

GEOLOGY, MINERALOGY AND GEOCHEMISTRY
OF THE BORATE DEPOSITS AND ASSOCIATED
ROCKS AT THE EMET VALLEY, TURKEY

by

CAHIT HELVACI, B.Sc., M.Sc.



Thesis submitted to the University of Nottingham
for the degree of Doctor of Philosophy,
January, 1977.

BEST COPY

AVAILABLE

Variable print quality

**PAGE
NUMBERS
CUT OFF
IN THE
ORIGINAL**

CONTENTS

Page

ABSTRACT

Chapter I:

INTRODUCTION

- | | |
|--------------------------|----|
| 1. Area of present study | 1 |
| 2. Previous work | 6 |
| 3. The present study | 9 |
| 4. Acknowledgements | 10 |

Chapter II:

DISTRIBUTION AND CLASSIFICATION OF BORATE DEPOSITE AND MINERALS

- | | |
|--|----|
| 1. Geochemical behaviour of boron | 12 |
| 2. Distribution and classification of borate deposits and minerals | 13 |
| 3. Borate deposits and minerals in Turkey | 23 |

Chapter III:

GENERAL GEOLOGY OF THE EMET DISTRICT

- | | |
|---|----|
| 1. Introduction | 27 |
| 2. Basement rocks and their petrography | 32 |
| 3. General stratigraphy of the sediments | 34 |
| (a) Conglomerate and sandstone | 34 |
| (b) Lower limestone | 35 |
| (c) Red formation | 35 |
| (d) Borate zone | 36 |
| (e) Upper limestone | 36 |
| 4. Petrography and geochemistry of volcanic rocks | 39 |
| (a) Classification of volcanic rocks | 39 |
| (b) Petrography of volcanic rocks | 40 |
| Spherulitic rhyolite | 40 |
| Dacite | 41 |
| Pyroxene andesite | 42 |
| (c) Geochemistry of volcanic rocks | 42 |
| 5. Structure | 49 |
| 6. Thermal springs | 54 |
| 7. Geological history | 56 |

Chapter IV:

PETROGRAPHY AND GEOCHEMISTRY OF THE SEDIMENTS

- | | |
|----------------------------------|----|
| 1. Petrography of the sediments | 59 |
| 2. Geochemistry of the sediments | 68 |
| (a) Introduction | 68 |

	<u>Page</u>
(b) Distributions, variations and inter-element correlations	69
(c) Geochemistry of clay and tuff	69
SiO ₂	70
Al ₂ O ₃ , TiO ₂ and K ₂ O	70
Iron (Fe ₂ O ₃ and FeO)	73
MgO	74
CaO, Mn and CO ₂	79
Na ₂ O	79
P ₂ O ₅	80
H ₂ O	80
B ₂ O ₃	84
S	85
Cl	85
Cr and Ni	86
Cu	87
Zn	88
As	89
Br	90
Sr	90
Ba	91
Ce	92
Pb	92
Th and U	93
Summary	94
(d) Geochemistry of upper limestone	95

Chapter V:

DETAILED STRATIGRAPHY AND STRUCTURE OF THE BORATE DEPOSITS

1. Introduction	119
2. Stratigraphy	123
3. Structure and thickness	134

Chapter VI:

MINERALOGY AND PETROGRAPHY OF THE EMET BORATE DEPOSITS

1. Introduction	145
2. Textural relationships of borate and other minerals in the Emet borate deposits	149
Calcium borates	149
Colemanite	149
Meyerhofferite	168

	<u>Page</u>
Sodium-calcium borates	173
Ulexite	173
Strontium borates	177
Veatchite	177
Tunellite	177
Magnesium-calcium borates	180
Hydroboracite	180
Complex borates	184
Teruggite	184
Compound borates	187
Cahnite	187
Non-borate minerals	190
Native sulphur	190
Realgar	190
Orpiment	192
Celestite	194
Gypsum	194
Calcite	198
Quartz	198
3. Geographical distribution and mineral assemblages	201

Chapter VII: GEOCHEMISTRY OF THE BORATES AND OTHER MINERALS

1. Introduction	205
2. Distributions, variations and inter-element correlations	209
B_2O_3 , CaO and H_2O	213
The elements Mg, Na, Sr, As and S	221
The elements Si, Al, Ti, Fe, Mg, K, Mn and P	226
The elements Cl, Cr, Ni, Cu, Zn, Sn, Ce, Pb and Th	228
The elements Br, Ba and U	229
3. Interpretation of chemistry	230
4. Colour variations in colemanite and the other borates	232

Chapter VIII: ORIGIN AND DIAGENESIS OF THE EMET BORATE DEPOSITS

1. The geological setting	267
2. Source of the Boron, Arsenic, Sulphur, Calcium, Sodium, Magnesium and Strontium	268
3. Mineral phases formed penecontemporaneously with the clastic sediments	272
Origin of the early formed colemanite	272
4. Diagenetic mineralization	278
5. Depositional and post-depositional history	283

	<u>Page</u>
<u>Chapter IX:</u>	
<u>COMPARISON OF THE FORMATION OF CALCIUM BORATES OF EMET WITH THE KIRKA DEPOSIT AND OTHERS IN TURKEY</u>	
1. Introduction	287
2. Kernite and other borate minerals from the Kirka deposit	291
Kernite	292
3. Inyoite mineral from Bigadiç deposits	296
 <u>Chapter X:</u>	
<u>ECONOMIC ASPECTS AND FUTURE PROSPECTS</u>	
1. Economic aspects	299
2. Future prospects	301
 <u>Chapter XI:</u>	
<u>SUMMARY AND CONCLUSIONS</u>	305
 <u>Appendix A:</u>	
<u>SAMPLE COLLECTION AND PREPARATION</u>	
1. Collection	316
2. Preparation	317
 <u>Appendix B:</u>	
<u>MAJOR ELEMENT ANALYSIS BY WET CHEMICAL METHODS</u>	319
 <u>Appendix C:</u>	
<u>MAJOR AND TRACE ELEMENTS ANALYSES BY X-RAY FLUORESCENCE SPECTROMETRY</u>	
1. Introduction	322
2. Preparation of fusion beads	327
3. Preparation of powder pellets	328
4. Calibration procedure	328
5. Determination of unknowns	330
6. Corrections for contaminations and interference	330
 <u>REFERENCES</u>	332

ABSTRACT

The Emet borate deposits are shown to be older and mineralogically more complex than previously thought. They are considered to have formed within the muds of separate or interconnected playa lakes, in areas of volcanic and seismic activity, fed partly by thermal springs and partly by streams draining the catchment areas, under arid or semi-arid climatic conditions during the Middle Oligocene.

The borate minerals formed in two geochemically distinct sedimentary basins and are interbedded with limestone, marls, volcanic tuffs and clays, much of which appear to have been derived mostly from a volcanic terrain. The borates show mineralogical and geochemical features in the two basins which are sufficiently different to suggest that the chemical compositions of ground and surface waters in the two basins differed at least from time to time. Basement metamorphic rocks and Tertiary limestone might also have been exposed and erosion of these may have contributed Ca and Sr to the lake waters.

Sediments in the borate lakes are cyclical with both lateral and vertical facies changes. The clastic sediments in both

basins are similar but are very much thicker in the northern basin. The total Tertiary sedimentary thickness exceeds 750 metres. The borate zone varies in thickness between 0-100 metres and reaches its maximum thickness in the northern deposits.

The Middle Oligocene sedimentary formations, including the borate zone, are far more faulted than previously thought. Thermal springs, which at present deposit travertine and sulphur, are active and widespread west of the Emet River.

Colemanite predominates and occurs in many different forms. Other borates include meyerhofferite, ulexite, tunellite, teruggite, cahnite, hydroboracite and either veatchite or p-veatchite. Cahnite has not hitherto been identified from borate deposits. Calcite, gypsum, celestite, native sulphur, realgar and orpiment are the principal associated minerals. Montmorillonite and illite are the only clay mineral groups identified.

Volcanic rocks, closely related to the Middle Oligocene lacustrine sediments, range from rhyolites to basalts and are very rich in potash relative to soda. A complete transition exists between tuffs and clays in the Emet borate zone sediments and is reflected in their geochemistry. All tuffs, clays and limestones are characterized by a relatively high concentration of B, As, S and Sr, and high $\text{Fe}_2\text{O}_3:\text{FeO}$ ratios which indicate strongly oxidising conditions of sedimentation, with a very low rate of leaching.

The deposits are characterized by high Ca borate (colemanite), very low Na, poor Cl and relatively high Mg, Sr, As and S concentrations compared with other borate deposits. Like the sediments, the borates are also characterized by a relatively high $\text{Fe}_2\text{O}_3:\text{FeO}$ ratio, suggesting strongly oxidising conditions of precipitation.

The geochemical investigations suggest that the most likely sources of B, As and S were from the Tertiary volcanic rocks and associated thermal springs. The major sources of Ca, Mg and Sr are considered to be due to leaching of underlying basement rocks and Tertiary limestone by thermal springs.

Investigation of the genesis of colemanite reveals no field evidence to unambiguously support its formation by replacement of ulexite or dehydration of inyoite after burial. The early colemanite nodules were probably formed directly from brines, penecontemporaneously within the unconsolidated sediments below the sediment/water interface, and continued to grow as the sediments were compacted. Possibly the brines were never sufficiently concentrated to allow borate precipitation until the lakes were partially or wholly dried up.

Later generations of colemanite occur in vughs, veins and as fibrous margins to colemanite nodules. Other diagenetic changes include the partial replacement of colemanite by hydroboracite, calcite, cahnite and a veatchite mineral. When weathered, colemanite is often almost completely replaced by calcite. Realgar, celestite and sulphur appear to have been deposited both during and after the formation of the borates.

Quantitatively known reserves in the Emet district are more adequate but their quality is less assured. The presence of arsenic in both the sulphide and borate phases can present problems during mineral processing. However, the Emet borates are high-grade colemanite deposits and should supply a substantial quantity of the world's needs for many years.

CHAPTER I

INTRODUCTION

1. Area of present study

The Emet borate deposits are located in the middle of the known borate deposits of western Anatolia, between Eskişehir and Bigadiç borate districts (Fig. 1). They are in the west of the province of Kütahya in the area between Gediz, Simav and Tavşanlı. The depositional basin of the borate beds is aligned north-south and outcrops on the east side of the Koca Çay (Emet River) from Dereköy north almost to Killik. The main mining operations are at Espey and Killik north of Emet town and at Hisarcik village which is south of Emet. The borate is transported along the 30 kilometer road running north of Emet to Emirler railway station. The climate permits work to be carried out throughout the year.

The Emet district contains the upland basin of the Emet River (Koca Çay) which is almost entirely enclosed by higher land, except to the north near Köprücek where there is an outlet to the Tavşanlı area and to the south east near Kaya village, leading to the Gediz area.

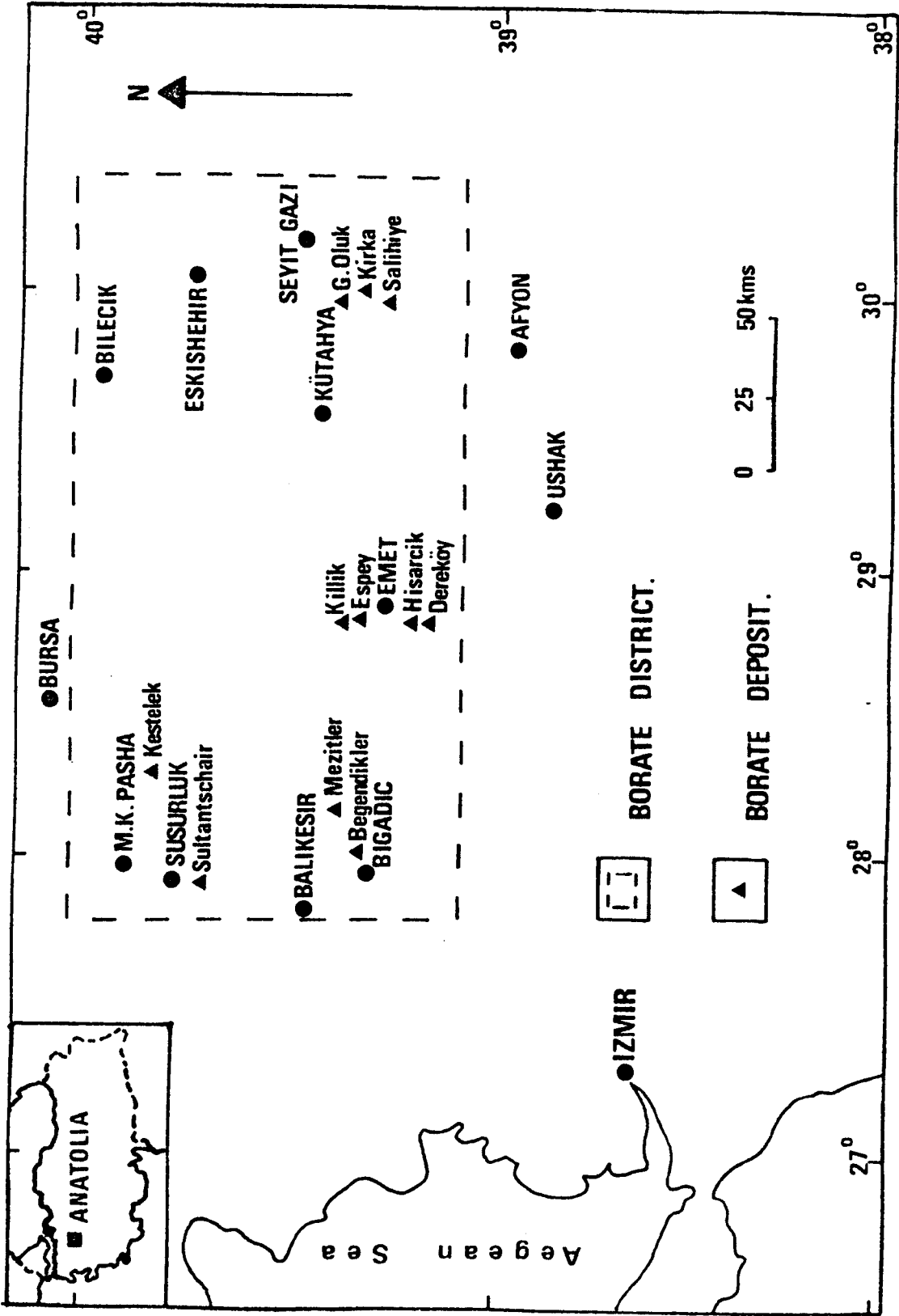


Fig.1. Location map of Emet and other borate deposits in Western Anatolia.

The Emet valley lies at altitudes of between 700 and 1000 metres, the river itself flowing at between 700 and 750 metres. The ranges lying to the west of the valley are higher and rise more steeply from the plateau than those to the east.

The topography of the area is closely related to the underlying geology. In the west, the more resistant igneous rocks of Eğrigöz and Katran mountains rise up to 2181 metres at the northernmost part of the range. To the south, the volcanic and metamorphic rocks of Şaphane mountain reach 2121 metres. The Kocadağ ranges to the east of the Emet basin are of metamorphic origin and rise to only 1814 metres. North and north-east of Emet is another region of mainly metamorphic and volcanic rocks, the highest point at Köprücek Hill - an isolated andesite outcrop - being 1320 metres.

The Emet valley itself consists mainly of recent alluvium formations and Middle Oligocene lacustrine sediments containing borate deposits which outcrop at elevations of between 800 and 950 metres (Plate 1).

The recent Gediz earthquake of 1970 resulted in severe disturbances to topography, geology and landscape within the Emet and Gediz valleys along the lines of NW-SE trending faults.

The variations in intensity of the earthquake depended largely on the tectonic structure of the area and the rock types.

Earth movements resulted in features such as tension fissures and landslides within the landscape; new thermal springs were generated by the movement of NW-SE trending faults. Much damage was caused to houses and mining properties; landslips affected opencast workings but underground operations were only slightly disturbed (Plate 2; Fig. 2).



Plate 1. General view of Middle Oligocene lacustrine formation in the Emet valley. Succession starts with lower limestone, continues with red formation, borate zone (foreground Hisarcik opencast mine-workings) and upper limestone. In the background metamorphic complex extending along a N-S direction .



Plate 2. The Dereköy village, south of Hisarcik, after the Gediz earthquake shocks. Photo shows the disturbances of earthquake.

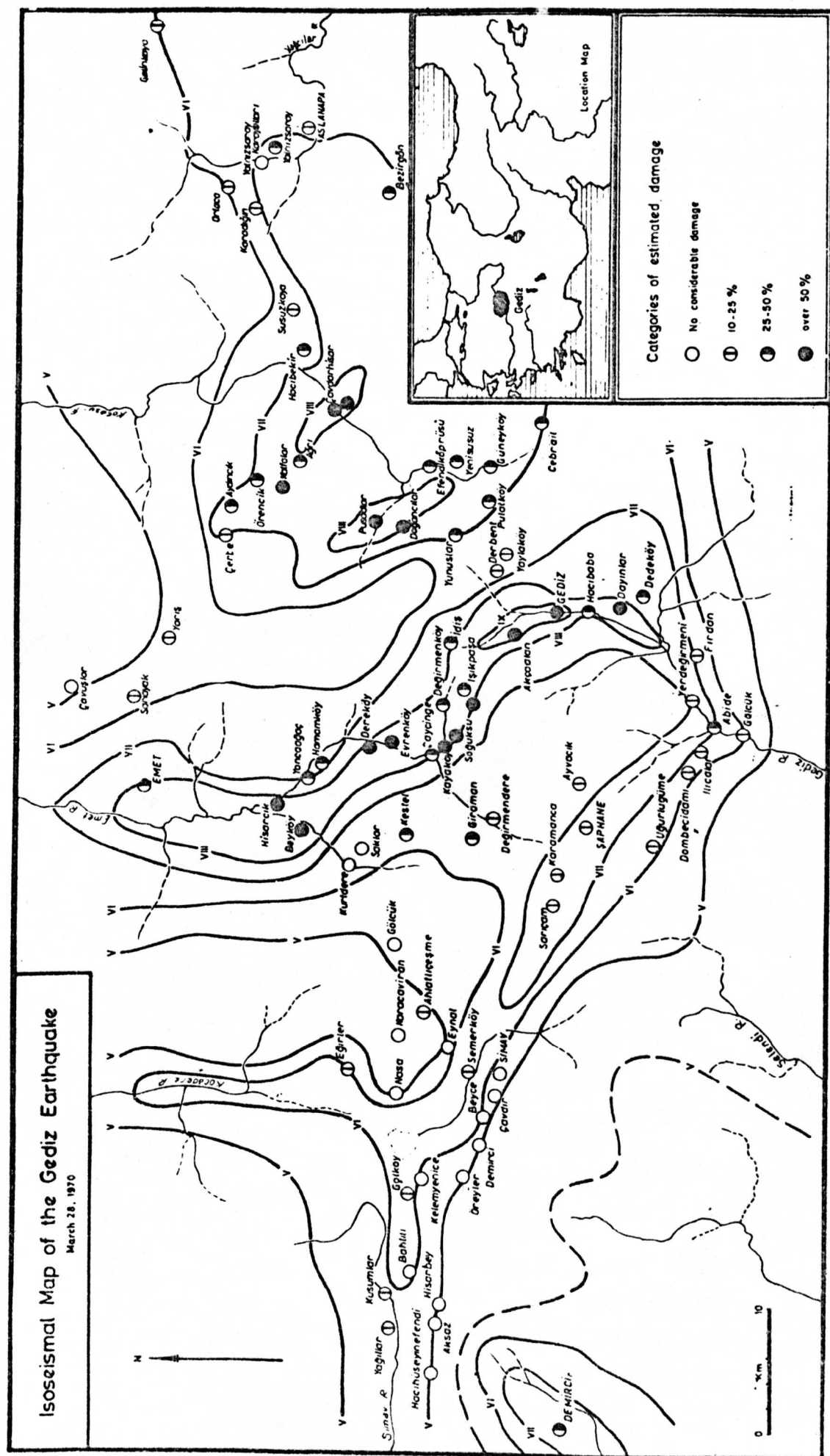


Fig. 2. Isoseismal map of the Gediz earthquake (after Yazar, Demir, Kumbasar and Trupia, 1970).

2. Previous work

The Emet borate district is the most important source of calcium borates in the world. Most of the deposits are owned and operated by Etibank (Turkish mining and banking company), and on the northern border a small part of the deposits is owned and operated by the Turkish Borax Company at Espey and Killik.

The Emet borate deposits were discovered accidentally by Dr. J. Gawlik whilst carrying out a survey of lignite deposits for M.T.A. (The Mineral Research and Exploration Institute of Turkey) in April, 1956. The only mineral recorded was colemanite, a very common calcium borate known in the other Turkish borate deposits (Gawlik, 1956, Meixner, 1952, 1953, Özpeker, 1969).

The Turkish Borax Company has been operating mines in the Espey and Killik areas since September 1956 and an extensive exploratory drilling programme was undertaken by M.T.A. in 1958 and 1959, on behalf of the Etibank Company, in the Hisarcik and Espey localities. The deposits are mined by open pit mining methods at Hisarcik and underground mining methods at Espey and Killik, which will be converted to opencast mining in the near future. Table 1 gives the reserves (expressed in tonnes) in this area.

A paper in Turkish (Özpeker, 1969) which surveyed most of the known Turkish borate deposits provides the only published account of the geology of the Emet Valley. It listed borate and other minerals that occur in the Emet deposits (Table 2).

Teruggite from the Hisarcik deposit was subsequently identified and the crystal structure described by Negro, Kumbasar and Ungaretti, 1973; several other minerals have been identified during the present study.

Reserves in Tonnes

Location	Proved	Probable	Total	Average wt% B ₂ O ₃ content	Minerals
Hamamköy (Etibank)	Reserve figures are unreliable				See Table 3
Hisarcik (Etibank)	7,175,440	5,125,807	12,938,282	43% B ₂ O ₃	See Table 3
Espey (Etibank)	53,690,000	39,662,000	93,425,500	46% B ₂ O ₃	See Table 3
Espey (Turkish Borax Company)	20,000	640,000	660,000	49.5% B ₂ O ₃	See Table 3
Killik (Turkish Borax Company)	181,900	2,379,000	2,560,900	45 % B ₂ O ₃	See Table 3

Table 1 Borate minerals reserves in the Emet borate deposits.

Mineral Name	Formula	Locality
Colemanite	$\text{Ca}_2\text{B}_6\text{O}_{11} \cdot 5\text{H}_2\text{O}$	Espey, Göktepe, Hisarcik, Hamamköy
Ulexite	$\text{NaCaB}_5\text{O}_9 \cdot 8\text{H}_2\text{O}$	Göktepe, Hisarcik
Celestite	SrSO_4	Hisarcik
Realgar	AsS	Hisarcik
Orpiment	As_2S_3	Hisarcik
Gypsum	$\text{CaSO}_4 \cdot 2\text{H}_2\text{O}$	Göktepe
Calcite	CaCO_3	Espey, Göktepe, Hisarcik, Hamamköy

Table 2 Minerals listed by Özpeker in the Emet borate deposits.

3. The present study

The borate deposits in the Emet Valley were first visited by the writer in the summer of 1972. The deposits have been visited subsequently in the summers of 1973 and 1974 for the purpose of making detailed maps, observations and collecting samples. Most of the samples collected were obtained in the open pit in the Hisarcik locality and in the underground workings of the Espey and Killik mines. Specimens of sedimentary and volcanic rocks have also been collected from the deposits and adjacent area. The results of drilling and subsequent exploration by both companies have been made available to the writer and access to all mines and opencast workings has been freely granted.

The major purpose of the present study is to contribute to the understanding of geology, mineralogy, geochemistry and origin of borate deposits. The main aims of the present research can be listed as follows.

1. Detailed mapping of the Emet borate deposits and the adjacent area.

2. Detailed geology and mineralogy of the Emet borate deposits and associated rocks.

3. Geochemistry of the borate deposits and associated sedimentary and volcanic rocks.

4. The application of geological, mineralogical and geochemical data together with field observations to explain the origin and diagenesis of the Emet borate deposits and associated rocks.

4. Acknowledgements

The research project was made possible by the Turkish Ministry of Education Scholarship which the author gratefully acknowledges. The author wishes to take this opportunity to express his gratitude to the management and technical staff of Etibank's mineral production divisions for their generous assistance during visits to the Emet and Kirka borate deposits.

The author is greatly indebted to Dr. R.J. Firman for his very considerable assistance, encouragement and supervision throughout the whole period of this study and for critically reading the manuscript.

I am grateful to Professor the Lord Energlyn for his encouragement and for the facilities in the Department of Geology at the University of Nottingham; to members of staff and research students for advice and help, and particularly to Dr. P.K. Harvey for his interest, encouragement and many rewarding discussions on geochemical work; Dr. R.B. Elliott, Dr. J.A.D. Dickson, Dr. D. Field and Mr. P. Redfern for their unfailing help in some aspects of the research work.

The Technical Staff are thanked for their help in the preparation of research materials, in particular, Mr. D. Jones for his invaluable assistance in the production of photographs; Mr. E. Mitchell for rock-crushing; Mr. R.D. Hendry and Mr. T. Foster for preparation of thin sections; Mr. J. Eyett and Mr. W. Wilson for their help with XRF and XRD works and Mr. I.H. Beaumont for his help during geochemical work in the silicates laboratory.

Dr. R.H. Bate of the British Museum examined fossils from the Upper Limestone and I am most grateful to him for his assistance. Dr. M.G. Barker in the Chemistry Department is thanked for his kind help with single crystal work. Mr. F. Akdogan in the Mechanical Engineering Department is also thanked for his kind help with some programming.

I would like to thank Miss A.M. Hargreaves and Mrs. J. Pearson who typed this thesis as fast as it was written and Mrs. J. Wilkinson for cartographic assistance. Finally, my gratitude goes to Miss R.A. Lockwood, not only for her help with maps and diagrams, but also for many other considerable contributions too numerous to mention.

CHAPTER II

DISTRIBUTION AND CLASSIFICATION OF BORATE DEPOSITS AND MINERALS

1. Geochemical behaviour of boron

Boron has a very low atomic weight (10.811) and presents both metallic and non-metallic properties. It is one of the most mobile and least abundant elements, the average amount of boron in the Earth's crust being estimated at less than 10 parts per million. However, it is found in minerals which occur in nearly all geologic environments and it forms many unusual compounds with unusual properties due to its dual nature. Because of the high ionic potential ($i = 13.0$) B^{3+} is unlikely to exist as a free ion.

Boron occurs in several plutonic and metamorphic rocks, usually in the mineral tourmaline (Rankama and Sahama, 1950; Goldschmidt, 1954). In sedimentary rocks it occurs mainly in detrital tourmaline and as a trace or minor element in illitic clays. The marine argillaceous sediments contain relatively larger amounts of boron than the non-marine argillaceous sediments (Landergrén, 1945). It has also been claimed that there is a

direct relationship between the boron in the sediments and the salinity of the water where they were deposited. The average values accepted by most authors for marine sediments are in the range of 110 to 120ppm B (Goldschmidt, 1954). There are considerable amounts of boron in the sea water (4.6ppm B) (Sverdrup, Johnson and Fleming, 1942). The concentration of boron in lake and thermal spring waters varies widely and most of them are associated with volcanic activity.

The greatest concentration of borate minerals is found in the non-marine evaporite deposits, but the rest of the continental clastic sediments are usually extremely low in boron. Large quantities of boron are concentrated in deposits of hydrated borate minerals; these deposits occur in closed basins and under arid conditions within areas of volcanic activity. The boron minerals precipitate as a result of the concentration by evaporation of natural boron-bearing waters in both non-marine and marine sedimentary environments.

In connection with the studies on problems of the geochemical abundance of boron in the Earth's crust, its cyclic behaviour was discussed by previous authors such as Goldschmidt, Landergren, Harder and Watanabe. Although boron is not abundant in the Earth's crust, the cycle and concentration of boron in the crust have been reasonably well established (Fig. 3).

2. Distribution and classification of borate deposits and minerals

Borate minerals, not necessarily of commercial value, occur in a number of places in the world. They are found in Turkey

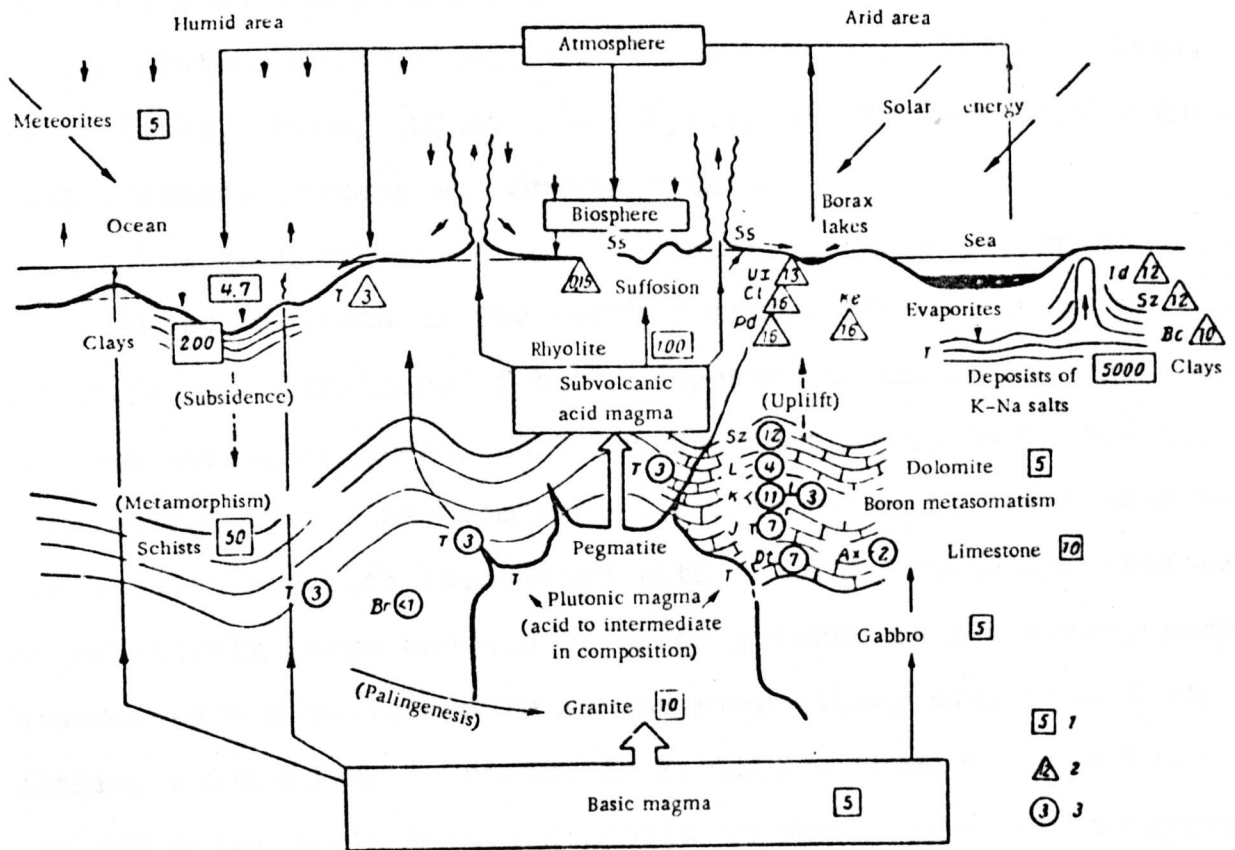


Fig.3. Scheme for the cycle and concentration of boron. The geochemical abundance of boron in rocks is cited according to Goldschmidt, Landergrén and Harder. (After Watanabe, 1964).

- 1 - average content of boron in rocks (g/ton);
- 2 - exogenic concentration of boron (%);
- 3 - endogenic concentration of boron (%);
- S's - sassolite; Ux - ulexite; Cl - colemanite;
- Pd - pandermite; Ke - kernite; In - inderite;
- Bc - boracite; Sz - szaibelyite; L - ludwigite;
- K - kotoite; J - "jimboite" $[\text{Mn}_3(\text{BO}_3)_2]$;
- Dt - datolite; Ax - axinite;
- T - tourmaline; Br - braunite.

(Western Anatolia), U.S.S.R. (Inder district), the Western United States (California), Canada, Argentina, Chile, Bolivia, Peru, Tibet, China, India, Iran, Syria, New Zealand, New Guinea, Italy, Japan, Germany and Great Britain.

Although boron is one of the rarer and more unevenly distributed elements in the Earth's crust, there are extraordinary concentrations of boron deposits on an industrial scale in some localized areas. All the United States, South American, Turkish and many other commercial borate deposits are brackish-fresh water deposits associated with volcanic activity. Because of relatively large amounts of boron present in sea water, borate minerals are also formed in marine evaporites, e.g. Stassfurt Permian salts and a trace amount in Yorkshire Permian deposits. Contact metasomatic borate deposits in skarns adjacent to granites have great economic importance in the Soviet Union. Similar occurrences of borate minerals in the Isle of Skye, Scotland, have no economic value. The thermal spring waters from South America and Japan and volcanic exhalation of volcanic regions from Tuscany in Italy also contain an appreciable amount of boron.

Although borate deposits formed in various environments and very different conditions, the economically most important deposits are very closely related to the recent extensive volcanic activity along orogenic belts, characterized by andesitic-rhyolitic magmas, in the arid or semi-arid climates and non-marine evaporite environments (closed basins) during the Tertiary period. The main source of boron appears to have been volcanic emanations from such magma (Fig. 4).

Several authors have suggested various genetic classifications for the known major borate deposits in the world (Meixner, 1953;

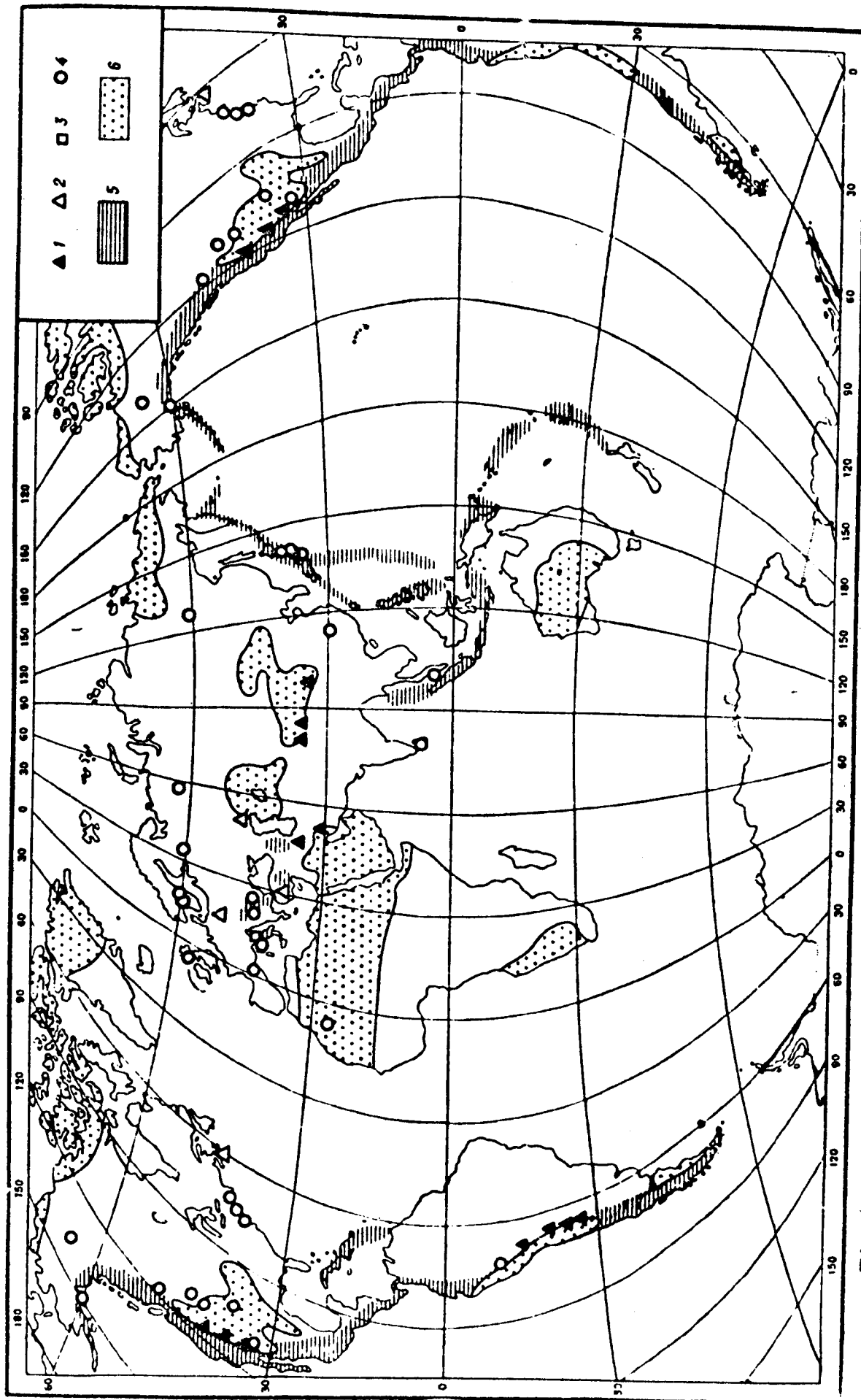


Fig.4. Distribution map of boron deposits. (After Watanabe, 1964)
 1 - exogenic deposits (surface); 2 - exogenic deposits (buried);
 3 - exhalation deposits; 4 - endogenic deposits; 5 - volcanic zone;
 6 - arid region.

Shabynin, 1957; Watanabe, 1964; Aristarain and Hurlbut, 1972).

The latest classification has been done by Aristarain and Hurlbut (1972). They suggested the borate deposits are related to three principal geological environments:-

- A. Deposits related to intrusive rocks
- B. Deposits related to volcanic activity
- C. Deposits related to marine sediments

The deposits, types A and B are the most important economically, e.g. type A in U.S.S.R. and type B in Turkey and California deposits. The largest production of boron minerals comes from type B of borate deposits. All Turkish borate deposits appear to be associated with volcanic activity, classified in type B. Aristarain and Hurlbut (1972) give a more detailed subdivision for volcanic activity deposits, type B:-

Deposits related to volcanic activity

1. Steam vents (= soffioni) natural and drilled, recovered as sassolite (Tuscany, Italy)
2. Thermal spring solutions (Japan; Sulphur Bank Spring, California, U.S.A.)
3. Thermal spring deposits (Jujuy, Argentina; Chetco, U.S.A.)
4. Mud flow (Jujuy, Argentina)
5. Desert Lake (brine) (Searles Lake, U.S.A.)
6. Playa (= marsh) on or near surface (Nevada, U.S.A.; Tibet; Bolivia; Peru)
7. Old playa, buried, highly deformed, low to no chemical changes (Salta, Argentina)
8. Old playa or lake deposit, buried, highly deformed, low to moderate chemical changes (Emet, Kirka, Bigadiç, Kestelek etc., Turkey; California, U.S.A.; Salta, Argentina)

All of these examples are non-marine and are Tertiary or younger in age. Marine borate deposits associated with volcanic activity have not been recorded.

The composition and structure of borate minerals vary from one place to another a great deal, but they mainly occur as Ca, Ca-Na, Na, Mg and Sr borates. The Ca and Na borate minerals are the major constitutions of most economic non-marine borate deposits. The important borate minerals with their chemical compositions and geological environments are listed in Table 3.

Table 3. Common borate minerals

<u>Mineral Name</u>	<u>Oxide Formula</u>	<u>B₂O₃ Content wt%</u>	<u>Environment</u>	<u>References</u>
<u>Boric acid</u>				
Sassolite	B ₂ O ₃ ·3H ₂ O	56.30	Volcanic subli- mate (steam vents)	Zachariassen (1954)
<u>Hydrated borates</u>				
Inyoite ⁺	2CaO·3B ₂ O ₃ ·13H ₂ O	37.62	Non-marine	Clark (1959)
Meyerhofferite ^{†*}	2CaO·3B ₂ O ₃ ·7H ₂ O	46.72	"	Christ and Clark (1956)
Colemanite ^{†*}	2CaO·3B ₂ O ₃ ·5H ₂ O	50.81	"	Christ et al (1958)
Tertschite ⁺	4CaO·5B ₂ O ₃ ·20H ₂ O	37.32	"	Meixner (1953)
Priceite(=pandermite) [†]	4CaO·5B ₂ O ₃ ·7H ₂ O	49.84(54.59)	"	Schlüter (1922)
Ginorite	2CaO·7B ₂ O ₃ ·8H ₂ O	65.54	"	D'Achiardi (1934)
Nobleite	CaO·3B ₂ O ₃ ·4H ₂ O	61.98	"	Erd et al (1961)
Ulexite ^{†*}	Na ₂ O·2CaO·5B ₂ O ₃ ·16H ₂ O	42.95	"	Clark et al (1964)
Probertite	Na ₂ O·2CaO·5B ₂ O ₃ ·10H ₂ O	49.56	"	Rumanova et al (1966)
Borax [†]	Na ₂ O·2B ₂ O ₃ ·10H ₂ O	36.51	"	Morimoto (1956)
Tincalconite [†]	Na ₂ O·2B ₂ O ₃ ·5H ₂ O	47.80	"	Christ et al (1959)
Kernite [†]	Na ₂ O·2B ₂ O ₃ ·4H ₂ O	51.02	"	Christ et al (1959)

Table 3 (continued)

<u>Mineral Name</u>	<u>Oxide Formula</u>	<u>B₂O₃ Content wt%</u>	<u>Environment</u>	<u>References</u>
Ezcurrite	2Na ₂ O.5B ₂ O ₃ .7H ₂ O	58.21	Non-marine	Muessing et al (1957)
Hydroboracite ^{†*}	CaO.MgO.3B ₂ O ₃ .6H ₂ O	50.53	Marine and non-marine	Rumanova et al (1964b)
Inderborite [†]	CaO.MgO.3B ₂ O ₃ .11H ₂ O	41.49	"	Palach et al (1951)
Inderite [†]	2MgO.3B ₂ O ₃ .15H ₂ O	37.32	Non-marine and endogenic deposit	Rumanova et al (1964a)
Kurnakovite [†]	2MgO.3B ₂ O ₃ .15H ₂ O	39.89	Marine, non-marine and endogenic deposit	Palache et al (1951)
Szaibelyite(=ascharite)	2MgO.B ₂ O ₃ .H ₂ O	41.38	Marine and endogenic (skarn) deposit	Palache et al (1951)
Tunnellite ^{†*}	SrO.3B ₂ O ₃ .4H ₂ O	54.32	Non-marine	Erd et al (1961)
Veatchite ^{†*}	4SrO.11B ₂ O ₃ .7H ₂ O	58.16	"	Clark et al (1971)
p-Veatchite ^{†*}	" " "	58.5	Marine and non-marine (?)	Braitsch (1959) and this study (?)
Teruggite ^{†*}	4CaO.MgO.6B ₂ O ₃ .As ₂ O ₅ .20H ₂ O	32.76	Non-marine	Aristarian and Hurlbut (1968)
Howlite [†]	Ca ₂ SiB ₅ O ₉ (OH) ₅	44.49	Non-marine	Murdoch (1957)

Table 3 (continued)

<u>Mineral Name</u>	<u>Oxide Formula</u>	<u>B₂O₃ Content</u> <u>Wt%</u>	<u>Environment</u>	<u>References</u>
Bakerite	$\text{Ca}_4\text{B}_4(\text{BO}_4)(\text{SiO}_4)_3(\text{OH})_3\text{H}_2\text{O}$	27.92	Non-marine	Giles (1903)
Kaliborite	$\text{KMg}_2\text{B}_{11}\text{O}_{19}\cdot 9\text{H}_2\text{O}$	56.92	Marine and endo- genic deposit	Palache et al (1951)
Landerellite	$(\text{NH}_4)_2\text{O}\cdot 5\text{B}_2\text{O}_3\cdot 5(?)\text{H}_2\text{O}$	71.01	Volcanic subli- mate	Clark and Christ (1959b)
<u>Anhydrous borates</u>				
Ludwigite	$(\text{Mg}, \text{Fe})_2\text{Fe}^{III}\text{B}_5\text{O}_5$	17.02	Non-marine and endogenetic (skarn) deposit	Palache et al (1951)
Kotoite	$3\text{MgO}\cdot \text{B}_2\text{O}_3$	36.54	Endogenetic (skarn) deposit	Watanabe (1939)
<u>Borates containing hydro- xyl or halogen</u>				
Boracite	$\text{Mg}_3\text{B}_7\text{O}_{13}\text{Cl}$	62.15	Marine	Braitsch (1960a&b)
<u>Compound borates</u>				
Cahnite ⁺ *	$4\text{CaO}\cdot \text{B}_2\text{O}_3\cdot \text{As}_2\text{O}_5\cdot 4\text{H}_2\text{O}$	11.69	Vein cut by peg- matite and non- marine	Palache and Bauer (1927) and this study

Table 3 (continued)

<u>Mineral Name</u>	<u>Oxide Formula</u>	<u>B₂O₃ Content Wt%</u>	<u>Environment</u>	<u>References</u>
<u>Borosilicates</u>				
Datolite	CaB[SiO ₄](OH)	21.76	Contact metaso- matic deposits in skarns	Kurman and Usacheva (1937)
Tourmaline	Na(Mg, Fe, Mn, Li, Al) ₃ Al ₆ [Si ₆ O ₁₈](BO ₃) ₃ (OH, F) ₄	10.53	Granites, peg- matites, peg- pneumatolytic veins and meta- morphic rocks	Donnay and Buerger (1950)

+ Minerals occur in the Turkish borate deposits

* Minerals occur in the Emet borate deposits

3. Borate deposits and minerals in Turkey

The known borate deposits of Turkey occur in Western Anatolia, south of the Marmara Sea, and within an area roughly 300 kilometers east-west by 150 kilometers north-south. They are located mainly in the following districts:- M. Kemalpaşa, Bursa province; Susurluk and Bigadiç, Balıkesir province; Emet, Kütahya province; and Kirka, Eskişehir province (Fig.1).

The early history of borate mining in Turkey goes back to Roman times. Substantial amounts of borates have been produced in Turkey since the end of the last century. In 1865 a French company was operating the Sultançayırı mine in Balıkesir province. There is a record of production since 1887, which indicates that production has been continuous except for war periods. Until 1954 all recorded production came from Sultançayırı but since 1950 extensive exploration has resulted in the discovery of several important new Turkish deposits. Bigadiç deposit, Balıkesir province, has operated since 1950 and major production in the M. Kemalpaşa deposit, Bursa province, began about 1952. In 1956 the Emet borate deposits, Kütahya province, were discovered accidentally by Dr. J. Gawlik whilst carrying out a survey of lignite deposits for M.T.A. After their discovery the Emet deposits became the main source of colemanite in the western world. Finally, the most outstanding discovery was the Kirka borate deposit which is mainly a massive borax body, with estimated reserves several times greater than those of Boron, California (Dunn, 1966; Arda, 1968; Inan, 1972; Baysal, 1972). Today, however, borate mining is confined to three distinct areas:- Emet, Kirka and Bigadiç.

Turkey is currently the second largest producer of borate minerals and has the world's largest reserves. Output is rapidly catching up on that of the U.S.A.. Production more than doubled in 1975 to over one million tonnes (1.075.533 tonnes) and further increases, particularly of borax from Kirka, are likely to lead to Turkey dominating the world markets. Already Turkey is the major world producer of colemanite, much of which comes from the Emet valley.

The known borate deposits of Turkey were deposited in the lacustrine sediments of Tertiary age during the period of volcanic activity which commenced in the early Tertiary period and continued at least to the beginning of the Quaternary. Although the lithology of the borate deposits shows some differences from one to another, they are, generally, interbedded with conglomerate, sandstone, tuff, clay marl and limestone. Sediments in the borate lakes show often a clear evidence of cyclicity. Pyroclastic and volcanic rocks of rhyolitic, dacitic, trachytic, andesitic and basaltic composition are intercalated with these lacustrine sediments. The existence of volcanic rocks in every borate district suggests that volcanic activity may have been necessary for the formation of borates.

The known Turkish borate deposits, including the Emet borates, were considered by previous authors to be of Neogene age (Meixner, 1953; Gawlik, 1956; Özpeker, 1968; Inan, 1972; Baysal, 1973). Fossils collected from the Emet area by the present author suggest that the deposits are in fact older than was previously thought. Some ostracods from limestone overlying the borates in Emet indicate brackish-fresh water deposits of Middle Oligocene age. The occurrence of Eocene conglomerate and

fossiliferous limestone underlying unconformably the borates in the Kirka deposit suggests that this deposit may also be older than was previously thought. Formations of Eocene age occasionally outcrop at the north and north-west of the Kirka basin (Inan, Ph.D. thesis, 1973) and the rest of the borate deposits could have been formed at the same time. There is not enough data available to prove their age conclusively and the suggestion of Özpeker (1969) that they are of Neogene age may be wrong. Borate minerals were deposited in separate or possibly inter-connected lake basins under arid or semi-arid climatic conditions.

Although colemanite, a very common calcium borate, is the predominant mineral in all borate districts apart from Kirka, the detailed mineralogy and geochemistry of the Turkish borate deposits vary; roughly they may be classified as follows:-

1. Ca borate deposits (Emet, Bigadiç, Kestelek, Sultançayırı)
2. Na borate deposit (Kirka)

Borate minerals hitherto recorded from Turkish deposits are mainly Ca, Ca-Na, Ca-Mg, Na and Mg borates. A rare Sr borate has been found at Kirka (Baysal, 1972) and the writer has found Ca-As and Sr borates in the Emet district. The complete list of borate minerals from Turkish deposits is given in Table 4.

Generally, borate minerals are associated with calcite, dolomite, gypsum, celestite and sulfides. The mineralogy and geochemistry of the Emet borate deposits are unique among the other Turkish borates deposits, because of unusual occurrences of Ca-As and Sr borates and the high content of S, As, Sr. Sulphur, realgar, orpiment, celestite, gypsum and calcite minerals are formed with borate minerals in the Emet deposits.

Mineral Name	Locality	References
Inyoite	Kirka, Bigadiç	Meixner (1953b)
Meyerhofferite	Emet, Kirka, Bigadiç	Meixner (1953b), this study
Colemanite	Emet, Kirka, Bigadiç, Kestelek	Meixner (1952)
Tertschite	Bigadiç	Meixner (1952)
Pandermite (=priceite)	Bigadiç, Sultançayiri	Schlüter (1928)
Ulexite	Emet, Kirka, Bigadiç	Meixner (1953b); this study
Borax	Kirka	Inan (1972); Baysal (1972)
Tincalconite	Kirka	Inan (1972)
Kernite	Kirka	This study
Hydroboracite	Emet, Kirka, Bigadiç	Özpeker (1969); Helvacı (1974)
Inderborite	Kirka	Baysal (1973)
Inderite	Kirka	Inan (1972); Baysal (1973)
Kurnakovite	Kirka	Inan (1973); Baysal (1973)
Tunellite	Emet, Kirka	Inan (1972); Baysal (1972); this study
Veatchite (sensu lato)	Emet	Helvacı (1974); this study
Teruggite	Emet	This study; Negro et al. (1973)
Howlite	Bigadiç	Özpeker (1969)
Cahnite	Emet	This study

Table 4. Borate minerals found in the Turkish borate deposits.

CHAPTER III

GENERAL GEOLOGY OF THE EMET DISTRICT

1. Introduction

In the Emet area, the borates are in beds of Middle Oligocene lacustrine sediments, which lie unconformably on the Paleozoic(?) metamorphic rocks.

Emet borates were considered by Gawlik and all subsequent authors to be of Neogene age (Fig. 5) but fossils collected by the present writer suggest that the deposits are older than was previously thought. Some ostracods from limestones overlying the borates were examined by Dr. R. H. Bate (personal communication) and the following were identified; Candona (Pseudocandona) fertilis fertilis, Erpetocypris sp., Timiriaseria sp. and Cypris sp. indicating brackish-fresh water deposits of the Middle Oligocene. Also some gastropods, plants (Angiosperm leaf fossils) and algae (Myxophyte algal nodules) from the Emet Sediments were examined and the gastropods identified by Dr. A. J. Rundle and Mr. J. Cooper are as follows:- Lymnaea, Helix, Planorbis and Planorbis, all of which indicate a fresh water-brackish environment.

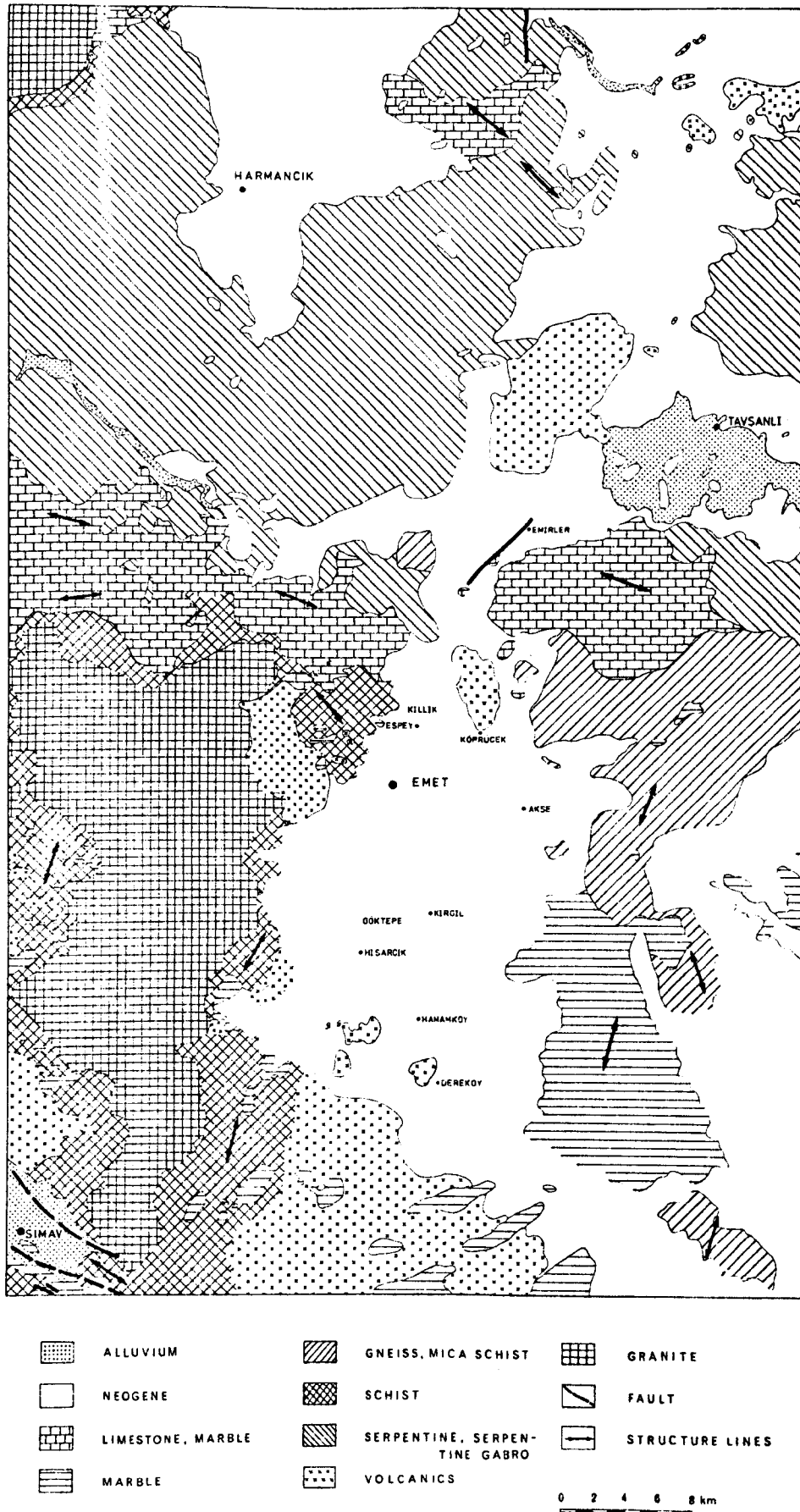


Fig.5. Geology and tectonic map of Emet and Tavşanlı area, Kütahya (after H.Holzer, 1954). Note that the age of the sediments containing borate deposits is shown as Neogene and the major fault extending NW-SE directions, along the Emet River, is not marked on the map.

The sediments of the Emet district consist of the following predominantly lacustrine sequence, from top to bottom:-

- (e) Upper limestone containing clay, marl and chert layers.
- (d) Clay, tuff and marl containing borate deposits.
- (c) Red formation; conglomerate, sandstone, clay, marl, limestone with coal and gypsum bands.
- (b) Thin bedded lower limestone with lenses of marl and tuff.
- (a) Conglomerate and sandstone.

This sequence rests directly and unconformably on the Paleozoic(?) metamorphic complex containing marble, mica schist, calc-schist and chlorite schist, with an angular unconformity. Figs. 6 and 7 are, respectively, a geological map and a generalized stratigraphic section of the Emet borate district. (Figs. 6 & 7)

Basal conglomerate and sandstone do not outcrop throughout the Emet area, but intervene between the lower limestone and the basement metamorphic complex beyond the mapped area, mainly in the southern part of the district. Sediments in the borate lakes show clear evidence of cyclicity. Above the basement, sedimentation begins with carbonate, followed by conglomerate, sandstone, clay and marl with interbedded tuff and borate, and returns to carbonate.

A sequence of volcanic rocks in the Emet district has been well established and they are discussed later on in this chapter.

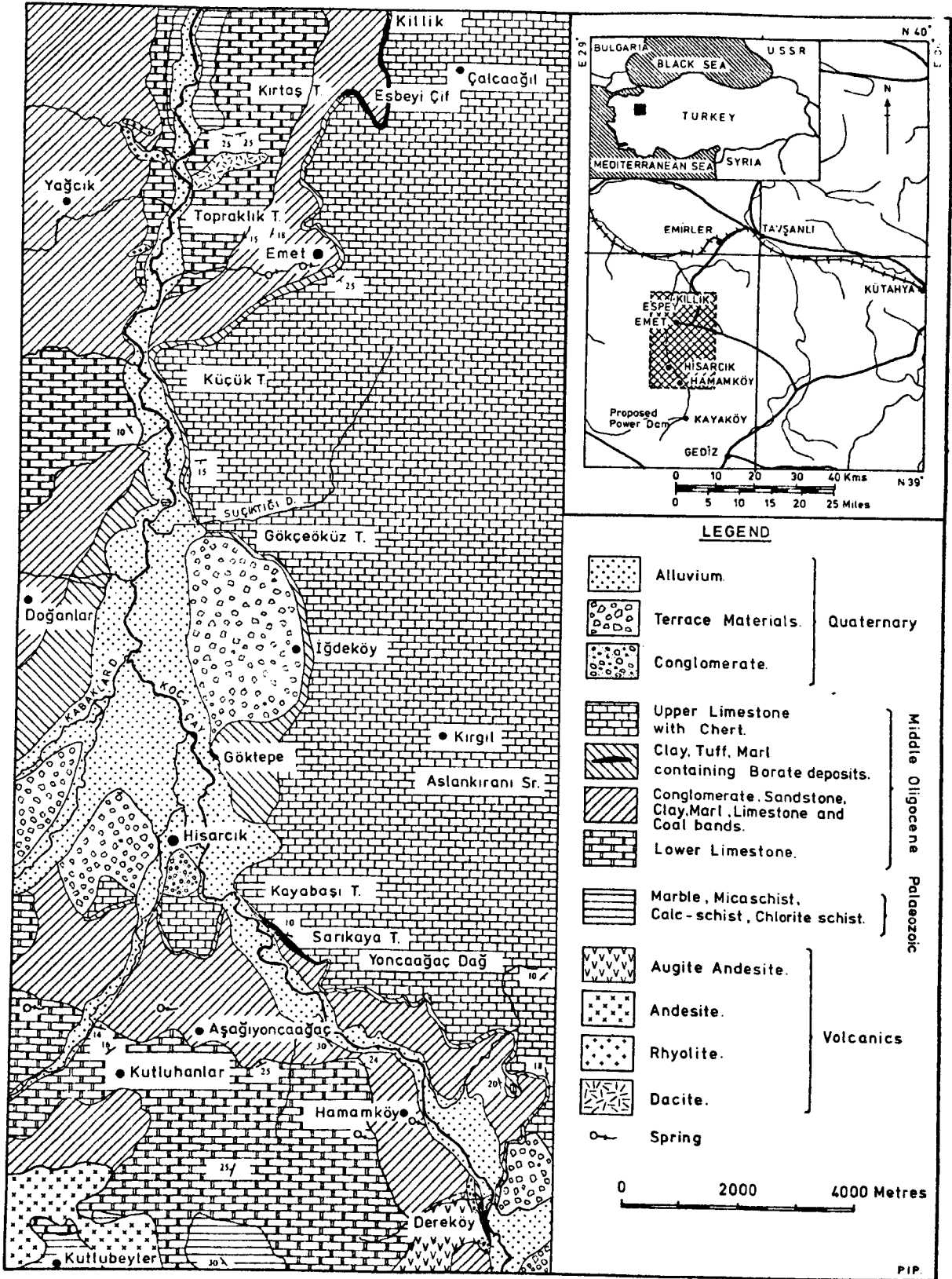


Fig.6. Locality and geological map of Emet borate district.
(After Dr. Özpeker, 1969, with additions and minor
corrections by C.Helvaci.)

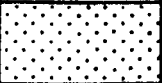


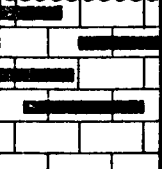
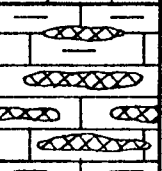
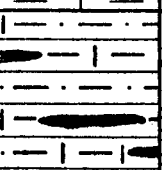
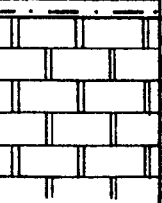

GEOLOGICAL TIME			THICKNESS	LITHOLOGY	DESCRIPTION
ERA	PERIOD	EPOCH			
C a e n o z o i c	Quaternary				ALLUVIUM
					TERRACE MATERIALS
					CONGLOMERATE
	Tertiary	Middle Oligocene	400 m		UPPER LIMESTONE. CONTAINING CLAY, MARL AND CHERT LAYERS.
			0-100m		CLAY, TUFF, MARL CONTAINING BORATE DEPOSITS.
			125 m		CONGLOMERATE, SANDSTONE, CLAY, MARL, LIMESTONE, WITH COAL BANDS.
Palaeozoic			150 m		LOWER LIMESTONE
			?		MARBLE, MICA SCHIST, CALC-SCHIST, CHLORITE SCHIST.

Fig.7. Generalized stratigraphic and geological column of Emet borate district.

2. Basement rocks and their petrography

The metamorphic complex, which consists mainly of marble, mica schist, calc-schist, chlorite schist, quartzite and gneiss, lies unconformably beneath Middle Oligocene lake sediments containing borate deposits in the Emet area. They outcrop mainly east and west of the younger lake sediments and extend in a north-south direction, thus limiting the Emet borate beds to the east and west (see Fig. 5). North and south of the Emet area, the metamorphic complex outcrops from place to place, and is associated with recent volcanic rocks, which cut and metamorphose them. The Egrigöz granite, which appears on the west side of the Emet valley, and the Tertiary volcanic activity caused the thermal metamorphism of these rocks which are believed to be Paleozoic metasedimentary formations.

Hand specimens collected from the area indicated that the major metamorphic rock groups frequently incorporate other rock types which occur in the field, but they are not distinct mappable bands.

Marbles occur as two distinct mappable types, mainly in the east and north part of the Emet basin. One type is massive, dark blue in colour and its composition is mainly large grain-sized calcite crystals, which are highly strained, and polygonal grains of calcite crystals which are up to 2mm in diameter (Plate 3). The other type of marble is pale blue or grey coloured, shows a granular blastix texture and contains very fine grained calcite crystals of up to 10-25 microns which indicate recrystallization. The two different marble types contain trace amounts of quartz and biotite. The grain of quartz crystals are approximately up to 30-50 μ . It seems likely that these marbles were important



Plate 3 Massive marble outcropping near Egrigöz village in the north part of the Emet valley.

sources of Ca, Mg and probably some other trace elements when the borates formed during the Tertiary period.

Mica schist, calc-schist, chlorite schist, gneiss, quartzite and banded ironstone occur mainly in the west and north part of the Emet valley. Their colours are usually green, green-grey and sometimes yellow and yellow-red. The common constituents of the rocks are quartz, muscovite, biotite, plagioclase, orthoclase, chlorite and calcite in the veins, with occasionally garnet, apatite, epidote, hematite and limonite. Usually quartz is heavily strained and banded. Grain size varies considerably. A poor foliation is commonly delineated by the phyllosilicate minerals, biotite, muscovite and chloritized biotite. Plagioclase and orthoclase are always altered when observed in thin sections, but occasionally orthoclase shows simple twinning. Concentrations of heavy minerals include apatite, rutile, tourmaline, zircon, hematite and limonite.

3. General stratigraphy of the sediments

Borate containing sediments of Middle Oligocene age overlies unconformably the basement metamorphic complex. Quaternary alluvial deposits cover these sediments along the Emet River. The Middle Oligocene sedimentary formations strike roughly parallel to the Emet river; their thickness varies considerably from one place to another and the total thickness exceeds 750 m (see Figs. 6 and 7). The succession of Middle Oligocene sediments downwards is given on page 29 and shown on Fig. 7. The Emet Middle Oligocene sequence is described in detail below, starting from the base.

(a) Conglomerate and sandstone:

Beyond the mapped area (Fig. 6) basal conglomerate and

sandstone intervene between the lower limestone and the basement metamorphic complex. They outcrop at the southern part of the Emet valley towards the Gediz and Simav areas.

Conglomerate occurs, generally, as very large rock fragments of varying size which are derived from the basement rocks. The fragments are cemented together with calcite. The colour is mostly medium to dark red, due to high oxidation.

Succession, towards the top of conglomerate, goes to sandstone. This occurs in a coarse and fine grained state, containing mainly quartz grains and mica. Amounts of mica increase towards the top of succession. The colour is mostly green to grey. Much of the constituents of sandstone are derived from the basement. The thickness of conglomerate and sandstone varies considerably and the lack of measurable sections makes reasonable estimation of their thickness difficult.

(b) Lower limestone

Lower limestone occurs as thin bedded layers with lenses of marl and tuff. The colour is mostly white and white-grey. Usually it outcrops on the west bank of the Emet valley, but in the north part of the field it rests directly and unconformably on the basement complex, with an angular unconformity. Near Hamamköy - Dereköy and Kutlubeyler this unit contains lignite seams 0.8-1.2 meters thick. The thickness of lower limestone increases to 150 meters in the field (see Figs. 6 and 7).

(c) Red formation

The red formation is composed of conglomerate, sandstone, clay and limestone, and these beds occasionally enclose lignite and gypsum bands. Generally this formation shows green, grey and often red colours. It outcrops on both sides of the Emet river,

along a N-S direction, with varying thickness from one place to another up to 125 meters (Plate 4, see also Figs. 6 and 7). Grain size varies considerably and they are very loosely cemented. In some places, the red formation interfingers with clay, sandstone and conglomerate along the abrupt northern edge of the local basin of deposition. It encloses lenses of tuff.

(d) Borate zone

This unit, about 0-100 meters thick, contains the borate deposits interbedded with clay, tuff, marl and soft thinbedded limestone. It shows clearly lateral and vertical facies changes, which will be discussed in detail separately. Borates and interbedded sedimentary formations strike and outcrop roughly parallel to the Emet river conformably overlying the top of the red formation. Colemanite occurs as nodules and stringers in clay with minor associated other borate and non-borate minerals. (Fig. 8; see also Figs. 6 and 7).

Around the outer part of the local basins of deposition, the borate zone consists entirely of the barren facies; the colemanite-bearing clay and tuff grades outwardly into green or green-grey coloured altered tuff and clay which are mainly montmorillonitic and illitic clay groups. Along the abrupt northern and southern termination of the basin, the barren facies dies out. The distribution of the borate zone indicates that this formation was deposited in deeper parts of the basin.

(e) Upper limestone

Upper limestone, containing clay, marl and chert layers, forms a prominent marked bed on top of the borate zone. It is generally white, or a white-grey colour and varies considerably in its bedding thickness of up to 400 meters. Towards the edges

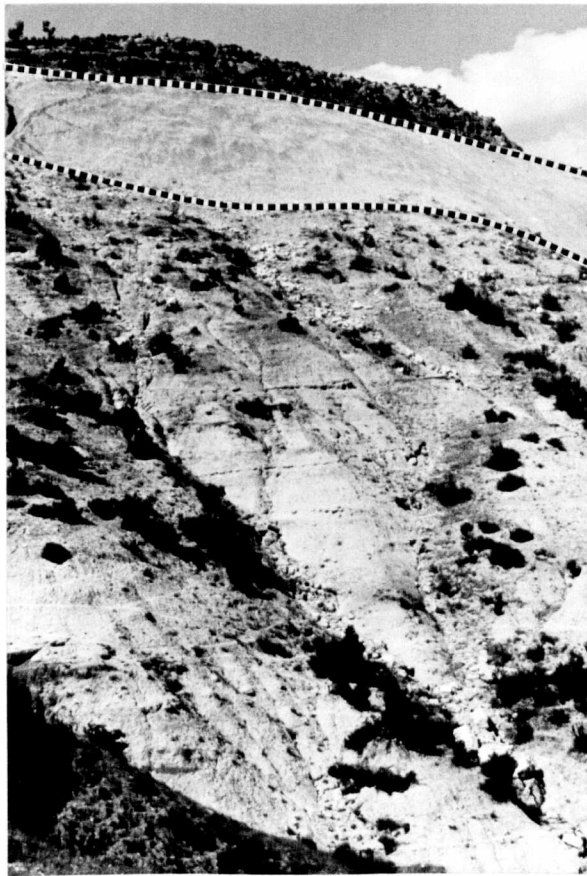


Plate 4 The succession of the Emet lacustrine sediments, red formation, borate zone and upper limestone upwards.

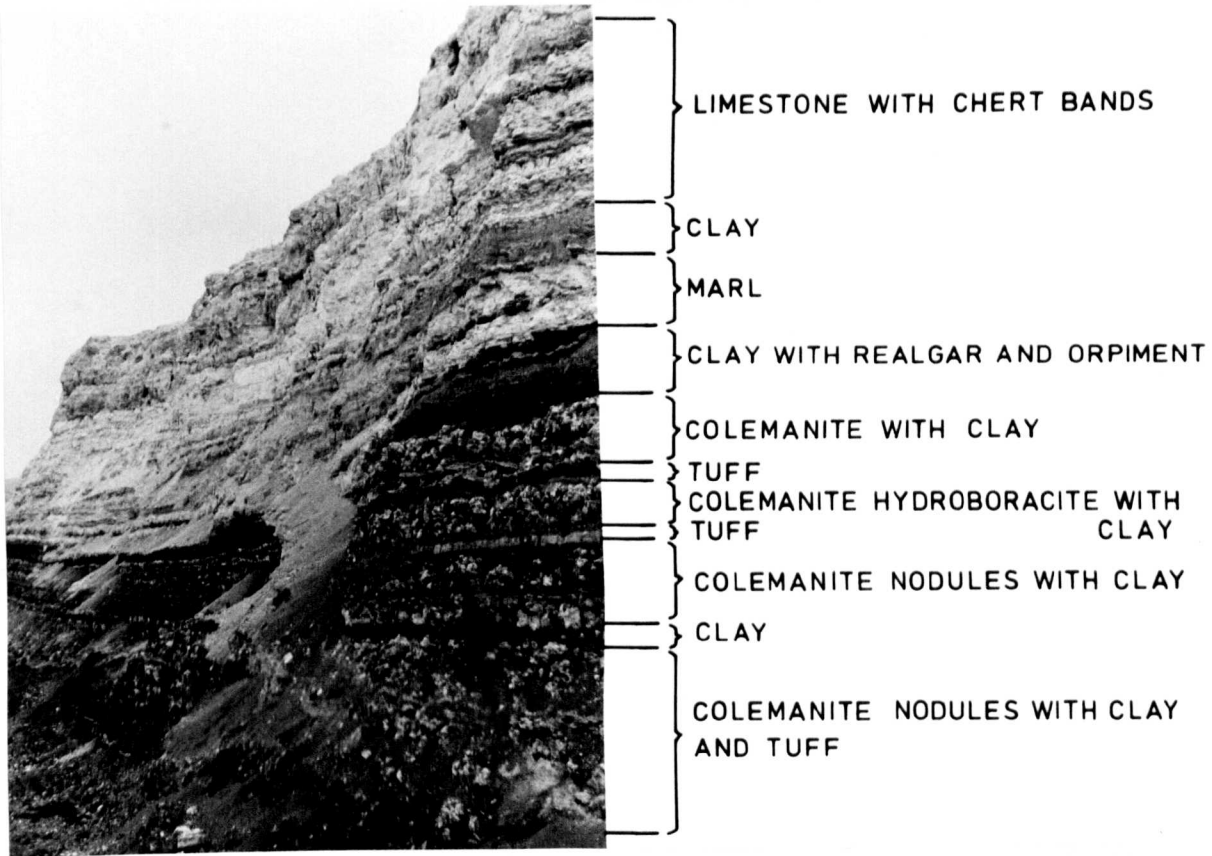


Fig. 8 Section from Sarikaya (Hisarcik) showing the borate zone (colemanite, hydroboracite and other minerals) interbedded with clay, tuff and marl and the upper limestone overburden.

of the Emet valley, it rests on the red formation or conglomerate. It is, usually, a very hard resistant limestone, which forms the cap-rock for the borate zone (Figs. 6, 7 and 8).

Occasionally illitic clay, marl and chert layers, up to 1 meter thickness, occur inbetween the upper limestone. The colour of the illitic clay is generally greenish-grey whereas the cherts show blue, dark blue and greyish colours.

Quaternary conglomerate, terrace materials and alluvium were deposited on top of the Middle Oligocene sediments along the Emet river. They show a difference in thickness from one place to another. The conglomerate at Hisarcik village is very loosely cemented.

4. Petrography and geochemistry of volcanic rocks.

(a) Classification of volcanic rocks:

Volcanic activity in the Emet area commenced in the early Tertiary period and continued at least to the beginning of the Quaternary. The earliest recorded lava flows are of rhyolitic, dacitic and trachytic types. The next lava flows are trachy-andesitic-andesitic and finally more recent flows, younger than the formation containing borate minerals, are olivine-rich andesitic basalts.

The volcanic activity occurred mainly in the north-west and south-west parts of the area. The earliest volcanic rocks are located in the north, whereas the more recent volcanic rocks are in the south. Much of the sediment in the borate basins seems to have been derived from volcanic terrain.

Classification of volcanic rocks based on mineral compositions (e.g. Streckeisen, 1967) are difficult to apply

to these rocks, because of the intense alteration. Therefore the classification suggested by Taylor (1969) has been used in this study. The classification of volcanic rocks is summarised on the basis of silica, alumina and potash percentage as follows: -

1. High-Al basalt: $<53\% \text{SiO}_2$
2. Low-Silica andesite: $53-56\% \text{SiO}_2$; $0.7-2.5\% \text{K}_2\text{O}$
3. Low-K andesite: $<0.7\% \text{K}_2\text{O}$; $53-62\% \text{SiO}_2$
4. Andesite: $56-62\% \text{SiO}_2$; $0.7-2.5\% \text{K}_2\text{O}$
5. High-K andesite: $>2.5\% \text{K}_2\text{O}$; $53-62\% \text{SiO}_2$
6. Dacite: $62-68\% \text{SiO}_2$
7. Rhyolite: $>68\% \text{SiO}_2$

The chemical analyses of the volcanic rocks from the Emet district fall into high-Al basalt, high-K andesite, dacite and rhyolite volcanic rock groups. Volcanic rocks, which are closely related to the Middle Oligocene lacustrine sediments, are mainly spherulitic rhyolite, dacite, pyroxene andesite and olivine-augite basalt. Volcanic tuff interbedded with the lacustrine sediments occurs in the borate basin.

(b) Petrography of volcanic rocks

Spherulitic rhyolite:

This outcrops in the northern part of the mapped area near the village of Köprücek to form the Köprücek Hill. The hand specimen shows that it is usually white, grey and light brown to dark brown in colour. Phenocrysts of quartz, feldspar and biotite are quite visible by the unaided eye, but the crystals in the groundmass are too small to be seen.

Microscope analysis of the thin section shows phenocrysts of quartz, andesine, sanidine and reddish-brown biotite in a microfelsitic and spherulitic groundmass containing amygdules of opal and radiating chalcedony. The feldspar phenocrysts in the spherulitic rhyolite display, when fresh, oscillatory zoning, simple and albite twinning, but they have mainly suffered corrosion and alteration. The quartz is mainly corroded and has cracks in it. Biotite shows a reddish-brown colour and alters to iron minerals. The groundmass contains opal, radiating chalcedony, quartz, alkali-feldspar, hematite and accessory minerals which are mainly apatite and zircon (Plate 5). The groundmass is highly variable in texture, becoming more glassy with increasing acidity.

Northwards the rhyolite passes into a rhyolitic crystal tuff in character.

Dacite:

Dacite occurs as an intrusive rock in the north of part of the district, on the east bank of the Emet river. Its outcrop extends in a SW-NE direction north of the Topraklik Hill and cuts the basement metamorphic complex. In the hand specimen, its colour is, generally, grey, when fresh, or greyish yellow and sometimes pink, when altered. Phenocrysts of quartz, feldspar and biotite are quite big enough to be noticed by the unaided eye, but the groundmass has invisible small crystals.

In the thin section, this rock type carries phenocrysts of plagioclase, orthoclase, quartz, and generally fewer of biotite and hornblende. The groundmass is usually glassy or felsitic and is composed chiefly of quartz and orthoclase. It sometimes displays a flow structure.

The plagioclase feldspar is andesine and is the most abundant phenocryst phase. Andesine shows very good zoning, simple and albite twinning, when fresh, but it has often suffered corrosion and alteration in the middle or edge of the crystals. Its' alteration product is mainly chlorite. Orthoclase is often altered, mainly to sericite, kaolin or chlorite and phenocrysts of orthoclase are seldom.

Phenocrysts of quartz are present and they are mainly corroded. Quartz occurs in the groundmass as small crystals.

Mafic minerals are almost porphyritic. Biotite and hornblende are the only mafic constituents. The biotite phenocrysts show very good cleavages and they are resorbed by andesine. Hornblende occurs mainly as altered crystals and, sometimes, smaller specks are visible inside the hornblende. It is usually resorbed by andesine.

The groundmass is composed chiefly of quartz and orthoclase and sometimes shows flow structures or is very glassy and stippled with crystallites (Plate 6).

Pyroxene andesite:

This rock unit outcrops in the southern part of the Emet district, around Dereköy Village. The younger lava flows of this unit pass into an olivine-augite basalt, towards the west of the area. The rocks in this group are mineralogically transitional between andesite and basalt.

In the hand specimen, its' colour is, usually, dark grey, but sometimes it shows a greyish yellow colour due to an alteration. Grain sized phenocrysts of feldspar and biotite could be identified by the unaided eye. Hematite and pyrite minerals are very common. Calcite is often found as amygdale-fillings (Plate 7).



Plate 5. Plate showing spherulitic rhyolite containing phenocrysts of quartz, feldspar, biotite and a microfelsitic and spherulitic groundmass. Plane polarized light, x10.

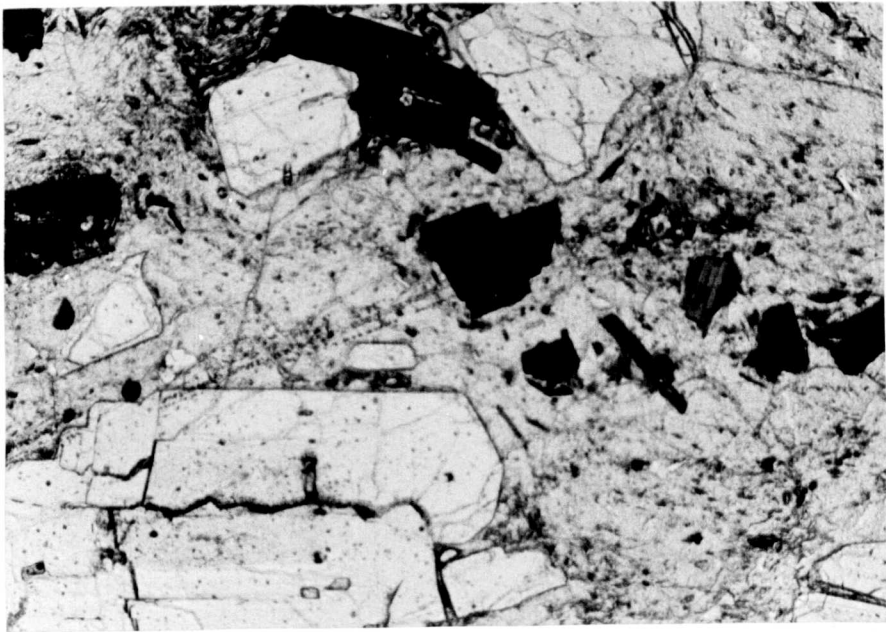


Plate 6. Dacite showing phenocrysts of plagioclase, quartz, biotite and felsitic groundmass. Plane polarized light, x10.



Plate 7. Hand specimen of pyroxene andesite showing calcite as amygdule-fillings, phenocrysts of feldspar and biotite, pyrite. Due to alteration it shows a greyish yellow and blue colouring.

In the thin section, this rock unit has phenocrysts of pyroxene, plagioclase, biotite, muscovite and olivine. The groundmass contains vesicules set in a matrix of black or brownish glass, generally of porphyritic texture.

The plagioclase feldspar is albite and it occurs as small needle shaped crystals or as a lath in the groundmass generally showing albite twinning.

Biotite and muscovite occur as flaky crystals showing perfect cleavages.

A clino-pyroxene, augite, is the most common of the pyroxene phenocryst phases. Phenocrysts of augite show prismatic and eight-sided transverse sections with perfect cleavages, when fresh, but they are mainly altered. Occasionally this pyroxene shows reverse zoning.

Euhedral crystals of olivine are altered to serpentine and show cracks. The alteration of the outer iron-rich rims of olivine to brownish-red iddingsite is fairly common. The alteration is marked by a network of iron-oxide. Iron ore is, mainly, represented by hematite, magnetite and pyrite.

Secondary calcite, usually, fills the cavities, veins and amygdules of the rocks.

The groundmass shows generally a vesicular texture and is made up of black or brownish glass. Accessory minerals include magnetite, pyrite, hematite, apatite and occasionally zircon (Plate 8).

Olivine-augite basalt or andesitic basalt shows a more porphyritic texture and flow structure. The amounts of iron ores (e.g. pyrite, hematite, magnetite), biotite and vesicle-filling calcite are increased. The groundmass becomes more black or brown glass (Plate 9).



Plate 8. Plate showing pyroxene andesite containing phenocrysts of pyroxene, plagioclase, biotite, and porphyritic groundmass. Plane polarized light, x10.



Plate 9. Olivine-augite basalt or andesitic basalt showing phenocrysts of olivine, augite, biotite and porphyritic groundmass. Plane polarized light, x10.

(c) Geochemistry of volcanic rocks:

In the present study, a total number of 10 volcanic rock samples were collected from the Emet district. Samples were analysed for up to 28 elements, mostly by the use of X.R.F. spectrometer. B_2O_3 , CO_2 and H_2O were analysed by wet-chemical methods. Following the normal practice, the major element constituents are described by their oxides (weight percent) and the trace constituents by their elements (in parts per million).

In order to demonstrate chemical relationships and variation in the volcanic rocks, the Harker variation diagram, in which total alkali are plotted against weight percent SiO_2 (Fig. 9), and the KCN diagram (Fig. 10) have been used.

The Harker variation and KCN diagrams for the volcanic rocks do not show a distinct trend, because of the limited number of samples and intense alteration of the volcanic rocks; but the KCN diagram indicates that these volcanic rocks associated with the Emet borate deposits are very rich in potash in comparison to Cascade volcanic province (Fig. 10).

Figs. 9 and 10 indicate that these volcanic rocks associated with the Emet borate deposits are very rich in potash and soda. At this stage, it is difficult to say whether, generally, borate deposits are associated with alkaline-rich volcanic rocks or not, because of the general lack of chemical analysis of volcanic rocks from different borate deposits.

The main purpose of the chemical analysis of the volcanic rocks was to establish the level of boron in various samples. The results showed that boron was only a minor element in some of the basalt and dacite samples, but it was a trace amount in the rest.

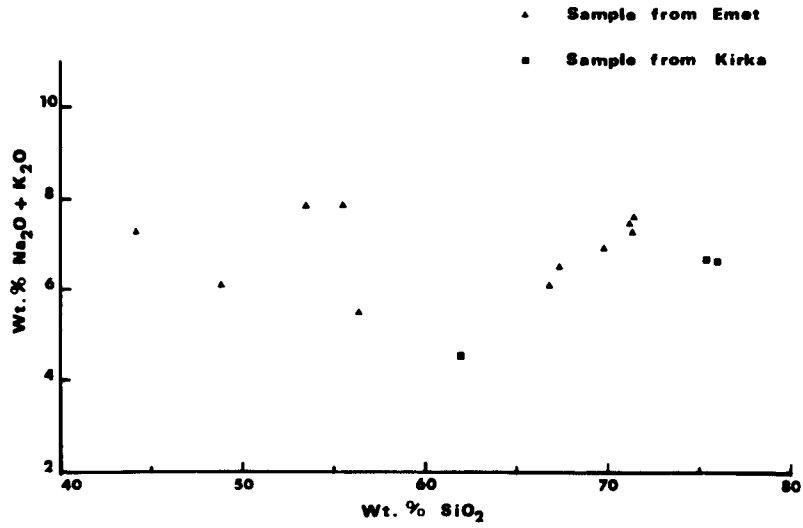


Fig. 9. Harker partial variation diagram for total alkali Wt% against SiO₂ Wt% data of the Emet volcanic rocks.

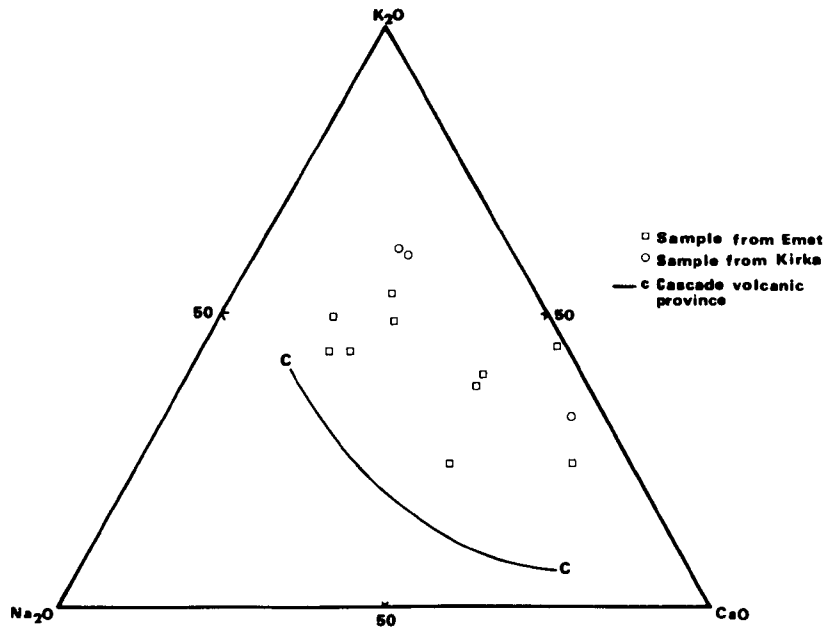


Fig. 10. The KCN diagram for the Emet volcanic rocks.

Table 5 summarises the chemical composition of the volcanic rocks for the Emet district. Sample number 181 (tuff), which comes from the Middle Oligocene lacustrine sediments, is used for comparison with the other volcanic rock types.

5. Structure:

The Middle Oligocene sediments of the Emet region were deposited on the Eocene and Lower Oligocene paleotopography, infilling the valleys of those periods. This can be observed in the east and west of the Emet district where the basement metamorphic complex still forms the high hills.

The thickness of the Tertiary sediments varies from one place to another, probably because of deposition in a chain of inter-connected lakes. The total Tertiary sedimentary thickness exceeds 750m (see Fig. 7). The Emet lake beds are preserved in an elongated structural basin which trends roughly north-south. The depositional basin of the borate deposits is aligned north-south and outcrops on the east side of the Emet river (Koca Çay) from Dereköy north almost to Killik (see Fig. 6). The lake beds appear to be eroded on the west side of the Emet river by a NW-SE trending major fault (Fig. 11).

The Middle Oligocene sedimentary formations strike roughly parallel to the Emet river, their dip ranging from nearly horizontal to over 20° , and they are dislocated by NW-SE trending gravity faults, many of which are still active. NE-SW trending gravity faults occurred after the deposition of borates, but they are not active at present. The predominant faults are normal with dips ranging from 30° to vertical. These structures are strikingly reflected in the stepped topography (Plate 10; see also Fig. 11).

Table 5 The chemical composition of the Emet volcanic rocks.

<u>Number</u>	<u>181</u>	<u>182</u>	<u>183</u>	<u>184</u>	<u>185</u>
SiO ₂	43.93	55.25	53.26	48.66	67.14
Al ₂ O ₃	12.21	15.32	13.13	13.91	13.58
TiO ₂	0.63	1.88	1.79	1.66	0.38
Fe ₂ O ₃	3.08	6.01	6.11	4.76	1.81
FeO	0.60	0.80	0.59	0.72	0.44
MgO	6.06	4.93	5.57	3.94	0.70
CaO	8.54	6.47	6.42	12.13	2.10
Na ₂ O	0.24	2.46	2.16	1.84	1.92
K ₂ O	7.09	5.41	5.68	4.29	4.61
MnO	0.13	0.12	0.12	0.16	0.06
P ₂ O ₅	0.18	0.61	0.60	0.55	0.13
H ₂ O+	6.53	2.88	2.29	3.32	4.63
CO ₂	3.86	0.00	0.00	1.61	0.00
B ₂ O ₃	0.72	0.00	0.00	0.24	0.32
SO ₃	0.88	0.08	0.07	0.07	0.06
Total	94.68	102.22	97.79	97.86	97.88
Cl	359	135	252	136	1001
Cr	52	256	275	263	8
Ni	84	166	186	138	29
Cu	15	31	35	31	1*
Zn	129	79	76	65	86
As	1367	55	41	15*	78
Br	0*	1*	1*	0*	4*
Sr	1077	598	643	609	258
Ba	544	1135	1091	1056	1293
Ce	494	145	138	135	84
Pb	46	15	12	17	59
Th	35	18	11	14	25
U	7	6	7	11	8

*Indicates values below the detection limit

181 - Tuff
 182,183 - Andesite
 184 - Basalt
 185 - Dacite

Table 5 (continued)

<u>Number</u>	<u>186</u>	<u>187</u>	<u>188</u>	<u>189</u>	<u>190</u>
SiO ₂	66.70	56.13	69.67	71.28	71.04
Al ₂ O ₃	14.59	17.46	14.61	14.04	14.16
TiO ₂	0.40	1.29	0.33	0.35	0.32
Fe ₂ O ₃	1.90	8.09	2.34	2.43	2.22
FeO	0.49	0.20	0.08	0.12	0.08
MgO	0.74	0.54	0.53	0.40	0.30
CaO	2.26	5.02	2.08	1.98	1.59
Na ₂ O	2.04	2.96	3.06	3.44	3.01
K ₂ O	4.07	2.55	3.89	4.18	4.49
MnO	0.07	0.03	0.04	0.09	0.07
P ₂ O ₅	0.19	0.31	0.16	0.17	0.13
H ₂ O+	4.68	3.79	1.96	0.86	1.64
CO ₂	0.00	0.00	0.00	0.00	0.00
B ₂ O ₃	0.00	0.00	0.00	0.00	0.00
SO ₃	0.08	0.08	0.06	0.02	0.02
Total	98.21	98.45	98.81	99.36	99.07
Cl	1058	74	715	259	148
Cr	7	15	9	6	5
Ni	12	19	7	10	8
Cu	9	10	8	5	7
Zn	71	77	53	46	45
As	93	835	51	33	30
Br	6*	0*	4*	1*	1*
Sr	251	535	263	240	217
Ba	1318	1473	1464	1481	1386
Ce	84	273	75	72	65
Pb	51	33	55	49	50
Th	25	16	32	31	27
U	12	4	6	8	9

*Indicates values below the detection limit

186 - Dacite

187 - Andesitic tuff

188,189,190-Rhyolite

Table 5 (continued)

<u>Number</u>	<u>191</u>
SiO ₂	71.19
Al ₂ O ₃	13.66
TiO ₂	0.31
Fe ₂ O ₃	2.16
FeO	0.22
MgO	0.34
CaO	1.85
Na ₂ O	3.31
K ₂ O	4.01
MnO	0.04
P ₂ O ₅	0.14
H ₂ O ⁺	0.82
CO ₂	0.00
B ₂ O ₃	0.00
SO ₃	0.06
Total	98.11
Cl	303
Cr	6
Ni	7
Cu	4
Zn	33
As	70
Br	2*
Sr	234
Ba	1411
Ce	77
Pb	47
Th	29
U	5

* Indicates values below the detection limit

191 - Rhyolite

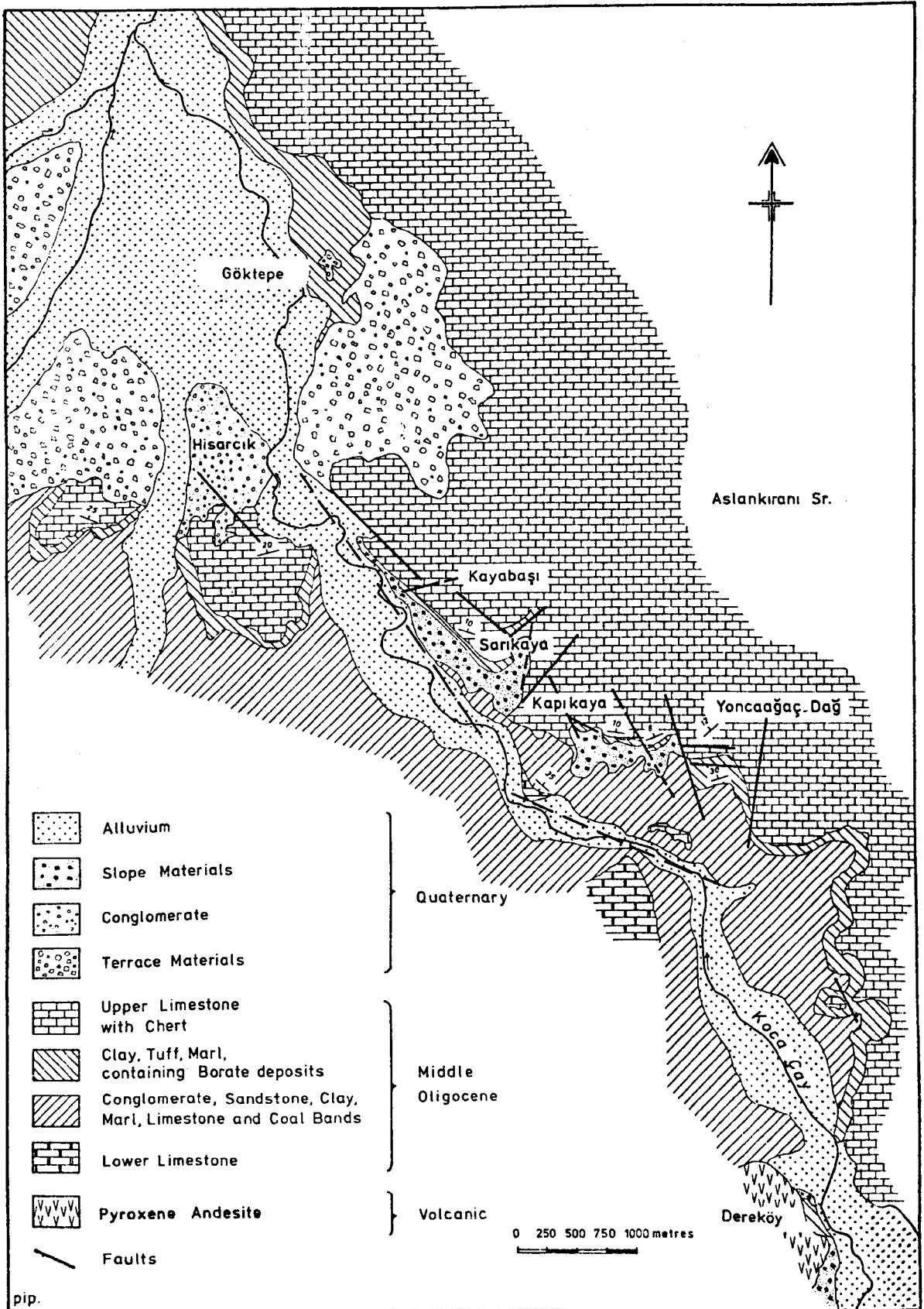


Fig.11. Detailed geological map of Hisarcik area.

6. Thermal springs:

Thermal springs are widespread throughout the area. They are located on both sides of the Emet river, mainly around the town of Emet, Yenice, Aşağıyoncaagaç and Hamamköy villages. They discharge from the lower limestone and red formation (see Fig. 6).

Thermal springs at present deposit travertine and sulphur (Plate 11), and new springs were generated by movement of NW-SE trending faults during the Gediz earthquake in 1970.

Water samples collected from six of the thermal springs were analysed for B, Ca, Mg, Na, Sr and As elements. Boron was determined by the volumetric method, calcium, magnesium, sodium and strontium by atomic absorption and arsenic by the colormetric method. Results of the chemical analysis for these elements may be too low because of precipitation on cooling after the water samples were collected. Water samples were not analysed for S and Fe because of the difficulties associated with the rapid precipitation of these elements.

Springs at Emet (S_1 , S_4 , S_5) are very rich in sulphur and they precipitate CaCO_3 . Springs near Hamamköy village (S_2 , S_3) contain high amounts of sulphur and iron and precipitate travertine. Springs around Yenice village (S_6) likewise carry high concentrations of calcium and iron and precipitate travertine. These springs, in the vicinity of Yenice, emerge from the lower limestone; they contain the highest concentration of boron recorded. There are no known borate deposits in the catchment area so although leaching of undiscovered borates is theoretically possible, a volcanic source of boron seems much more likely. Similarly springs west of the river Emet seem unlikely to receive



Plate 10. Plate showing stepped topography in the Hisarcik borate deposit.



Plate 11. Ca, S and Fe rich thermal springs precipitating travertine near Yenice village on the west side of the Emet river.

boron by the leaching of borate deposits east of the river and again a volcanic source of boron seems more likely.

It should be noted that compared with thermal springs in volcanic regions in Japan the springs in the Emet valley are relatively impoverished as suggested by the elements analysed, possibly because of waning volcanic activity in the Emet region.

The chemical analysis of the thermal springs for six elements is given on Table 6. A range of water sample analysis from Japan (Kitano, 1963) is added to table 6 for comparison purposes.

7. Geological history:

The evidence suggests that no later than the early Oligocene, playa lakes, the area of the future borate basin, were established in seismically active areas as a single or very likely as a chain of inter-connected lakes. This area was already topographically low due to downward movement. The deepest part of the basin was close to its northern border. To the east and west the rise out of the basin was more sharp, whereas to the south it was more gradual. In the structural setting described above, these playa lakes started to be fed by thermal springs and surface streams.

In these lakes, first the thin bedded lower limestone, which was distributed very evenly, was deposited. Towards the top, the lower limestone accumulated with clay and volcanic ash, which was derived from the adjacent volcanic activity. This indicates that volcanic activity started during the upper part of the lower limestone formation.

After the deposition of the lower limestone, the size of the basin increased and the red formation, which is mainly clastic

Table 6. Chemical analysis of thermal spring waters from the Emet district.

Spring	Locality	pH	Electrical Conductivity (μ S)	Temperature (°C)	milligrammes per litre (mg/l)					
					B ³⁺	Ca ²⁺	Mg ²⁺	Na ⁺	Sr ²⁺	As ⁵⁺
S ₁	Emet	7.2	6.2 x 100, at 30.5°C	47.53	4.39	34	25	35	n.d.	0.108
S ₂	Hamamköy	7.0	14 x 100, at 28°C	45.32	4.81	196	47.5	64	1.44	0.064
S ₃	Hamamköy	7.0	10.2 x 100, at 30.5°C	51.29	6.37	103.6	40	35	0.76	0.048
S ₄	Emet	7.2	6.6 x 100, at 30.5°C	43	5.43	35	25.3	47	0.06	0.093
S ₅	Emet	7.2	9.9 x 100, at 27°C	41	4.52	82.4	23.2	60	0.12	0.038
S ₆	Yenice	6.9	34 x 100, at 27°C	46	25.95	196	61.4	300	3.71	0.5
S ₇ [*]	Futamata (Japan)	6.5-6.6	-	35-50	39.52- 148.2	540- 830	110- 160	1500- 2500	7-12	-

n.d. : Not detected
 * : Data taken from Kitano (1963) for comparison purposes.
 - : Data not available

sediments, was formed very rapidly. The rate of the sedimentation in this period was very high, which also indicates the rate of erosion from the adjacent source rocks. The occurrence of lignite in the red formation indicates that the deposition basin became a shallow lake or swamp from time to time. Volcanic activity occurred occasionally in this period.

At the end of the red formation, clay and volcanic ash were deposited in these lakes, and borates, mainly Ca borate nodules, were developed within the unconsolidated sediments during periods of evaporation, together with small amounts of sulphur and realgar. The genesis of these minerals is discussed in detail later on. The rate of the sedimentation in this period was very slow. Successive beds of borates protected by layers of clay, tuff and marl were progressively built up as the basin sank.

After the completion of the borate zone, as the sediments accumulated in the borate lakes, the deposition basin sank and its size and depth increased while the upper limestone was forming. The upper limestone, containing occasionally chert, marl and clay layers was deposited and then the sedimentation was completed. Either local thermal springs or underground water circulating the sediments was the most likely source of silica which caused the chert formation in the upper limestone.

CHAPTER IV

PETROGRAPHY AND GEOCHEMISTRY OF THE SEDIMENTS

1. Petrography of the sediments

The general appearance and stratigraphy of the sediments in the Emet borate deposits has already been described in the previous chapter. The succession of sediments is shown on page 29 and Fig. 7. The petrography of the sediments is briefly described below.

Microscope analyses of sandstone samples from conglomerate and sandstone formations show grains of quartz, plagioclase, orthoclase, biotite and muscovite. This sandstone, which is fairly pure, and moderately sorted, is a micaceous arkose or arkosic arenite. In the thin sections, it consists of fairly well-sorted angular-to-subangular grains of feldspar (plagioclase and orthoclase) (300-400 μ) and quartz (300-500 μ); abundant parallel oriented flakes of muscovite and chloritized biotite (up to 400 μ). Long and thin flakes of muscovite and biotite usually lie parallel to the bedding. The rock is weakly cemented by scattered grains of calcite and secondary quartz outgrowths. A few schist particles are distributed randomly. The rock is generally free from clay and its porosity is high (Plate 12).

Samples collected from the lower limestone consist of calcite, detrital quartz and often clay minerals. It is an impure limestone. Calcite appears as a fine-grained to microcrystalline calcite mosaic. Laminae are usually distinguished by abrupt variations in grain size of calcite. Subrounded detrital quartz grains up to 20μ are set in fine grained calcite. Clay minerals occur along the bedding plane and have a cloudy appearance (Plate 13). According to the staining tests, there is no dolomite in the lower limestone. No macro or micro-fossils have been found and the limestone appears to be a chemical precipitate.

The red formation consists of conglomerate, sandstone, clay, marl, limestone with coal and gypsum bands but sandstone and clay are more abundant.

Conglomerate in the red formation is mainly made up of quartz pebbles (1-8cm); gneiss, schists and granodiorite rock fragments. The rock is loosely cemented by clay minerals which contain a fair amount of silt and sand grains. The size of grains in the conglomerate varies considerably; sometimes the grain size decreases to 3mm (Plate 14). This fine-grained conglomerate contains considerable amounts of plagioclase, biotite and muscovite minerals as well as metamorphic rock fragments. Calcite grains are scattered in the cement.

Sandstones in the red formation are usually impure and appear as a lithic graywacke. This rock shows grains of quartz, plagioclase, orthoclase, biotite and muscovite. Biotite grains are up to 200μ , and altered, usually to chlorite or iron oxides and hydroxides. When they are fresh, biotite shows perfect cleavages. Muscovite has a flaky character. Quartz grains are up to 200μ , angular or sub-rounded. They are either very clear

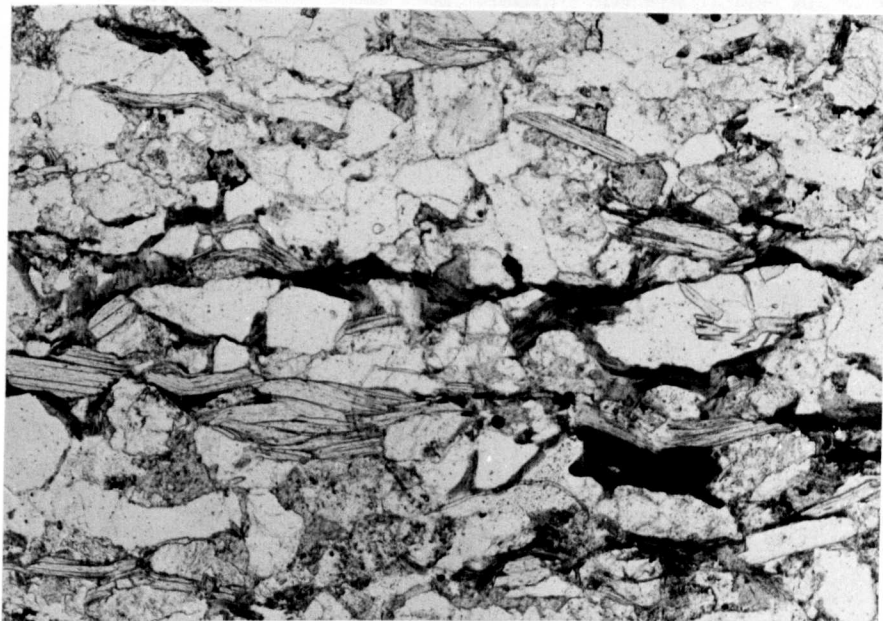


Plate 12. Sandstone showing grains of quartz, feldspar, biotite and muscovite and calcitic cement. Flakes of muscovite and biotite lie parallel to the bedding. Plane polarized light, x10.

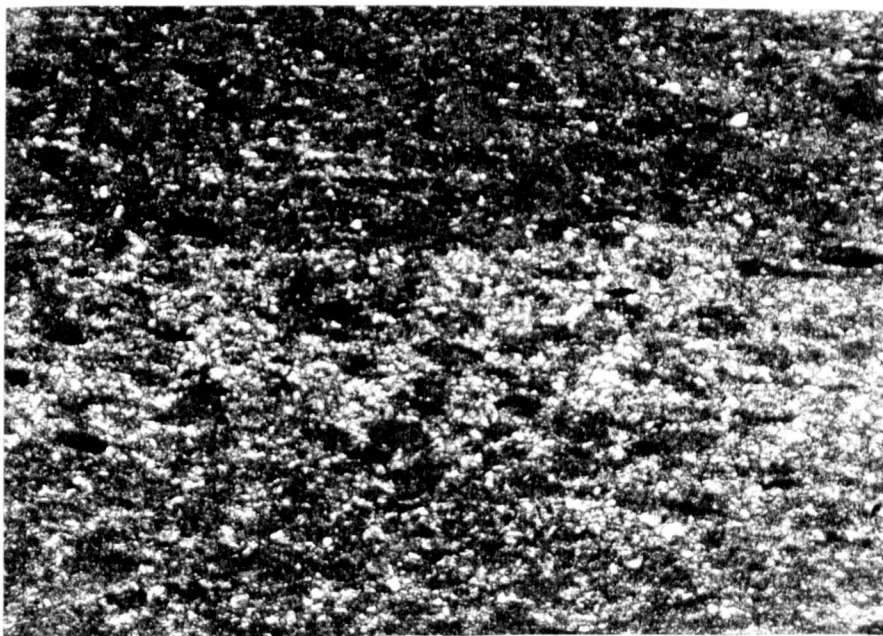


Plate 13. Lower limestone containing a fine-grained to microcrystalline calcite and clay minerals which show a cloudy appearance. Plane polarized light, x10.

or lightly stippled. Feldspar grains are sub-rounded and usually altered. An unsorted aggregate of angular or sub-angular grains is set in an abundant argillaceous matrix. Unsorted grains are cemented by microgranular calcite and clay minerals. No preferred orientation of grains is visible (Plate 15).

Some clay, limestone and marl layers are interbedded in the red formation. The clay minerals are too fine-grained to be identified under the microscope; but X-ray diffractometer analyses show that montmorillite and illite are the only clay mineral groups identified. Limestones in the red formation are soft, thin-bedded and consist of fine-grained calcite crystals.

The borate zone sediments consist of clay, tuff and marl containing borate minerals, as mentioned in the previous chapter. The clay minerals in the claystone are too fine-grained to be identified by microscope analysis. Direct-recording X-ray diffractometer analyses using standard powder and oriented-sample techniques show that montmorillonite and illite are the clay mineral groups. The former is the dominant mineral and is probably derived from volcanic tuff and ash. Quartz, biotite and muscovite grains occur occasionally. Biotite and muscovite flakes appear as thin flattened crystals. Fine-grained calcite crystals, iron oxides and organic matter are observed in the clay. In the marl specimens, fine-grained clay minerals and fine-grained-to-microcrystalline calcite have been observed. Sometimes calcite is very coarsely crystalline and it is parallel to the bedding.

Volcanic tuff shows a clear clastic texture and consists of quartz, orthoclase, biotite and muscovite grains. The matrix is usually altered to clay minerals and volcanic ash containing very



Plate 14. Conglomerate containing grains of quartz, plagioclase, mica and metamorphic rock fragments, with calcite cement. Plane polarized light, x10.

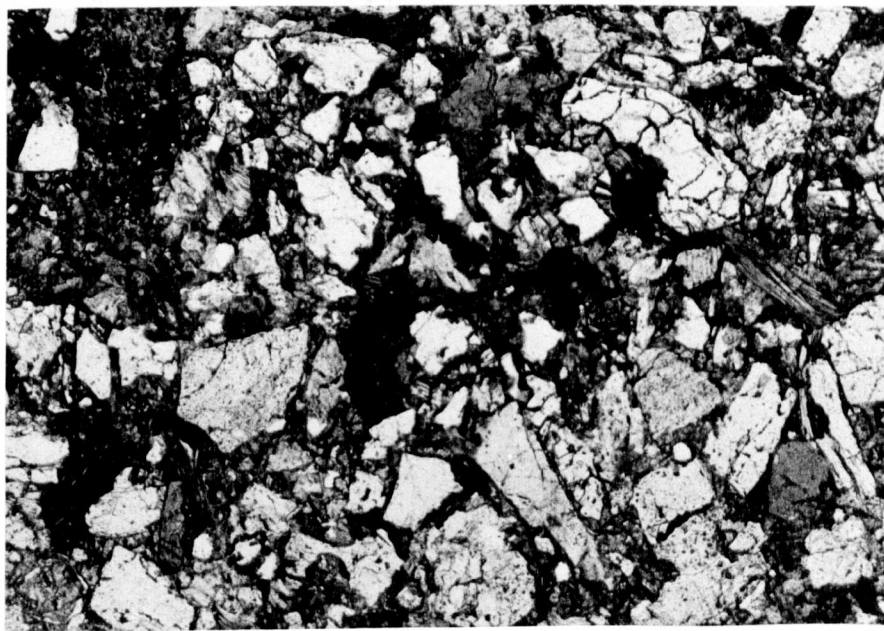


Plate 15. Graywacke showing unsorted grains of quartz, feldspar and mica, which are cemented by microgranular calcite and clay minerals. Plane polarized light, x10.

fine crystals, when the tuff is fresh. Quartz grains are rounded or subrounded, varying in size up to 400 μ . The orthoclase feldspar varies in grain size, but it is mainly very small and shows alteration. Subrounded small biotite crystals and needle-shaped muscovite crystals occur very seldom; their flakes lie parallel to the bedding plane. Biotite crystals show alteration and are orientated parallel with the bedding planes. The matrix is mainly volcanic ash which often shows alteration to clay minerals. The volcanic tuff has a grading structure, because of the abrupt variation in grain size. (Plate 16).

The upper limestone is extremely variable in texture. It shows an impure, organic and oolitic limestone character, and it consists of mainly a fine-grained-to-microcrystalline calcite mosaic, quartz and mica grains, and also chert and clay. Coarse crystalline calcite is recrystallized in the cracks and cavities of limestone. The staining test gives no evidence of dolomite in the limestone. There are some orpiment spots spread throughout the limestone. This rock has a very high porosity with solution cavities.

Sandy limestone shows a fine-grained-to-microcrystalline calcite mosaic, and grains of quartz and mica (mainly muscovite). The sub-rounded detrital quartz and mica grains are set in calcite and they are clearly separated by calcite. There are occasionally carbonaceous remains. Laminae are characterised by abrupt variations in the grain size of calcite (Plate 17).

The upper limestone is fossiliferous containing mainly ostracods and gastropod shells. Ostracods are abundant with varying size in diameter up to 1mm. The matrix is microcrystalline calcite containing patches of clear coarser calcite. Larger shells

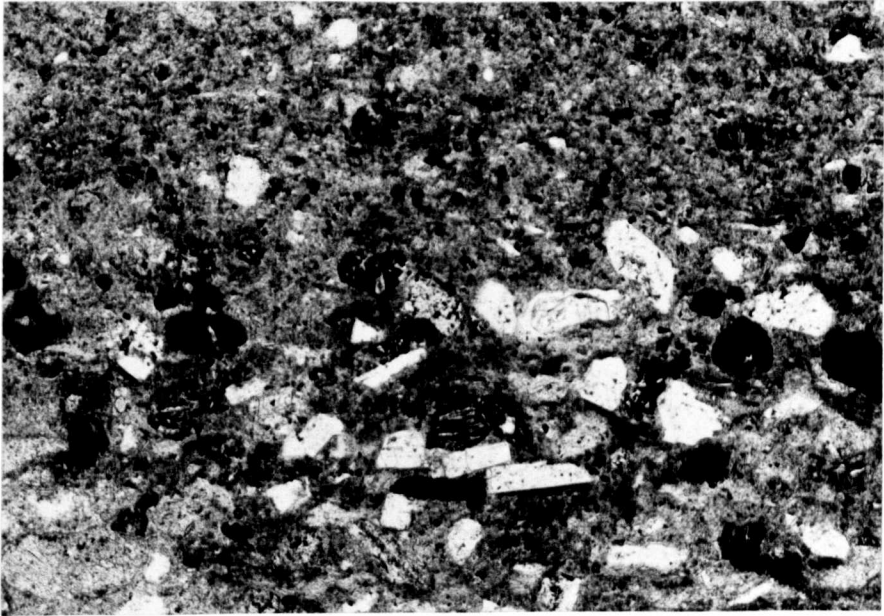


Plate 16. Volcanic tuff containing quartz, orthoclase, biotite and muscovite, volcanic ash and a matrix, which is usually altered to montmorillonitic clay. Plane polarized light, x 10.

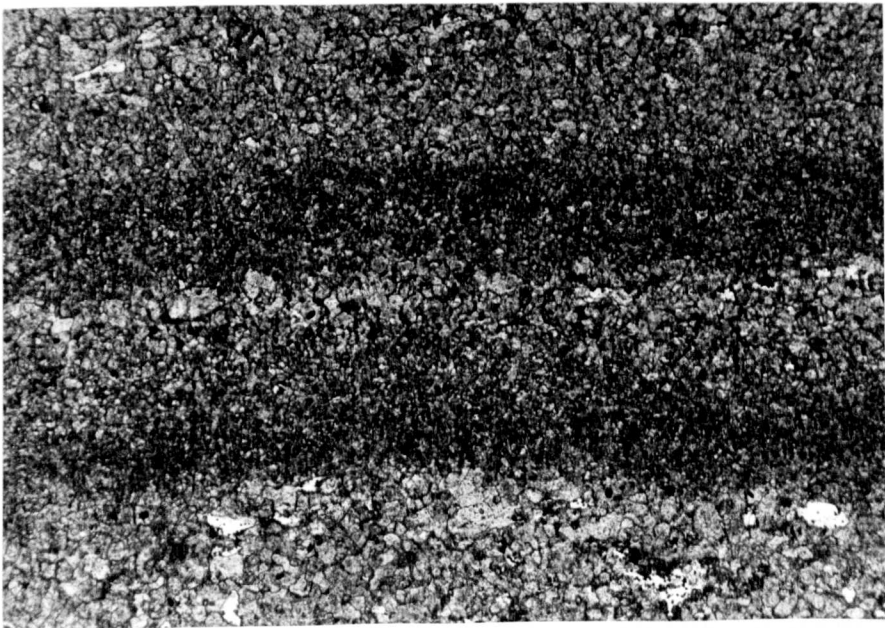


Plate 17. Plate showing sandy limestone containing a fine-grained-to-microcrystalline calcite mosaic, and occasionally grains of quartz and mica. Plane polarized light, x 10.

were only partly filled with lime mud at the time of deposition. Voids remaining within shells, and also cavities under shell fragments, were later filled with coarser clear calcite as a result of authigenic precipitation. Ostracods and gastropods fragments are enclosed in a matrix which is mainly fine-grained mosaic calcite. Larger fragments are recrystallized and filled with clear, relatively coarse calcite. Algal remains are also recrystallized to coarse calcite (Plate 18).

The upper limestone shows also an oolitic character, especially the lower part of it. This is observed mainly on the northern part of the deposits, in the Espey-Killik area. Ooliths consist of radial fibrous calcite, but with rare distinct concentric banding, firmly cemented by fine-to-coarse grained and bladed calcite crystals. Nuclei in ooliths are mostly microcrystalline calcite pellets, but a few appear to be shell fragments. The diameter of ooliths varies considerably up to 1 or 2mm. Detrital quartz and clay grains appear occasionally (Plate 19).

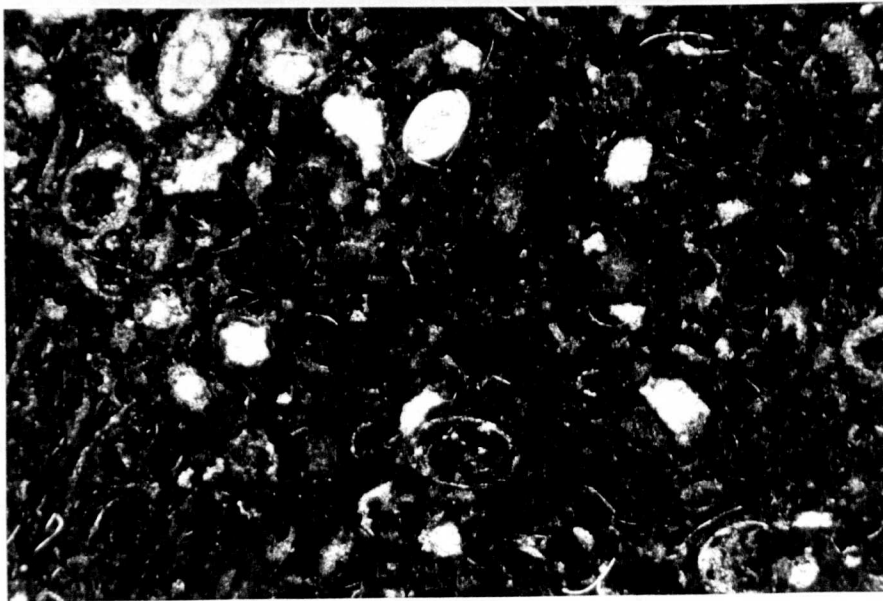


Plate 18 Fossiliferous limestone containing mainly ostracods and gastropod shells. The matrix is microcrystalline calcite. Plane polarized light, x 10.

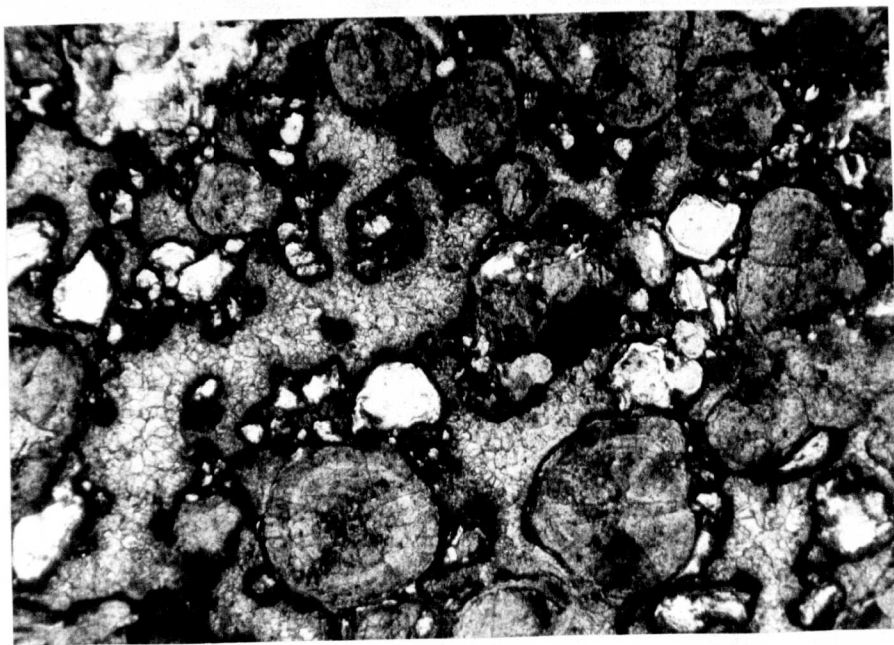


Plate 19 Plate showing oolitic limestone containing occasionally detrital quartz and clay grains. Plane polarized light, x 10.

2. Geochemistry of the sediments.

(a) Introduction:

Eighty-four clay, tuff, marl and limestone samples were collected from the top of the red formation, mainly from the borate zone, and from the upper limestone. Most of the samples were collected from several sections along the borate zone in order to find out the geochemistry of the sediments interbedded with borate minerals. Additional samples were collected from above and below the borate zone in order to find out the vertical distribution of boron. Most of the samples collected were obtained in the open pit in the Hisarcik locality and in the underground workings and drillings of the Espey and Killik mines (see Figs. 6, 8 and 11).

Samples were analysed for up to 28 elements, mostly by the use of an X.R.F. spectrometer. Following the normal practice, the major constituents are described by their oxides (weight percent) and the trace constituents by their elements (parts per million). Summary statistics of the chemical analyses for clay, tuff and limestone samples are given in Tables 7, 8 and 11. Correlation matrices of elements for clay, tuff and limestone samples are given respectively in Tables 9, 10 and 12. The chemical analyses for individual samples are given in Table 13.

The main purposes of geochemical investigation of the sediments from the Emet borate deposits are summarised as follows:

- 1) To establish the chemistry and to provide chemical analyses for the Middle Oligocene sediments associated with the Emet borate deposits.

- 2) To study the presence of elements and their correlation with each other.

3) To investigate the distribution of boron in the sediments.

4) To study the relationship between borate minerals and associated minerals.

5) To explain the problem of the origin and diagenesis of the sediments, which might help to solve the origin and diagenesis of associated borate deposits.

(b) Distributions, variations and inter-element correlations:

Element distributions, variations and correlations are discussed in the light of chemical analyses (Tables 7, 8 and 11) and the correlation matrix of clay, tuff and limestone sample populations (Tables 9, 10 and 12).

Significant positive correlations of elements with each other may result from isomorphous substitution of one element for another; association of two elements in the same mineral or associated minerals, and precipitations or accumulations of minerals of the elements under similar environments without interfering with each other. Negative or insignificant correlations indicate the absence of these conditions and suggest that the two elements may precipitate at the expense of each other, that is, one is formed from the breakdown of the other.

(c) Geochemistry of clay and tuff:

Most of the clay minerals in the Emet deposits seem to be formed by the breakdown or alteration of volcanic tuff. The transition between tuff and clay can be easily observed in the field and deduced from the chemical analyses. These two different rock types vary due to the different stages of alteration.

Samples numbered 48, 51 and 53 are fairly fresh and unaltered tuff, whereas 146, 162, 166, 171 and 174 are montmorillonitic clays, which are alteration products of volcanic tuff (Table 13).

No detailed mineralogical study of these rocks has been attempted but some idea of the mineralogical composition can be gained from the major element compositions. General geochemical behaviour of elements is taken from Wedepohl (1969).

SiO₂

The average silica content of clay and tuff is, respectively, 49.11% and 58.65% (Tables 7 & 8). In these rocks, silica occurs as a major constituent of the clay minerals; montmorillonite and illite, feldspar and biotite; and as free SiO₂ in the mineral quartz.

In the clay and tuff analyses, silica is positively correlated with Na₂O, indicating the presence of the plagioclase feldspar both in the clay and tuff (Tables 9 and 10). Positive correlation of SiO₂ and FeO in the clay suggests that Fe-montmorillonite and biotite are present (Table 9).

Al₂O₃, TiO₂ and K₂O

These three oxides are positively correlated with each other. (Table 9 and 10). The elements Al and K are the essential constituents of the clay mineral illite, and also Al but not K occurs in montmorillonitic clays.

Al₂O₃ is positively correlated with the oxides of Fe₂O₃, MnO, CaO and H₂O both in the clay and tuff analyses, indicating the presence of montmorillonite in both rock types, whereas its positive correlation with K₂O and H₂O suggest illite occurrence in the clay only. The strong correlation in the tuff of K₂O with

Table 7 Summary statistics for clay

<u>Element</u>	<u>Mean</u>	<u>St.Dev</u>	<u>Maximum</u>	<u>Minimum</u>	<u>Range</u>
SiO ₂	49.11	2.82	52.50	44.64	7.86
Al ₂ O ₃	16.03	3.43	21.03	11.35	9.68
TiO ₂	0.53	0.14	9.82	0.34	0.48
Fe ₂ O ₃	3.88	1.11	5.62	1.82	3.80
FeO	0.79	0.27	1.18	0.46	0.72
MgO	7.54	3.34	14.19	4.12	10.07
CaO	2.74	2.37	7.40	0.28	7.12
Na ₂ O	0.70	1.27	4.08	0.16	3.92
K ₂ O	4.28	1.85	6.01	0.09	5.92
MnO	0.08	0.04	0.15	0.03	0.12
P ₂ O ₅	0.19	0.13	0.47	0.00	0.47
H ₂ O	10.51	2.36	15.41	7.66	7.75
CO ₂	0.98	1.37	3.57	0.00	3.57
B ₂ O ₃	0.60	0.37	1.09	0.18	0.91
SO ₃	0.46	0.21	0.97	0.25	0.72
Cl	114	65	243	64	179
Cr	140	82	268	26	242
Ni	240	143	499	95	404
Cu	59	18	90	36	54
Zu	158	51	241	81	160
As	2791	6281	19487	237	19250
Br	0*	1	1*	0*	1
Sr	2327	1676	5702	413	5289
Ba	623	334	1120	0*	1120
Ce	349	410	1436	153	1283
Pb	115	51	209	49	160
Th	35	8	52	26	26
U	6	5	17	0*	17

* Indicates values below the detection limit.

Table 8 Summary statistics for tuff

<u>Element</u>	<u>Mean</u>	<u>St.Dev</u>	<u>Maximum</u>	<u>Minimum</u>	<u>Range</u>
SiO ₂	58.65	7.33	67.50	48.02	19.48
Al ₂ O ₃	15.17	1.62	17.76	13.15	4.61
TiO ₂	0.51	0.13	0.70	0.38	0.32
Fe ₂ O ₃	2.22	0.82	3.75	1.26	2.49
FeO	0.80	0.65	2.06	0.36	1.70
MgO	4.89	1.26	6.16	2.53	3.63
CaO	2.96	2.48	7.91	1.25	6.74
Na ₂ O	0.42	0.24	0.85	0.17	0.68
K ₂ O	8.27	0.79	9.66	7.38	2.28
MnO	0.05	0.03	0.10	0.03	0.07
P ₂ O ₅	0.11	0.04	0.16	0.07	0.09
H ₂ O	2.44	2.96	5.69	0.00	5.69
CO ₂	0.03	0.09	0.24	0.00	0.24
B ₂ O ₃	0.18	0.20	0.58	0.00	0.58
SO ₃	1.56	1.32	4.12	0.43	3.69
Cl	220	88	342	106	236
Cr	26	10	42	14	28
Ni	58	65	202	20	182
Cu	24	20	66	9	57
Zn	105	36	162	61	101
As	1507	1495	4572	436	4136
Sr	1036	778	2406	130	2276
Ba	813	182	1045	513	532
Ce	166	94	349	86	263
Pb	64	27	112	32	80
Th	37	7	50	29	21
U	6	7	21	0*	21

* Indicates values below the detection limit

Al_2O_3 and iron oxides is probably caused by biotite. The positive correlation of K^+ and SO_3 in the tuff might indicate the presence of K^+ sulphates.

In the clay and tuff, it is likely that titanium is either chemically or physically bound to clay minerals or that it substitutes for Fe^{3+} , because of its strong correlation with Al_2O_3 , K_2O , Fe_2O_3 , CaO and MnO . Titanium is present in both illite and montmorillonite, but its strong correlation with K_2O suggests that the amount of titanium in illite is greater than in montmorillonite.

The average alumina content of clay and tuff is 16.03% and 15.17%, whereas the potassium content is 4.28% and 8.27%, respectively (Table 7 & 8). Volcanic tuff contains a very high amount of K^+ in its chemical composition (Table 13). Probably, some of the K^+ is removed in solution during the alteration of volcanic tuff to clay. The average titanium content of clay and tuff is almost negligible; 0.53% and 0.51%, respectively (Table 7 & 8).

Iron (Fe_2O_3 and FeO)

Iron in the clay and tuff has been calculated as Fe_2O_3 (Fe^{3+}) and FeO (Fe^{2+}), because both valency oxides are present and affect the colour of the sediments. The considerable amount of Fe^{3+} in the sediments occurs in the minerals hematite and iron hydroxides, which are responsible for the colour of the sediments.

In the clay analyses, Fe_2O_3 is positively correlated with K_2O , indicating Fe_2O_3 presence in illite, which does not occur in the tuff.

An excess of Fe^{3+} is present in the octahedral layers of the clay minerals (illite, montmorillonite), substituting for Al (Carroll, 1958) and the strong correlation of Fe_2O_3 with the oxides Al_2O_3 , TiO_2 , CaO , MnO and H_2O in the clay and tuff samples as discussed above is probably due to montmorillonite (possibly Fe montmorillonite). The positive correlation between iron and P_2O_3 might be explained by the presence of iron phosphates in the clay and tuff

As at present, some iron may have been supplied by the thermal springs while the sediments were forming. The average Fe_2O_3 content for the Emet clay and tuff is 3.88% and 2.22%, whereas the average FeO content is very low (0.79% and 0.80% respectively).

The high $\text{Fe}^{+++}/\text{Fe}^{++}$ ratios suggest deposition under strongly oxidising conditions, probably with little or no decomposable organic matter, under arid or semi-arid conditions where aerobic bacterial activity is so rapid that organic matter is destroyed before burial. Under such conditions, the Fe^{3+} oxides can be buried without undergoing reduction by bacteria to ferrous iron.

MgO

The average magnesium content of the clay and tuff is, respectively, 7.54% and 4.89% (Tables 7 & 8). The higher magnesium content of clay can be explained by the greater clay mineral content in clays than in tuffs. It further is suggested that the amount of MgO increased relatively during the alteration of volcanic tuff to montmorillonitic clay.

The oxide MgO occurs mainly in the clay mineral montmorillonite but the high CO_2 in clay suggests that some dolomite might be present. It is positively correlated with FeO and P_2O_5 in the tuff analyses whereas in the clay the strong correlation of MgO with H_2O and SO_3 suggests the presence of Mg sulphates.

Table 9.

CLAY - CORRELATION MATRIX						
SI02	1.0000					
AL203	-0.0267	1.0000				
TI02	-0.2994	0.3791	1.0000			
FE203	-0.4138	0.4177+	0.9380*	1.0000		
FEO	0.7317*	0.3093	-0.5438	-0.5837	1.0000	
MGO	0.2558	-0.7989	-0.7339	-0.8189	0.1493	1.0000
CAO	-0.5970	0.3995	0.3386	0.4480+	-0.1910	-0.5911
NA2O	0.4174+	0.4284+	-0.0867	-0.1742	0.4268+	-0.1961
K2O	-0.4629	-0.0845	0.5341*	0.6167*	-0.5765	-0.2248
MNO	-0.2350	0.7463*	0.2743	0.2766	0.0457	-0.6631
P2O5	-0.5646	-0.1107	0.7360*	0.6991*	-0.7714	-0.2848
H2O	-0.3524	-0.6446	-0.3877	-0.2992	-0.3667	0.5631*
CO2	-0.5361	-0.2726	0.1876	0.2743	-0.5939	-0.2004
R2O3	-0.4579	-0.0069	0.2012	0.3137	-0.6096	-0.0371
SO3	0.3848	-0.3248	-0.6650	-0.8399	0.4765+	0.7331*
CL	-0.1225	-0.4121	0.5015+	0.3098	-0.4572	0.0767
CR	0.4634+	0.5294*	-0.1452	-0.0122	0.6150*	-0.4021
NI	0.5435*	0.4498+	-0.3002	-0.1912	0.7445*	-0.2332
CU	0.3035	-0.3139	-0.0375	-0.1384	0.0499	0.4052+
ZN	-0.4233	-0.4974	0.4927+	0.3714	-0.7787	0.1434
AS	0.2238	-0.5553	-0.4887	-0.6813	0.2382	0.7661*
BR	-0.2612	0.7079*	0.0240	0.1040	0.2480	-0.5808
SR	0.2042	-0.7399	-0.7212	-0.7822	0.1455	0.9653*
BA	-0.3557	0.5108+	0.7387*	0.7632*	-0.3478	-0.8561
CE	0.2033	-0.5540	-0.4508	-0.6542	0.2047	0.7598*
PB	-0.4863	0.1250	0.8482*	0.7891*	0.7111	-0.4411
TH	-0.2289	-0.1013	0.7750*	0.7130*	-0.6270	-0.4501
U	0.3708	0.1035	-0.0720	-0.0169	0.5058+	-0.0576
	SI02	AL203	TI02	FE203	FEO	MGO

Table 9. (contd.)

CAO	1.0000					
NA2O	-0.3828	1.0000				
K2O	0.4483+	-0.8560	1.0000			
MNO	0.3403	0.6752*	-0.4057	1.0000		
P2O5	0.2632	-0.5196	0.6997*	-0.1876	1.0000	
H2O	-0.2726	-0.3690	0.0559	-0.4980	0.2850	1.0000
CO2	0.4447+	-0.2191	0.1369	0.1213	0.4027+	0.3452
B2O3	-0.1285	-0.2213	0.4138+	0.0145	0.2951	0.2658
SO3	-0.3257	0.0784	-0.3968	-0.2150	-0.5781	-0.0313
CL	-0.0077	-0.2561	0.3321	-0.2719	0.5679*	-0.0387
CR	-0.0702	0.5900*	-0.5020	0.3548	-0.4824	-0.2782
NI	-0.1248	0.5187+	-0.5320	0.2090	-0.5304	-0.1847
CU	-0.1657	-0.5168	0.4753+	-0.6105	-0.0057	-0.1824
ZN	0.0764	-0.5679	0.6402*	-0.3542	0.7074*	0.1608
AS	-0.2169	-0.1829	-0.1435	-0.4169	-0.2988	0.0455
BR	0.5474*	0.5030+	-0.3938	0.8819*	-0.3546	-0.4513
SR	-0.5670	-0.1788	-0.1961	-0.6049	-0.3423	0.4804+
BA	0.5040+	0.2092	0.1065	0.5902*	0.5004+	-0.2517
CE	-0.2159	-0.2028	-0.1115	-0.4229	-0.2509	0.0511
PB	0.3796	-0.4775	0.7944*	-0.0012	0.8277*	-0.1517
TH	0.1888	-0.0926	0.3277	0.0534	0.7249*	-0.0399
U	0.1495	-0.3120	0.2075	-0.4521	0.0188	-0.0370
	CAO	NA2O	K2O	MNO	P2O5	H2O

Table 9. (Contd.)

CO2	1.0000					
B2O3	-0.0120	1.0000				
SO3	-0.4004	-0.2158	1.0000			
CL	0.1420	-0.1907	-0.0768	1.0000		
CR	-0.1664	-0.3769	-0.3209	-0.5449	1.0000	
NI	-0.2467	-0.4662	-0.1614	-0.5863	0.9673*	1.0000
CU	-0.4518	0.1796	0.4947+	0.2165	-0.5306	-0.4417
ZN	0.2673	0.3322	-0.0500	0.7960*	-0.8773	-0.9228
AS	-0.2742	-0.3064	0.8763*	0.3517	-0.5442	-0.4017
BR	0.1129	-0.2149	-0.1442	-0.3668	0.4555+	0.3581
SR	-0.3146	0.0261	0.7204*	0.1009	-0.4008	-0.2605
BA	0.5400*	-0.1008	-0.7742	0.1540	0.2792	0.1259
CE	-0.2735	-0.2795	0.8699*	0.3765	-0.5838	-0.4406
PB	0.2128	0.4584+	-0.4185	0.4730+	-0.5654	-0.6570
TH	0.5973*	-0.0646	-0.6464	0.6592*	-0.1372	-0.2728
U	-0.2403	-0.5460	-0.1461	-0.0661	0.4144+	0.5436*
	CO2	B2O3	SO3	CL	CR	NI

Table 9. (Contd.)

CU	1.0000					
ZN	0.4404+	1.0000				
AS	0.5565*	0.2957	1.0000			
BR	-0.6223	-0.5183	-0.2926	1.0000		
SR	0.4220+	0.1529	0.7847*	-0.4926	1.0000	
BA	-0.6314	0.0162	-0.7170	0.4552+	-0.9034	1.0000
CE	0.5759*	0.3366	0.9980*	-0.3178	0.7739*	-0.7045
PB	0.3017	0.7442*	-0.2367	-0.2285	-0.4477	0.4267+
TH	-0.2365	0.5377*	-0.3701	-0.1513	-0.5194	0.7366*
U	0.1268	-0.3263	-0.0710	-0.1759	-0.1110	-0.0245
	CU	ZN	AS	BR	SR	BA
CE	1.0000					
PB	-0.1852	1.0000				
TH	-0.3471	0.5861*	1.0000			
U	-0.0828	-0.1632	-0.0692	1.0000		
	CE	PB	TH	U		

SIGNIFICANT AT 95% - SYMBOL +
SIGNIFICANT AT 99% - SYMBOL *

CaO, MnO and CO₂

These three oxides are strongly correlated with each other and constitute most of the chemically precipitated carbonate fraction. Additionally CaO and MnO occur in the authigenic minerals of the clay and tuff. It is believed that most of the minerals with these oxides were formed either within the basin of deposition or later within the sedimentary deposit itself.

The oxide CaO is positively correlated with CO₂, indicating calcite occurrence in the clay and tuff, whereas the positive correlation of CaO and CO₂ with the oxides Fe₂O₃, TiO₂, P₂O₅ and H₂O shows that these oxides occur in montmorillonite in both clay and tuff analyses. CaO is also positively correlated with K₂O in the clay, suggesting the presence of CaO in illite. The strong correlation of CaO with B₂O₃ and H₂O indicates the presence of borate in the sediments. MnO is strongly correlated with Al₂O₃, TiO₂, Fe₂O₃ as well as CaO. It occurs mainly in psilomelane and montmorillonite in the clay and tuff samples (Tables 9 & 10).

The average calcium, manganese and carbon dioxide content of the clay is, respectively, 2.74%, 0.08% and 0.98%; whereas they are slightly lower in the tuff; 2.96%, 0.05% and 0.03% respectively (Tables 7 & 8).

Na₂O

The average content of sodium in clay and tuff is, respectively, 0.70% and 0.42% (Table 7 & 8). Although in the clay analyses, the oxide Na₂O is positively correlated with SiO₂, Al₂O₃ and MnO, indicating that the sodium fixation took place by cation

exchange in the clay minerals (illite and montmorillonite). The low sodium content and the low Na:K ratio in the clay suggests that Na adsorbed in the clay is insignificant.

The strong correlation between Na_2O and SiO_2 in the tuff samples indicates the occurrence of alkali feldspar, which is also observed by the microscope work. The lack of correlation between sodium and Cl suggests that there is no halite present in the deposits.

P_2O_5

The average contents of P_2O_5 in clay and tuff are 0.19% and 0.11%, respectively (Table 7 & 8). P_2O_5 in the clay and tuff is positively correlated with TiO_2 , Fe_2O_3 , MnO, H_2O , indicating its association with the clay mineral montmorillonite; but its strong correlation with K_2O in the clay shows that it occurs in illite as well. It is believed that some phosphorus is adsorbed on the clay minerals. The correlation of P_2O_5 with Al_2O_3 suggests that it is possible that some PO_4^{3-} is adsorbed by the clay minerals.

P_2O_5 is correlated very strongly with Fe_2O_3 in the clay and tuff analyses. It is likely that some iron phosphates are present in these rocks, but there is no clear evidence to suggest concentration of phosphorus in organic matter and the occurrence of apatite and monazite in the deposits.

H_2O

The average water contents of clay and tuff are, respectively 10.51% and 2.44% (Table 7 & 8), which shows clearly that the water

Table 10

===== TUFF - CORRELATION MATRIX =====

SI02	1.0000					
AL203	-0.4127	1.0000				
TI02	-0.7962	0.1341	1.0000			
FE203	-0.5195	0.6361*	0.5917*	1.0000		
FEO	-0.4691	-0.1133	0.2130	-0.4122	1.0000	
MGO	-0.2364	-0.4054	0.2830	-0.1511	0.6174*	1.0000
CAO	-0.8175	0.0095	0.8993*	0.4499+	0.2062	0.1910
NA2O	0.8154*	-0.1862	-0.5085	-0.3098	-0.6093	-0.6086
K2O	-0.2316	0.5296*	-0.1155	-0.1390	0.5525*	-0.1017
MNO	-0.8338	0.2143	0.8555*	0.5843*	0.0754	0.0350
P2O5	-0.8954	0.3546	0.7507*	0.5409*	0.5060+	0.5610*
H2O	-0.8319	0.5998*	0.7190*	0.7759*	-0.0649	-0.2577
CO2	-0.6400	-0.3081	0.6637*	0.0286	0.3641	0.2636
B2O3	-0.7099	-0.2058	0.6257*	0.0238	0.4597+	0.1422
SO3	-0.5628	0.0605	0.2843	-0.2380	0.9768*	0.6128*
CL	0.1605	-0.4880	0.4442+	0.1210	-0.3385	0.1309
CR	-0.7966	0.3211	0.7966*	0.7397*	-0.1093	-0.0924
NI	-0.3413	0.7697*	-0.0076	0.4242+	-0.2538	-0.7592
CU	-0.3289	0.7102*	0.0499	0.4788+	-0.3487	-0.8004
ZN	-0.4215	0.0329	0.2823	0.4005+	0.1000	0.6035*
AS	-0.5831	0.3953	0.6819*	0.6248*	0.2675	0.4219+
SR	-0.2176	0.0978	0.4295+	0.7597*	-0.4056	0.2836
BA	0.6236*	-0.0346	-0.4701	0.1533	-0.9028	-0.4569
CE	-0.7808	0.5770*	0.7713*	0.7509*	0.2446	0.2538
PB	-0.0429	0.5748*	-0.4324	0.0850	-0.0654	-0.5437
TH	-0.0509	0.6567*	-0.1464	0.5614*	-0.6717	-0.7786
U	-0.1087	0.6522*	-0.0737	0.3158	-0.4214	-0.9192
	SI02	AL203	TI02	FE203	FEO	MGO

Table 10 (Contd.)

CAO	1.0000					
NA2O	-0.5339	1.0000				
K2O	-0.2711	-0.1902	1.0000			
MNO	0.9680*	-0.5009	-0.2486	1.0000		
P2O5	0.6642*	-0.9030	0.1669	0.6593*	1.0000	
H2O	0.7640*	-0.4629	0.0440	0.8759*	0.6186*	1.0000
CO2	0.8952*	-0.4528	-0.3229	0.8109*	0.4559+	0.4849+
B2O3	0.8207*	-0.5295	-0.0223	0.7230*	0.4518+	0.5428*
SO3	0.2186	-0.6938	0.6317*	0.1147	0.6271*	0.0466
CL	0.3578	0.3617	-0.6856	0.2668	-0.1109	-0.0429
CR	0.8922*	-0.4874	-0.2633	0.9573*	0.6208*	0.9380*
NI	0.1154	-0.0202	0.3512	0.3150	0.0368	0.6650*
CU	0.1727	0.0210	0.2522	0.3624	0.0041	0.7016*
ZN	0.3570	-0.7181	-0.3937	0.3799	0.6588*	0.2487
AS	0.3450	-0.5578	0.2990	0.3198	0.7619*	0.4175+
SR	0.2848	-0.3413	-0.4929	0.3093	0.4393+	0.3250
BA	-0.3688	0.5974*	-0.6332	-0.2412	-0.5863	-0.1875
CE	0.5222*	-0.6376	0.3205	0.5506*	0.8506*	0.6852*
PB	-0.3706	-0.0738	0.5927*	-0.2408	-0.1250	0.1892
TH	-0.0346	0.1692	-0.0452	0.1914	-0.1417	0.5256*
U	0.0317	0.3210	0.2468	0.2235	-0.2319	0.5322*
	CAO	NA2O	K2O	MNO	P2O5	H2O

Table 10 (Contd.)

CD2	1.0000					
B203	0.8936*	1.0000				
S03	0.2870	0.4107+	1.0000			
CL	0.3135	0.0624	-0.3993	1.0000		
CR	0.6650*	0.6399*	-0.0362	0.1870	1.0000	
NI	-0.0416	0.1210	-0.1713	-0.5178	0.4392+	1.0000
CU	-0.0032	0.1678	-0.2696	-0.4112	0.5065+	0.9858*
ZN	0.2849	0.1041	0.1619	-0.0647	0.4045+	-0.1674
AS	-0.0039	0.1021	0.4359+	0.0690	0.3568	-0.0958
SR	-0.0175	-0.0849	-0.2839	0.3153	0.4668+	-0.1533
BA	-0.3840	-0.5817	-0.9256	0.2259	-0.1049	0.1126
CE	0.1530	0.2586	0.4219+	-0.0324	0.5927*	0.1899
PB	-0.4290	-0.0971	0.0124	-0.9599	-0.0622	0.7436*
TH	-0.2325	-0.1776	-0.5856	-0.3057	0.3915	0.8599*
U	-0.0958	0.0110	-0.3774	-0.2770	0.3204	0.9299*
	CD2	B203	S03	CL	CR	NI
CU	1.0000					
ZN	-0.1887	1.0000				
AS	-0.0888	0.2919	1.0000			
SR	-0.0726	0.6528*	0.5641*	1.0000		
BA	0.1627	0.0583	-0.5157	0.2749	1.0000	
CE	0.1922	0.3286	0.9417*	0.5138+	-0.5112	1.0000
PB	0.7036*	-0.1978	-0.1083	-0.2098	0.0132	0.0194
TH	0.8837*	0.0023	-0.1844	0.1809	0.5680*	0.0414
U	0.9364*	-0.4274	-0.2515	-0.2764	0.2594	0.0044
	CU	ZN	AS	SR	BA	CE
PB	1.0000					
TH	0.6195*	1.0000				
U	0.5916*	0.8340*	1.0000			
	PB	TH	U			

SIGNIFICANT AT 95% - SYMBOL +
SIGNIFICANT AT 99% - SYMBOL *

content of clay is much higher than that of the tuff. Water in tuff and especially in clay is mainly fixed or absorbed in the clay minerals, in which water is an essential part of the sheet structure.

In the present study, water is present in both clay minerals (montmorillonite, illite) and the authigenic borate minerals. In the clay analyses, water is positively correlated with MgO, suggesting that very small amounts of sepiolite may be present. Water is also positively correlated with the oxides of Al_2O_3 , TiO_2 , Fe_2O_3 , CaO, MnO and P_2O_5 in the tuff and clay samples, indicating its presence in the montmorillonitic clay group. The positive correlation between H_2O and B_2O_3 shows the association of water with the borate minerals precipitated in the deposit and with the clay and tuff.

B_2O_3

The boron content of clay (0.60%) is much higher than the boron content in tuff (0.18%)(Table 7 &8), because it is well established that the clay minerals, especially illite, adsorb up to 1% boron. The positive correlation between B_2O_3 and K_2O in the clay analyses indicates that boron is mainly adsorbed by the illitic clay. In the tuff, however, boron is positively correlated with the oxides of TiO_2 , FeO, MnO, P_2O_5 , suggesting that a small amount of boron is present in montmorillonite. The strong correlation of boron with CaO and H_2O shows that most of the boron occurs in the borate minerals such as colemanite.

S

In the clay and tuff analyses, sulphur occurs mainly in three forms; native sulphur, sulphates and sulphides.

Native sulphur occurs as a very thin layer up to 5 or 10cm thick interbedded with clay and tuff. The average sulphur content of clay (0.46%) is less than the sulphur content of tuff (1.56%) (Table 7 & 8). Very high sulphur concentration in tuff samples indicates that the source of sulphur is very likely thermal springs and a volcanic origin.

Sulphur occurs as a major constituent of sulphate evaporites such as celestite and gypsum, which occurs rarely. The Sr sulphate, celestite, is much more common than the others and in fact the strong correlation of sulphur with Sr in the clay proves that celestite is the most abundant evaporite mineral. However the correlation between sulphur and Cu in the clay and the very strong correlation of sulphur with MgO in the clay and tuff suggests that Mg sulphates and Cu sulphates or sulphides are present in limited amounts.

Sulphur also occurs in the form of sulphides which are mainly realgar, orpiment and pyrite. Sulphur is strongly positively correlated with As in the clay and tuff analyses. The most common As sulphides in the sediments are realgar and its alteration product, orpiment. The strong correlation between sulphur and iron in the tuff suggests that there is some pyrite present in the rocks.

Cl

In the clay and tuff analyses, the chlorine content is generally low and the tuff has a higher Cl average (220ppm) than

the clay (114ppm) (Tables 7 & 8). In general, clay minerals have a low chlorine content, but some comparatively high values have been quoted. A small fraction of insoluble chlorine is bound to the surface of sediment particles. It is also well known that marine sediments usually contain higher amounts of chlorine than non-marine sediments and that the chlorine content is derived from connate water during sediment accumulation and diagenesis. Chlorine can also be derived from volcanic emanations, and this is probably the reason for the higher chlorine content of tuff in the Emet deposits. It is likely that the weathering of tuff to montmorillonitic clay resulted in a very marked decrease in the chlorine content.

Chlorine is positively correlated with the oxides TiO_2 , P_2O_5 , B_2O_3 and it is weakly correlated with K_2O , Na_2O and CaO in both the clay and tuff analyses, indicating that chlorine is mainly adsorbed on the clay minerals (montmorillonite) rather than it occurring in evaporite minerals.

Cr and Ni

These two elements are closely correlated with each other and strongly correlated with the clay mineral montmorillonite (Table 9 & 10) suggesting that most of these elements are present within the clay minerals. Their close correlation suggests that they have similar geochemical mobility during weathering of parent rocks and during sedimentation. The geochemical mobility of Cr and Ni is rather low and these elements tend to be transported as fine suspensions in surface waters.

The ionic radii of Cr and Ni are very close to the radii of Al, Mg, Fe and Ti, which enables them to replace the latter in

the crystalline lattice and be concentrated in the clay minerals. Chromium substitutes mainly for Fe^{3+} and Al^{3+} , whereas Ni substitutes usually for Mg^{2+} and Fe^{3+} . In the clay and tuff analyses, chromium and nickel are strongly correlated with iron oxides, suggesting the substitution of Cr and Ni for iron or their adsorption on iron oxides. Probably chromite is also present.

Cr and Ni are positively correlated with the oxides of SiO_2 , Al_2O_3 , TiO_2 , Fe_2O_3 , MnO and P_2O_5 in the clay and tuff analyses, indicating their close association with the montmorillonitic clay groups. The average chromium and nickel contents of the clay (140ppm and 240ppm, respectively) are much higher than in the tuff, which has a very low Cr (26ppm) and Ni (58ppm) content (Tables 7 & 8).

Cu

The clay contains an average of 59ppm copper, as compared with only 24ppm in the tuff (Tables 7 & 8). The relatively high concentrations of copper can be adsorbed on clay minerals and iron oxides. Also leaching of country rocks by thermal springs could explain the origin of the higher copper concentrations. In the clay and tuff analyses, copper is positively correlated with Al_2O_3 , MgO , and Fe_2O_3 , as well as with K_2O in the clay, indicating its close association with the clay minerals (montmorillonite and illite) and iron oxides (Tables 9 and 10).

The positive correlation of Cu with Cr and Ni is probably due to the presence of biotite in the tuff. In the clay also, the positive correlation of copper and S and As suggests that

some Cu sulphides or sulphates and copper arsenide may be present in the deposits. Copper has a very high affinity for sulphur under the conditions of sedimentary rock formation and minerals composed of copper-sulphur are important. Arsenic can easily combine with Cu, especially native copper, to form copper arsenide.

Zn

The average Zn content of the clay is 158ppm as compared with 105ppm in the tuff (Tables 7 & 8).

Zn has similar ionic radii of Mg^{2+} , Fe^{2+} , Co^{2+} , Ni^{2+} and Mn^{2+} and substitutes or replaces mainly ferrous iron and magnesium in certain structural positions of silicates (biotite, feldspar) and oxides. The positive correlation of zinc with iron and magnesium in the tuff samples proves that zinc is either substituting or replacing iron and magnesium.

The importance of zinc adsorption on clay minerals has been experimentally proved by Krauskopf (1956) and others. Zinc adsorption depends on temperature, pH, salinity etc... of the solution (adsorbate) and several properties such as composition, structure, grain size etc... of the adsorbent. Montmorillonite, illite and precipitated iron oxides adsorb zinc most effectively. The positive correlation of zinc with the oxides of TiO_2 , P_2O_5 , Fe_2O_3 , MgO in the clay and tuff analyses, and its strong positive correlation with K_2O in the clay, shows its close association with the montmorillonitic and illitic clay minerals (Tables 9 & 10).

Zinc in the deposit therefore, is likely to be present in Fe and Ti minerals and adsorbed on the clay minerals. The origin of the high zinc concentration is probably due to the leaching of country basement rocks by hot springs. Zinc is usually

transported and accumulated in the sedimentary environment in detrital matter, especially in colloidal iron oxides and iron oxide coatings on other minerals.

As

The clay and tuff samples contain exceptionally high arsenic concentrations in the Emet deposits, with average contents of 2791 ppm and 1507 ppm As, respectively (Tables 7 & 8).

The origin of the very high arsenic concentration in the Emet clay and tuff sediments is probably due to widespread occurrence of hot springs, connected with volcanic activity in the Emet district. The chemical analyses of the thermal springs for arsenic is given on Table 6, page 57 (Chapter III). Data on the arsenic content of hot spring waters shows values of up to 5.99ppm As. Japanese hot springs gave an average of 0.3ppm As (Watanuki, 1963).

In rock-forming minerals, arsenic (ionic radii As^{3+} 0.58 and As^{5+} 0.46 Å) can probably substitute for Si^{4+} (0.43), Al^{3+} (0.51), Fe^{3+} (0.64), and Ti^{4+} (0.68 Å). In general, arsenic is present in iron sulphides, clay minerals (possibly in an adsorbed form), organic matter, etc... in shales and clays. Arsenic is positively correlated with the oxides of MgO , TiO_2 , Fe_2O_3 , P_2O_5 and H_2O in the clay and tuff analyses, suggesting that it is mainly adsorbed in the montmorillonitic clays. Arsenic is also very strongly correlated with sulphur in the clay and tuff samples, indicating its close association with sulphur as sulphide forms such as realgar and orpiment. Realgar and its alteration product, orpiment, are widespread throughout the clay and tuff formations. Chemical analyses of these two minerals and arsenic occurrence in the borate phases will be discussed in

detail in the mineralogy of the Emet borate deposits.

Br

Bromine contents of clay and tuff are below the detection limit. But clay samples contain between 0-1ppm of bromine as compared with the tuff (Table 7).

In the lacustrine sediments, the average bromine content is 1-30ppm, whereas in evaporites it is high. The similarity in the ionic radii of bromine and chlorine, 1.96\AA and 1.8\AA respectively, enables the bromide ion to replace the chlorine ion in lattice sites (Weast, 1971), such as carnallite mineral ($\text{KMgCl}_3 \cdot 6\text{H}_2\text{O}$). In the Emet sediments, the non-existence of K, Na and Mg salts probably causes the low concentration of bromine; the strong correlation of bromine with Al_2O_3 , CaO, Na_2O and MnO in the clay analyses indicates that the negligible bromine is associated with the montmorillonitic clay.

Sr

The clay and tuff lacustrine sediments in the Emet deposits contain very high amounts of strontium and they are comparatively enriched in strontium concentrations. The clay contains an average of 2327ppm strontium as compared with 1036 ppm strontium in the tuff samples (Tables 7 & 8).

In the clay and tuff analyses, strontium occurs as follows: adsorbed on the clay minerals (especially montmorillonite); in isomorphous substitution for Ca in calcite; and mainly as independent sulphate phases, celestite (SrSO_4). The ionic radius of Sr^{2+} is between those of Ca^{2+} and Ba^{2+} and is somewhat smaller

than the Pb^{2+} radius. In a number of minerals, Sr is replaced by Ca^{2+} , Ba^{2+} and Pb^{2+} and also replaces them, e.g. celestite, strontianite, barite..., but not with calcite which forms an isomorphous series with carbonates of smaller cations.

Sr is positively correlated with the oxides of MgO , TiO_2 , Fe_2O_3 , P_2O_5 and H_2O in the clay and tuff samples. This correlation indicates that a small amount of strontium is adsorbed on the montmorillonite (Tables 9 & 10).

Much of the strontium in the Emet sediments is present as celestite. The strong positive correlation of Sr with sulphur in the clay samples indicates the presence of celestite in the deposits. The chemical analyses of the thermal springs for Sr is given on Table 6, at page 57 (Chapter III). The chemical analysis and occurrence of celestite in the Emet deposits will be discussed later on.

Ba

The clay and tuff formations in the Emet deposits have a very high barium concentration. The average barium contents of the clay and tuff samples are, respectively 623ppm and 813ppm. The barium content of tuff is higher than in the clay (Tables 7 & 8).

Ba in the sedimentary rocks occurs mainly adsorbed on clay minerals, as Ba-sulphate precipitates or incorporated with carbonate minerals. Ba is usually adsorbed from solution by clay minerals (montmorillonite, illite), hydroxides (ferric oxide) and organic matter. In the clay and tuff analyses, Ba is strongly correlated with the oxides of SiO_2 , Al_2O_3 , TiO_2 , Fe_2O_3 , CaO , Na_2O , MnO and P_2O_5 , indicating its close association with montmorillonite. It is mainly adsorbed on montmorillonitic clay groups.

The strong correlation between Ba and CaO in the clay samples suggests that a small amount of Ba is replacing or is an isomorphous substitution for Ca in the carbonate fraction. Ba is also strongly correlated with CO₂ in the clay, suggesting a probable occurrence of Ba carbonate.

Ce

In the present study, the clay and tuff samples were analysed for only one of the rare earth elements, namely cerium. Those samples analysed for Ce appear to be enriched with an average of 349ppm and 166ppm respectively, in clay and tuff samples (Tables 7 & 8). The Ce enrichment in the sediments suggests that some of the elements may have been oxidized under the oxidizing environments.

Ce in general is strongly positively correlated with the oxides of Al₂O₃, TiO₂, Fe₂O₃, MgO, CaO, MnO and H₂O in the clay and tuff analyses, indicating the cerium adsorption on the clay minerals (montmorillonite).

Ce is also positively correlated with P₂O₅ in the tuff samples. The correlation is probably due to cerium in phosphate minerals such as monazite.

Pb

The lead contents of the clay and tuff samples are, respectively, 115ppm and 64ppm. (Tables 7 & 8). The lead concentration of clay is higher than tuff, because of high adsorption effects of the clay minerals.

Lead from weathering of magmatic and metamorphic rocks is expected to have mainly accumulated in detrital sediments in their

potassium-bearing minerals mica and feldspar. Some lead is transported into the sedimentary environments being adsorbed on clay minerals and ferric iron oxides. Lead is usually adsorbed on clay minerals (montmorillonite), iron oxide and on organic substances. In the tuff analyses, lead is positively correlated with Al_2O_3 and K_2O , indicating the presence of lead in the mica and feldspar minerals of the tuff. Usually mica contains less lead than potassium feldspar. In general, it is accepted that lead replaces K^+ in its minerals. In the clay samples, lead is positively correlated with the oxides of TiO_2 , Fe_2O_3 , K_2O and P_2O_5 , suggesting the lead was adsorbed on clay minerals (illite) and ferric iron oxides (Tables 9 & 10). The insignificant correlation of Pb with S indicates that there is no lead-sulphide (Galena, PbS) present in the Emet lacustrine sediments.

Th and U

The geochemistry of thorium is intimately associated with that of uranium. Thorium and uranium have a similar geochemical behaviour in igneous and metamorphic rocks, but are different in sedimentary rocks, because of their different fractionation during the weathering of the parent rocks. During weathering and rock alteration, the comparatively immobile thorium is concentrated in resistate minerals or is adsorbed on clays, whereas uranium is redistributed in surface and ground waters. Thorium and uranium are commonly fractionated during surficial processes owing to oxidation of uranium to the soluble uranyl ion. In the present study, Th and U are positively correlated in the tuff analyses, whereas in the clay samples their correlation

is insignificant, indicating fractionation during the formation of clay sediments in the weathering zone (Tables 9 & 10).

Th is positively correlated with the oxides of Al_2O_3 , TiO_2 , Fe_2O_3 , P_2O_5 and H_2O in the clay and tuff analyses, indicating its adsorption on the clay minerals (montmorillonite) and concentration in resistant minerals (probably monazite, hematite, quartz, etc.). The correlation of U with Al_2O_3 , FeO and H_2O suggests that some of the uranium is also adsorbed on montmorillonitic clay and not all of the uranium is oxidized and leached away by surface and ground waters.

The thorium contents of the clay and tuff are very close to each other with 35ppm and 37ppm, respectively, but the clay and tuff contain less uranium concentrations. Both clay and tuff have an average of 6ppm U in their chemical compositions (Tables 7 & 8).

Summary

A complete gradation exists between tuff and clay in the Emet borate zone sediments and is reflected in their geochemistry. Clays on average have less SiO_2 and K_2O and significantly more Fe_2O_3 , MgO , Na_2O and H_2O than the average tuff at Emet. This seems to be the result of the prevalence of quartz and biotite in the tuffs compared with the relatively higher proportions of clay minerals (both illite and montmorillonite) in the clays.

Both tuffs and clays are characterised by high $\text{Fe}_2\text{O}_3:\text{FeO}$ ratios indicating strongly oxidizing conditions of sedimentation. Unusually high concentrations of B, As, Sr and S suggest the formation of suites of evaporite and hydrothermal minerals within the sediments similar to those found in the interbedded

borate layers. Low Cl and negligible Br tend to confirm the non-marine character of the sediments. It is, therefore, concluded that both the tuffs and the clays were deposited in non-marine basins under strongly oxidising conditions.

Small quantities of borates, strontium sulphates and arsenic sulphides were precipitated from brines which were partly derived from thermal springs but apart from these, all minerals in the tuffs and clays could have been formed by the chemical weathering of igneous and metamorphic source rocks, or in the case of the tuffs by direct ash fall into the basins.

(d) Geochemistry of upper limestone:

In order to find out the general chemical composition of the limestone and the vertical distribution of boron in the sequence, samples were collected and analysed from the upper limestone overlying the borate zone in the Emet lacustrine deposits. The geochemistry of the upper limestone is discussed in the light of average chemical analysis (Table 11) and the correlation matrix (Table 12). The chemical analyses for individual samples are also given in Table 13.

CaO and CO₂ make up the bulk of the analysed samples (90% and above). Ca, Mg, Mn, Sr and probably Ba are mainly restricted to the carbonate fraction (calcite). B, As and Sr are represented respectively in borates (mainly colemanite), sulphides (realgar, orpiment) and sulphates (celestite), which all are chemical (or authigenic) precipitates from the brines. Si occurs in two different forms in the limestone such as in the clay (detrital) fraction and in the chemically precipitated chert which is a common occurrence in the upper limestone. The detrital clay

Table 11 Summary statistics for limestone

<u>Element</u>	<u>Mean</u>	<u>St.Dev</u>	<u>Maximum</u>	<u>Minimum</u>	<u>Range</u>
SiO ₂	3.84	2.14	8.14	1.46	6.68
Al ₂ O ₃	2.91	2.62	8.22	0.75	7.47
Fe ₂ O ₃	0.17	0.02	0.66	0.00	0.66
FeO	0.10	0.09	0.28	0.00	0.28
MgO	1.01	1.27	4.27	0.15	4.12
CaO	51.68	2.77	55.30	46.20	9.10
Na ₂ O	0.26	0.04	0.33	0.20	0.13
K ₂ O	0.16	0.08	0.34	0.10	0.24
MnO	0.03	0.01	0.05	0.00	0.05
P ₂ O ₅	0.05	0.03	0.12	0.03	0.09
H ₂ O	0.73	0.63	2.10	0.21	1.89
CO ₂	38.68	1.77	40.63	35.00	5.63
B ₂ O ₃	0.21	0.08	0.32	0.00	0.32
SO ₃	0.23	0.14	0.60	0.10	0.50
Cl	124	42	237	62	175
Cr	10	6	22	4	18
Ni	16	11	42	3*	39
Cu	15	4	21	9	12
Zn	15	9	31	4	27
As	249	617	2291	24	2267
Br	1*	1	3*	0*	3
Sr	740	866	2925	146	2779
Ba	41	48	169	0*	169
Ce	148	46	288	101	187
Pb	10	10	37	0*	37
Th	3*	4	15	0*	15
U	3*	4	16	0*	16

* Indicates values below the detection limit

Table 12

===== LIMESTONE - CORRELATION MATRIX =====

SI02	1.0000					
AL203	0.0117	1.0000				
FE203	0.5042+	0.3374	1.0000			
FEO	-0.0882	-0.3364	-0.1446	1.0000		
MGO	0.6104*	-0.1872	-0.2719	0.0385	1.0000	
CAO	-0.9320	-0.1838	-0.4536	0.0999	-0.6486	1.0000
NA2O	-0.0039	-0.0416	-0.1111	0.1945	-0.1437	0.0671
K2O	0.4414+	0.4136+	0.8981*	-0.2209	-0.2645	-0.3817
MNO	0.1807	0.5540*	0.2681	0.3913	0.1304	-0.2758
P2O5	0.0896	-0.1888	-0.1119	-0.1273	0.2646	-0.1769
H2O	0.3362	-0.3070	-0.2976	0.0137	0.6850*	-0.3603
CO2	-0.3382	-0.6141	-0.0101	0.3782	-0.3759	0.3378
B2O3	-0.4698	0.4041+	0.0835	0.0416	-0.5053	0.4201
SO3	0.2807	-0.3839	-0.2335	0.2929	0.3280	-0.1898
CL	-0.3583	0.3774	-0.0418	0.1470	-0.1994	0.2312
CR	-0.1946	-0.0771	0.2840	-0.1642	-0.4061	0.1704
NI	0.2040	0.0594	0.5775*	0.2701	-0.4393	-0.1501
CU	0.4905+	0.0361	0.3524	0.0441	0.3248	-0.4804
ZN	0.3465	0.2224	0.7649*	0.1936	-0.4346	-0.2806
AS	0.1809	-0.2715	0.0556	0.5273*	-0.0119	-0.1148
BR	-0.2097	0.1981	-0.0675	-0.0851	-0.2276	0.0523
SR	0.5560*	-0.2446	-0.2531	0.3014	0.9814*	-0.5584
BA	-0.0309	0.0300	0.0788	0.0311	0.0140	-0.0680
CE	-0.0091	-0.1063	0.2779	0.3888	-0.4359	0.1076
PB	0.4564+	0.3253	0.8398*	-0.0832	-0.0987	-0.4614
TH	0.3620	0.2730	0.8460*	-0.2279	-0.2914	-0.2973
U	-0.2062	0.5956*	-0.0060	-0.3434	-0.1459	0.1397
	SI02	AL203	FE203	FEO	MGO	CAO

Table 12 (Contd.)

NA2O	1.0000					
K2O	-0.1593	1.0000				
MNO	-0.0786	0.2402	1.0000			
F2O5	-0.5934	-0.2328	-0.0761	1.0000		
H2O	0.0210	-0.3200	-0.1228	0.0133	1.0000	
CO2	-0.0044	-0.1199	-0.3863	0.0999	-0.2638	1.0000
B2O3	-0.3742	0.1520	0.3186	-0.0239	-0.2142	-0.0943
SO3	0.2354	-0.4678	0.1007	0.2703	0.3859	-0.0768
CL	0.1745	0.0560	0.5037+	-0.3360	-0.2758	-0.0302
CR	-0.6404	0.3410	-0.2148	0.4856+	-0.4263	0.4799+
NI	0.1087	0.4212+	0.3223	-0.0173	-0.4509	0.3053
CU	-0.2460	0.0949	0.2159	0.1918	0.5018+	-0.2725
ZN	0.2205	0.5949*	0.2936	-0.1492	-0.3598	0.1144
AS	0.4519+	-0.2281	0.3119	0.0123	0.0009	0.2149
BR	0.2938	0.1480	-0.1955	-0.3876	0.1299	0.0819
SR	-0.0855	-0.3533	0.3282	0.2808	0.6825*	-0.3295
BA	-0.6007	-0.0118	-0.0539	0.7441*	-0.2078	0.1176
CE	0.4308+	0.0438	0.2815	-0.1287	-0.3336	0.2926
PB	-0.4620	0.7648*	0.2193	0.1090	-0.2089	-0.0592
TH	-0.4075	0.8203*	0.0711	0.0049	-0.3784	-0.0020
U	-0.1283	0.1110	0.3658	0.0427	-0.3193	-0.5278
	NA2O	K2O	MNO	F2O5	H2O	CO2

Table 12 (Contd.)

B203	1.0000					
S03	-0.1301	1.0000				
CL	0.0188	-0.3650	1.0000			
CR	0.4407+	-0.3311	-0.2658	1.0000		
NI	0.1858	0.3089	0.0247	0.2634	1.0000	
CU	0.1880	0.4397+	-0.5358	-0.0774	0.1026	1.0000
ZN	0.2209	0.1973	-0.1739	0.1868	0.8647*	0.3393
AS	-0.1586	0.7961*	0.0267	-0.3132	0.6625*	0.2142
BR	-0.0006	-0.4367	0.3523	-0.0513	-0.1068	-0.4194
SR	-0.2808	0.6675*	-0.2421	-0.4315	-0.1497	0.5275*
BA	0.1800	-0.1259	-0.3951	0.5563*	-0.0928	0.2491
CE	0.0747	0.5417*	0.1392	-0.0837	0.8455*	0.0499
PB	0.1532	-0.3498	-0.2074	0.3844	0.3045	0.4717+
TH	0.1024	-0.4024	-0.1124	0.4115+	0.4080+	0.2307
U	0.1069	-0.2714	0.6342*	-0.1702	-0.0940	-0.3468
	B203	S03	CL	CR	NI	CU
ZN	1.0000					
AS	0.5046+	1.0000				
BR	-0.0804	-0.3069	1.0000			
SR	-0.1863	0.3614	-0.4037	1.0000		
BA	0.0093	-0.2667	-0.2960	-0.0158	1.0000	
CE	0.6938*	0.8873*	-0.2028	-0.0628	-0.2998	1.0000
PB	0.5266*	-0.2233	-0.1319	-0.1433	0.4778+	-0.0865
TH	0.5237*	-0.2225	-0.0687	-0.3600	0.2925	0.0267
U	-0.2111	-0.2121	0.1058	-0.2292	-0.0356	-0.0672
	ZN	AS	BR	SR	BA	CE
PB	1.0000					
TH	0.9132*	1.0000				
U	-0.0071	0.1473	1.0000			
	PB	TH	U			

SIGNIFICANT AT 95% - SYMBOL +
SIGNIFICANT AT 99% - SYMBOL *

fraction includes the major elements Si, Al, Fe, Mg and K which are the main constituents of the clay minerals (illite, montmorillonite). Fe is also occluded in the carbonate fraction, but it is not in the lattice of calcite crystals.

Most of the trace elements in the limestone are in the clay and heavy minerals fraction. The minor and trace elements which are either adsorbed on the clay minerals or within their crystal lattices in the clays fraction of the limestone, include mainly Cl, Cr, Ni, Cu, Zn, Br, Ce, Pb, Th and U. Small amounts of As, Sr and Ba are also included in the clay fraction. All the trace elements show strong positive correlation with SiO_2 , Al_2O_3 , MgO and K_2O oxides of the clay minerals (illite and montmorillonite). Elements grouping in one portion of the samples, for example, in detrital or carbonate minerals, show positive correlation among themselves.

Dolomite does not occur in the upper limestone, although it has a fairly high concentration of magnesium (1.01%). It is likely that the high content of magnesium is due to the clay minerals fraction (mainly montmorillonite) in the limestone. The titanium content of the limestone is below the detection limit. The negative correlation of P_2O_5 with CaO (-0.18) rules out the presence of apatite or carbonate-apatite in the limestone. It seems likely that some of the trace elements such as Cr, Sr and Ba replace or substitute for Ca^{2+} and Mg^{2+} in the carbonate fraction, whereas Ni, Zn and Pb substitute for iron in the non-carbonate fraction.

The upper limestone is characterized by a relatively high $\text{Fe}_2\text{O}_3:\text{FeO}$ ratio (1.7) indicating strongly oxidising conditions of sedimentation and arid to semi-arid environments with a very low rate of leaching.

The Upper Limestone is thus not untypical of reasonably pure limestones containing chert and detrital clay minerals but like the tuffs and clays in the borate zone it is characterised by relatively high concentrations of B, As and Sr.

Table 13. The chemical analyses of the Middle Oligocene sediments. (Clay, tuff, marl and limestone samples.)

<u>Number</u>	<u>1</u>	<u>3</u>	<u>5</u>	<u>7</u>	<u>13</u>
SiO ₂	52.33	43.52	49.62	52.50	54.93
Al ₂ O ₃	15.97	11.68	15.33	19.97	12.13
TiO ₂	0.41	0.38	0.45	0.49	0.42
Fe ₂ O ₃	3.18	2.65	2.75	3.33	3.53
FeO	1.18	0.82	1.88	1.12	0.84
MgO	8.88	5.19	5.04	5.42	4.18
CaO	1.60	13.19	6.39	5.89	5.91
Na ₂ O	0.29	0.31	0.28	0.28	0.43
K ₂ O	3.99	3.34	4.16	4.08	2.84
MnO	0.03	0.27	0.08	0.09	0.04
P ₂ O ₅	0.16	0.18	0.14	0.15	0.09
H ₂ O+	12.18	7.16	8.29	7.91	9.48
CO ₂	0.00	9.55	3.27	0.00	3.59
B ₂ O ₃	0.18	0.37	0.48	0.37	0.16
SO ₃	0.40	0.55	0.70	0.52	0.33
Total	100.78	99.16	98.86	102.12	98.90
Cl	69	72	64	72	46
Cr	254	191	258	268	269
Ni	499	295	545	438	471
Cu	56	33	34	36	32
Zn	90	70	82	81	82
As	596	408	717	333	251
Br	0*	2*	0*	1*	0*
Sr	2644	1683	1717	1633	764
Ba	492	449	735	774	666
Ce	188	164	184	165	123
Pb	59	47	58	49	48
Th	30	31	23	32	31
U	17	0*	4	2*	5

*Indicates values below the detection limit

Table 13 (continued)

<u>Number</u>	<u>14</u>	<u>15</u>	<u>16</u>	<u>17</u>	<u>19</u>
SiO ₂	43.11	3.07	36.29	2.64	8.46
Al ₂ O ₃	13.03	1.78	7.67	0.73	1.82
TiO ₂	0.41	0.00	0.21	0.00	0.00
Fe ₂ O ₃	2.69	0.00	1.35	0.04	0.00
FeO	0.88	0.39	0.52	0.00	0.28
MgO	3.94	0.83	11.35	1.22	3.55
CaO	14.70	49.70	16.10	49.56	44.94
Na ₂ O	0.36	0.32	0.15	0.23	0.15
K ₂ O	3.71	0.35	1.98	0.10	0.13
MnO	0.07	0.04	0.03	0.00	0.05
P ₂ O ₅	0.17	0.14	0.11	0.02	0.13
H ₂ O+	4.28	1.00	11.29	1.10	2.57
CO ₂	10.91	39.05	9.56	39.39	35.31
B ₂ O ₃	0.48	0.27	0.27	0.48	0.58
SO ₃	1.20	0.35	0.92	0.15	0.40
Total	99.94	97.29	97.80	95.66	98.37
Cl	95	111	114	135	547
Cr	163	9	15	5	9
Ni	204	18	29	4	14
Cu	16	27	13	21	12
Zn	59	19	57	6	14
As	345	17689	371	1566	544
Br	6*	0*	5*	0*	0*
Sr	1001	1043	757	7440	2564
Ba	1210	1347	291	185	33
Ce	83	0*	52	207	158
Pb	23	1*	30	13	20
Th	19	4*	13	0*	3*
U	0*	15	2*	1*	7

*Indicates values below the detection limit

Table 13 (continued)

<u>Number</u>	<u>20</u>	<u>21</u>	<u>23</u>	<u>25</u>	<u>26</u>
SiO ₂	4.98	25.74	34.00	66.62	24.12
Al ₂ O ₃	5.41	5.81	7.45	0.61	7.67
TiO ₂	0.00	0.23	0.16	0.00	0.11
Fe ₂ O ₃	0.00	1.46	1.37	0.00	1.04
FeO	0.56	0.56	0.28	0.16	0.25
MgO	3.89	7.63	13.05	0.07	5.34
CaO	47.60	26.74	18.20	16.52	31.50
Na ₂ O	0.24	0.32	0.24	0.32	0.32
K ₂ O	0.11	1.78	1.02	0.10	1.30
MnO	0.02	0.04	0.03	0.00	0.03
P ₂ O ₅	0.13	0.14	0.09	0.02	5.01
H ₂ O+	0.71	6.05	10.51	1.85	5.01
CO ₂	37.40	21.01	11.73	12.00	22.74
B ₂ O ₃	0.37	0.37	0.08	0.37	0.08
SO ₃	0.15	0.85	0.25	0.80	0.28
Total	101.57	98.73	98.46	99.44	104.80
Cl	179	193	88	267	65
Cr	5	55	28	4	39
Ni	4	90	59	7	86
Cu	19	28	26	6	18
Zn	9	59	54	6	38
As	382	2316	1032	3421	113
Br	2*	0*	2*	0*	4*
Sr	2806	2383	3068	889	1654
Ba	36	219	107	0*	128
Ce	127	269	149	205	89
Pb	6*	39	33	3*	28
Th	3*	18	11	3*	12
U	5	5	3*	0*	0*

*Indicates values below the detection limit

Table 13 (continued)

<u>Number</u>	<u>27</u>	<u>28</u>	<u>31</u> #	<u>33</u>	<u>38</u>
SiO ₂	4.83	1.46	42.22	50.84	48.02
Al ₂ O ₃	1.15	7.95	6.15	11.35	14.04
TiO ₂	0.00	0.00	0.10	0.34	0.70
Fe ₂ O ₃	0.10	0.07	0.95	1.82	2.27
FeO	0.00	0.04	0.00	0.99	1.34
MgO	1.44	0.45	18.13	14.19	5.64
CaO	50.40	53.90	2.19	1.56	7.99
Na ₂ O	0.33	0.26	0.15	0.16	0.17
K ₂ O	0.15	0.16	0.52	3.43	7.69
MnO	0.00	0.05	0.02	0.04	0.10
P ₂ O ₅	0.04	0.04	0.13	0.08	0.15
H ₂ O+	0.77	0.21	14.19	10.64	5.69
CO ₂	39.60	35.91	0.00	0.00	0.24
B ₂ O ₃	0.00	0.27	0.48	0.27	0.58
SO ₃	0.15	0.13	2.05	0.97	2.42
Total	98.96	100.90	87.28	96.68	97.04
Cl	133	237	111	168	282
Cr	6	5	14	26	42
Ni	7	12	27	98	52
Cu	9	10	168	85	24
Zn	9	7	151	193	128
As	42	40	123746	19487	1494
Br	3*	2*	0*	0*	0*
Sr	146	279	2691	5702	1005
Ba	0*	0*	0*	0*	655
Ce	126	150	553	1436	199
Pb	0*	2*	17	81	38
Th	0*	1*	9	26	34
U	2*	16	4	5	4

*Indicates values below the detection limit

Sulphur expressed as S

Table 13 (continued)

<u>Number</u>	<u>40#</u>	<u>42</u>	<u>43</u>	<u>44</u>	<u>45</u>
SiO ₂	34.54	49.51	32.64	18.35	48.19
Al ₂ O ₃	4.49	9.42	2.29	3.72	7.95
TiO ₂	0.18	0.22	0.04	0.05	0.22
Fe ₂ O ₃	1.05	0.80	0.13	0.38	1.23
FeO	0.96	0.92	0.24	0.32	0.54
MgO	15.89	23.23	15.86	18.28	18.74
CaO	12.25	1.14	20.30	23.45	4.66
Na ₂ O	0.21	0.11	0.17	0.26	0.17
K ₂ O	0.55	0.68	0.24	0.28	1.35
MnO	0.06	0.02	0.03	0.05	0.03
P ₂ O ₅	0.15	0.05	0.10	0.10	0.15
H ₂ O ⁺	12.46	11.88	9.26	5.76	14.80
CO ₂	0.21	0.00	15.95	22.90	0.00
B ₂ O ₃	0.27	0.18	0.18	0.78	0.37
SO ₃	3.50	0.77	0.30	0.65	0.60
Total	86.77	98.93	97.73	95.33	99.00
Cl	138	63	86	71	60
Cr	36	37	9	19	41
Ni	70	59	18	35	89
Cu	94	24	17	22	27
Zn	127	47	31	30	54
As	68546	533	1220	3840	746
Br	0*	0*	0*	0*	0*
Sr	2152	2044	3012	4079	1954
Ba	0*	249	75	0*	151
Ce	3772	89	130	376	160
Pb	27	16	5*	17	28
Th	0*	10	8	1*	13
U	3*	0*	9	8	0*

*Indicates values below the detection limit

Sulphur expressed as S

Table 13 (continued)

<u>Number</u>	<u>46</u>	<u>48</u>	<u>51</u>	<u>52</u>	<u>53</u>
SiO ₂	8.14	67.50	66.16	41.22	63.50
Al ₂ O ₃	3.11	14.50	13.15	8.57	14.58
TiO ₂	0.00	0.47	0.42	0.17	0.38
Fe ₂ O ₃	0.08	1.75	1.68	1.31	2.13
FeO	0.00	0.36	0.44	0.16	0.48
MgO	4.27	4.22	4.41	7.22	5.80
CaO	46.20	1.72	1.43	17.36	1.40
Na ₂ O	0.23	0.85	0.58	0.17	0.35
K ₂ O	0.13	7.90	7.97	4.97	7.38
MnO	0.03	0.04	0.03	0.05	0.04
P ₂ O ₅	0.08	0.07	0.07	0.07	0.11
H ₂ O+	2.10	0.00	0.00	5.91	0.28
CO ₂	35.00	0.00	0.00	10.12	0.00
B ₂ O ₃	0.18	0.00	0.22	0.27	0.00
SO ₃	0.47	0.43	0.62	1.15	0.85
Total	100.02	99.81	97.18	98.54	97.28
Cl	62	342	240	112	193
Cr	6	18	20	13	22
Ni	6	20	25	18	24
Cu	21	13	19	22	12
Zn	9	61	75	93	162
As	215	533	736	2155	436
Br	0*	0*	0*	0*	0*
Sr	2925	466	1124	4832	1606
Ba	43	944	871	389	1045
Ce	101	87	86	174	91
Pb	8	32	74	137	59
Th	0*	35	36	27	39
U	2*	7	3*	5	0*

* Indicates values below the detection limit

Table 13 (continued)

<u>Number</u>	<u>55</u>	<u>57#</u>	<u>60</u>	<u>62#</u>	<u>64</u>
SiO ₂	56.99	27.45	16.32	25.89	52.15
Al ₂ O ₃	15.31	9.59	3.53	10.78	16.86
TiO ₂	0.45	0.06	0.01	0.38	0.68
Fe ₂ O ₃	1.26	0.60	0.21	0.98	3.75
FeO	2.06	0.00	0.18	1.92	0.56
MgO	6.16	12.75	7.22	4.31	5.44
CaO	1.25	0.77	35.56	22.05	4.41
Na ₂ O	0.24	0.13	0.23	0.24	0.24
K ₂ O	9.66	0.31	0.20	3.66	8.34
MnO	0.03	0.05	0.18	0.20	0.07
P ₂ O ₅	0.13	0.16	0.10	0.18	0.16
H ₂ O+	0.00	12.13	5.19	4.46	5.44
CO ₂	0.00	0.00	27.94	0.00	0.00
B ₂ O ₃	0.18	0.18	0.13	0.18	0.13
SO ₃	4.12	11.39	1.72	16.93	1.62
Total	97.84	75.57	98.72	92.16	99.85
Cl	113	103	89	291	262
Cr	14	8	7	19	36
Ni	26	14	16	27	58
Cu	9	325	26	88	26
Zn	94	185	26	211	130
As	2195	247554	12846	62721	4572
Br	0*	0*	0*	0*	0*
Sr	130	126	3672	17735	2406
Ba	513	0*	0*	242	768
Ce	188	1664	1044	2441	349
Pb	75	21	7*	68	58
Th	29	12	5*	17	39
U	0*	8	6	1*	4

* Indicates values below the detection limit

Sulphur expressed as S

Table 13 (continued)

<u>Number</u>	<u>66</u>	<u>67</u>	<u>68</u>	<u>74</u>	<u>75</u>
SiO ₂	4.42	34.97	3.30	47.23	56.25
Al ₂ O ₃	0.98	1.58	1.16	16.78	17.76
TiO ₂	0.00	0.00	0.00	0.54	0.44
Fe ₂ O ₃	0.00	0.00	0.03	4.34	2.68
FeO	0.28	0.08	0.16	0.76	0.38
MgO	3.22	11.66	0.47	4.12	2.53
CaO	50.26	23.10	53.20	7.40	2.52
Na ₂ O	0.25	0.27	0.26	0.32	0.49
K ₂ O	0.10	0.11	0.19	4.41	8.93
MnO	0.04	0.02	0.02	0.11	0.06
P ₂ O ₅	0.04	0.02	0.03	0.17	0.10
H ₂ O+	1.27	0.89	0.60	9.31	5.66
CO ₂	39.49	24.00	39.47	3.57	0.00
B ₂ O ₃	0.13	0.18	0.27	0.18	0.18
SO ₃	0.18	0.13	0.23	0.33	0.87
Total	100.66	97.01	99.39	99.57	98.85
Cl	159	954	117	105	106
Cr	4	3	14	179	32
Ni	3*	1*	24	285	202
Cu	15	6	10	42	66
Zn	4	7	16	142	82
As	203	157	140	237	584
Br	1*	7*	3*	1*	0*
Sr	2036	1012	446	413	514
Ba	52	156	0*	1034	898
Ce	103	37	153	153	164
Pb	10	3*	3*	108	112
Th	0*	1*	2*	41	50
U	0*	3*	1*	7	21

*Indicates values below the detection limit

Figure 13 (continued)

<u>Number</u>	<u>76 #</u>	<u>79 #</u>	<u>82</u>	<u>85</u>	<u>86</u>
SiO ₂	34.18	34.92	39.81	35.44	11.18
Al ₂ O ₃	12.33	16.84	9.42	9.49	4.69
TiO ₂	0.35	0.37	0.34	0.34	0.03
Fe ₂ O ₃	3.15	3.17	2.81	3.57	0.61
FeO	0.44	0.56	0.36	0.19	0.08
MgO	3.31	3.37	8.56	2.57	1.96
CaO	14.39	12.69	11.95	20.30	44.45
Na ₂ O	0.23	0.28	0.43	0.21	0.15
K ₂ O	3.01	3.15	2.55	1.42	0.32
MnO	0.05	0.05	0.12	0.03	0.02
P ₂ O ₅	0.09	0.19	0.16	0.45	0.07
H ₂ O+	12.54	13.04	5.70	9.12	3.06
CO ₂	3.10	0.00	15.39	15.95	34.82
B ₂ O ₃	0.22	0.27	0.13	0.00	0.18
SO ₃	11.76	12.29	0.30	0.23	0.20
Total	99.15	101.19	98.03	99.31	101.82
Cl	66	84	40	69	72
Cr	146	153	144	145	33
Ni	271	313	243	559	79
Cu	28	37	26	48	20
Zn	87	88	81	104	22
As	176	243	224	81	34
Br	2*	3*	3*	14	2*
Sr	312	1390	468	1120	423
Ba	738	742	845	500	128
Ce	103	100	121	105	86
Pb	70	59	93	127	17
Th	23	20	29	30	7
U	3*	5	23	9	4

* Indicates values below the detection limit

Sulphur expressed as S

Table 13 (continued)

<u>Number</u>	<u>87</u>	<u>88</u>	<u>89</u>	<u>90</u>	<u>91</u>
SiO ₂	2.07	19.21	1.93	13.87	4.21
Al ₂ O ₃	1.63	7.37	3.96	6.55	8.22
TiO ₂	0.00	0.16	0.00	0.13	0.00
Fe ₂ O ₃	0.07	2.07	0.00	1.44	0.40
FeO	0.00	0.19	0.11	0.08	0.08
MgO	0.55	1.31	0.15	0.89	0.27
CaO	53.90	38.36	55.30	42.35	49.04
Na ₂ O	0.21	0.17	0.30	0.19	0.27
K ₂ O	0.10	0.90	0.10	0.91	0.25
MnO	0.01	0.04	0.02	0.05	0.04
P ₂ O ₅	0.06	0.11	0.03	0.07	0.03
H ₂ O+	0.27	3.58	0.25	2.74	0.55
CO ₂	40.48	27.41	37.07	30.62	38.53
B ₂ O ₃	0.22	0.18	0.27	0.27	0.32
SO ₃	0.20	0.28	0.25	0.15	0.10
Total	99.77	101.34	99.74	100.31	102.31
Cl	109	65	81	91	134
Cr	15	96	6	38	13
Ni	16	268	6	57	24
Cu	14	25	15	21	17
Zn	8	55	15	76	27
As	24	54	51	50	46
Br	0*	3*	0*	0*	3*
Sr	254	350	312	212	199
Ba	44	323	64	140	43
Ce	140	84	139	120	145
Pb	8	30	5*	29	19
Th	4*	11	0*	11	4*
U	2*	5	2*	0*	0*

* Indicates values below the detection limit

Table 13 (continued)

<u>Number</u>	<u>92</u>	<u>93</u>	<u>94</u>	<u>95</u>	<u>96</u>
SiO ₂	16.96	4.13	7.33	1.58	17.35
Al ₂ O ₃	8.98	1.56	4.84	0.91	7.74
TiO ₂	0.15	0.00	0.00	0.00	0.16
Fe ₂ O ₃	1.42	0.43	0.66	0.07	1.16
FeO	0.10	0.08	0.06	0.09	0.51
MgO	1.09	0.35	0.55	0.28	1.67
CaO	38.50	52.85	47.95	54.60	37.45
Na ₂ O	0.20	0.24	0.23	0.27	0.28
K ₂ O	1.24	0.28	0.34	0.11	1.38
MnO	0.04	0.03	0.03	0.01	0.05
P ₂ O ₅	0.11	0.04	0.05	0.03	0.19
H ₂ O+	3.38	0.43	0.24	1.90	4.51
CO ₂	28.08	39.70	37.68	39.15	27.32
B ₂ O ₃	0.00	0.27	0.18	0.27	0.00
SO ₃	0.20	0.13	0.13	0.25	0.43
Total	100.45	100.52	100.27	99.52	100.20
Cl	67	129	106	119	54
Cr	33	17	12	7	35
Ni	50	19	28	6	74
Cu	22	15	18	18	34
Zn	50	19	29	10	61
As	66	36	52	64	900
Br	0*	0*	1*	3*	0*
Sr	228	315	253	453	2076
Ba	246	17	86	11*	210
Ce	131	157	154	136	173
Pb	45	15	37	6*	34
Th	21	5*	15	1*	8
U	0*	0*	6	1*	1*

* Indicates values below the detection limit

Table 13 (continued)

<u>Number</u>	<u>99</u>	<u>100</u>	<u>101</u>	<u>102</u>	<u>103</u>
SiO ₂	45.08	41.44	1.78	53.89	4.76
Al ₂ O ₃	17.03	13.44	1.58	23.62	0.75
TiO ₂	0.48	0.41	0.00	0.54	0.00
Fe ₂ O ₃	3.47	2.79	0.06	6.63	0.23
FeO	0.96	0.86	0.12	0.24	0.24
MgO	8.11	5.57	0.54	3.42	0.58
CaO	6.50	14.52	53.20	1.69	51.10
Na ₂ O	0.18	0.39	0.20	0.17	0.32
K ₂ O	4.01	4.17	0.11	2.88	0.11
MnO	0.10	0.33	0.02	0.03	0.04
P ₂ O ₅	0.17	0.19	0.12	0.22	0.05
H ₂ O+	9.94	6.40	0.32	7.35	0.58
CO ₂	0.00	8.04	40.63	0.00	40.15
B ₂ O ₃	3.18	0.97	0.27	0.08	0.18
SO ₃	0.43	0.43	0.23	0.18	0.60
Total	99.64	99.95	99.18	100.94	99.69
Cl	56	62	101	58	131
Cr	99	79	22	416	5
Ni	174	147	15	827	42
Cu	42	42	14	48	17
Zn	123	105	12	187	31
As	646	461	34	121	2291
Br	2*	0*	1*	0*	0*
Sr	3360	2134	473	86	1523
Ba	624	512	169	760	0*
Ce	181	161	130	143	288
Pb	84	71	12	66	3*
Th	29	23	2*	44	0*
U	3*	2*	3*	2*	0*

*Indicates values below the detection limit

Table 13 (continued)

<u>Number</u>	<u>104</u>	<u>105</u>	<u>108</u>	<u>109</u>	<u>110</u>
SiO ₂	28.59	44.33	37.31	24.17	10.42
Al ₂ O ₃	14.39	20.32	11.10	9.47	6.52
TiO ₂	0.25	0.50	0.38	0.19	0.07
Fe ₂ O ₃	1.98	2.97	3.04	1.66	0.87
FeO	0.52	0.24	0.72	0.44	0.24
MgO	4.49	4.06	7.81	7.64	2.46
CaO	27.30	11.54	12.17	28.70	43.40
Na ₂ O	0.33	0.31	0.24	0.23	0.30
K ₂ O	2.02	1.80	2.70	1.07	0.93
MnO	0.09	0.03	0.08	0.05	0.13
P ₂ O ₅	0.21	0.22	0.22	0.11	0.15
H ₂ O+	5.50	12.57	12.21	7.26	2.31
CO ₂	11.88	2.38	0.00	19.24	31.63
B ₂ O ₃	0.37	0.00	6.65	0.00	0.00
SO ₃	0.40	0.30	2.52	0.25	0.30
Total	98.32	101.57	97.15	100.48	99.73
Cl	48	79	86	42	110
Cr	49	107	82	46	18
Ni	109	111	146	88	33
Cu	24	40	42	38	26
Zn	78	101	119	60	30
As	622	6355	3476	219	397
Br	0*	0*	0*	1*	0*
Sr	1523	1681	9213	4060	4155
Ba	253	23	461	242	75
Ce	169	622	287	86	167
Pb	41	37	53	56	30
Th	11	16	15	9	6
U	1*	3*	0*	1*	3*

* Indicates values below the detection limit

Table 13 (continued)

<u>Number</u>	<u>112</u>	<u>115</u>	<u>116</u>	<u>117</u>	<u>118</u>
SiO ₂	42.04	45.87	45.04	37.66	4.33
Al ₂ O ₃	13.93	14.44	19.61	7.33	3.32
TiO ₂	0.38	0.45	0.44	0.24	0.00
Fe ₂ O ₃	3.29	3.99	3.95	1.64	0.30
FeO	0.53	0.66	0.60	0.64	0.24
MgO	10.12	11.21	11.02	16.10	8.48
CaO	10.31	6.37	7.34	1.99	42.14
Na ₂ O	0.27	0.17	0.19	0.12	0.21
K ₂ O	2.49	3.22	3.11	0.80	0.20
MnO	0.08	0.07	0.08	0.05	0.04
P ₂ O ₅	0.23	0.18	0.19	0.14	0.03
H ₂ O ⁺	11.75	10.33	7.69	6.67	0.40
CO ₂	0.00	0.00	0.00	0.00	33.21
B ₂ O ₃	2.35	1.28	1.54	0.69	0.00
SO ₃	1.50	0.40	1.32	4.17	1.00
Total	99.27	98.64	102.12	78.24	93.90
Cl	131	56	130	76	127
Cr	82	92	92	54	9
Ni	146	163	160	94	12
Cu	35	57	33	296	36
Zn	114	135	134	151	9
As	495	530	481	100319	116
Br	0*	1*	2*	0*	1*
Sr	7681	6763	4738	77364	13147
Ba	675	1085	784	0*	304
Ce	116	153	120	3785	105
Pb	56	154	57	34	15
Th	17	25	19	2*	0*
U	1*	0*	3*	0*	0*

*Indicates values below the detection limit

Table 13 (continued)

<u>Number</u>	<u>119</u>	<u>127</u>	<u>135</u>	<u>146</u>	<u>156</u>
SiO ₂	3.91	42.01	9.51	39.31	51.86
Al ₂ O ₃	4.64	15.57	3.99	14.34	18.46
TiO ₂	0.00	0.51	0.04	0.35	0.47
Fe ₂ O ₃	0.29	4.01	0.48	2.47	3.94
FeO	0.18	0.64	0.12	0.40	0.56
MgO	3.08	4.25	0.70	10.45	6.40
CaO	48.30	9.24	49.70	7.67	4.62
Na ₂ O	0.22	0.29	0.26	0.40	0.25
K ₂ O	0.27	4.64	0.43	3.26	5.44
MnO	0.03	0.10	0.31	0.06	0.15
P ₂ O ₅	0.04	0.20	0.06	0.30	0.17
H ₂ O+	0.24	5.48	1.09	8.54	7.70
CO ₂	35.11	0.00	32.90	0.00	0.00
B ₂ O ₃	0.16	12.20	0.00	13.56	0.88
SO ₃	1.30	0.50	0.08	0.47	0.33
Total	97.77	99.64	99.67	101.58	101.23
Cl	105	73	125	57	74
Cr	6	88	7	51	74
Ni	18	190	21	109	140
Cu	39	34	18	41	35
Zn	13	125	75	121	144
As	698	375	78	455	358
Br	0*	2*	1*	0*	1*
Sr	17765	1520	199	9417	1734
Ba	180	530	82	476	818
Ce	165	193	130	164	150
Pb	16	135	124	84	84
Th	0*	16	9	31	29
U	0*	3*	28	6	8

* Indicates values below the detection limit

Table 13 (continued)

<u>Number</u>	<u>161</u>	<u>162</u>	<u>164</u>	<u>165</u>	<u>166</u>
SiO ₂	51.60	43.50	44.64	42.73	48.57
Al ₂ O ₃	18.11	15.42	21.03	6.89	12.47
TiO ₂	0.60	0.50	0.56	0.28	0.55
Fe ₂ O ₃	4.51	3.84	4.43	1.71	4.48
FeO	0.84	0.70	0.76	0.60	0.53
MgO	5.90	9.80	4.85	11.51	8.51
CaO	2.59	4.53	5.73	7.40	1.20
Na ₂ O	0.19	0.17	0.26	0.16	0.19
K ₂ O	6.01	4.24	5.50	2.12	5.44
MnO	0.07	0.10	0.12	0.07	0.05
P ₂ O ₅	0.16	0.31	0.22	0.16	0.21
H ₂ O+	7.66	9.14	10.05	11.67	11.41
CO ₂	0.00	0.00	0.00	10.09	0.92
B ₂ O ₃	0.97	6.19	0.93	3.08	0.88
SO ₃	0.50	0.35	0.40	1.05	0.28
Total	99.71	98.88	99.48	99.52	95.69
Cl	65	119	71	98	172
Cr	132	91	121	36	130
Ni	219	155	203	60	176
Cu	90	50	53	43	62
Zn	163	171	146	130	199
As	529	515	453	7809	1950
Br	0*	0*	1*	0*	0*
Sr	1387	4893	1634	2629	3530
Ba	489	486	667	0*	481
Ce	217	221	207	729	273
Pb	163	120	141	78	114
Th	32	25	26	19	39
U	6	3*	5	6	4

*Indicates values below the detection limit

Table 13 (continued)

<u>Number</u>	<u>167</u>	<u>168</u>	<u>171</u>	<u>174</u>
SiO ₂	47.85	47.77	46.47	49.93
Al ₂ O ₃	7.73	16.25	12.31	14.73
TiO ₂	0.14	0.82	0.42	0.43
Fe ₂ O ₃	0.99	5.62	3.21	3.27
FeO	0.22	0.46	0.48	0.40
MgO	17.67	4.77	10.76	14.32
CaO	1.99	3.26	1.04	1.05
Na ₂ O	0.14	0.35	0.47	0.48
K ₂ O	0.80	5.96	3.69	3.80
MnO	0.05	0.08	0.07	0.08
P ₂ O ₅	0.24	0.47	0.25	0.26
H ₂ O+	15.92	10.00	15.41	7.88
CO ₂	0.00	1.68	2.69	0.00
B ₂ O ₃	0.62	0.52	1.09	4.08
SO ₃	1.40	0.25	0.47	0.26
Total	95.76	98.26	98.83	100.97
Cl	123	243	64	60
Cr	15	66	82	113
Ni	35	95	151	110
Cu	61	58	47	62
Zn	100	241	170	128
As	36688	852	683	474
Br	0*	0*	0*	0*
Sr	1617	623	3379	3883
Ba	0*	1120	546	533
Ce	2641	273	226	185
Pb	33	209	109	65
Th	9	52	34	39
U	5	6	0*	0*

* Indicates values below the detection limit

CHAPTER V

DETAILED STRATIGRAPHY AND STRUCTURE OF THE BORATE DEPOSITS

1. Introduction

The general stratigraphy and structure of the borate deposits and associated rocks were discussed briefly in Chapter III. A generalized stratigraphic and geological column of the Emet borate district (Fig.7) and a section from Sarikaya (Hisarcik) showing the borate zone (Fig.8) were given on pages 31 and 38, respectively.

This present chapter deals with stratigraphic and structural studies of the Emet borate deposits, based primarily on detailed mapping and observations undertaken during the summers of 1972, 73 and 74. The detailed mineralogy and geochemistry of the deposits will be discussed separately in the next two chapters. Detailed maps were completed for the localities where the commercially important borate deposits occur. Fig.12 shows the detailed mapping areas, which are indicated with cross-hatching on the locality map. The detailed geology of the Espey-Killik and Hisarcik areas, which contain most of the commercially viable borate deposits are shown on Figs. 13 and 14 respectively.

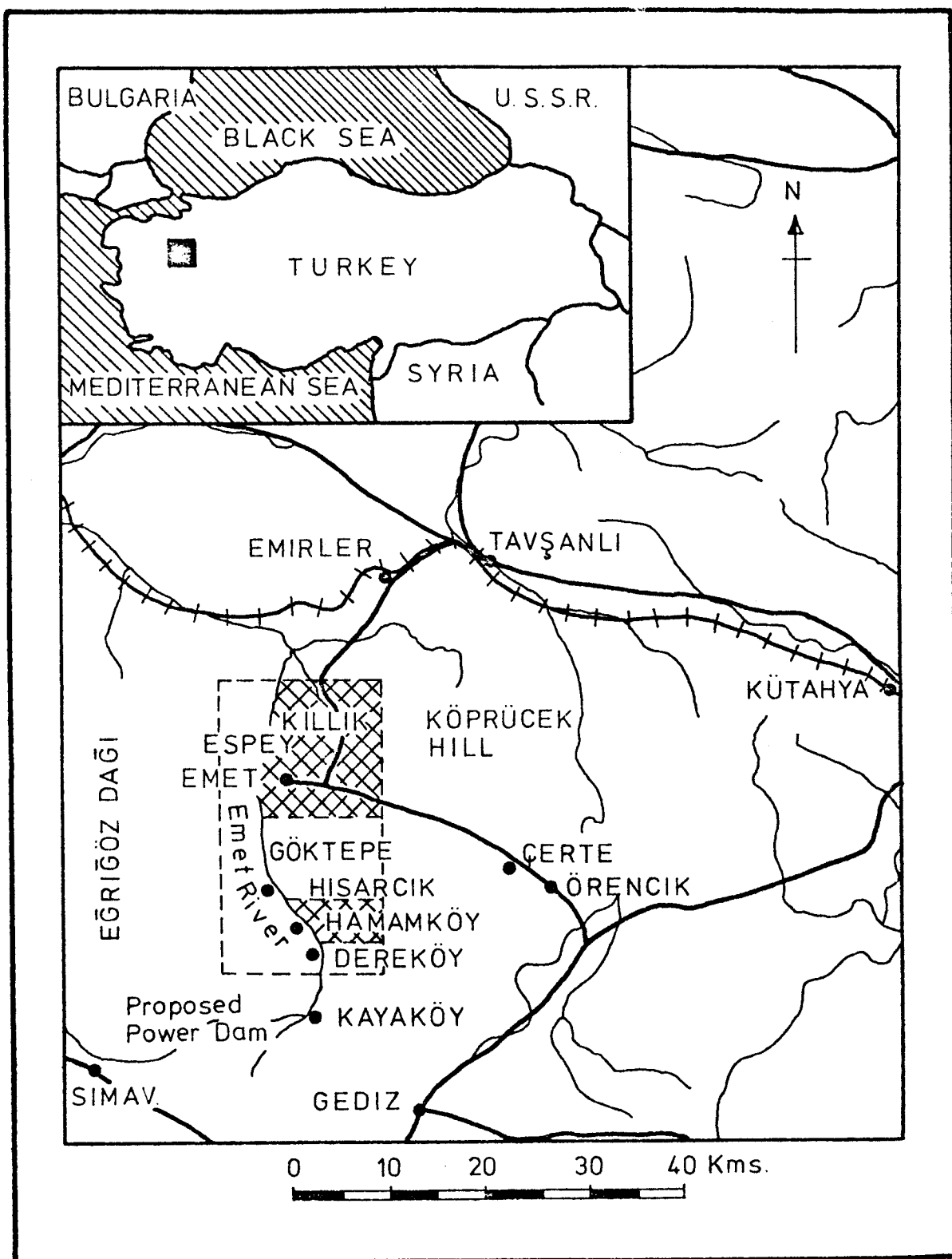


Fig.12. Locality map of the Emet borate district. Detailed mapping areas are indicated by cross-hatching.

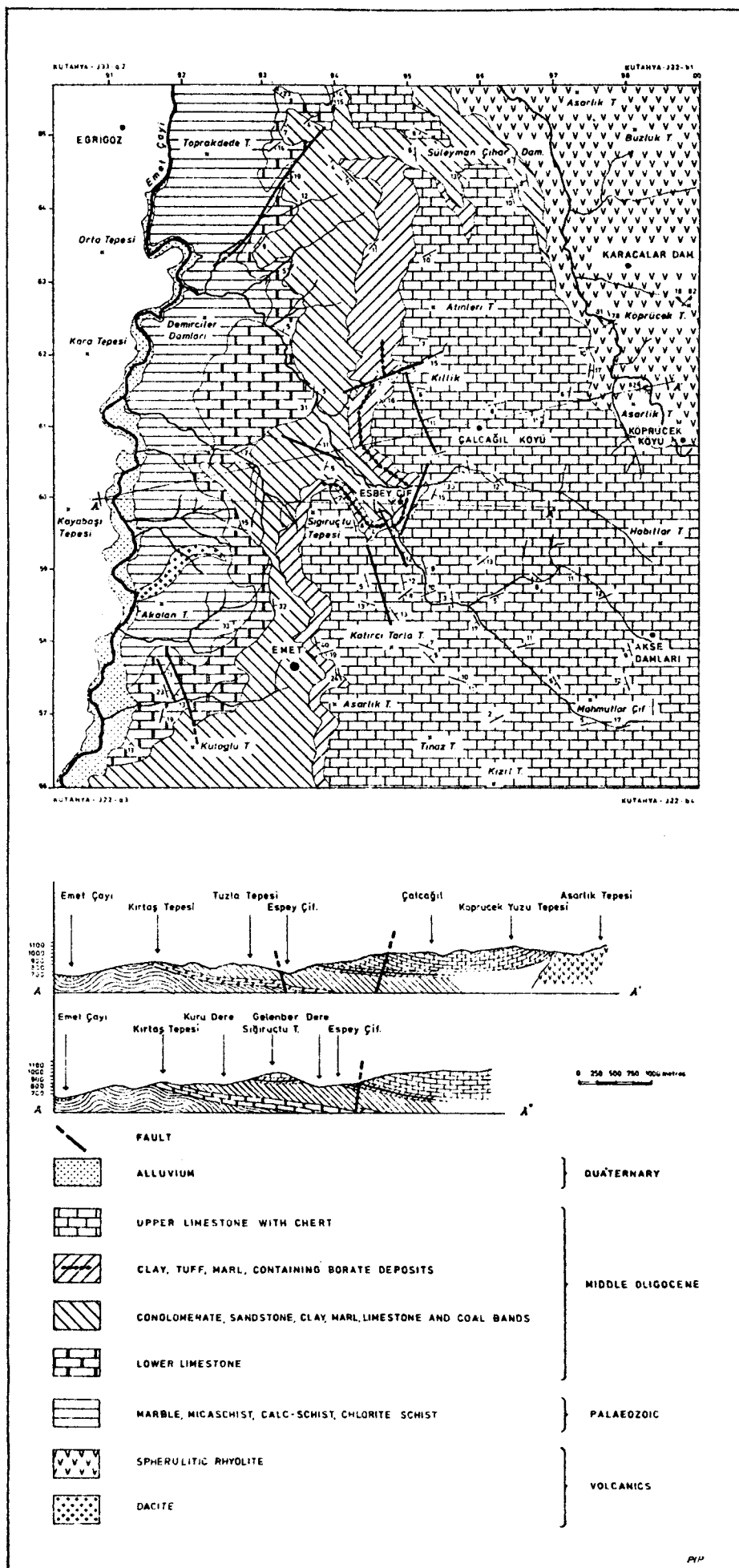


Fig.13. Detailed geological map of the Espey-Killik area.

Stratigraphic and structural studies indicate that the Emet borates were deposited in two distinct sedimentary, non-marine basins, elongated in a north-south direction and limited on the east and west by the basement metamorphic complex. The borate minerals are interbedded with marls, thin-bedded limestones, volcanic tuffs and clays which appear to have been derived mostly from a volcanic terrain.

The Emet borate deposits are shown to be older and mineralogically more complex than was previously thought. They are considered to have formed within the muds of playa lakes during the Middle Oligocene.

2. Stratigraphy

The borate zone varies in thicknesses between 0-100 metres. It consists mainly of nodules and stringers of colemanite and minor amounts of the other borate and non-borate minerals. These are interbedded with montmorillonitic and illitic clays, volcanic tuffs, marl and soft thin-bedded limestone (Figs. 13 and 14; see also Figs. 7 and 8). The borates and interbedded clay, tuff etc. formation rest conformably on the red formation (Figs. 12, 13 and 14; see also Fig. 6). Borates and associated clays and tuffs, which seem to have been derived mainly from a volcanic terrain, show a repetition of the rhythmic deposition and finally towards the top of the borate zone, are succeeded by limestone (Plates 20 and 21; see also Fig. 8).

The borate deposits of the Emet district occur in varying proportions and frequency throughout the Middle Oligocene sediments. The borate zone shows lateral and vertical facies changes throughout the deposits. The calcium borate facies



Plate 20

Plate showing rhythmic deposition of borates (mainly colemanite), clay and tuff, etc. (Sarıkaya locality, Hisarcik).

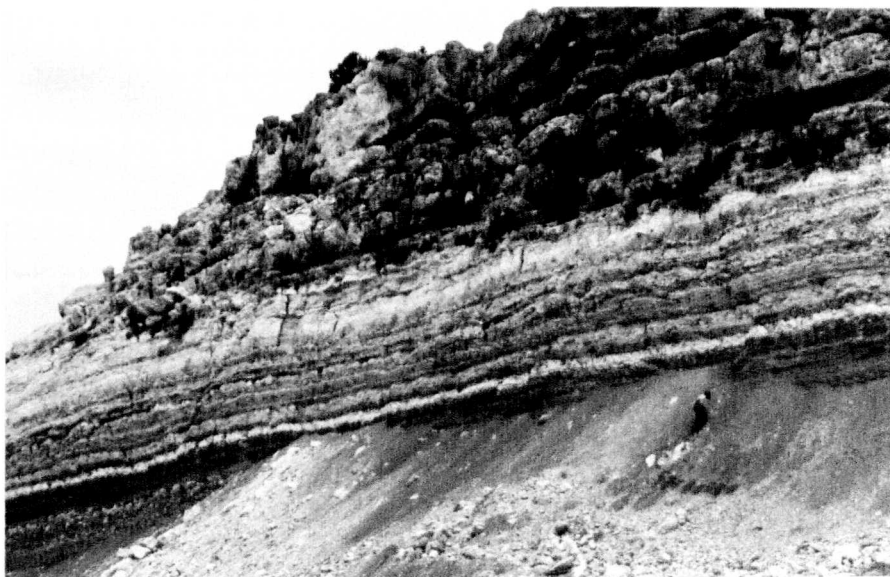


Plate 21

Plate showing the borate zone with daisy beds and the upper limestone overburden (Kapıkaya locality, Hisarcik).

is roughly lenticular, reaching its maximum thickness in the central parts of the basins. Around the outer parts of the local basins, colemanite-bearing clay and tuff grades laterally into green or green-grey coloured altered tuff and clay which are mainly montmorillonitic and illitic clay groups. Along the abrupt northern and southern termination of the Emet borate basins, the barren facies dies out. The facies correlation diagrams of the borate zone for Espey-Killik and Hisarcik localities are shown respectively on Figs. 15 and 16. As can be seen from Figs. 15 and 16, some of the borate and interbedded clay and tuff beds change laterally and show a lenticular character, as well as vertical facies changes.

The borate zone reaches its maximum thickness (up to 100 meters) at the Espey and Killik localities. Beyond the commercial areas, the borate zone is very thin or absent. There are six different borate (colemanite) seams occurring at different levels within the borate zone, but they show lateral facies changes within short distances, because of their lenticular occurrence. Fig. 17 shows the six different colemanite seams alternating with clay and tuff at Killik (see also Fig. 15 for the Espey locality). Colemanite seams and interbedded clay and tuff exhibit the same character at the Hisarcik locality. Fig. 16 illustrates the discontinuous nature of the colemanite seams. Total thickness of the borate zone at the Hisarcik locality is up to 30 meters with the highest borate concentrations in the upper zone (see Fig. 8) and the poor colemanite beds and high arsenic sulphides (realgar and orpiment) and sulphur concentrations in the lower zone (Plate 22).

At the Göktepe locality, north of Hisarcik, the borate zone

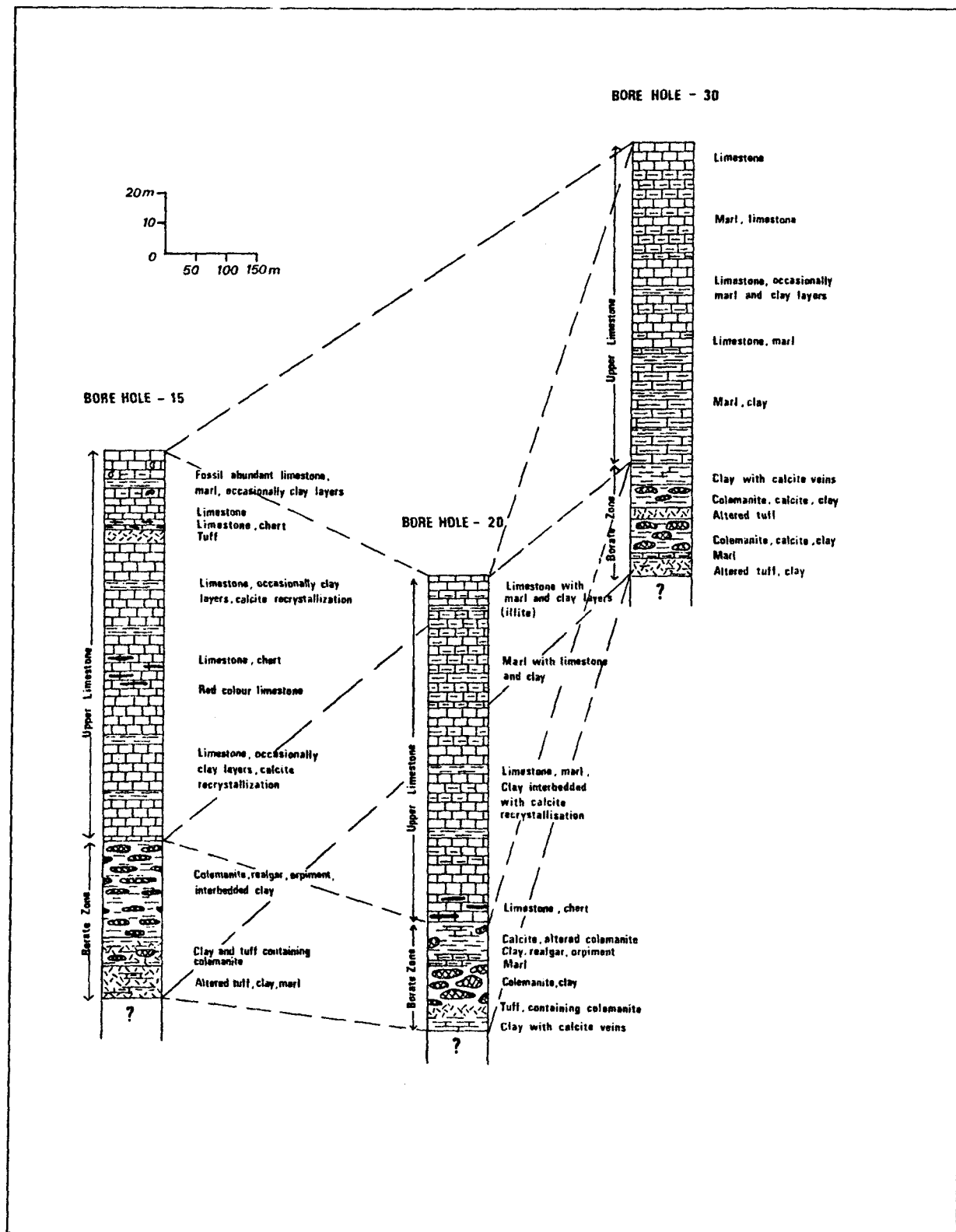


Fig.15. Facies correlation of bore holes 15, 20 and 30 in the Espey locality (Bore holes are shown on the isopach map of the Espey borate zone, part of the northern borate zone).

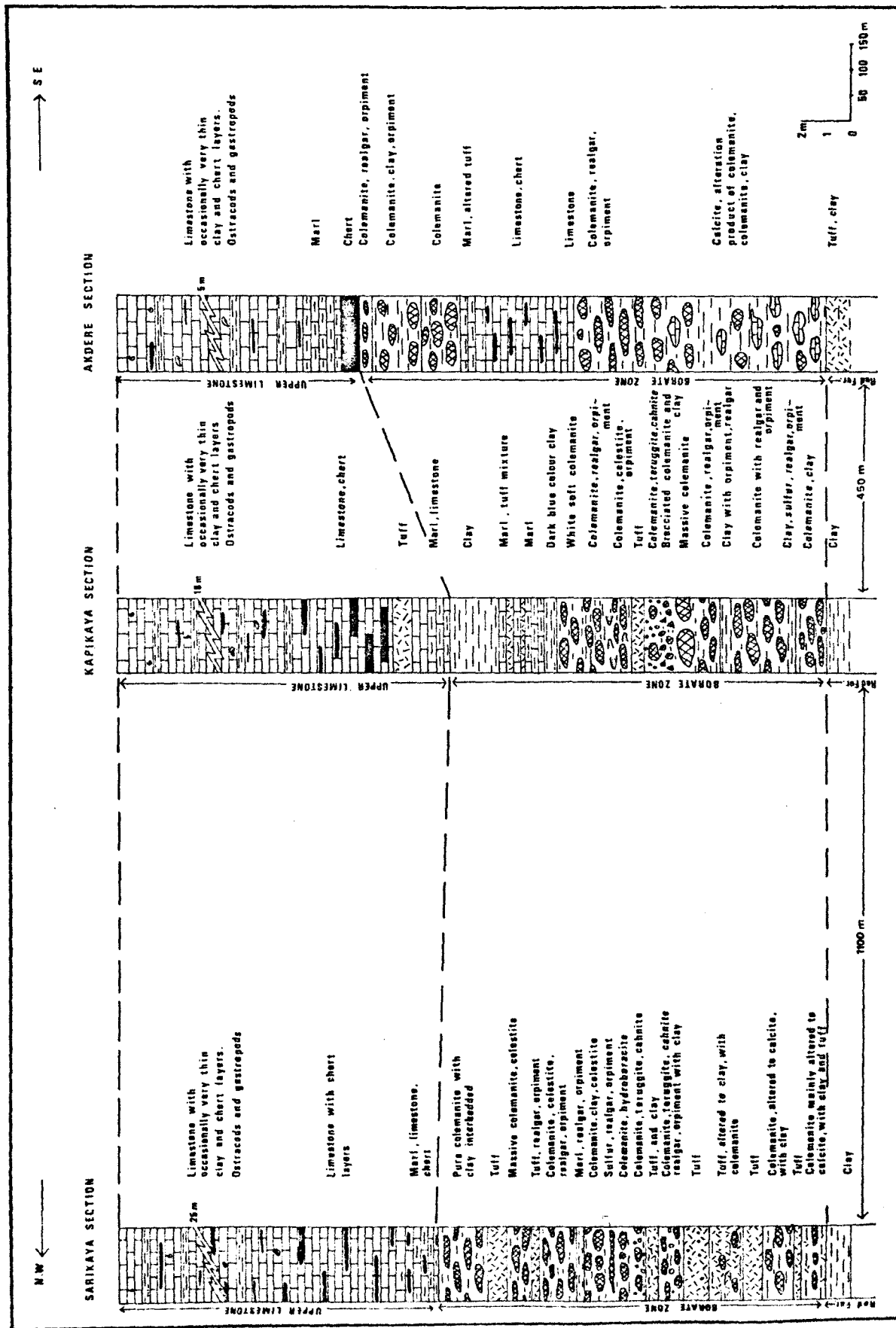


Fig.16. Facies correlation of the Sarikaya, Kapikaya and Akdere sections, Hisarcik. (The southern borate zone).

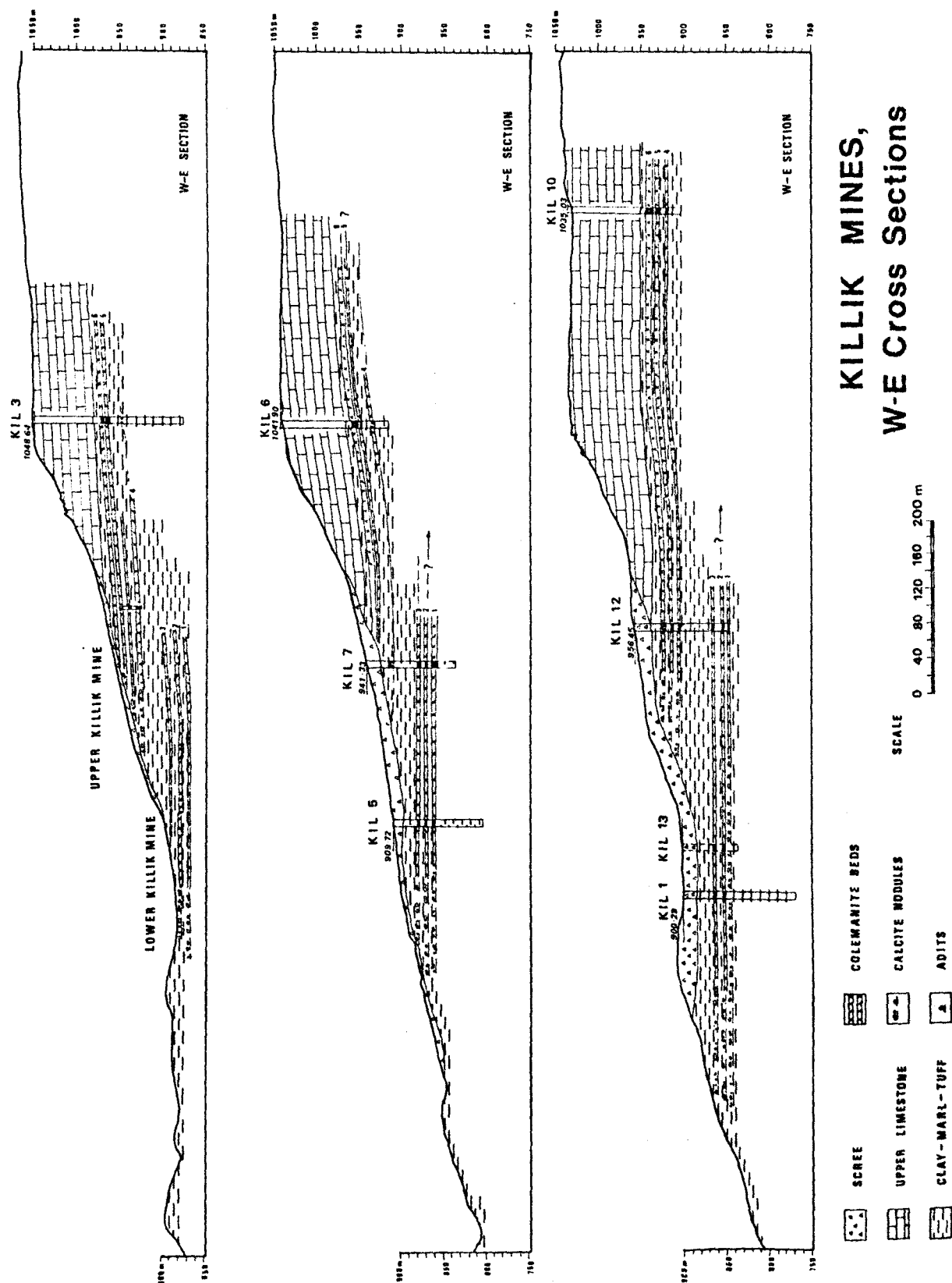


Fig.17. W-E cross sections of Killik borate deposit, showing six different colemanite seams alternating with clay and tuff.

becomes thinner with up to 2 meters of colemanite, probably because this is the outer edge of the local basin (Plate 23). The continuity of the borate zone in the Middle Oligocene has been traced further southeast of Hisarcik, to near Hamamköy and Dereköy, adjacent to the Emet River; here there are two outcrops of colemanite and interbedded sediments. The areas at Hamamköy and Dereköy which contain the borate ore are at least 10-20 meters wide and 100 meters long. The borate horizon may also be traced on the west bank of the Emet River, south of Hisarcik village and on the road to the Yenice village (see Fig.6). This extension of the borate beds on the west bank of the Emet River has no commercial importance, because they have been altered by weathering and erosion.

Due to the small number of bore holes and lack of analysis and sudden lateral and vertical facies changes of this formation, it is very difficult to correlate an individual layer of the borates and interbedded sediments. Also, correlation between individual beds in different localities is not easy because of the difficulty of distinguishing one bed from another and because of the discontinuous nature of beds when traced over large areas.

Clays occur interbedded with colemanite and tuff in varying thicknesses throughout the deposits. The clay appears dark green or green-grey in colour at different stages of the succession.

Tuff shows a fine to coarse grain size and sometimes gradation. Fine and coarse grained tuffs occur mainly as different beds. They appear usually grey in colour, but sometimes greenish-grey, when fresh. A typical tuff sample is shown on Plate 24.



Plate 22 Plate showing the poor colemanite beds and high arsenic sulphides and sulphur concentrated in the lower part of the borate zone, Hisarcik.



Plate 23 Plate showing the borate zone at the Goktepe locality, where colemanite has been replaced by calcite.

The detailed petrography of clay and tuff is described in Chapter IV.

Colemanite in the borate zone occurs in many different forms ranging from minute stellate clusters of crystals in clay to ovoid nodules up to 0.5 metres in diameter (Plate 25). Nodules with radiating structures are by far the commonest form of colemanite in the deposits, but these nodules exhibit a large variety of shapes and sizes (Plate 26 and Chapter VI). The majority of colemanite nodules are often surrounded by haloes of green clay about 5-10 cm thick, which closely follow the shape of the nodules. When massive colemanite occurs in large spherical nodules, the banded clay surrounding it appears to be heaved or pushed up (see Plate 25). At Kapikaya (Hisarcik) and Dereköy localities, the smaller colemanite nodules with spherical shapes make distinct borate beds (daisy beds) which occur very locally in the upper part of the borate zone (see Plate 21). Colemanite also occurs as massive (see Plate 25), granular, thin layers interbedded with clay, and sometimes as disseminated crystals in a clay matrix or as a colemanite-clay breccia in the upper part of the borate zone. Individual beds with characteristically shaped nodules can not be traced more than 200 meters laterally.

Colemanite is often almost completely replaced by calcite in surface outcrops and adjacent to faults, as a result of modern weathering. Due to alteration of colemanite to calcite, only pseudomorphs and the general outline of the original colemanite layers may remain near or at the surface. At the Espey and Killik localities, no colemanite is found in the first five or ten meters from the surface of the borate beds. The transition from the leached friable calcite in the altered zone to hard crystalline colemanite occurs in less than a metre.

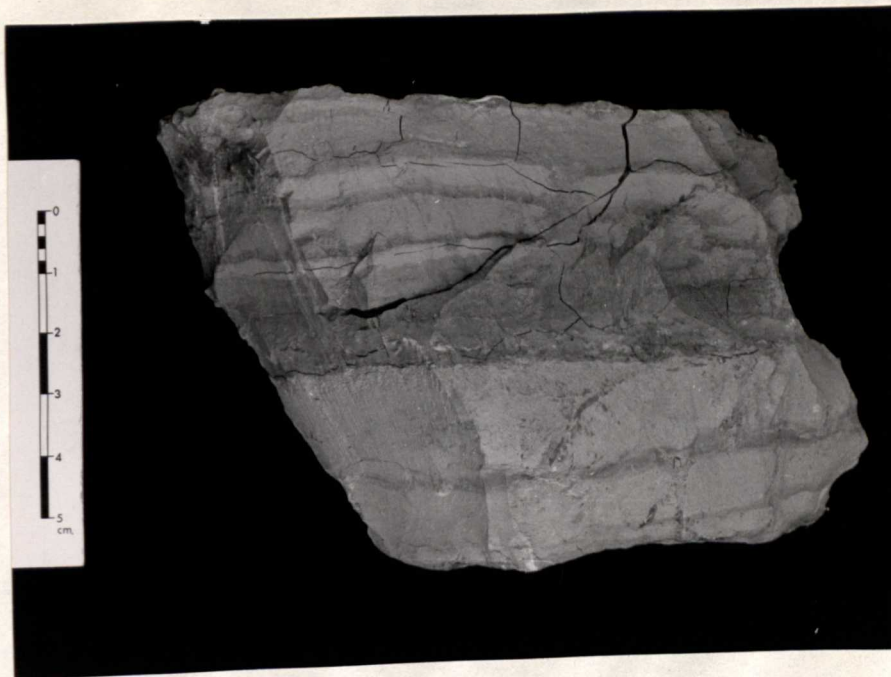


Plate 24 A typical tuff occurrence in the borate zone, sample taken from Kapikaya (Hisarcik).



Plate 25 Clay, colemanite, tuff and stellate clusters of colemanite crystals in clay in the borate zone. Note also vughs and veins of colemanite and arching-up of clay and tuff by colemanite nodules. (Sarıkaya, Hisarcik).

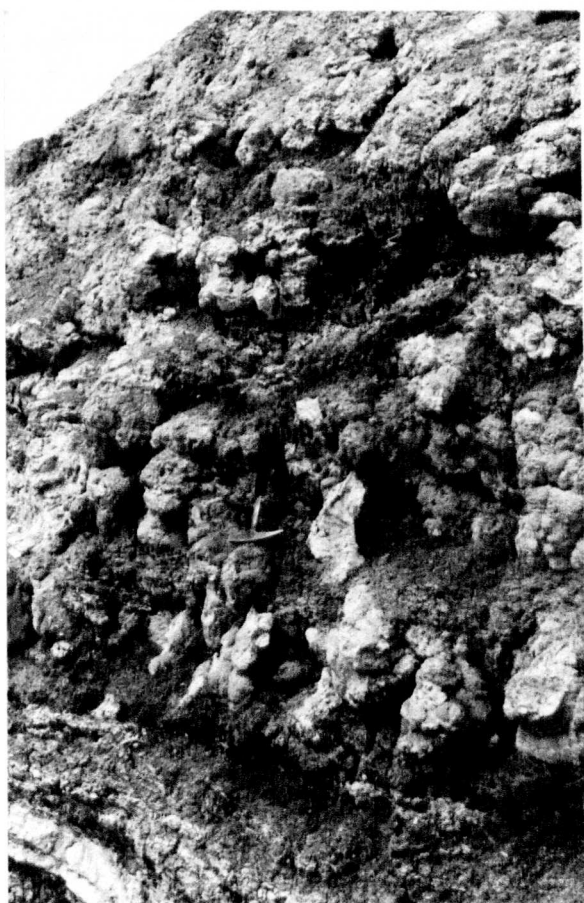


Plate 26 Colemanite nodules showing a large variety
of shapes and sizes (Kapikaya locality, Hisarcik).

This is also observed at Hisarcik, Göktepe and on the west side of the Emet River, where the cap-rock, the upper limestone, is almost stripped away by erosion. This is clearly seen at Göktepe locality, where colemanite is almost completely replaced by calcite on the outcrops of the colemanite beds in the borate zone (see Plate 23).

Fibrous gypsum veins and desert rose-shaped selenite crystals, which are a crystalline form of gypsum, occur in Kapıkaya (Hisarcik) and Göktepe localities. The borate zone is sometimes riddled with large numbers of thin, irregular and interconnected veins of fibrous gypsum, which are concentrated in very small areas within the borate zone, as observed at Göktepe locality.

The Emet borate zone is also characterized by relatively high levels of arsenic sulphides (as realgar and orpiment), strontium sulphate (celestite) and sulphur. The lower part of the borate zone contains more arsenic sulphide minerals and sulphur than the upper part (see Plate 22). Realgar and celestite occur as euhedral to sub-euhedral and disseminated crystals in the clay surrounding colemanite masses, as well as intergrowth with colemanite. Realgar frequently and celestite more rarely are found encrusted in vugs of colemanite nodules (see Plate 25).

3. Structure and thickness

The thickness of the borate zone varies from one place to another, probably because of deposition in a chain of interconnected lakes. The total thickness of the borate zone exceeds 100 metres (see Fig.7). Structurally, the thickest part of the borate basin is near the northern edge of the Emet district.

The depositional basin of the borate minerals is aligned north-south and mainly outcrops on the east side of the Emet River from Dereköy north almost to Killik(see Fig.12). The borate zone just like the rest of the Middle Oligocene sedimentary formations strikes roughly parallel to the Emet River, its dip ranging from nearly horizontal to over 20° towards the east. Detailed mapping (see Figs. 13 and 14) has shown that the Middle Oligocene sedimentary formations, including the borate zone, are far more faulted than was previously thought, hence lower grades of B_2O_3 in narrow fault zones may be more frequently found.

The borate zone is dislocated by NW-SE trending gravity faults, many of which are still active. NE-SW trending gravity faults occurred after the deposition of borates, but they are not active at present. The Gediz earthquake in 1970 has resulted in fresh NW-SE trending fissures and the borate deposits have been affected by movement of NW-SE trending faults.

The predominant faults are normal, with dips ranging from 30° to vertical. Steeply dipping beds are present near the principal faults. The major movement is vertical, occasional horizontal slickensides on the limestone suggest that a horizontal movement has also occurred. Thinning of the borate zone adjacent to northwest trending faults is evident at many localities. The thinning of the borate zone on up-throw blocks and the indications of greater fault displacement with depth are considered to be evidence of some structural movement contemporaneous with borate deposition. Although small folds have been observed in the borate zone at several localities, they do not appear to be a major cause of variation in the thickness of the ore body.

A major structural element in the southern area is a NW-SE trending fault, which extends along the Emet River and displaces the borate zone and the rest of the Middle Oligocene sediments vertically. The lake beds appear to be eroded on the west side of the Emet River, because of the downthrow of this side by the NW-SE trending major fault. This same movement resulted in the formation of a cliff-like feature northeast of the fault line, exposing the borate beds at the surface.

Along the borate zone, the ore body is cut in several places mainly by northwest trending faults. A few northeast trending faults with minor displacements are present in the ore body, but these are subordinate to the dominant northwest fracture pattern. These faults give rise to irregularities in the generally horizontal eastward sloping surface. These structures are strikingly reflected in the stepped topography. Plate 27 shows the general appearance of the borate deposits in the Hisarcik locality and a structure map on top of the borate zone for the Hisarcik locality is given on Fig. 18.

A similar occurrence of faults has been observed in the Espey and Killik localities. The ore body is cut by six major faults, which displace mainly the borate zone both vertically and horizontally. Plate 28 and 29 show the effect of the faults on the borate zone and the upper limestone, respectively in the Espey and Killik localities. The recent Gediz earthquake, 1970, has resulted in more obvious effects in the northern part of the area as demonstrated mainly by the abundance of fissures and landslides. A structural map of the base of the Espey borate zone is given on Fig. 19.

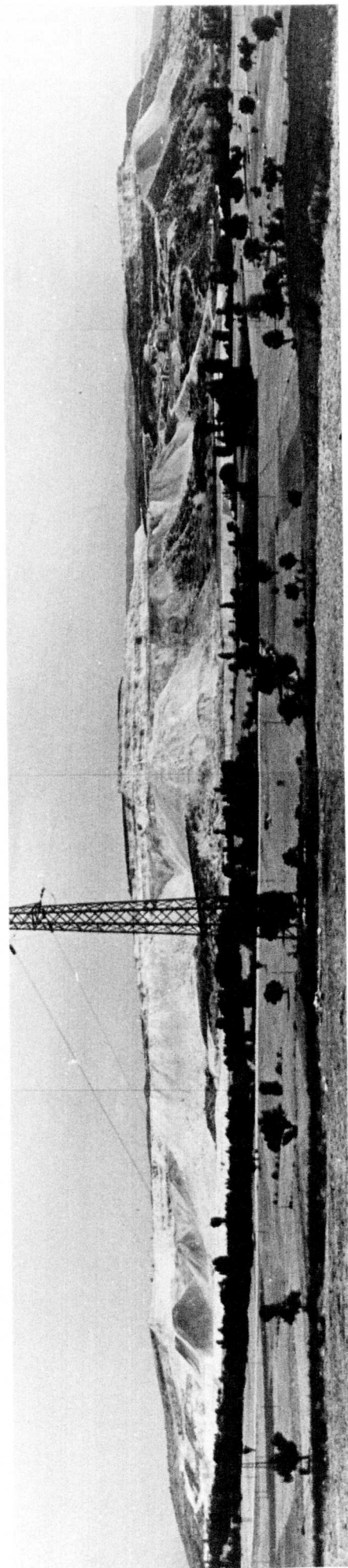


Plate 27 General appearance of the borate deposit in the Hisarcik locality.

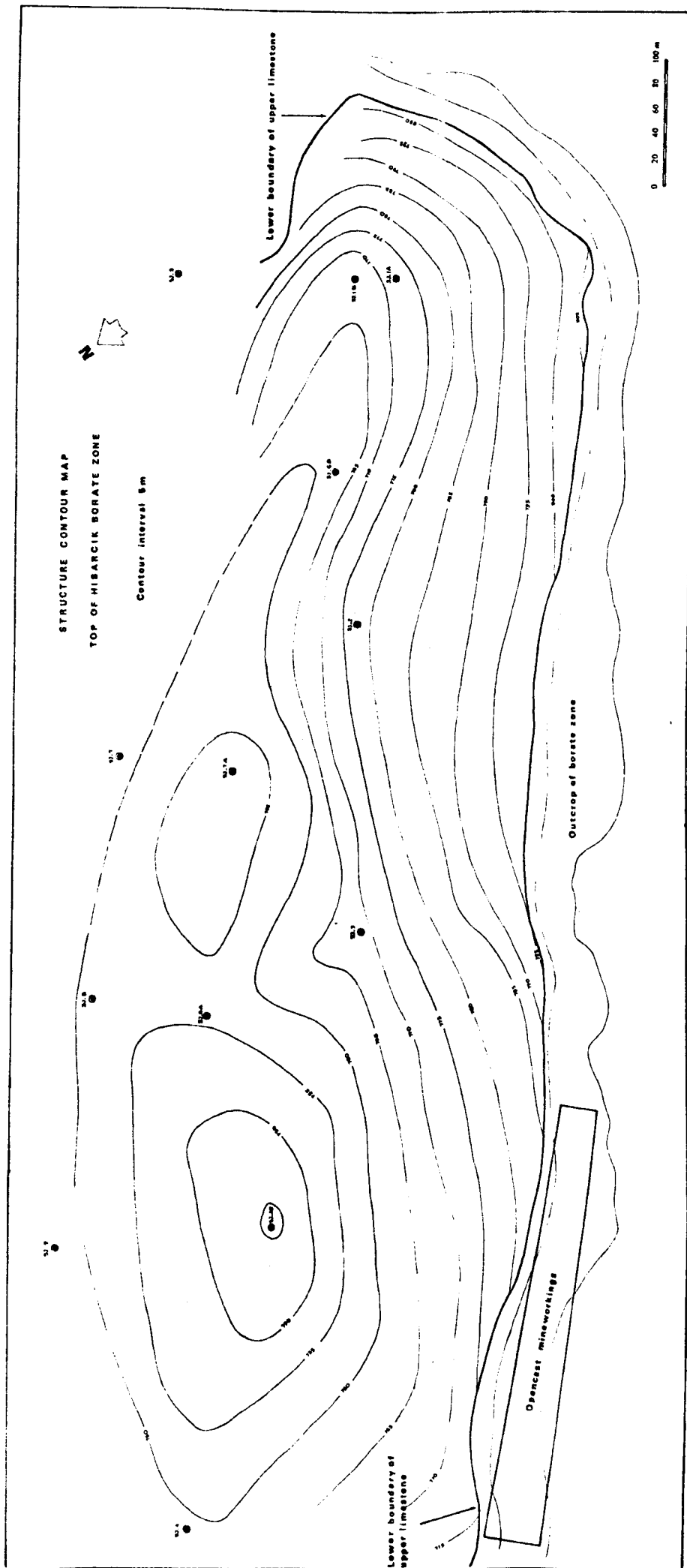


Fig.18. Structure map on top of the borate zone at Hisarcik.



Plate 28 Old Espey mineworkings and landslides after the Gediz earthquake, 1970.

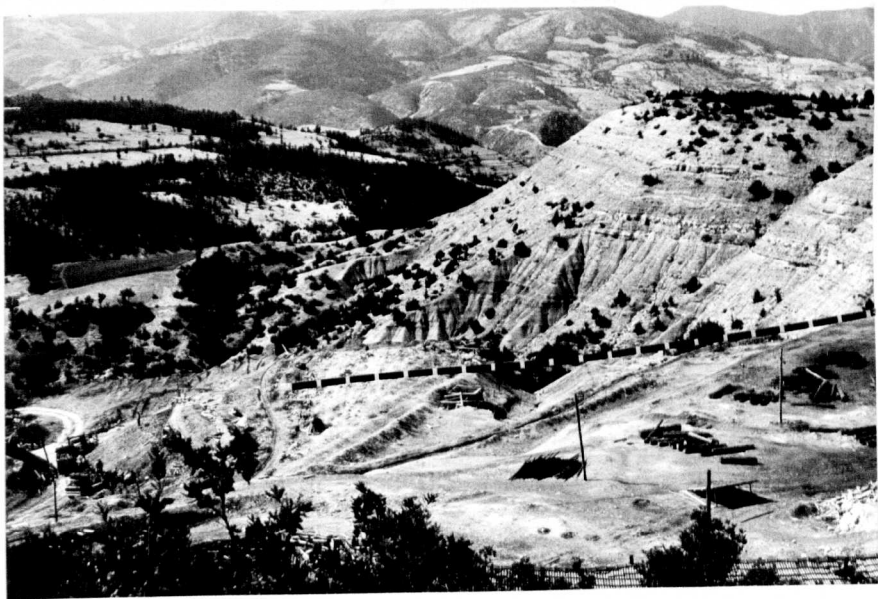


Plate 29 Plate showing Killik mineworkings and a
NE-SW trending fault.

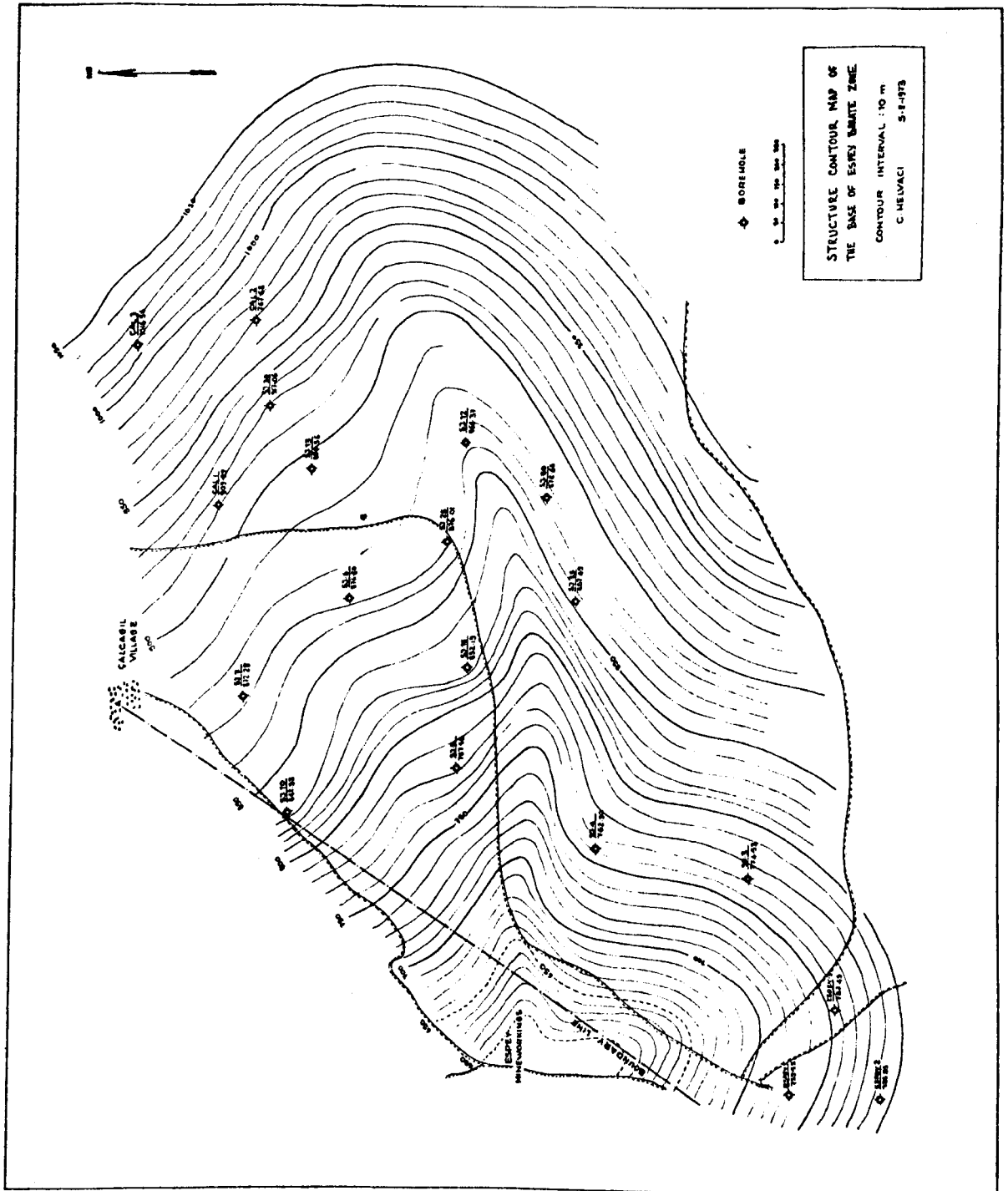


Fig.19. Structural map of the base of the Espey borate zone.

An attempt has been made to show the individual members of the borate zone by different isopach maps, but it is rather difficult to make separate isopach maps for the individual borate beds and interbedded clays and tuffs. Therefore, isopach maps have been done for the whole borate zone. Figs. 20 and 21 are, respectively, isopach maps of the borate zone in Hisarcik and Espey localities.

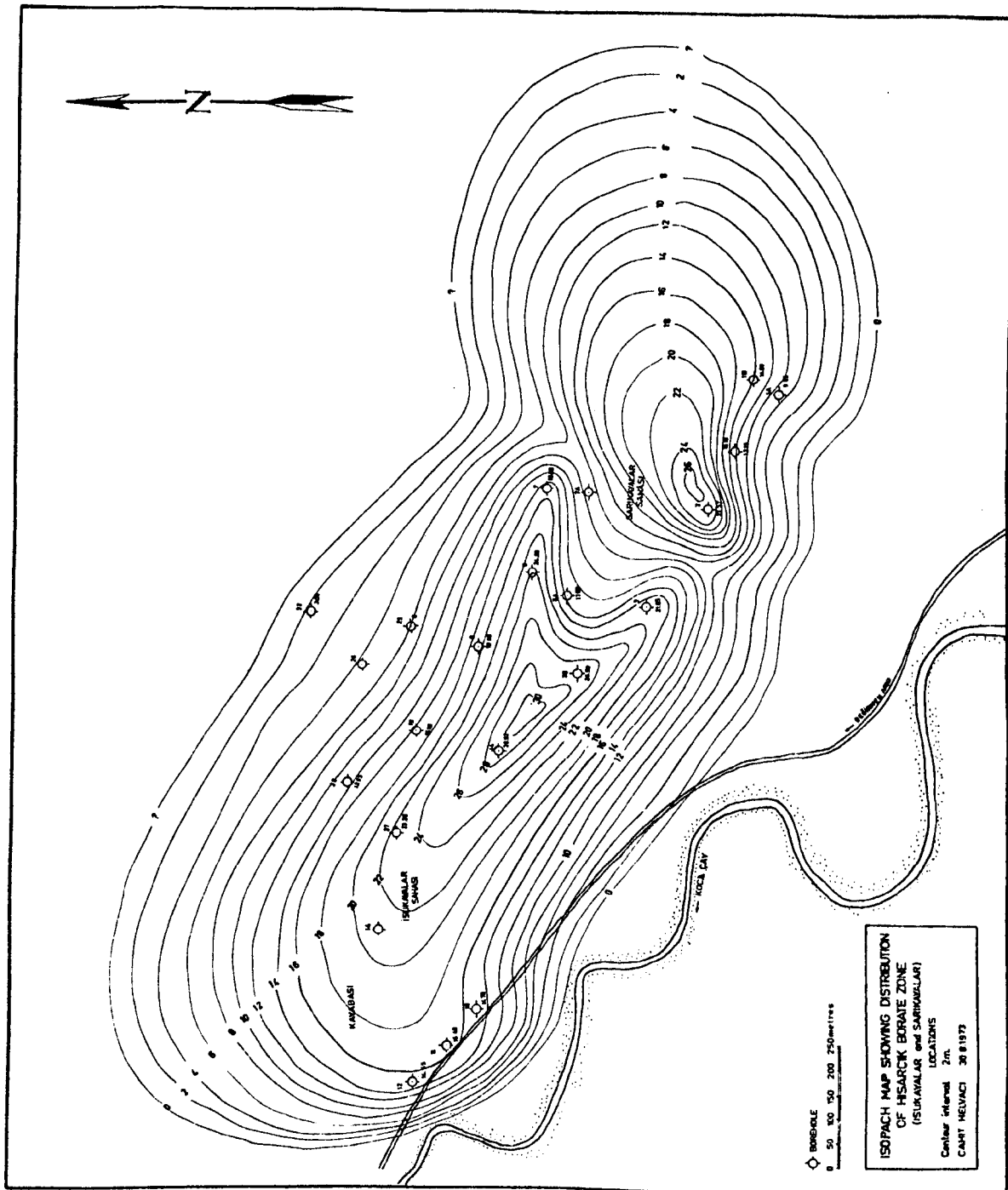


Fig.20. Isopach map showing distribution of the Hisarcik borate zone (i.e. clay, tuff, marl containing borate deposits as in Fig.7).

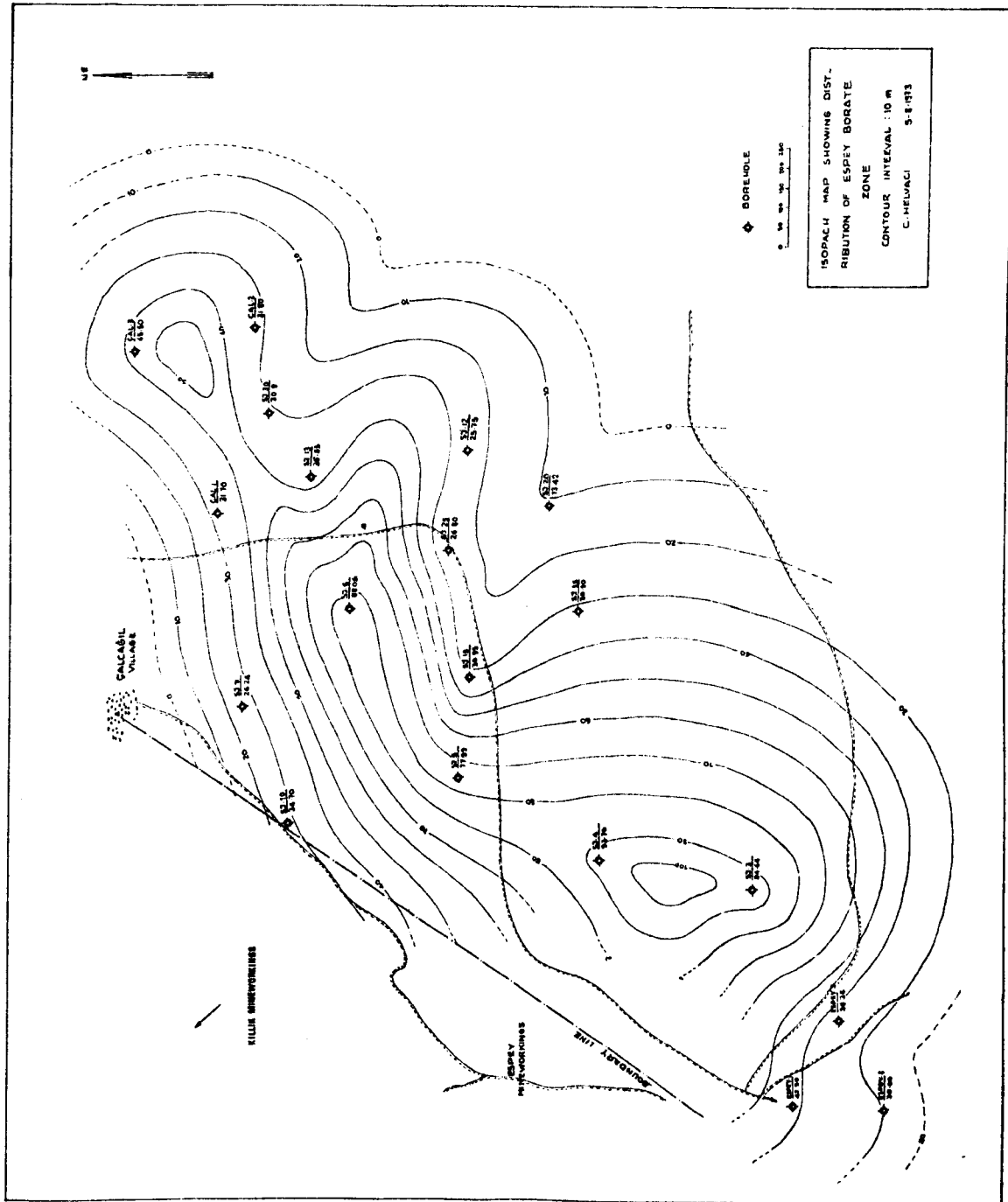


Fig.21. Isopach map showing the distribution of the Espey borate zone (i.e. clay, tuff, marl containing borate deposits as in Fig.7).

CHAPTER VI

MINERALOGY AND PETROGRAPHY OF THE EMET BORATE DEPOSITS

1. Introduction

Borate and other minerals from lacustrine deposits in the Emet borate district were determined by direct-recording X-ray diffractometer analyses using standard powder and oriented-sample techniques. For the X-ray diffraction studies of borate and associated minerals, powdered samples were mounted in an aluminium holder and its surface was smoothed to eliminate irregularities. Methods described by Carroll (1970) were used for the X-ray examination of clay minerals. The typical conditions used in this study were:- CuK radiation at 40 KV, 20 mA, Ni filter, scanning rate 1° /minute and usually silicon as an internal standard. Scanning was carried out from 5° to 60° , sometimes up to 70° for the borate minerals and 2° to 60° for the clay minerals. These ranges gave all the necessary information (d and I values) for borate, clay and other non-borate minerals identification.

Powder camera analyses and single crystal work have been carried out mainly seeking to confirm the identification of the veatchite and cahnite minerals. In addition to optical studies, the chemical analyses of individual borates and non-borates were also completed.

Mineralogical studies have shown that the borate deposits in the Emet district are far more complex than was first thought. Meyerhofferite, hydroboracite, a form of veatchite, tunellite and cahnite have been found during the present investigation, in addition to the minerals previously recorded (see Table 2). Also ulexite was found in the Espey and Killik areas, but it has not been observed in the Göktepe and Hisarcik localities where it was previously recorded by Özpeker. Table 14 lists the borate minerals so far recorded in the deposits.

Montmorillonite and illite are the only clay mineral groups identified, and the former is the dominant mineral in all of the samples studied. Native sulphur, arsenic sulphides (as realgar and orpiment) and strontium sulphates (as celestite) occur in the borate zone throughout the area and selenite and fibrous gypsum associated with borate minerals have been observed at the Göktepe and Hisarcik localities. Calcite also occurs frequently in surface outcrops and adjacent to faults as a result of modern weathering. Non-borate minerals found in the deposits are shown in Table 15.

Borates

Mineral Name	Oxide Formula	Structural Formula	Locality
1. Colemanite	$2\text{CaO} \cdot 3\text{B}_2\text{O}_3 \cdot 5\text{H}_2\text{O}$	$\text{Ca}[\text{B}_3\text{O}_4(\text{OH})_3] \cdot \text{H}_2\text{O}$	Killik, Espey, Göktepe, Hisarcik, Hamamköy, Dereköy
2. Meyerhofferite*	$2\text{CaO} \cdot 3\text{B}_2\text{O}_3 \cdot 7\text{H}_2\text{O}$	$\text{Ca}[\text{B}_3\text{O}_3(\text{OH})_5] \cdot \text{H}_2\text{O}$	Killik, Espey
3. Ulexite*	$\text{Na}_2\text{O} \cdot 2\text{CaO} \cdot 5\text{B}_2\text{O}_3 \cdot 16\text{H}_2\text{O}$	$\text{NaCa}[\text{B}_5\text{O}_6(\text{OH})_6] \cdot 5\text{H}_2\text{O}$	Killik, Espey
4. Veatchite* (sensu lato)	$4\text{SrO} \cdot 11\text{B}_2\text{O}_3 \cdot 7\text{H}_2\text{O}$	$2\text{Sr}_2[\text{B}_5\text{O}_8(\text{OH})]_2 \cdot \text{B}(\text{OH})_3 \cdot \text{H}_2\text{O}$	Killik, Espey
5. Tunellite*	$\text{SrO} \cdot 3\text{B}_2\text{O}_3 \cdot 4\text{H}_2\text{O}$	$\text{Sr}[\text{B}_6\text{O}_9(\text{OH})_2] \cdot 3\text{H}_2\text{O}$	Killik, Espey
6. Hydroboracite*	$\text{MgO} \cdot \text{CaO} \cdot 3\text{B}_2\text{O}_3 \cdot 6\text{H}_2\text{O}$	$\text{MgCa}[\text{B}_3\text{O}_4(\text{OH})_3]_2 \cdot 3\text{H}_2\text{O}$	Killik, Espey, Hisarcik
7. Teruggite	$4\text{CaO} \cdot \text{MgO} \cdot 6\text{B}_2\text{O}_3 \cdot \text{As}_2\text{O}_5 \cdot 20\text{H}_2\text{O}$	$\text{Ca}_4\text{Mg}[\text{AsB}_6\text{O}_{11}(\text{OH})_6]_2 \cdot 14\text{H}_2\text{O}$	Hisarcik
8. Cahnite*	$4\text{CaO} \cdot \text{B}_2\text{O}_3 \cdot \text{As}_2\text{O}_5 \cdot 4\text{H}_2\text{O}$	$2[\text{Ca}_2\text{B}(\text{OH})_4\text{AsO}_4]$	Killik, Espey, Hisarcik

Table 14 Typical compositions and structural formulas of borate minerals found in the Emet deposits.

*New occurrence of minerals found by C. Helvacı in the deposit for the first time.

Non-borates

Mineral Name	Formula	Locality
1. Sulphur	S	Throughout
2. Realgar	AsS	"
3. Orpiment	As ₂ S ₃	"
4. Celestite	SrSO ₄	"
5. Gypsum	CaSO ₄ ·2H ₂ O	Göktepe, Hisarcik
6. Calcite	CaCO ₃	Throughout
7. Quartz	SiO ₂	"
8. Montmorillonite	(Mg,Al) ₂ Si ₄ O ₁₀ ·(OH) ₂ nH ₂ O	"
9. Illite	(K,H ₃ O)Al ₂ (AlSi ₃ O ₁₀)(OH) ₂	"

Table 15 Names and compositions of non-borate minerals that occur in the Emet deposits.

2. Textural relationships of borate and other minerals in the Emet borate deposits.

Borate and non-borate minerals, according to their chemical composition and their mineralogical relationships with each other in the Emet deposits, may be divided into seven groups; namely the calcium borates, the sodium-calcium borates, the strontium borates, the magnesium-calcium borates, the complex borates, the compound borates, and the non-borates (mainly realgar, orpiment, celestite, etc.) (see Tables 14 and 15). There is no sodium borate mineral occurrence at Emet.

Borate minerals within each group have nearly the same chemical composition, differing from one to another only in the amount of water of hydration in the structure.

Calcium borates

Colemanite ($\text{Ca}[\text{B}_3\text{O}_4(\text{OH})_3] \cdot \text{H}_2\text{O}$)

Colemanite is by far the commonest mineral in both the Espey-Killik and Hisarcik areas, and for this reason the Emet borate deposits are usually referred to commercially as colemanite deposits. Colemanite occurs in many different forms ranging from minute stellate clusters of crystals in clay to ovoid nodules up to 0.5 metre in diameter. The individual crystals which make up the nodules are colourless, grey, pink and dark blue.

Among the commoner habits are:-

- a) Nodular forms with radiating structures (Plates 30, 31 and 32).
- b) Massive granular colemanite (Plates 33, 34 and 35).
- c) Disseminated crystals, often stellate, in a clay matrix (Plates 36, 37 and 38).

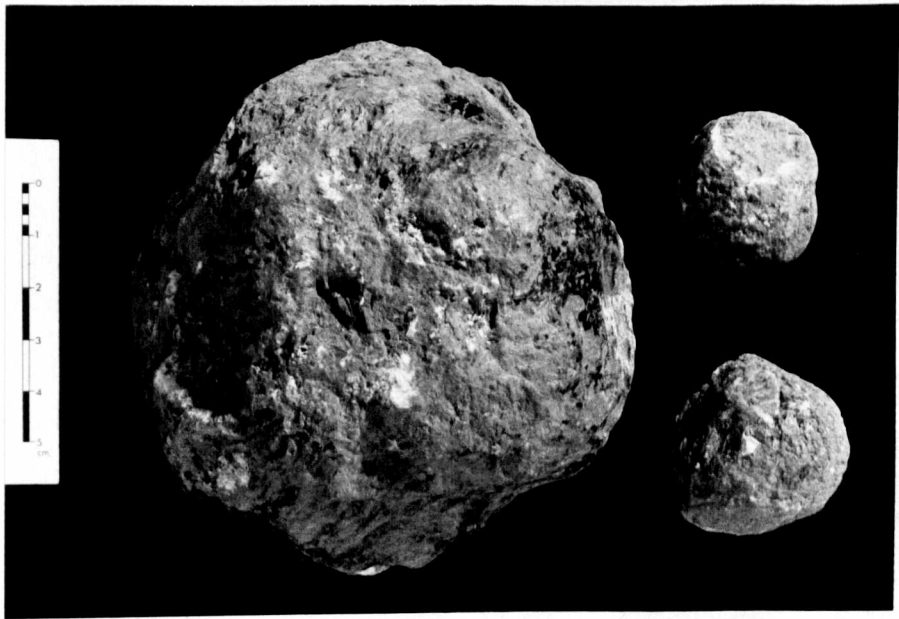


Plate 30 Colemanite nodules showing different sizes, surrounded by clay, Espey underground mine.



Plate 31 Colemanite nodules in the borate zone showing a radiating structure, surrounded by clays, Killik underground mine.



Plate 32 Section of colemanite nodule showing radiating structure with clay injection in between colemanite crystals, vugh in the centre filled with euhedral colemanite crystals and clay covering the outer edge of the nodule, Killik underground mine.



Plate 33 Massive granular colemanite with radial structure. Subeuhedral to euhedral crystals at the upper end. Sample used as standard, Sarikaya opencast mine.

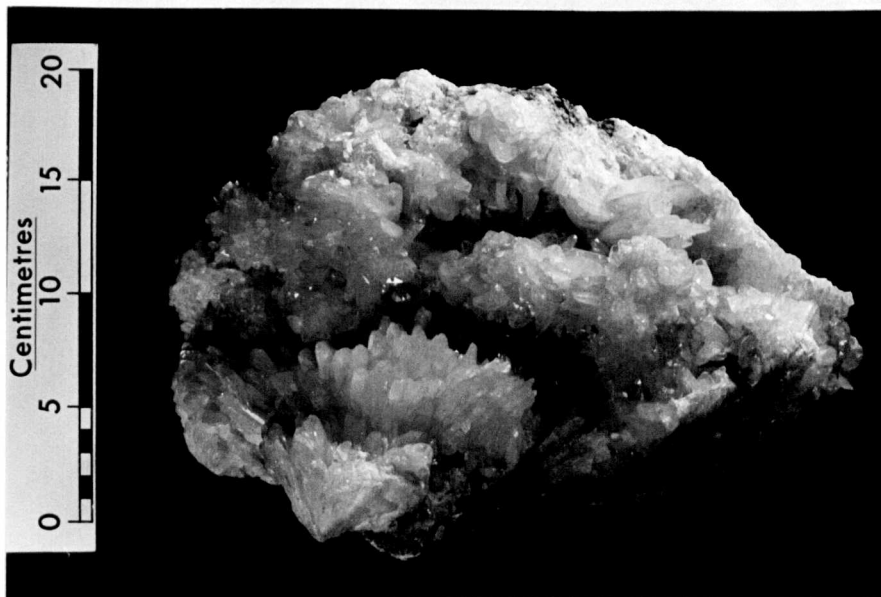


Plate 34 Euhedral colemanite crystals up to 5 cm in length in the vugh of colemanite nodule, Espey underground mine.



Plate 35 Cluster of bladed euhedral colemanite crystals, from the Espey underground mine.

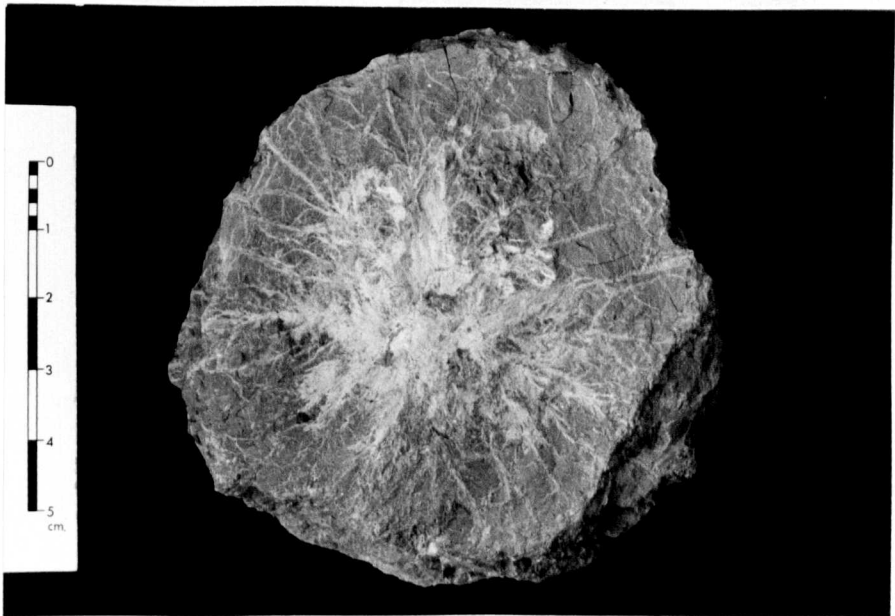


Plate 36 Undeveloped colemanite nodule showing radiating colemanite crystals in clay, Espey underground mine.

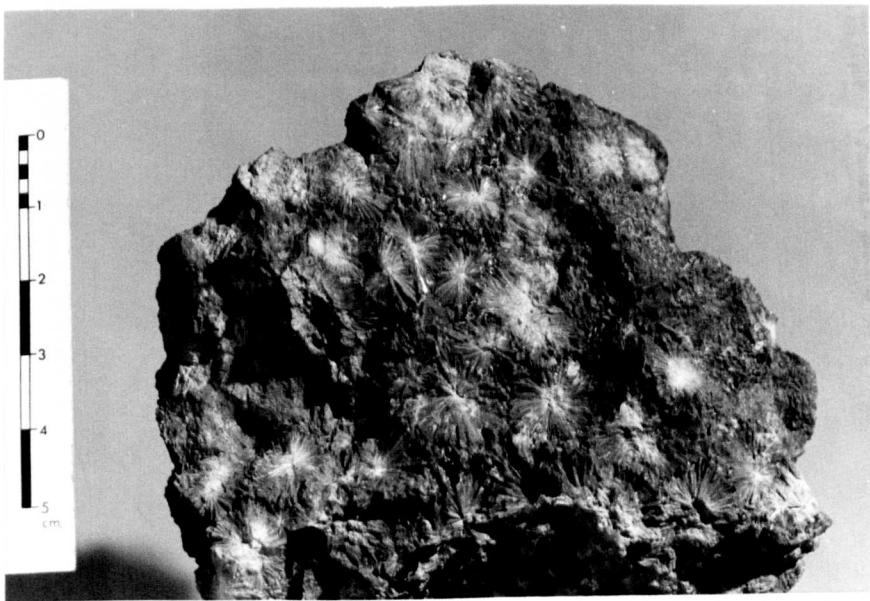


Plate 37 Radiating groups of colemanite crystals in clay, common occurrence of colemanite throughout the deposits, sample from Dereköy locality.

- d) Fibrous layers surrounding nodules (Plates 39 and 40).
- e) Thin layers interbedded with clay, sometimes brecciated (Plate 41).
- f) Vugh fillings (Plate 42).

Nodules are by far the commonest form of colemanite but these nodules exhibit a large variety of shapes and sizes (see Plate 30). There is a tendency for the smaller nodules to be spherical and the larger ones to be ovoid (Plate 43). Some, irrespective of size, contain vughs (Plate 44); others have a core of granular colemanite (Plates 45 and 46; see also Plate 32). Many of the larger nodules consist of aggregates of smaller spherical nodules composed of radiating crystals. In some of the medium size nodules (see Plates 31 and 39) the crystals are curved, as if they grew whilst the sediment was being compacted. Closer inspection reveals that these nodules grew in successive stages, each layer being separated by a thin discontinuous veneer of clay. Later generations of colemanite crystals radiate from separate centres of nucleation on the original nodule (see Plate 39).

Often it is difficult to identify all stages of nodule growth, but judging from the presence of included clay, it is clear that these nodules formed within the clays and tuffs below the sediment/water interface and probably continued to grow as the sediments were compacted.

The bulk of the colemanite nodules are made up of a mixture of fine-grained colemanite crystals and clay. In thin section, these colemanite crystals are elongated and radiate outwards from the nodule centre (Plate 47). These

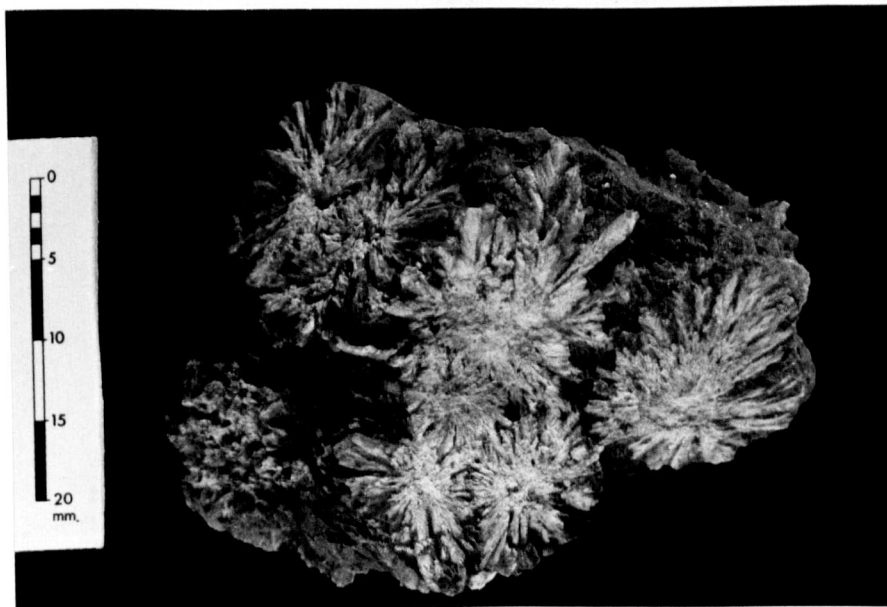


Plate 38 Semi-developed stellate colemanite crystals in a clay matrix showing radiating groups of colemanite crystals, Killik underground mine.

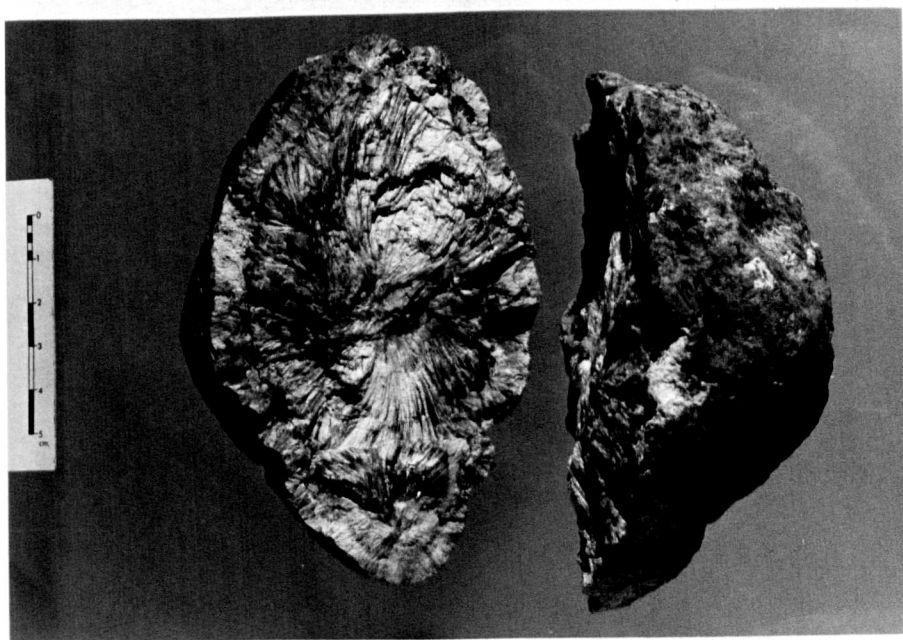


Plate 39 Photograph of colemanite nodule showing radiating colemanite crystals and fibrous colemanite crystals at the edge of the nodule. Radiating crystals are curved towards the edge, Espey underground mine.

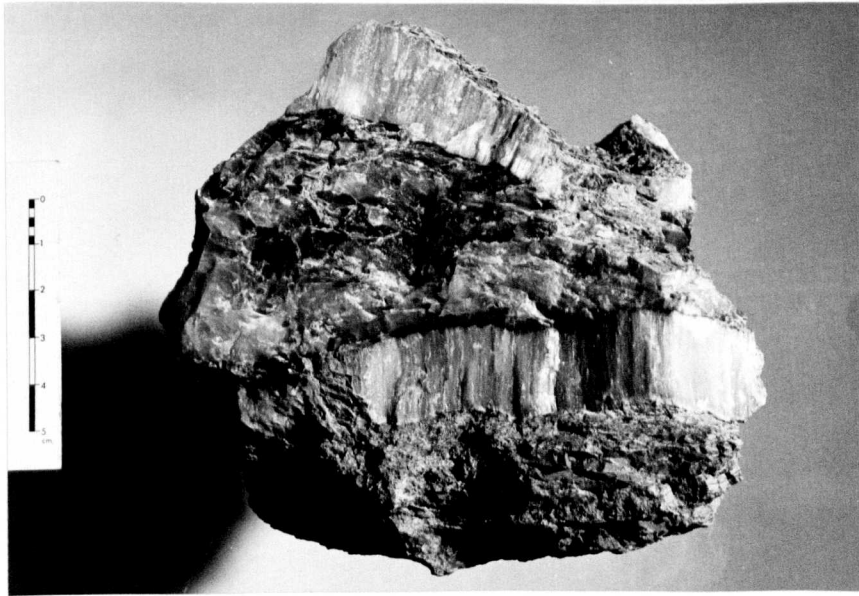


Plate 40 Massive colemanite surrounded by the layer of fibrous colemanite. Clay associated with colemanite is montmorillonite, Espey underground mine.

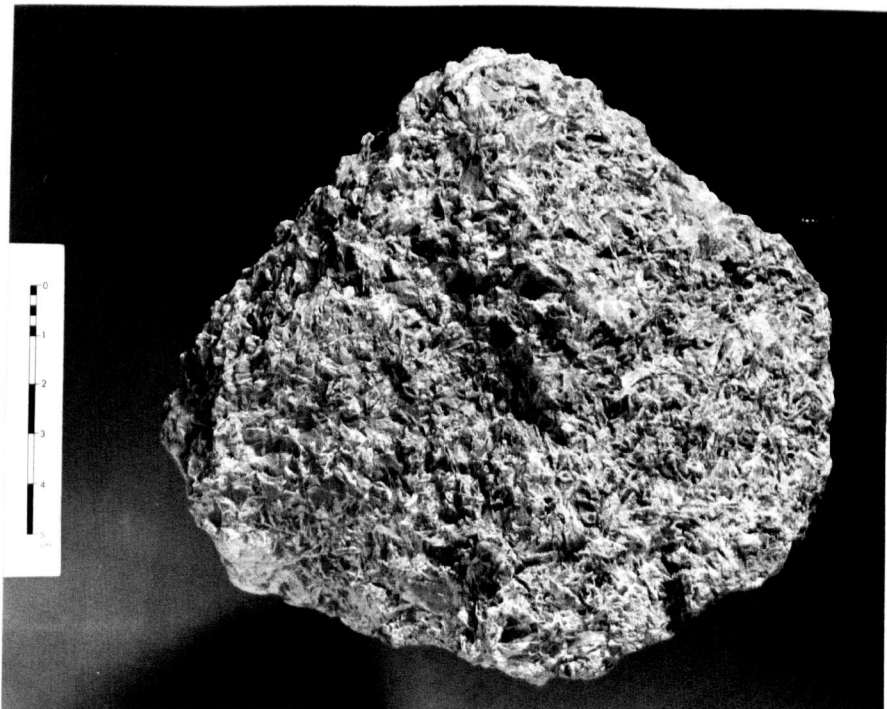


Plate 41 Photograph showing brecciated colemanite with clay admixture, sample comes from Espey underground mine near the fault zone.



Plate 42 Euhedral colemanite crystals filling vughs and cavities, Espey underground mine.



Plate 43 Colemanite nodules of different sizes and shapes, Hisarcik opencast mine.

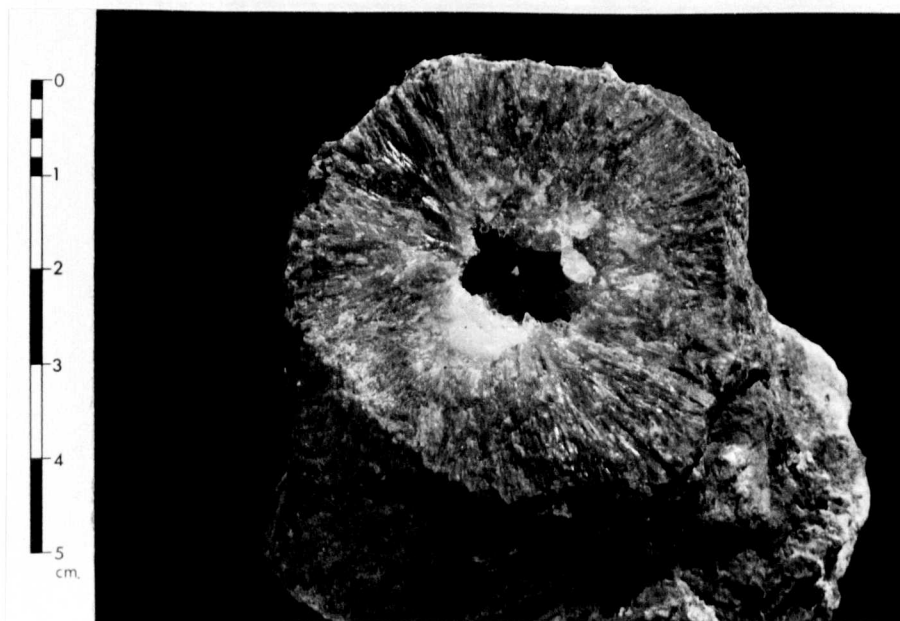


Plate 44 Colemanite nodule containing a vugh in the centre, Espey underground mine.

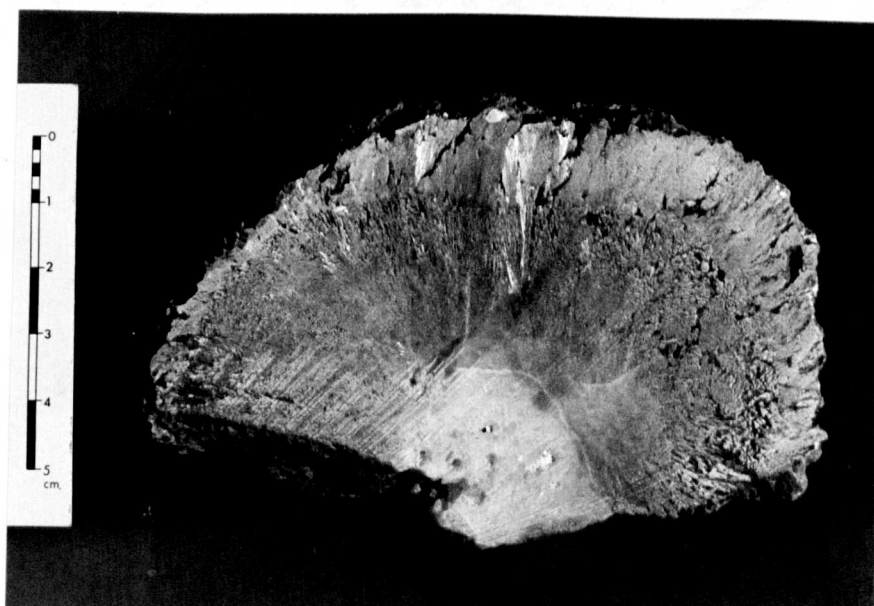


Plate 45 Colemanite nodule containing a vugh in the centre, filled with a core of granular colemanite, Espey underground mine.

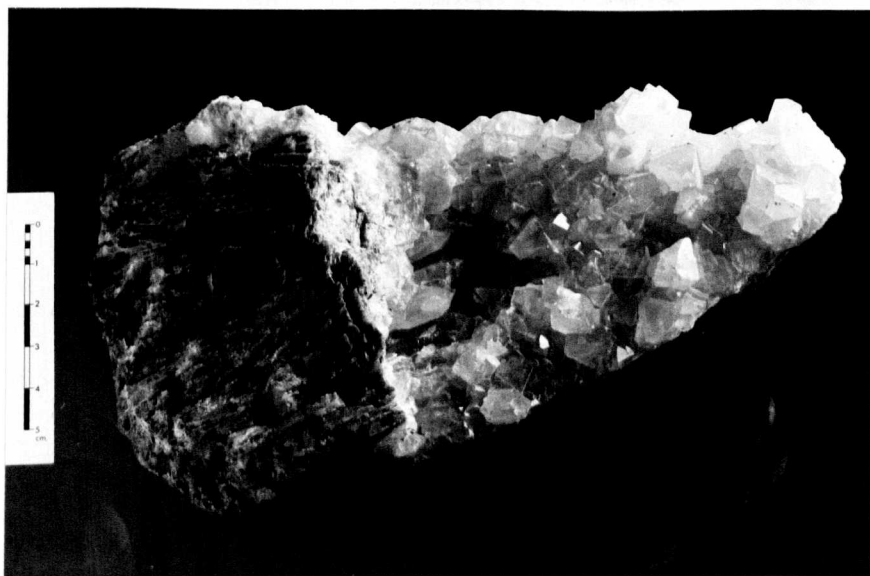


Plate 46 Part of the colemanite nodule showing massive radiating crystals and euhedral crystals in the centre, Killik underground mine.



Plate 47 Elongated and radiating colemanite crystals from the centre of the colemanite nodule. Crossed nicols, x10.

crystals appear on the outer surface of the nodule as thin radiating plates resembling a cauliflower or barite rosettes, but under the microscope they are fern-like (Plate 48). Each radiating crystal is clear, but small amounts of clay are attached to the outer surfaces of the crystals (see Plate 48).

Colemanite crystals also occur as veins of clear, medium to fine-grained crystals in the centre of each nodule (Plate 49). These veins are spindle-shaped in cross section, being thickest in the centre of the nodule and thinning toward the outer edges (see Plate 39). The veinlets intersect in such a way as to produce the so-called septarian structure. The veinlets (see Plate 39) commonly have an open space in the centre, which in some specimens is filled with fluid (see Plate 44); others have a core of granular and euhedral colemanite crystals (see Plates 32, 45 and 46).

Massive granular colemanite also occurs (see Plates 33, 34 and 35) as large, vuggy masses of medium to coarse-grained, radiating crystals containing variable amounts of intergranular clay, realgar and some other fine inclusions of foreign materials. Sometimes massive colemanite occurs as a very fine-grained crystal mixture with clay (Plate 50), whereas sometimes massive colemanite has medium to coarse-grained, elongated prismatic or tabular crystals (Plate 51). In thin section these colemanite crystals show many different forms, elongated-prismatic (Plates 52 and 53) to short-prismatic forms (see Plate 51) being dominant. In the hand specimens, individual crystals range in size from micro-crystalline to doubly terminated euhedra up to 5cm in length (see Plates 34 and 35). Often massive colemanite appears to be completely surrounded by montmorillonitic clay in the Espey-Killik area (Plate 54). This type of massive colemanite

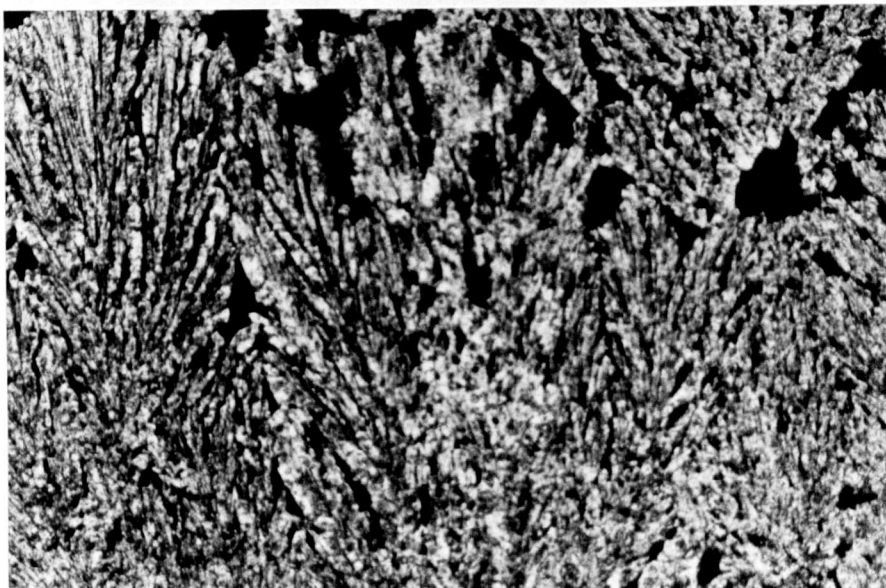


Plate 48 Plate showing the edge of a colemanite nodule. Outer edge of nodule is towards the top. Increase in the darkness is caused by increase in the clay content of the nodule. Plane polarized light, x10.

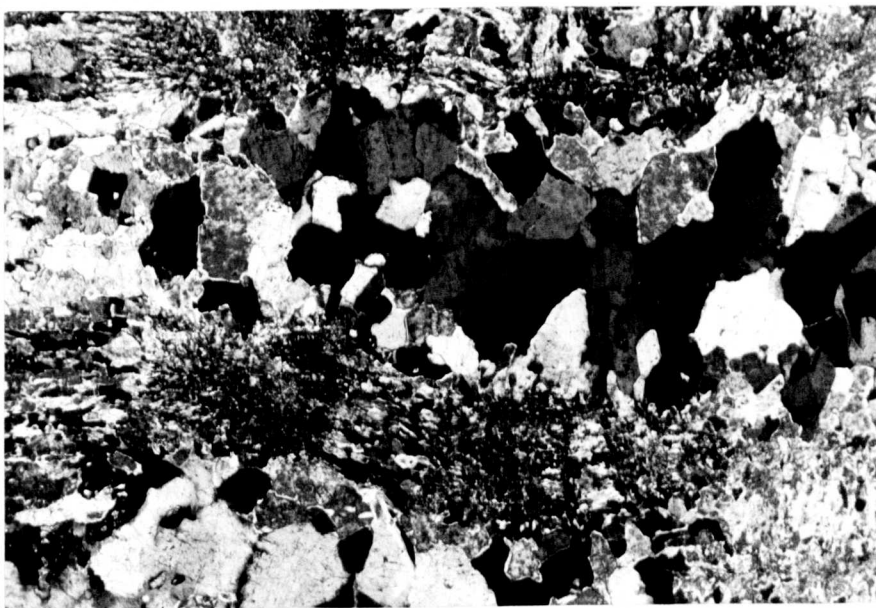


Plate 49 Colemanite crystals occurring as veins of clear, medium to fine-grained crystals in the centre of each nodule. Crossed nicols, x10.

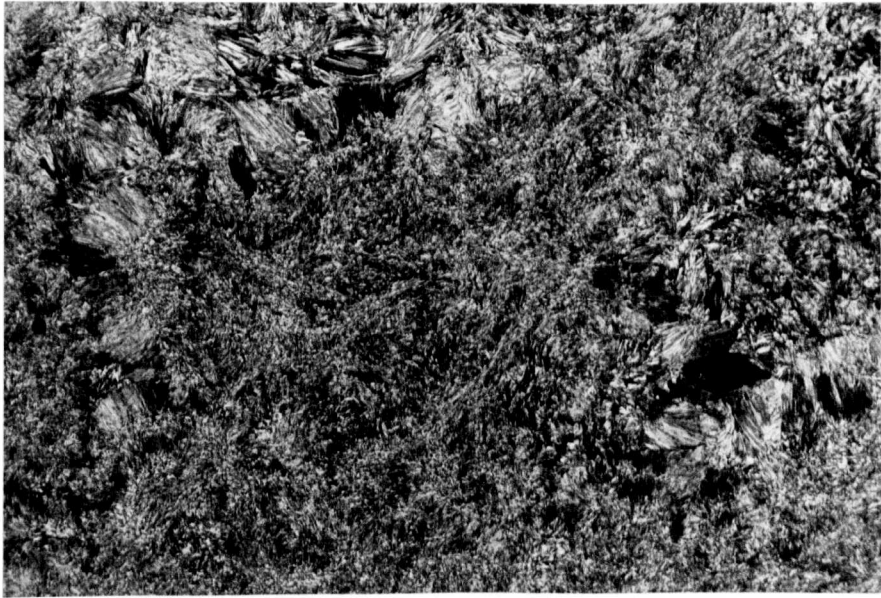


Plate 50 Plate showing massive colemanite occurrence as a very fine-grained crystal in a clay mixture. Crossed nicols, x10.

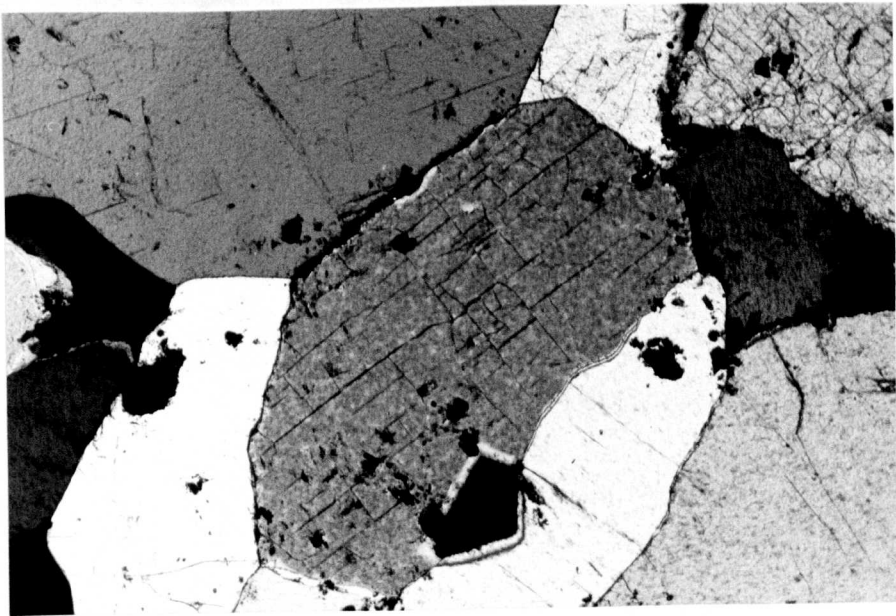


Plate 51 Coarse-grained, short-prismatic and tabular colemanite crystals. Crossed nicols, x10.



Plate 52 Plate showing elongated-prismatic colemanite crystals. Crossed nicols, x10.

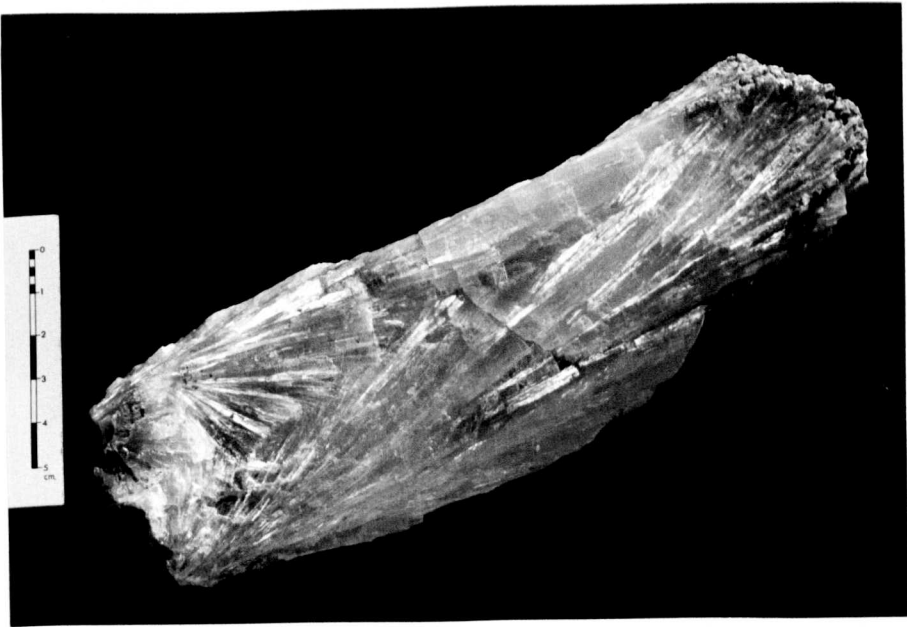


Plate 53 Elongated prismatic colemanite crystals in the massive body, Killik underground mine.

has a distinct dark blue colour due partly to clay and partly to celestine which give blue colouring to the colemanite. This will be discussed in the next chapter.

Often colemanite occurs as disseminated crystals and commonly stellate clusters in a clay matrix. These colemanite stellate and radiating groups of crystals in a clay matrix have been observed most frequently in the northern part of the deposits (Espey-Killik locality). As can be seen from Plates 36, 37 and 38, radiating groups of colemanite crystals in clay suggest that these crystals are growing within the clay matrix (Plate 55).

Nodules and massive colemanite are often coated by very thin layers (up to 2 cm thick) of fibrous colemanite which usually appears to be part of the nodule or massive colemanite, but sometimes fibrous colemanite is separated from the nodule or massive colemanite by very thin layers of clay (see Plates 39 and 40). Clay associated with this type of occurrence is generally green-grey coloured montmorillonitic clay (see Plate 40). In the thin section, medium to coarse-grained, elongated prismatic crystals pass gradually into fibrous crystals (Plate 56). Sometimes, fibrous colemanite crystals appear on the outer edges of the prismatic crystals (Plate 57).

Another common occurrence of colemanite is as thin layers (up to 5cm) interbedded with clay and sometimes brecciated. Brecciated colemanite crystals with clay admixture has been found along the dislocated zones (see Plate 41). Very thin veins of colemanite alternating with clay occur sporadically in the deposits. Plate 58 shows colemanite veins alternating with clay in the thin section. Sometimes, clay has a discontinuous character and is very thin compared with colemanite veins (Plate 59).



Plate 54 Massive colemanite is completely surrounded by montmorillonitic clay, colemanite is blue in colour, Espey underground mine.

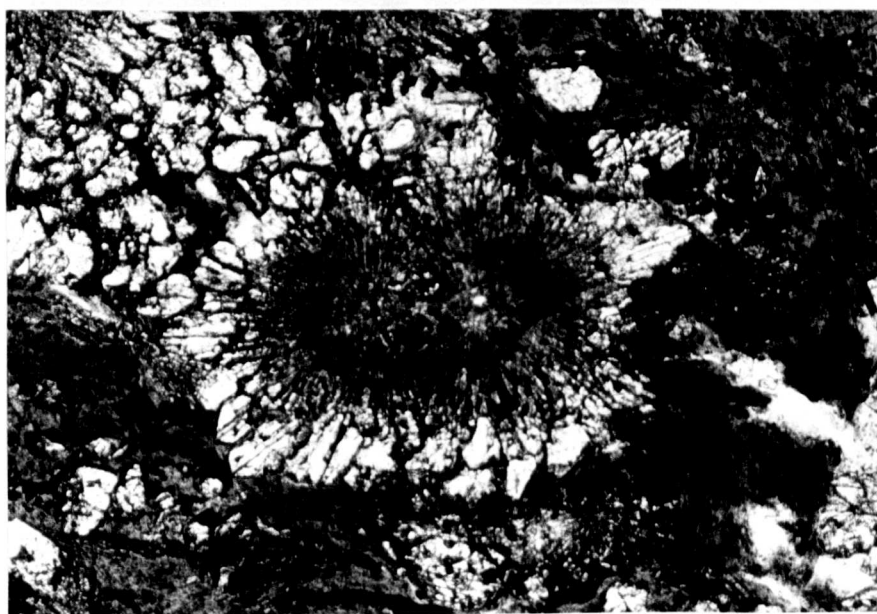


Plate 55 Star-like colemanite crystals growing in the clay matrix. Plane polarized light, x10.

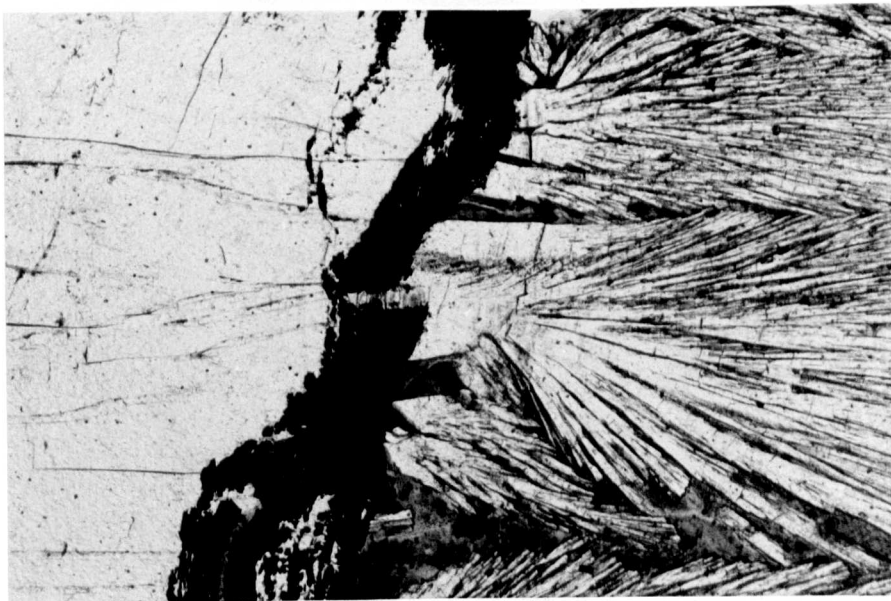


Plate 56 Plate showing clearly the relationship between prismatic and fibrous colemanite crystals. Prismatic crystals pass gradually into fibrous crystals. Note also realgar and orpiment vein cutting across. Plane polarized light, x10.



Plate 57 Prismatic colemanite crystals and fibrous crystals growing at their edges. Crossed nicols, x10.

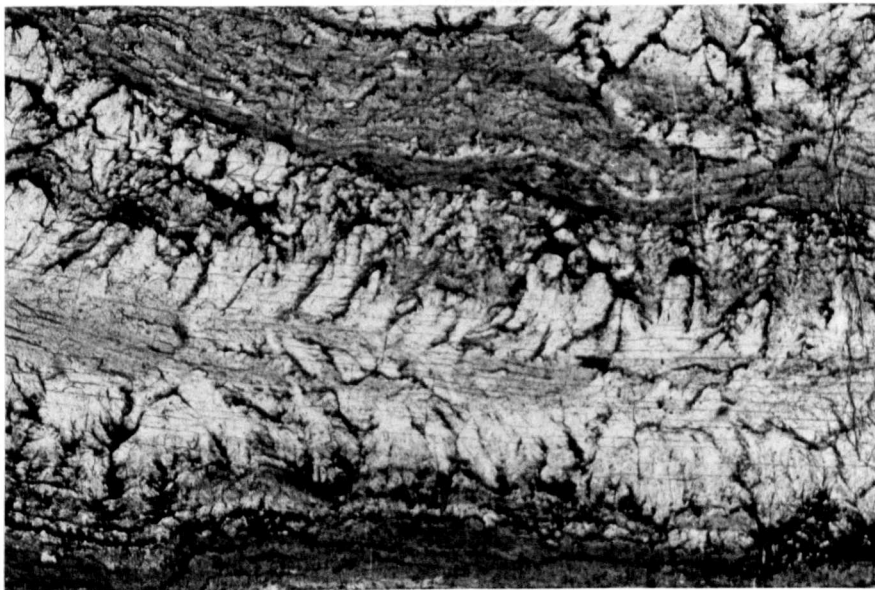


Plate 58 Colemanite veins and clay layers alternating in the thin section. Plane polarized light, x10.

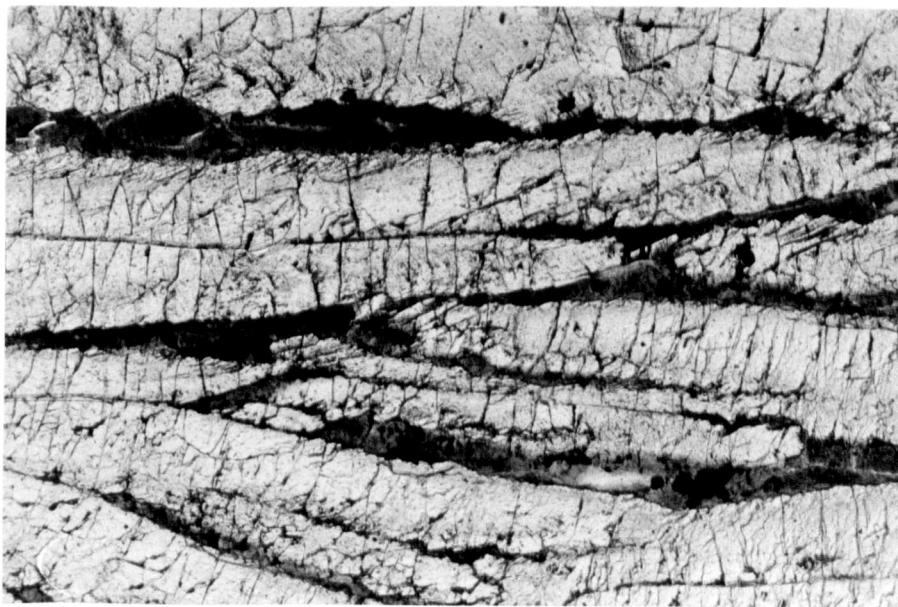


Plate 59 Very thin clay occurring inbetween colemanite crystals. Plane polarized light, x10.

Large euhedral crystals of colemanite are usually found in vughs and cavities created possibly after burial. The vughs of colemanite nodules are sometimes filled with euhedral colemanite crystals (see Plates 42 and 46).

Of the minerals in vughs and veins in colemanite nodules, colemanite is almost ubiquitous, but realgar frequently, and celestite (Plate 60) and cahnite (Plate 61) more rarely, are found encrusting colemanite crystals in vughs.

Common alteration products of colemanite are hydroboracite and calcite, and rarely a form of veatchite and cahnite. All colemanite samples analysed have a certain amount of hydroboracite and occasionally a form of veatchite which are commonly intimately intergrown with colemanite (Plate 62) and are sometimes cut by later colemanite veins (Plate 63). Alteration of colemanite to calcite has been observed in the field and revealed in many specimens by staining techniques and microscope studies. Colemanite alters to calcite mainly near the surface, near fault zones and along the radiating structure of colemanite nodules (Plates 64, 65 and 66).

Meyerhofferite $(\text{Ca}[\text{B}_3\text{O}_3(\text{OH})_5] \cdot \text{H}_2\text{O})$

Meyerhofferite is found in the northern basin in the Espey and Killik localities as small grey-bluish coloured nodules (up to 8cm in diameter) associated with colemanite in the lower part of the borate zone (Plate 67). It occurs as nodules of coarsely crystalline radiating crystals intergrown with clay at the margins. Small vughs in the centre of the nodules contain delicate acicular crystals (Plate 68),



Plate 60 Blue coloured celestite crystals in the vugh of the colemanite sample. Sample comes from Sarikaya locality.



Plate 61 Plate showing cahnite coating on euhedral colemanite crystals, Espey mine.

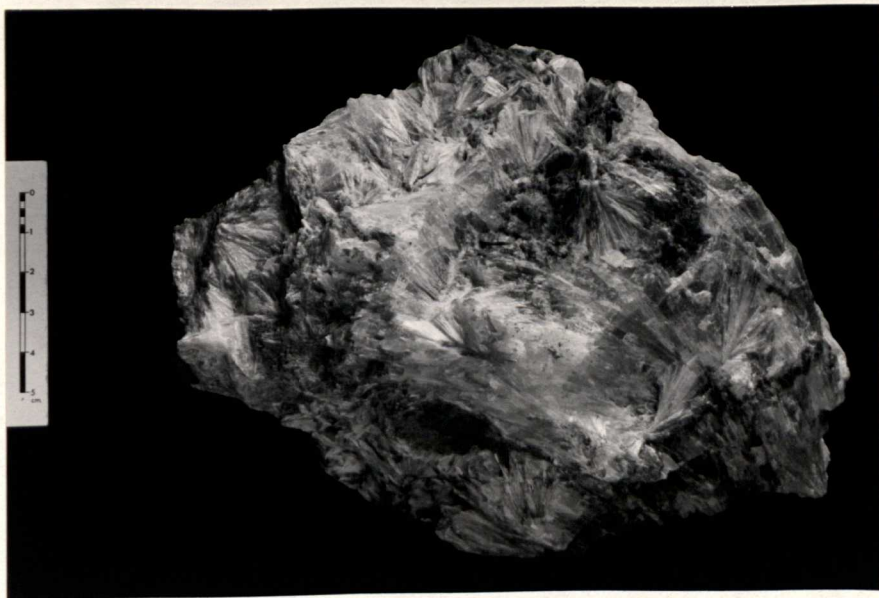


Plate 62 Plate showing coemanite alteration to hydroboracite. Also note that hydroboracite and coemanite are commonly intergrown, Sarikaya locality.

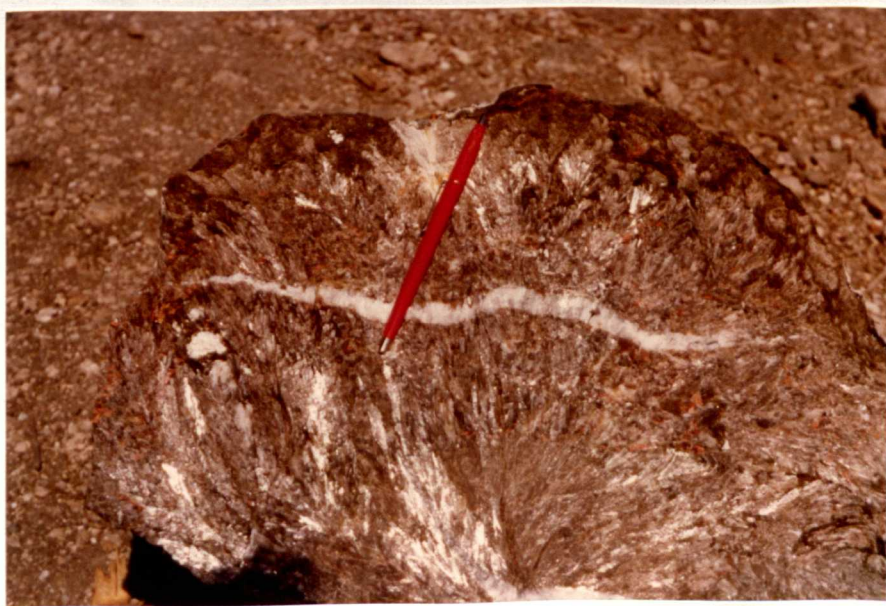


Plate 63 Coemanite nodule with orpiment and realgar minerals. Small amounts of hydroboracite and a form of veatchite on the left side (white coloured spots). Also two different coemanite veins, 1-1.5cm thick, cutting through the nodule, Killik mine.



Plate 64 Calcite, alteration product of colemanite, and colemanite crystals in the middle showing the relationships between colemanite and its alteration product, Espey mine.



Plate 65 Polished, etched and stained colemanite showing alteration to calcite, which has a pink colour after the staining.



Plate 66 Polished, etched and stained colemanite nodule showing alteration to calcite mainly along the radiating structure.



Plate 67 A group of Meyerhofferite nodules occurring as small and grey-bluish in colour, Killik underground mine.

which are also meyerhofferite, and no alteration to or from any other mineral has been observed.

Sodium-calcium borates

Ulexite $(\text{NaCa}[\text{B}_5\text{O}_6(\text{OH})_6] \cdot 5\text{H}_2\text{O})$

Ulexite is the only mineral of its series found in the deposit. It, like meyerhofferite, is restricted to the northern basin (Espey and Killik area), occurring sporadically. It occurs at three levels and always as massive and cauliflower-like nodules (Plate 69); veins and encrustations on other minerals are unknown in the Emet district. Sometimes, very thin fibrous ulexite crystals growing on top of the massive and cauliflower-like ulexite nodules have been observed (Plate 70).

Ulexite is commonly associated with colemanite and hydroboracite, but no alteration to colemanite or from any other mineral has been observed. It is usually very soft. The purest forms of ulexite are white but many are grey due to the nodule growing in the clay. In thin section, ulexite shows very fine-grained fibrous crystals growing in the clay mixture (Plate 71), but usually it has been compacted and is massive (Plate 72). Sometimes ulexite and clay admixture has many very thin veins extending from the edge of the nodules towards the centre. These veins usually have voids, but occasionally they are filled with fine-grained calcite crystals (Plate 73). These characters suggest that ulexite nodules, like colemanite and meyerhofferite, appear to have developed within and not on the sediments.

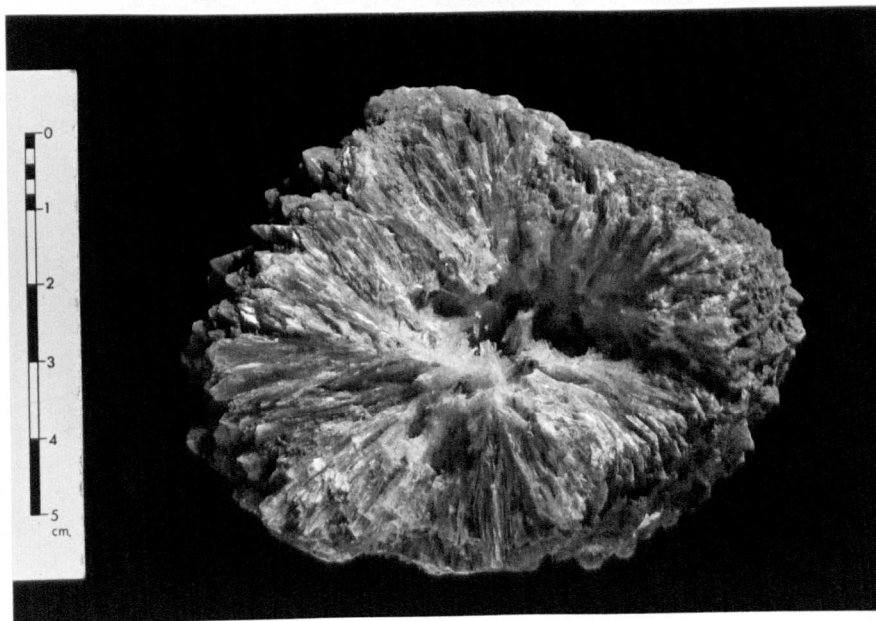


Plate 68 Meyerhofferite nodule showing coarsely crystalline radiating crystals and vugh in the centre, containing acicular crystals, Espey underground mine.

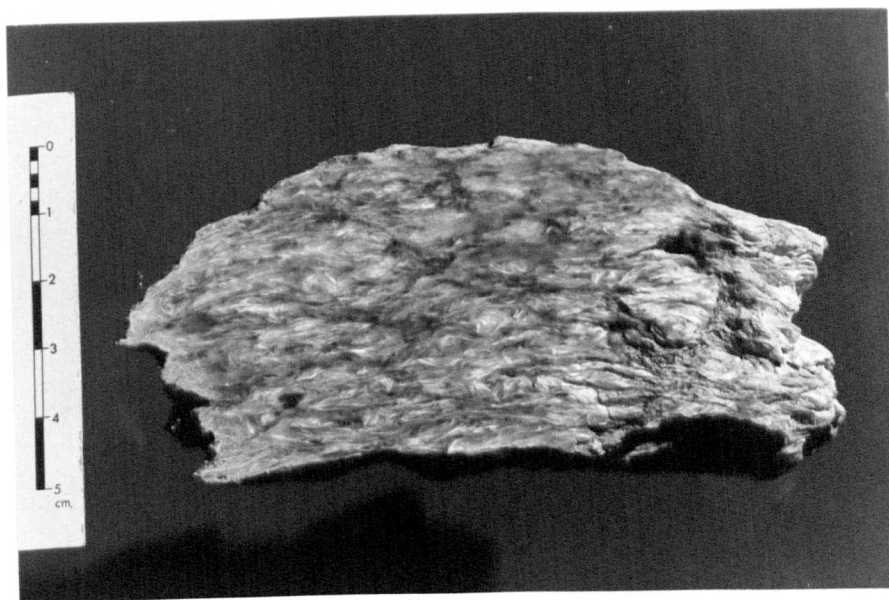


Plate 69 Occurrence of massive cauliflower-like ulexite nodule with silky appearance at the Killik mine.

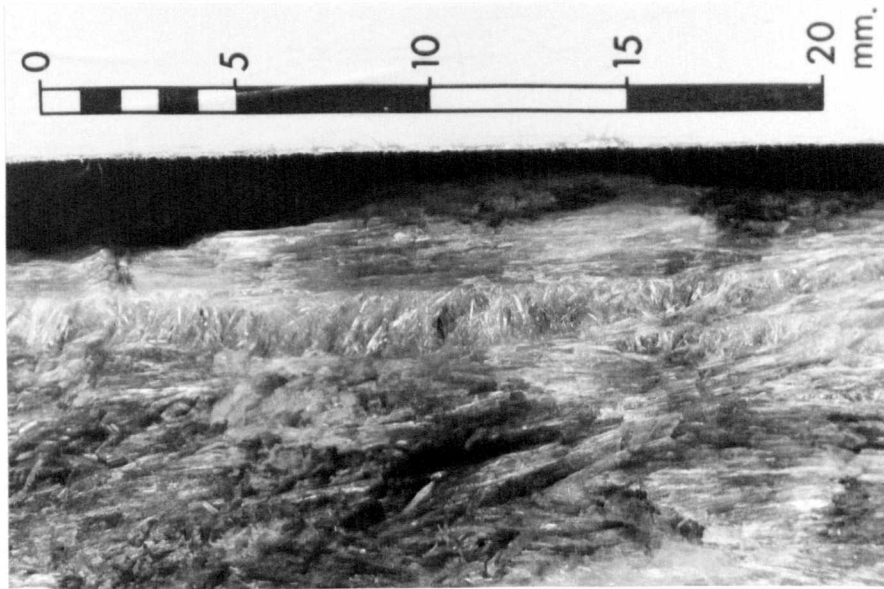


Plate 70 Thin fibrous ulexite crystals coating top of the cauliflower-like ulexite nodule, Killik underground mine.

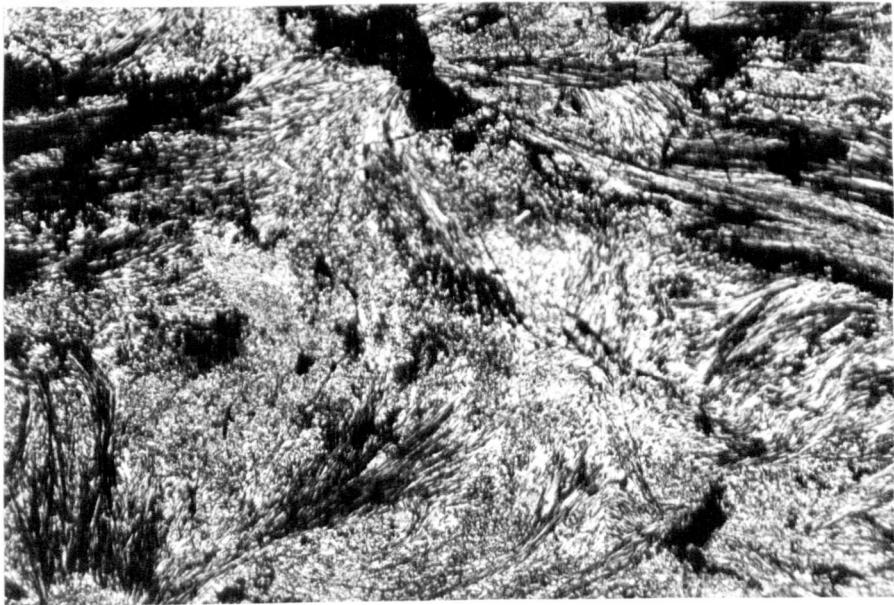


Plate 71 Plate showing very fine-grained fibrous ulexite crystals growing in the clay mixture. Crossed nicols, x10.



Plate 72 Massive ulexite admixture with clay. Crossed nicols, x10.



Plate 73 Ulexite and clay mixture showing very thin veins, occasionally filled by calcite crystals. Plane polarized light, x10.

Strontium borates

Veatchite ($2\text{Sr}_2[\text{B}_5\text{O}_8(\text{OH})]_2 \cdot \text{B}(\text{OH})_3 \cdot \text{H}_2\text{O}$)

A form of veatchite mineral is very rare, occurring sporadically at one horizon in the northern basin (Espey-Killik area). It appears as a very pure white mineral often with clay inclusions, with small (up to 2 cm in diameter) and large (up to 6cm in diameter) nodules made up of little needle-shaped crystals (Plate 74). Sometimes very small nodules are associated together and show mammillary appearance (Plate 75).

Veatchite (*sensu lato*) occurs as felted masses of very small crystals which are sufficiently curved to preclude a positive distinction between veatchite and p-veatchite by single crystals X-ray examination (Braitsch, 1959). Due to the absence of suitable crystal, the single crystal study has failed to distinguish between veatchite and p-veatchite.

This mineral is usually associated with colemanite. In thin sections, it shows very fine small crystals, which sometimes grow in or on top of colemanite nodule (Plate 76; see also Plate 63). Field and textural evidence shows that this mineral replaces colemanite and is not associated with the other Sr-borate, tunellite. This is the first record from Turkish borate deposits.

Tunellite ($\text{Sr}[\text{B}_6\text{O}_9(\text{OH})_2] \cdot 3\text{H}_2\text{O}$)

Tunellite, like the veatchite mineral, has a restricted distribution and has been found only in the lower part of the borate zone in the Espey and Killik localities.

Tunellite commonly occurs either as individual flattened crystals (Plate 77), 1-5cm in length, or as thin tabular-shaped

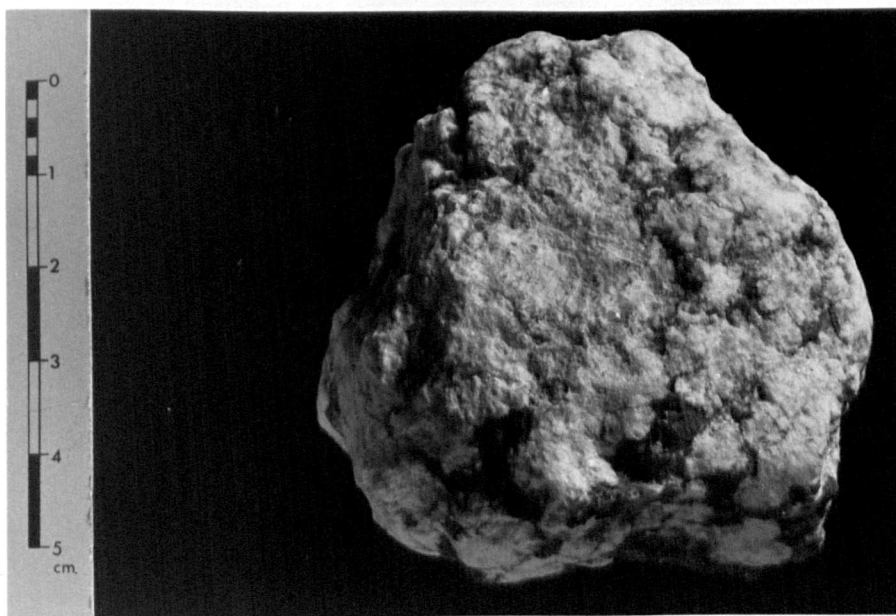


Plate 74 Plate showing a veatchite nodule made up of little needle-shaped crystals, Killik mine.

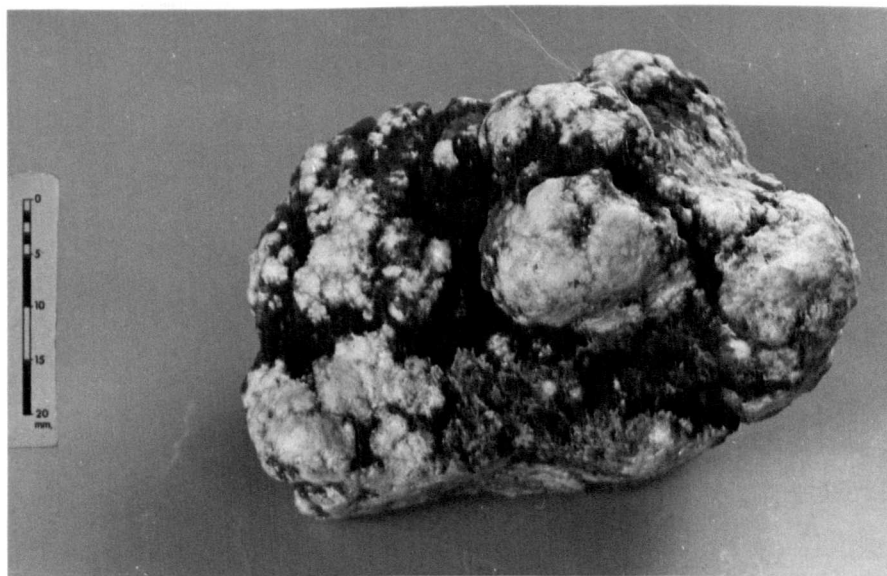


Plate 75 Very small nodules of a veatchite mineral associated together showing mamillary appearance, Killik mine.

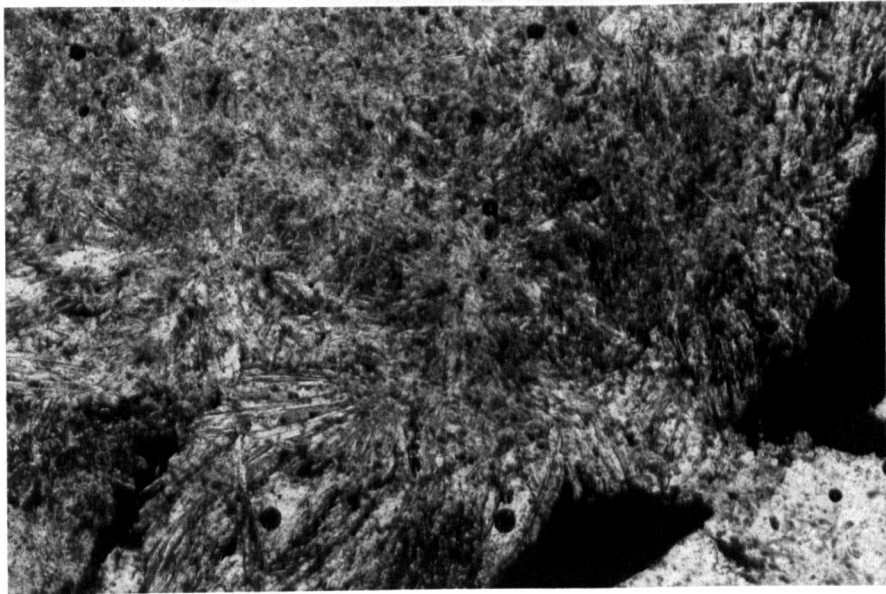


Plate 76 Plate showing very small crystals of veatchite mineral and colemanite crystals in the bottom right hand corner. Note also the appearance of clay and realgar. Plane polarized light, x10.

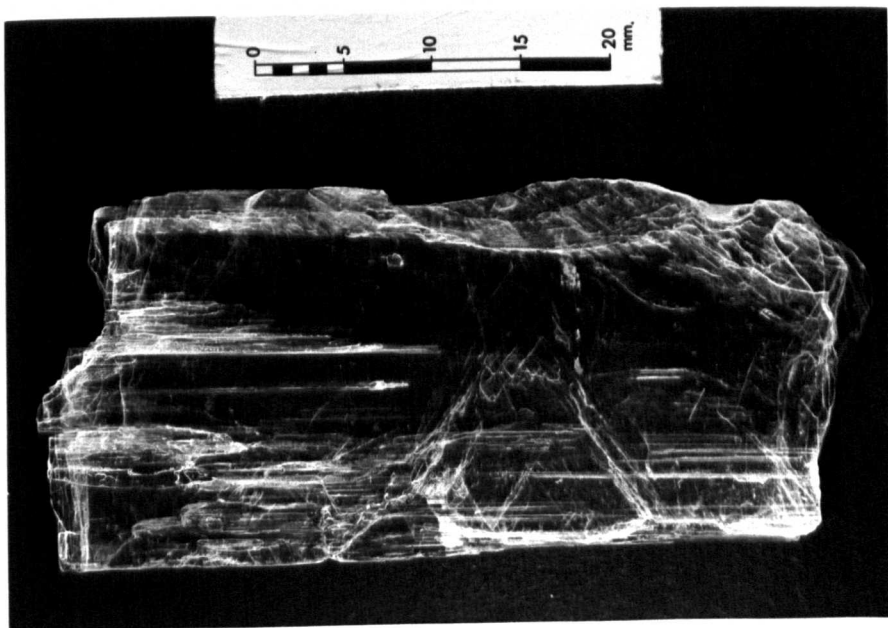


Plate 77 Individual flattened tunellite crystal showing perfectly developed cleavages and resembling muscovite flakes, Espey mine.

crystals which have nucleated on (but not replaced) ulexite (Plate 78). Pure flattened tunellite crystals are colourless, transparent and have perfectly developed cleavages parallel to flattened surfaces, which resemble muscovite flakes (see Plate 77). Alternatively tunellite occurs as small white nodules with radiating structures, which have apparently grown in the interbedded clays (Plate 79). In the Emet deposits, it is associated with ulexite and colemanite. Tunellite appears to have formed later than ulexite and colemanite, but not as a replacement. This mineral was first described from the Kirka deposit by Baysal (1972), but has not hitherto been identified in any other Turkish borate deposits.

Magnesium-calcium borates

Hydroboracite $(\text{MgCa}[\text{B}_3\text{O}_4(\text{OH})_3]_2 \cdot 3\text{H}_2\text{O})$

Hydroboracite is found throughout the deposits and occurs sporadically at three horizons in the northern basin and at one horizon in the southern basin. It forms small clusters (nodules) in which radiating needle-shaped crystals, 0.5-5cm, are randomly orientated (Plate 80). Radiating needle-shaped crystals of hydroboracite intersect with each other and groups of them show a conical appearance (Plate 81).

Sometimes, it forms thin layers within the interbedded clay. In the thin section, the needle-shaped crystals of hydroboracite have a fibrous texture. Plate 82 shows fibrous hydroboracite crystals with occasionally realgar, orpiment spots and clay particles.

This mineral is usually white, but sometimes it appears yellowish in colour due to the presence of realgar and orpiment. It is associated with colemanite and ulexite. It has no economic importance.

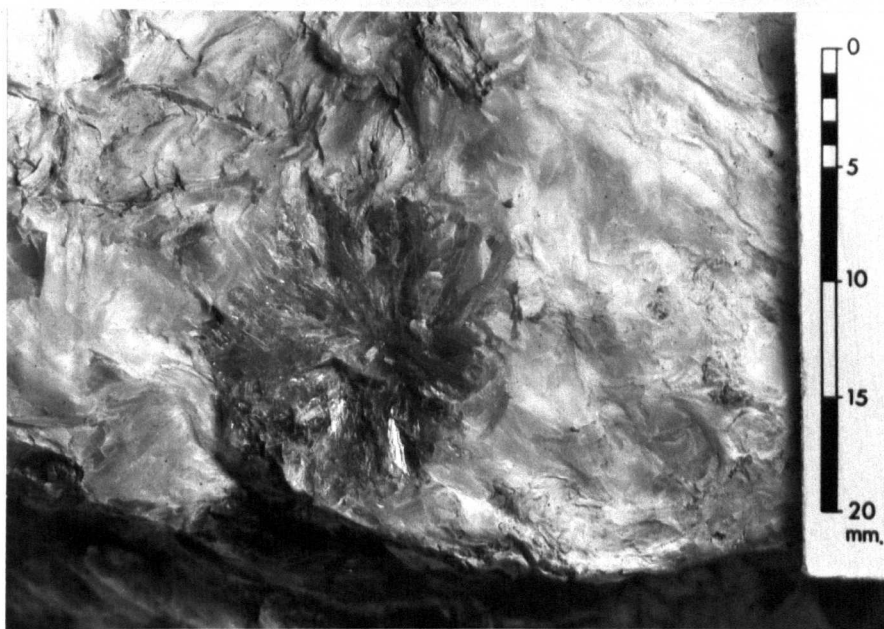


Plate 78 Plate showing thin tabular-shaped tunellite crystals nucleated on ulexite, Killik mine.

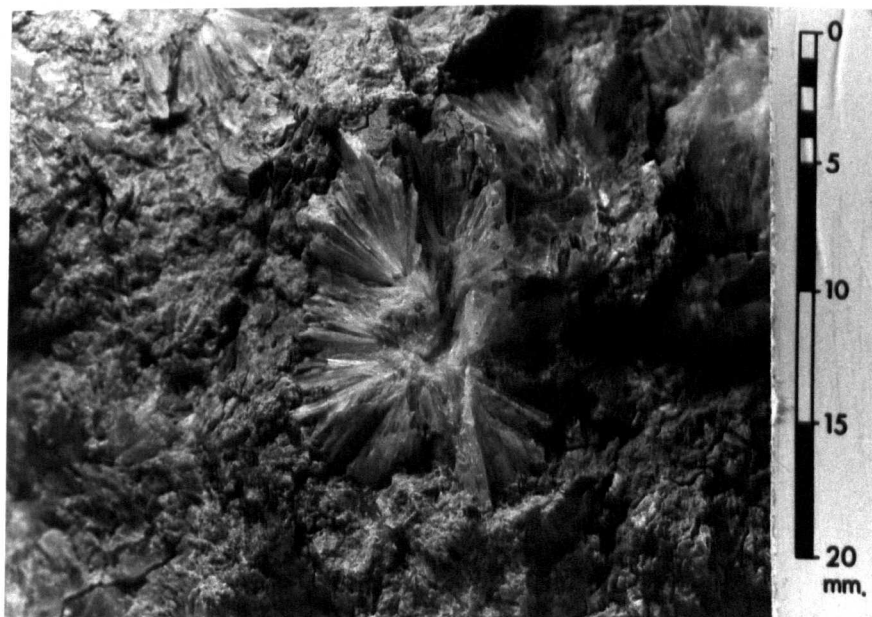


Plate 79 Small white tunellite nodules with radiating structures growing in the interbedded clays, Killik mine.

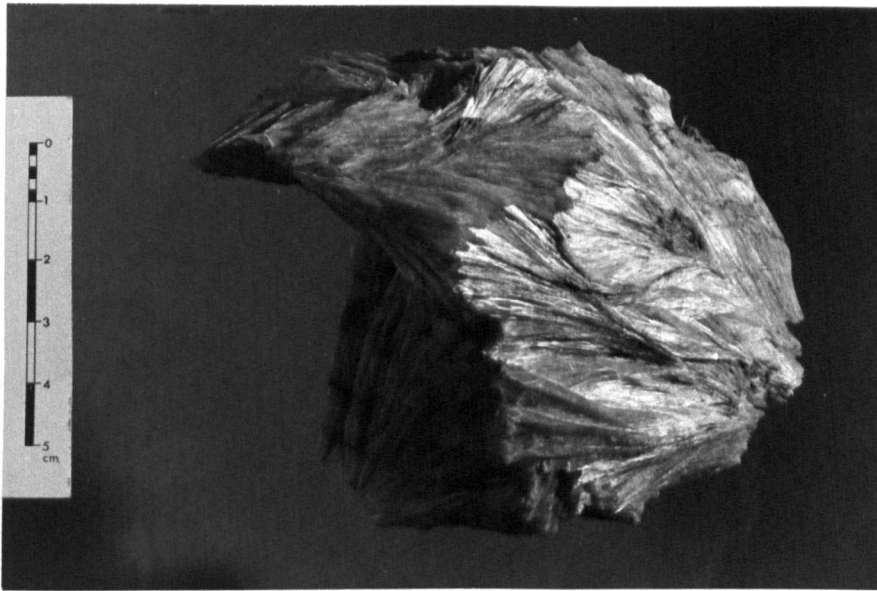


Plate 80 A small cluster of hydroboracite showing radiating needle-shaped crystals which are randomly orientated, Sarikaya locality.



Plate 81 Radiating crystals of hydroboracite intersecting with each other and groups of them showing a conical appearance, Killik locality.

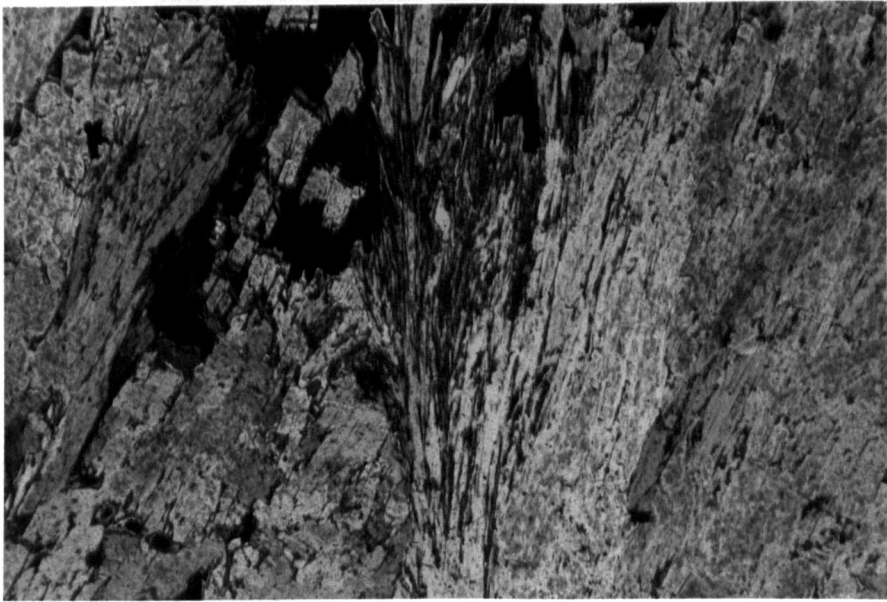


Plate 82 Plate showing fibrous hydroboracite crystals with occasional realgar, orpiment spots and clay particles. Crossed nicols, x10.

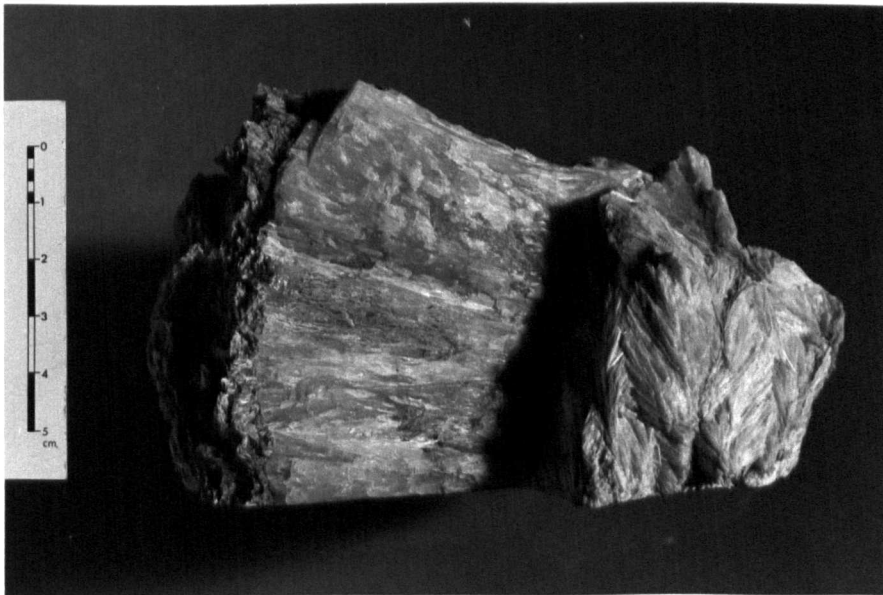


Plate 83 Plate showing colemanite alteration to hydroboracite. Colemanite gradually passing into hydroboracite towards the right hand corner, Sarikaya locality.

According to the field and textural evidence, hydroboracite appears to be an alteration product of colemanite. It is commonly intimately intergrown with colemanite (Plates 83 and 84) and is sometimes cut by later colemanite veins (see Plate 63). Plates 83 and 84 show clearly the textural relationship between colemanite and hydroboracite.

Complex borates

Teruggite $(\text{Ca}_4\text{Mg}[\text{AsB}_6\text{O}_{11}(\text{OH})_6]_2 \cdot 14\text{H}_2\text{O})$

Teruggite is rare, occurring sporadically at one horizon in the southern basin as very pure white, powdery potato-shaped nodules containing countless minute white euhedral crystals. The nodules of teruggite range from 2 to 10 cm in diameter (Plates 85 and 86).

Occasionally these powdery potato-shaped teruggite nodules contain very small spherulites of cahnite (Plate 87). This is the first record of this type of teruggite and cahnite occurrence from borate deposits. Teruggite was first recorded from the Loma Blanca deposit, province of Jujuy, Argentina, and described by Aristarian and Hurlbut (1968). The crystal structure of teruggite from the Emet deposits was described by Negro, Kumbasar and Ungaretti (1973).

The sporadic occurrence of teruggite and cahnite, compared with the almost universal distribution of arsenic sulphides in the Emet deposits, suggests that they developed in areas in which the brines were deficient in sulphides (probably H_2S) which would have otherwise precipitated the arsenic as realgar instead of arsenic bearing borates. Teruggite is associated with cahnite and colemanite.



Plate 84 Plate showing the association of hydroboracite and colemanite in the borate zone. Hydroboracite nodules are in the centre, Sarikaya locality.



Plate 85 A very pure white and powdery potato-shaped teruggite nodule, with rare clay inclusions, Kapikaya locality.

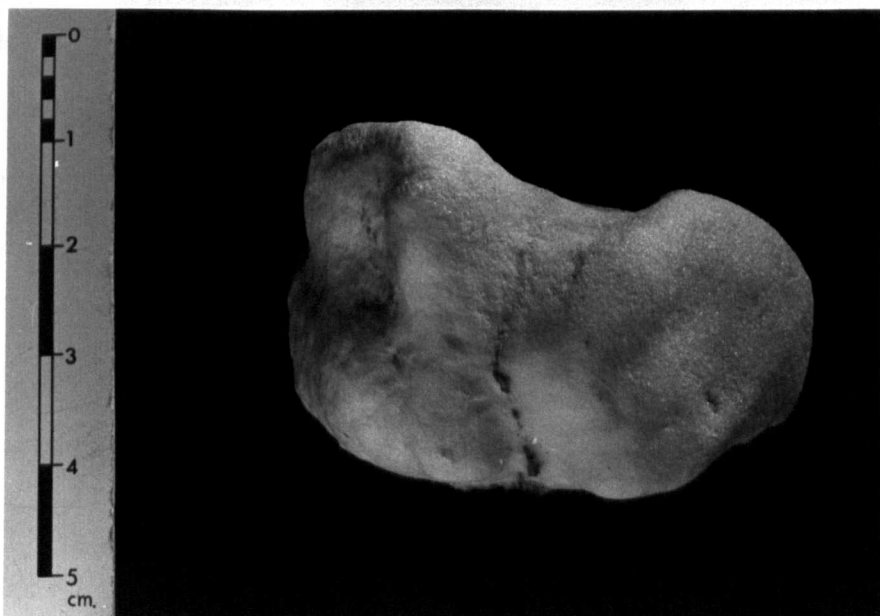


Plate 86 A very small, white and powdery teruggite nodule containing countless minute white crystals, Kapikaya locality.

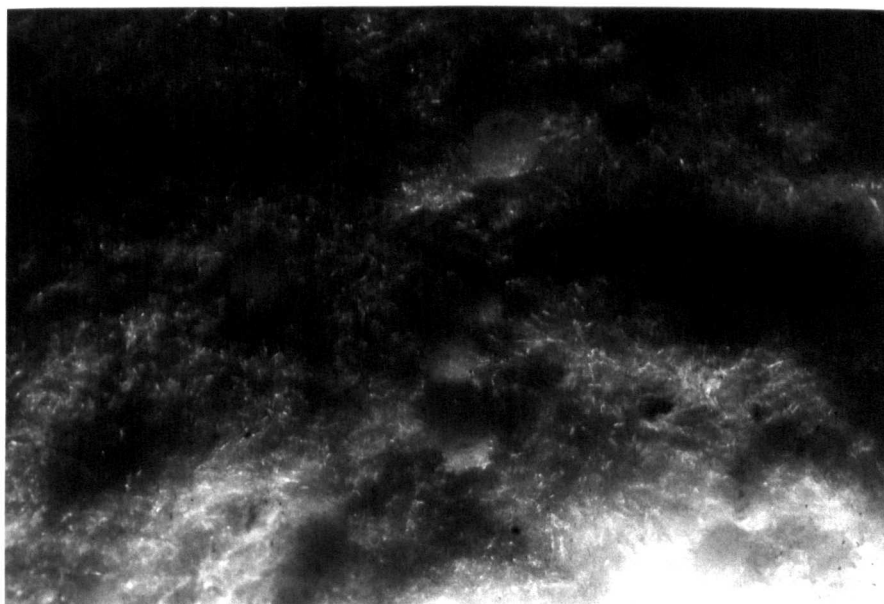


Plate 87 A powdery potato-shaped teruggite nodule containing very small spherulites of cahnite. Note also countless minute white euohedral crystals of teruggite, Kapikaya locality.

In the thin section, the crystals of teruggite are colourless, prismatic-shaped and are greatly elongated along the c axis. These crystals usually appear very small and needle-shaped (Plate 88). Occasionally spherulites of cahnite occur in the teruggite masses and fibrous crystals of cahnite show a radial texture (Plate 89).

Compound borates

Cahnite ($2[\text{Ca}_2\text{B}(\text{OH})_4\text{AsO}_4]$)

Cahnite, a very rare borate mineral, was first recorded from Franklin, New Jersey by Palache, et al (1927), appearing in the cavities of axinite veinlets associated with pegmatites cutting the main ore-body. Later discoveries of this mineral are associated with scarn zones as reported from the Klodeborg mine, Arendal, Norway, by B"ugge (1951) and from Eastern Siberia, U.S.S.R. by Malinko (1966). Cahnite was also recorded by Embrey (1960), from a cavity in dark grey leucitic lava at Capo di Bove, Rome, Italy, where it is found on calcite associated with phillipsite and chabazite.

Until now cahnite has not been identified from borate deposits. In the Emet borate deposits, cahnite occurs as very small spherulites in powdery potato-shaped teruggite nodules in the southern area (see Plate 87), and as a coating on euhedral colemanite crystals in vughs in colemanite nodules in the northern area (Plate 90; see also Plate 61). Cahnite is rare, occurring sporadically only at one horizon. It is associated with colemanite and calcite in the northern basin, whereas it is associated with teruggite and colemanite in the southern basin. The spherulites of cahnite are generally very small, rarely exceeding 2 mm in diameter and occurring usually singly, but occasionally two or three



Plate 88 Teruggite crystals appearing very small and needle-shaped in the thin section. Crossed nicols, x10.

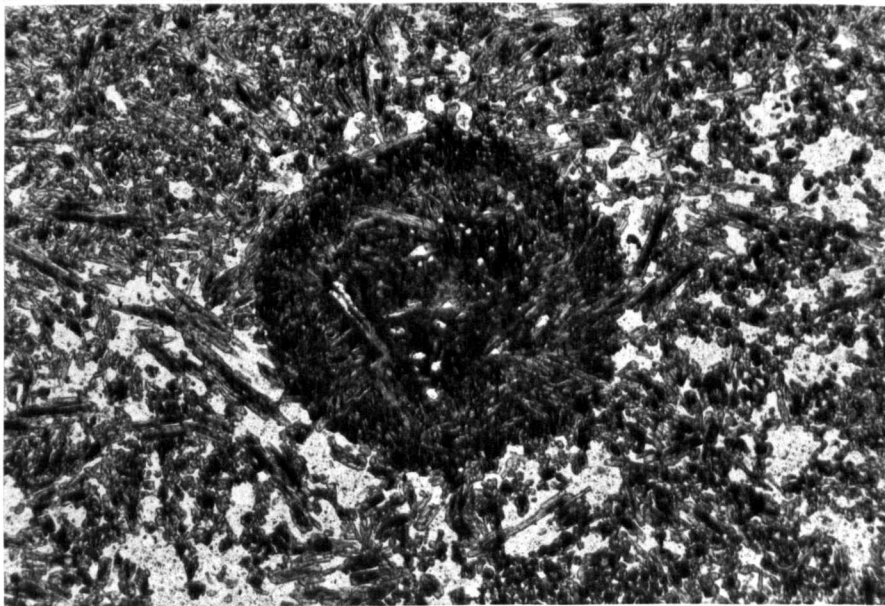


Plate 89 A spherulite of cannite occurring in the teruggite masses. Plane polarized light, x10.

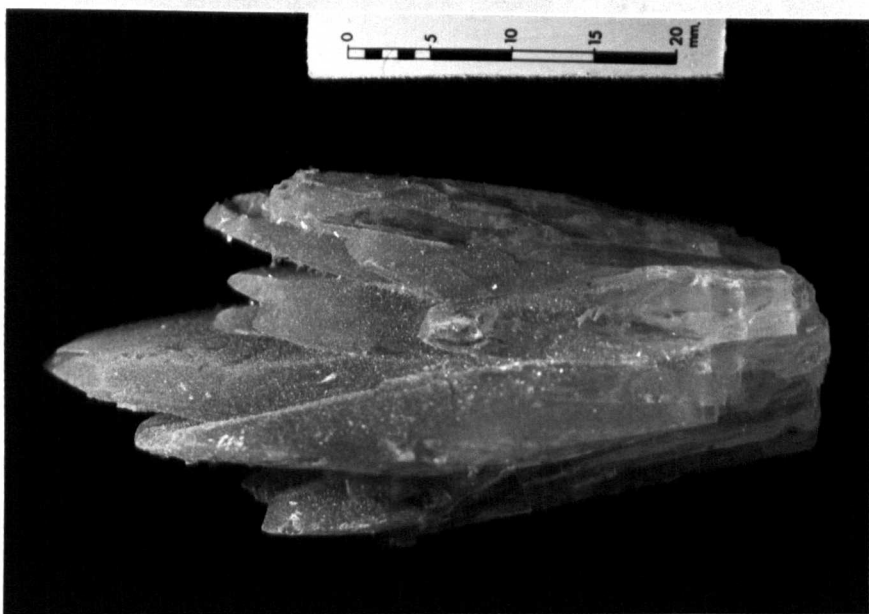


Plate 90 Cahnite occurring as a coating on euhedral colemanite crystals, Espey locality.

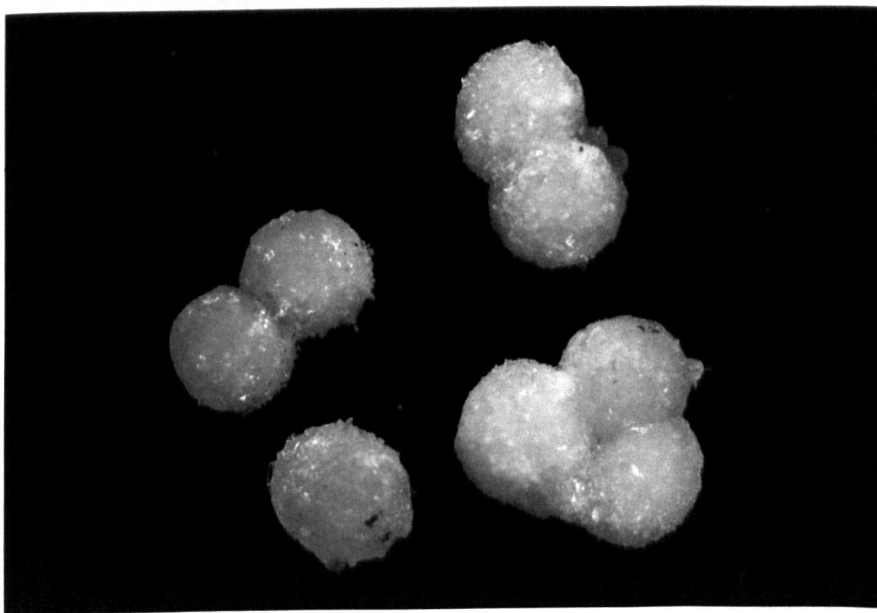


Plate 91 Plate showing spherulites of cahnite which rarely exceed 2mm in diameter

coalesce together (Plate 91). Cahnite is white and light brown in colour with a notable glassy lustre.

In the thin section, the cahnite spherulites contain needle-shaped and fibrous crystals which often show a radial texture (Plate 92; see also Plate 89).

Non-borate minerals

A number of non-borate minerals associated with borates occur in the borate zone (see Table 15). Realgar, orpiment and celestite are the common ones, but native sulphur, gypsum, calcite and quartz also occur. The occurrence of the clay minerals (such as montmorillonite and illite), and sulphide and sulphate minerals in the deposits is ubiquitous.

Native sulphur (S)

Native sulphur is almost ubiquitous in clays, tuffs and borates and appears to have formed at all stages during deposition and diagenesis. Sulphur occurs as very fine-grained crystals identified by X-ray diffractometer examination and has a pale yellow colour. Sulphur gives a yellow colouring to the clays and tuffs. It occasionally occurs as very thin layers up to 5-10 cm thick in the borate zone (see Fig.16 and Plate 22). It does not appear to be the result of the breakdown of sulphides. It is mostly concentrated in the lower part of the borate zone (see Plate 22).

Realgar (AsS)

By far the most widely occurring and most spectacular sulphide mineral at Emet is realgar. The brilliant red to blackish-red coloured realgar occurs in borate minerals (mainly colemanite), clays, tuffs and frequently in vughs of colemanite

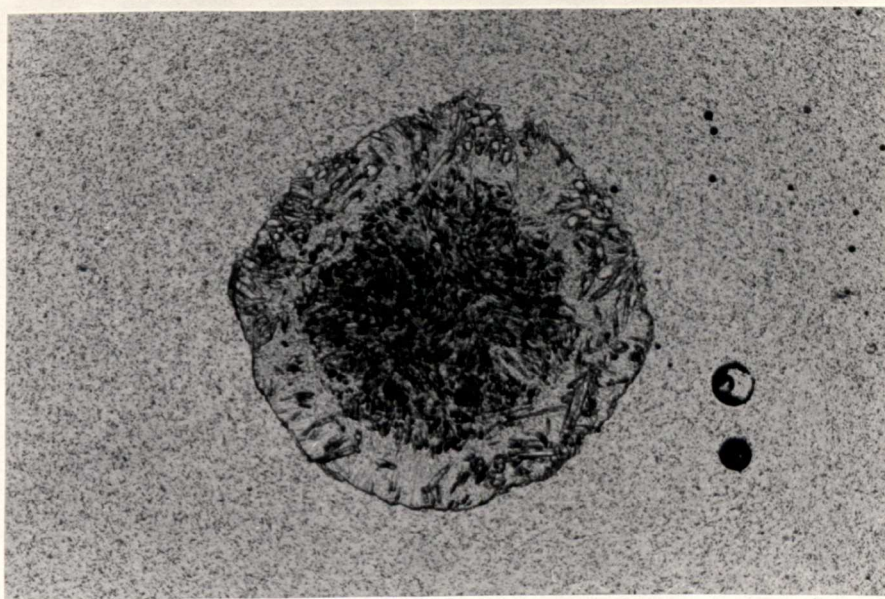


Plate 92 A cannite spherulite containing needle-shaped and fibrous crystals which show a radial texture. Plane polarized light, x10.



Plate 93 Plate showing realgar crystals exceeding 2cm in length, Sarikaya locality.

nodules (see Fig.8 and Plate 63). When realgar is exposed to the sunlight it decomposes, tarnishing to a dull orange or bright yellow orpiment. The clay of the borate zone is, usually, orange or red coloured from the included realgar and orpiment.

More rarely the realgar is found as euhedral columnar crystal aggregates growing on top of colemanite crystals, nodules and vughs, as well as in cavities. These realgar crystals exceed 2 cm in length (Plate 93). Often the realgar is also found included within single colemanite or other borate crystals as very fine-grained crystals.

Larger amounts of realgar occur with the colemanite. Realgar and orpiment-bearing colemanite nodules are quite common. However, the arsenic sulphide in the nodules is mostly concentrated in the included clay and rarely in the colemanite. These colemanites include realgar and orpiment and show a bright orange to red colour (Plate 94).

Orpiment (As_2S_3)

Orpiment is nearly always associated with realgar in the clays, tuffs and borate minerals. It is an alteration product of realgar, which decomposes readily to orpiment on exposure to the sunlight. It occurs, usually, as bright orange or yellow in colour and is very fine-grained (see Fig.8 and Plate 63). Some clay beds and borate minerals are coloured orange by their high realgar content (see Plates 25 and 42).

Orpiment is also often found in the vughs of minerals and in the thin section very thin orpiment and realgar veins are observed cross-cutting the colemanite and other borate minerals (see Plate 56).



Plate 94 Colemanite showing a bright orange to red colour, which includes realgar and orpiment, Killik locality.



Plate 95 Celestite crystals occurring in the vugh of a colemanite nodule, Sarikaya locality.

Celestite (SrSO_4)

Celestite occurs in colourless, pale blue or often blue, long orthorhombic crystals in the vughs of colemanite (Plates 95 and 96; see also Plate 60) and on top of the colemanite crystals or nodules (Plate 97). These pale blue perfect celestite crystals exceed 4 cm in length (Plate 98; see also Plate 96), but they lose their blue appearance and become almost colourless and transparent when they are exposed to the sunlight.

Celestite also occurs in thin veins up to 5-10 cm thick with medium to fine-grained crystals in the clays and tuffs, filling mainly cracks and joints. It is commonly intergrown with colemanite which also shows a blue colour due to the presence of celestite. Celestite is common, occurring sporadically at several horizons in the southern and northern basins.

Gypsum ($\text{CaSO}_4 \cdot 2\text{H}_2\text{O}$)

Selenite, a crystal form of gypsum, and fibrous gypsum associated with borate minerals have been observed only in the Göktepe and Kapıkaya (Hisarcik) localities. Fibrous gypsum and selenite occur commonly in the clays interbedded with the borates. Perfect monoclinic flattened crystals of selenite are up to 5 cm in length, are transparent or dark brown in colour due to clay inclusions and show "swallow-tails" twins (Plate 99). When selenite crystals appear together, they resemble barite rosettes. Often individual selenite crystals appear to be rounded and resemble desert roses (Plate 100).

Fibrous gypsum veins with median lines and clay inclusions (Plate 101) are tilted and cut the clay beds in the Göktepe locality. They are usually colourless but sometimes



Plate 96 Perfect long orthorhombic celestite crystals growing in the vugh of colemanite, Dereköy locality.

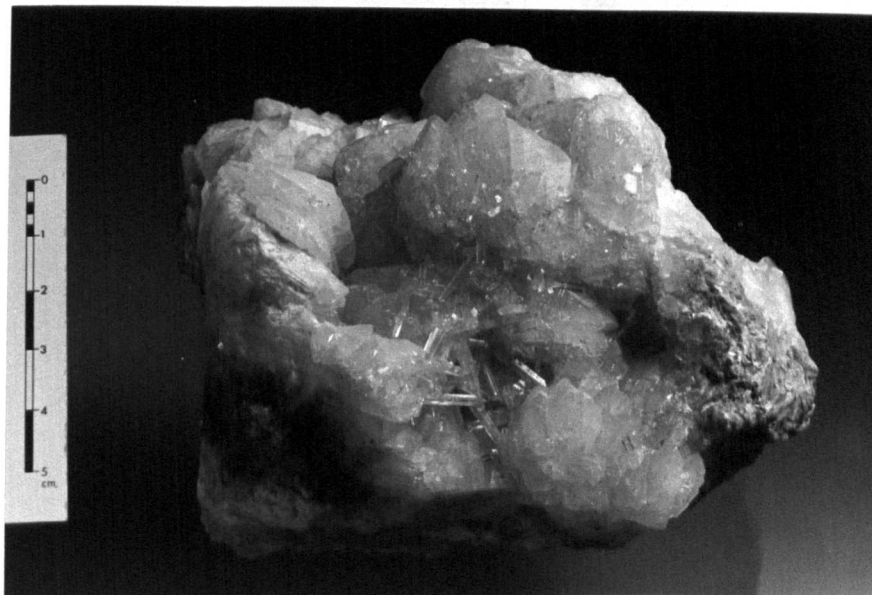


Plate 97 Perfect celestite crystals occurring on top of the colemanite crystals, Kapikaya locality.

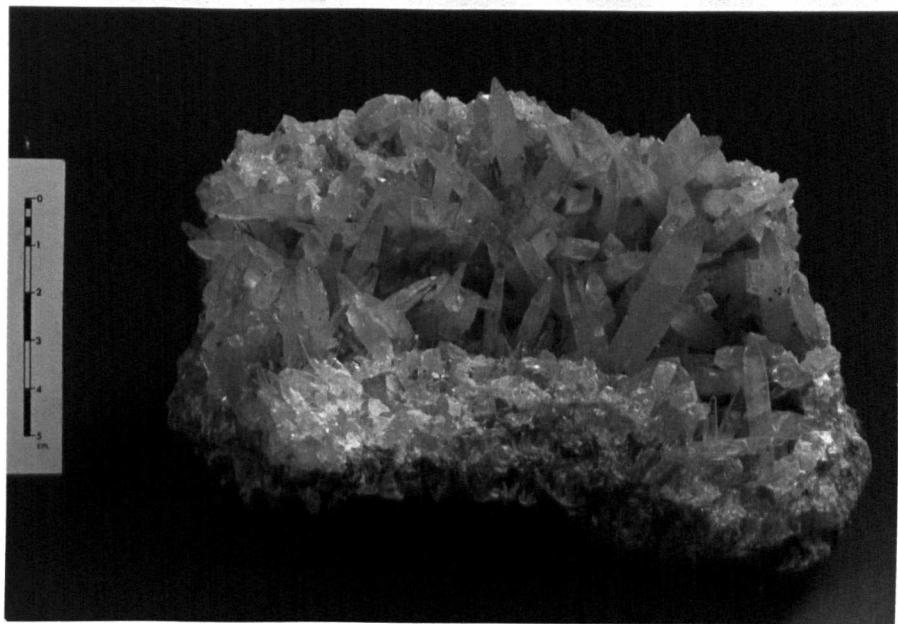


Plate 98 Pale blue perfect celestite crystals exceeding 4 cm in length, Kapikaya locality.

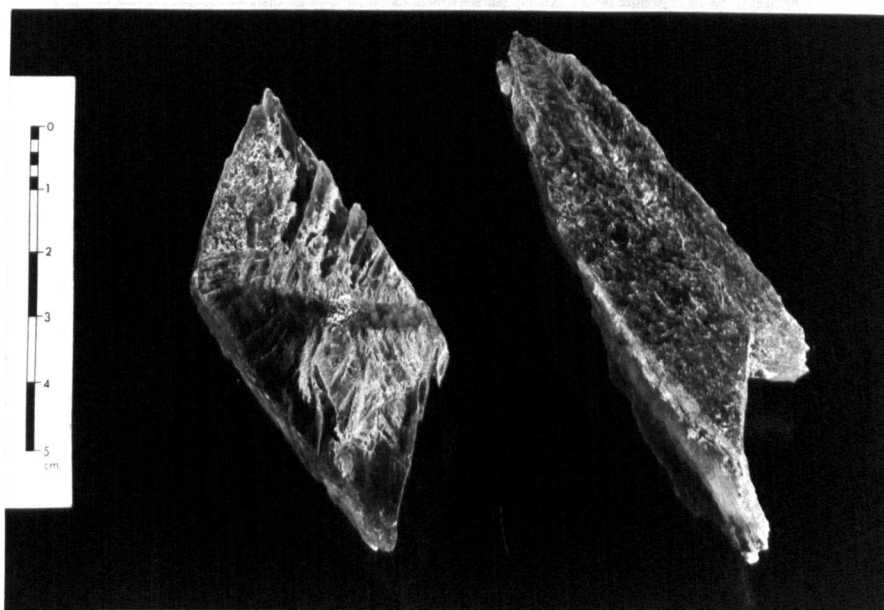


Plate 99 Plate showing perfect monoclinic flattened selenite crystal and the 'swallow-tails' twins of selenite, Göktepe, locality.

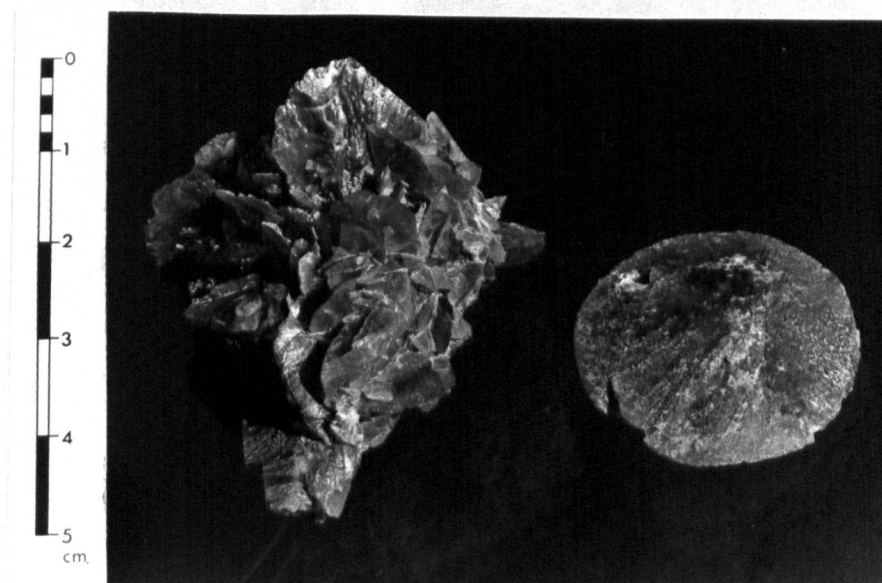


Plate 100 Plate showing selenite crystals resembling barite rosettes and a desert rose-like selenite crystal, Göktepe locality.

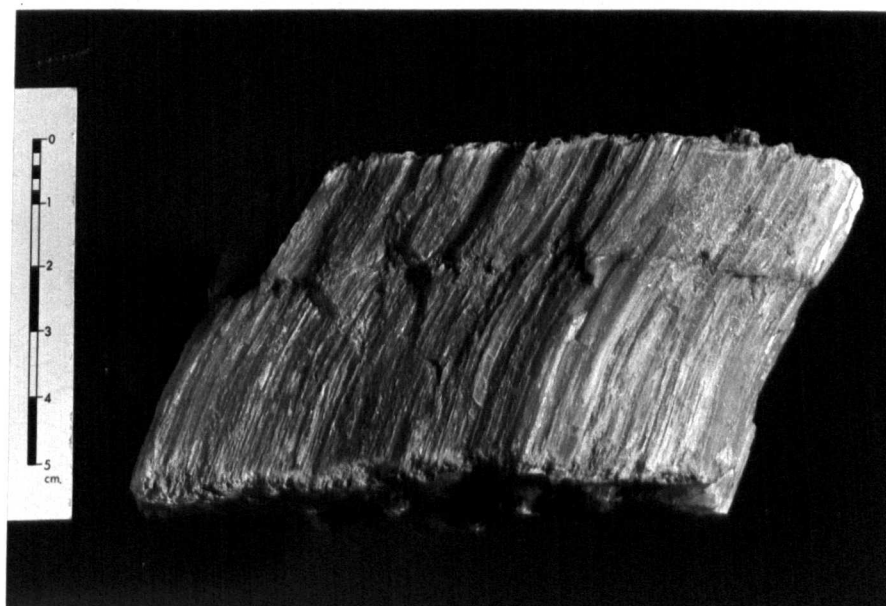


Plate 101 Fibrous gypsum veins with median lines and clay inclusions, Göktepe locality.

greyish in colour. In the thin section of fibrous gypsum, the fibres have well defined crystal boundaries and they appear as dark and light bands, similar to plagioclase lamellar twinning (Plate 102).

Calcite (CaCO_3)

Calcite occurs throughout the deposits at almost every horizon in the clays and as common intimate intergrowth with the borates due to the presence of carbonic acid during deposition and diagenesis. However, calcite also occurs in surface outcrops and adjacent to faults as a result of modern alteration of colemanite (Plate 103, see also Plate 64). This has been proved by using the staining methods of Dickson (1965 and 1966), field observations and microscope studies. After the staining tests, calcite was stained pink in colour (see Plates 65 and 66). In the thin section, the alteration of colemanite to calcite has also been observed and the alteration of colemanite starts from the outer edge of the crystals which are exposed to the air (Plate 104).

Occasionally calcite occurs as very thin layers up to 10-15 cm thick and its colour varies from colourless and white through various shades of yellow, brown and grey.

Quartz (SiO_2)

Quartz in one form or another is distributed throughout the deposits. Principally, it occurs as small grains in clays and as more or less discrete crystals in the tuff beds. The variety chert has been found as a grey to black layer up to 1 metre thick immediately above the borate zone in the upper limestone (Plate 105).



Plate 102 Fibrous gypsum with basal pinacoidal cleavage.
Crossed nicols, x10.

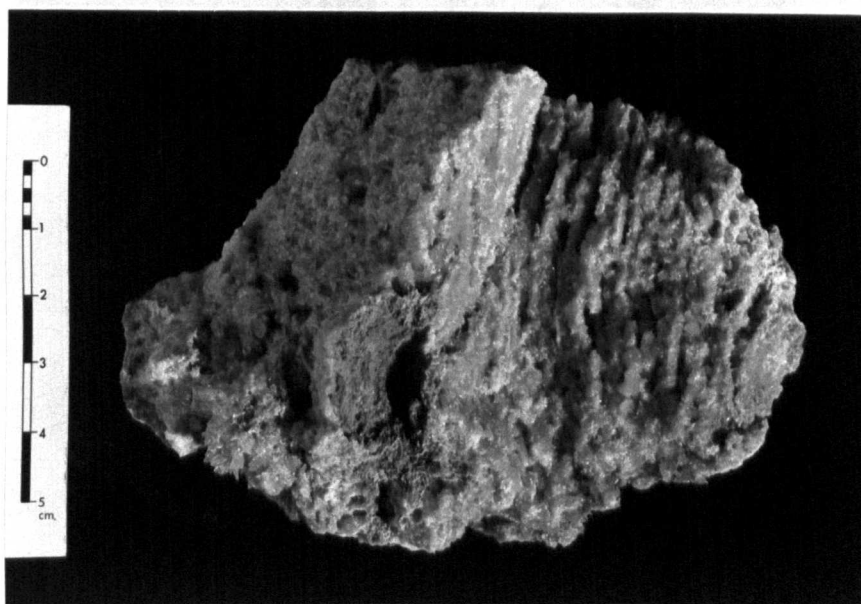


Plate 103 Scalenohedral crystals of calcite which is an
alteration product of colemanite, Espey locality.

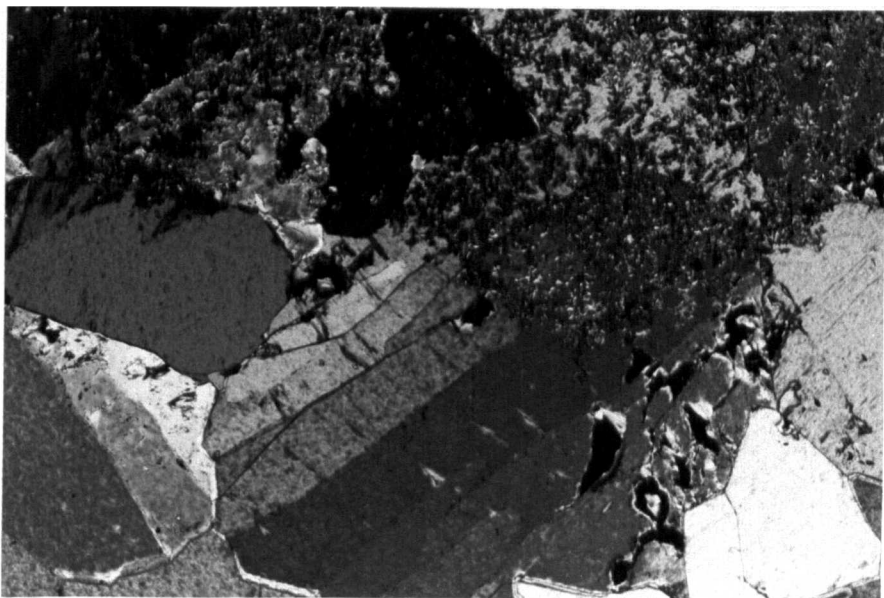


Plate 104 Colemanite crystals altering to calcite from their outer edges. Plane polarized light, x10.

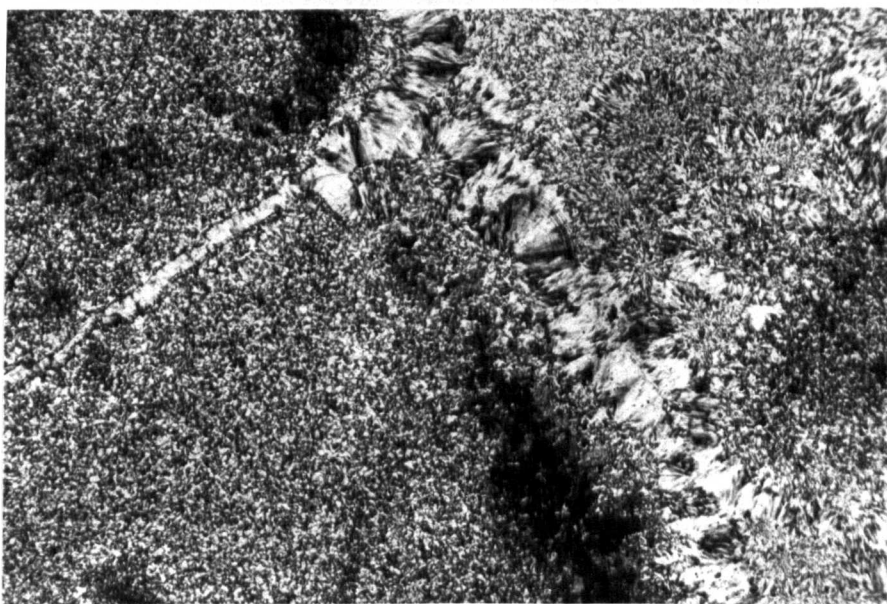


Plate 105 Chert (the variety of quartz) occurring in the upper limestone. Crossed nicols, x10.

3. Geographical distribution and mineral assemblages

The distribution and assemblages of minerals in the borate zone differ at different levels in the sequence. There is also an overall difference between the northern area (Espey-Killik) and the southern area (Hisarcik), sufficient to suggest that they were deposited in separate (but possibly occasionally inter-connected) basins.

Brines in the Emet borate deposits (palaeolakes) were evidently rich in Ca^{++} and B^{+++} in both northern and southern basins and the Ca borate mineral (colemanite) is present at every horizon throughout the sequence. Hydroboracite and cahnite occur sporadically throughout the deposits. Present observations also suggest that meyerhofferite, ulexite, tunellite and the veatchite mineral are restricted to the north and teruggite to the southern basin. Chemically this implies that conditions were more favourable from time to time for the formation of Na-Ca borates and Sr borates in the thicker northern deposits than in the south (Figs. 22 and 23).

Non-borate minerals (see Table 15) are almost ubiquitous and present throughout the Emet borate deposits (see Figs. 22 and 23).

The sequences of minerals in the Hisarcik area are different to those in the Espey-Killik localities, as is shown in Fig. 22 and Fig. 23. Nevertheless both areas show a similar trend, which is considered to represent one cycle of deposition, from carbonate to borate and back to carbonate.

The principal borate mineral assemblages observed are:- colemanite - meyerhofferite; colemanite - ulexite - hydroboracite; colemanite - hydroboracite; colemanite - veatchite; colemanite - ulexite - tunellite; colemanite - teruggite - cahnite; colemanite - cahnite; ulexite - hydroboracite;

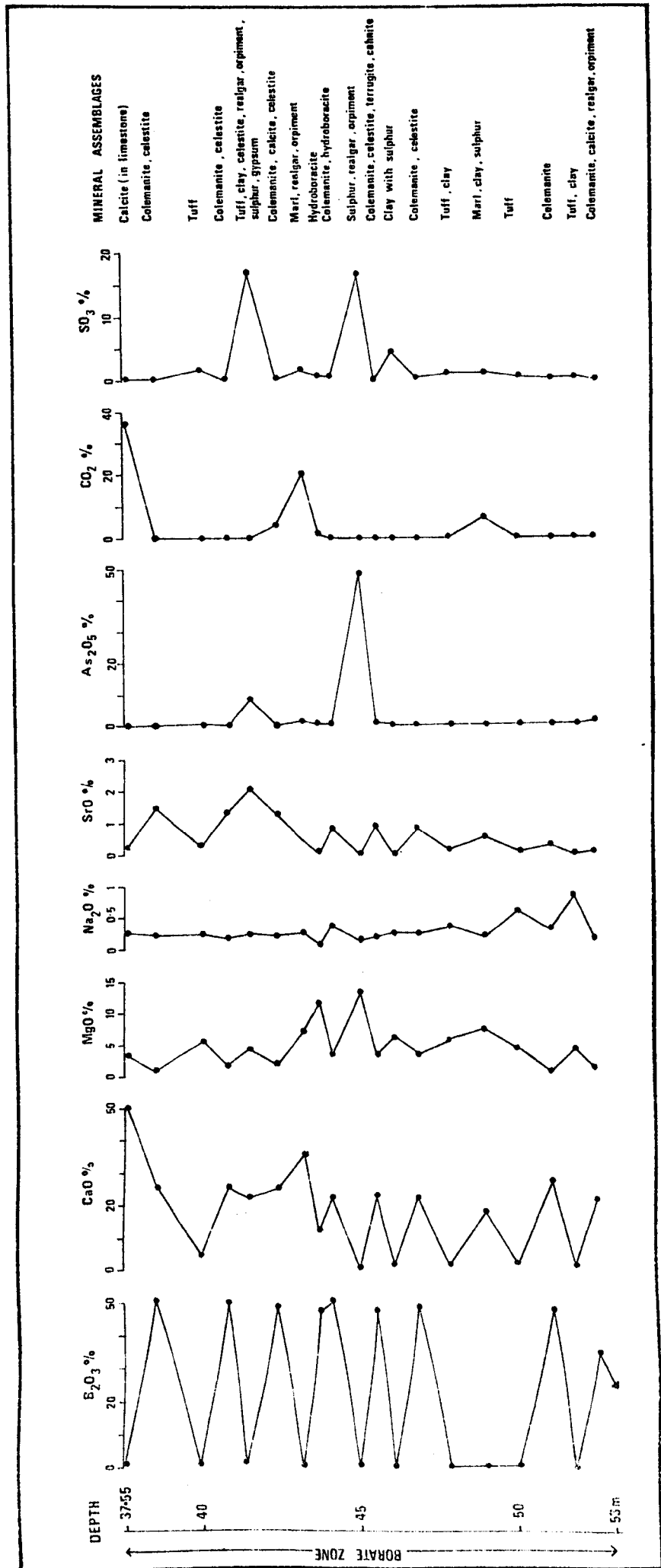


Fig.22. Major oxide and mineral assemblages variation with depth in the southern area (Sarikaya section, Hisarcik).

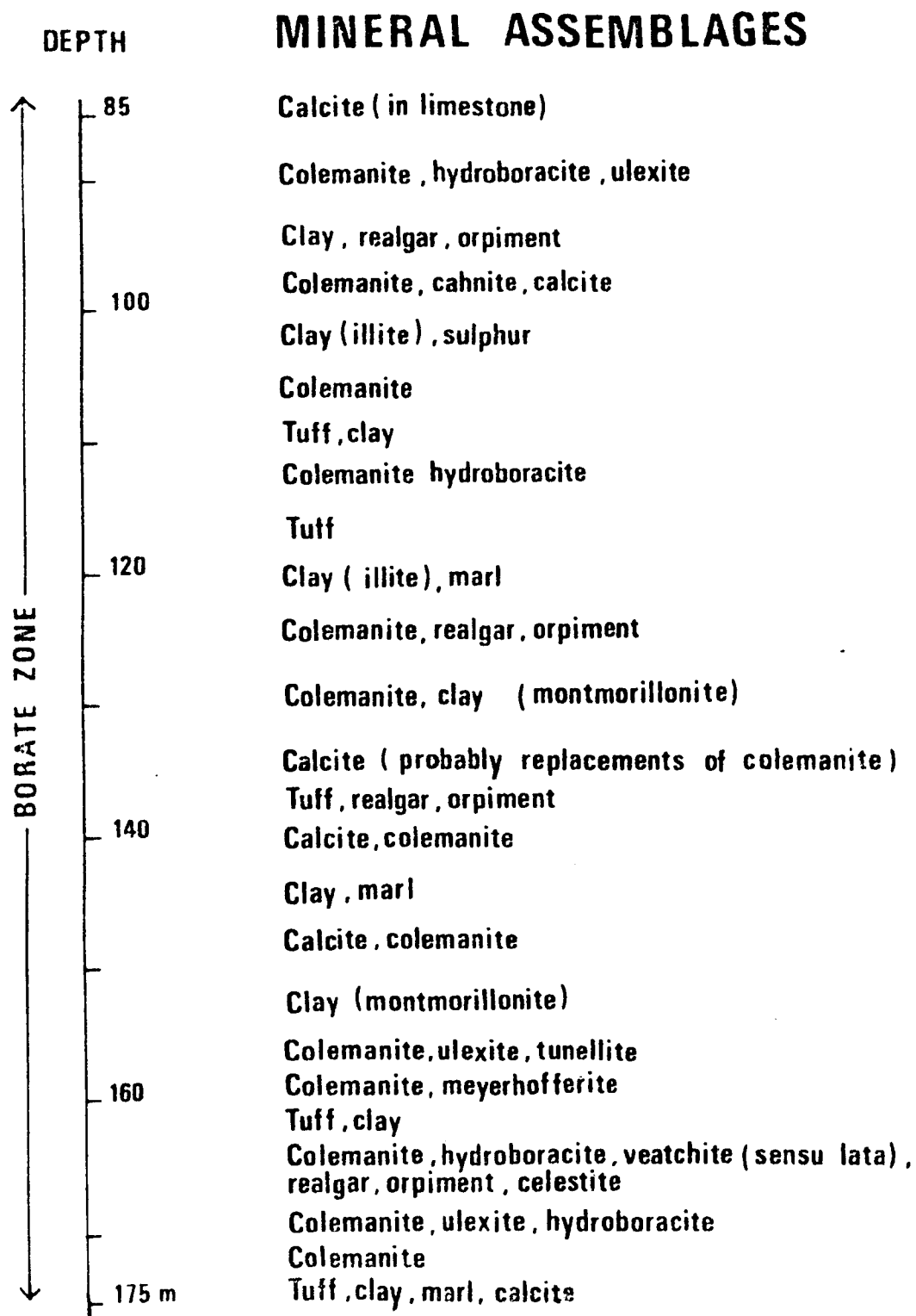


Fig.23. Mineral assemblages variation with depth in the northern area (Espey-Killik).

ulexite - tunellite and teruggite - cahnite (see Figs. 22 and 23). Colemanite - hydroboracite; colemanite - veatchite; colemanite - cahnite and teruggite - cahnite assemblages are believed to be developed during the secondary processes.

CHAPTER VII

GEOCHEMISTRY OF THE BORATES AND OTHER MINERALS

1. Introduction

In the present study, a total number of 59 colemanite, 11 colemanite with clay fractions, 31 other borate minerals and 15 non-borate mineral samples were collected from several sections along the borate zone. Most of the samples collected were obtained in the open pit in the Hisarcik locality and in the underground workings of the Espey and Killik mines. Additional samples were collected from the Göktepe and Dereköy localities. The location and distribution of samples is given in the Appendix (see also Figs. 12, 13 and 14).

Samples were analysed for up to 28 elements, mostly by the use of an X.R.F. spectrometer and atomic absorption spectrophotometry. The analytical methods for individual elements are given in more detail in the Appendix. Following the normal practice, the major constituents are described by their oxides (weight per cent) and the trace constituents by their elements (parts per million); but the listing of the major and trace elements for individual samples is reorganised in order to represent the chemical composition of the borate and non-borate minerals more systematically. As and S are expressed as both oxides and elements depending on individual mineral chemistry, but for convenience these elements

are always shown by their oxides in the tables.

Although the minerals are grouped as calcium borate (colemanite), other borates and non-borates, summary statistics and correlation matrices of the analyses were only carried out for the calcium borate (colemanite). This was because over 60% of the samples analysed were colemanite, which also comprises over 95% of the deposits. The other minerals are sporadic in occurrence, variable in mineralogy and hence do not provide a valid population for statistical analysis. Summary statistics of the chemical analyses for colemanite from the southern area (Hisarcik) and the northern area (Espey-Killik) are given separately in Tables 16 and 17. Correlation matrices of elements for the whole colemanite population is given in Table 18. The chemical analyses for individual samples of colemanite, colemanite and clay mixture, other borates and non-borate minerals are given respectively in Tables, 20, 21, 22 and 23.

The main purpose of geochemical investigation of the borates (mainly colemanite) from the Emet borate deposits are summarised as follows:-

*a) To establish the chemistry and to provide chemical analyses for large numbers of elements for the economically important colemanite and the other borates of the Emet district.

b) To provide chemical analyses for new occurrences of borate minerals and also for non-borate minerals.

*c) To study the presence of the elements and their correlation with each other in the colemanite.

d) To investigate the vertical and lateral distribution and variation of boron and other elements in the borate zone.

Table 16 Summary statistics for colemanite from
Hisarcik locality.

<u>Element</u>	<u>Mean</u>	<u>St.Dev</u>	<u>Maximum</u>	<u>Minimum</u>	<u>Range</u>
B ₂ O ₃	47.63	2.08	51.05	42.12	8.93 ✓
CaO	24.19	2.04	26.88	18.20	8.68
MgO	1.92	1.24	5.21	0.57	4.64
Na ₂ O	0.24	0.05	0.35	0.14	0.21
SrO	1.51	0.81	3.99	0.32	3.67
As ₂ O ₅	0.21	0.31	1.28	0.01	1.27
SiO ₂	2.63	2.02	8.09	0.48	7.61
K ₂ O	0.06	0.10	0.37	0.00	0.37
H ₂ O	19.91	0.70	21.35	18.72	2.63
SO ₃	0.30	0.26	1.13	0.05	1.08
Al	973	811	2863	133	2730
Fe	767	514	2318	0*	2318
Mn	22	16	56	3*	53
P	119	171	801	14*	787
Cl	132*	30	225	92*	133
Cr	8*	3	14	4*	10
Ni	5*	3	14	1*	13
Cu	27	12	61	6	55
Zn	7*	3	13*	3*	10
Br	0*	1	3*	0*	3
Sn	24	6	46	14	32
Ba	27*	38	149*	0*	149
Ce	214*	225	966*	60*	906
Pb	4*	7	31	0*	31
Th	2	2	7	0*	7
U	0*	1	2*	0*	2

* Indicates values below the detection limit

Table 17 Summary statistics for colemanite from Espey
and Killik localities

<u>Element</u>	<u>Mean</u>	<u>St.Dev</u>	<u>Maximum</u>	<u>Minimum</u>	<u>Range</u>
B ₂ O ₃	47.39	2.75	52.07	41.22	10.85
CaO	24.20	1.44	26.32	20.65	5.67
MgO	1.33	1.10	4.94	0.32	4.62
Na ₂ O	0.19	0.10	0.35	0.00	0.35
SrO	1.22	0.67	2.22	0.31	1.91
As ₂ O ₅	0.11	0.19	0.80	0.00	0.80
SiO ₂	2.29	2.33	8.33	0.04	8.29
K ₂ O	0.32	0.38	1.29	0.00	1.29
H ₂ O	20.35	1.08	22.41	17.20	5.21
SO ₃	0.36	0.49	2.51	0.06	2.45
Al	2439	2794	9881	0*	9881
Fe	1987	1980	9044	60	8984
Mn	37	40	153	0*	153
P	125	107	441	27*	414
Cl	165*	176	978	64*	914
Cr	12	7	29	4*	25
Ni	14	13	47	0*	47
Cu	22	17	59	0*	59
Zn	11*	7	28	3*	25
Br	1*	1	2*	0*	2
Sn	24	11	37	0*	37
Ba	104*	107	336	0*	336
Ce	132*	120	557	55*	502
Pb	8*	5	21	1*	20
Th	2	2	10	0*	10
U	0*	1	2*	0*	2

* Indicates values below the detection limit

*e) To study the relationships between borate and associated minerals.

*f) To help explain the problem of the origin and diagenesis of the borates and non-borates in terms of their minor and trace element contents.

g) To investigate the colour variation in the colemanite and other borates by using some of the minor and trace elements.

2. Distributions, variations and inter-element correlations

Element distributions, variations and correlations of colemanite samples are discussed in the light of summary statistics of the chemical analyses (Tables 16 and 17) and the correlation matrices of colemanite sample populations (Table 18). Major element variations with depth in the southemarea (Hisarcik) were given in Fig. 22.

Colemanite is a member of the Ca borates series in the $\text{CaO} - \text{B}_2\text{O}_3 - \text{H}_2\text{O}$ system. Although it can be of very high purity, natural specimens of colemanite nearly always contain small amounts of clay and other minerals.

Besides B_2O_3 , CaO and H_2O , colemanite contains minor and trace amounts of other elements which usually occur in the following ways:-

a) In isomorphous substitution for Ca, e.g. Mg, Sr and Ba.

b) Precipitation with calcium borate (colemanite) as evaporite minerals, e.g. the elements Mg, Sr, Na, As and S in the minerals hydroboracite, teruggite; veatchite, tunellite, celestite; ulexite; teruggite, cahnite, realgar, orpiment; and native sulphur, celestite, gypsum, realgar and orpiment respectively.

Table 18

===== COLEMANITE - CORRELATION MATRIX =====

203	1.0000					
AO	0.8649*	1.0000				
BO	-0.7828	-0.6806	1.0000			
CA20	-0.3970	-0.4089	0.1576	1.0000		
CO	-0.5872	-0.5822	0.4332+	0.4190+	1.0000	
AS205	-0.2495	-0.2724	0.2271	0.3898	0.3511	1.0000
BI02	-0.8653	-0.9321	0.6912*	0.3352	0.4150+	0.1480
FI02	-0.7633	-0.8733	0.5426*	0.2885	0.3197	0.1223
K20	-0.7804	-0.8741	0.5455*	0.2846	0.3297	0.0881
H20	0.6223*	0.5503*	-0.6883	-0.3530	-0.3314	0.0328
SO3	0.0219	0.0069	-0.1776	0.4013+	0.2874	0.2004
AL	-0.7791	-0.8891	0.5320*	0.3326	0.3508	0.1078
FE	-0.4207	-0.4983	0.1219	0.5103+	0.4004+	0.0716
MN	-0.8026	-0.8170	0.7068*	0.3716	0.4206+	0.2477
P	-0.5449	-0.5652	0.4026+	0.1312	0.2126	0.0015
CL	-0.1021	-0.0079	-0.0421	0.0811	0.2118	-0.0375
CR	-0.7287	-0.8403	0.4566+	0.2630	0.2695	0.1232
NI	-0.3226	-0.4647	0.0517	0.4910+	0.2504	-0.0053
CU	-0.7583	-0.7998	0.5044+	0.6086*	0.8356*	0.3778
ZN	-0.6285	-0.8404	0.5937*	0.2373	0.4048+	0.1449
BR	0.2494	0.1630	-0.2595	-0.1183	0.2001	-0.3754
SN	-0.6149	-0.4915	0.2031	0.6390*	0.3398	0.1554
BA	0.3991	0.1838	-0.1272	-0.6828	-0.1699	-0.4595
CE	-0.2220	-0.2436	0.2128	0.3231	0.3229	0.9926*
PE	-0.0697	-0.2519	0.2571	-0.0285	0.2249	-0.0715
TH	-0.4006	-0.4136	0.0729	0.1130	0.0272	-0.1634
U	0.1597	0.1856	0.0078	-0.2988	-0.2118	-0.1379
	BO03	CA0	MO0	NA20	SO0	AS205

Table 18 (continued)

SiO2	1.0000					
TiO2	0.9329*	1.0000				
K2O	0.9531*	0.9820*	1.0000			
H2O	-0.5870	-0.5864	-0.5981	1.0000		
SO3	-0.1577	-0.1451	-0.1709	0.0951	1.0000	
AL	0.9482*	0.9901*	0.9919*	-0.6026	-0.1458	1.0000
FE	0.4160+	0.4903+	0.4592+	-0.3025	0.7557*	0.4868+
MN	0.8640*	0.8910*	0.8698*	-0.6835	-0.0952	0.8809*
P	0.6652*	0.6264*	0.6815*	-0.3503	-0.1357	0.6298*
CL	0.0597	0.0970	0.0974	-0.2617	-0.0508	0.0997
CR	0.8738*	0.9492*	0.9358*	-0.5153	-0.1083	0.9491*
NI	0.4277+	0.5486*	0.5205*	-0.2932	0.5600*	0.5532*
CU	0.6498*	0.6159*	0.6242*	-0.5446	0.2719	0.6540*
ZN	0.8290*	0.8870*	0.8775*	-0.6101	-0.1106	0.8864*
BR	-0.2992	-0.3376	-0.3425	0.2380	0.3307	-0.3204
SN	0.5963*	0.5555*	0.6006*	-0.3766	0.1016	0.5877*
BA	-0.2581	-0.2181	-0.2513	0.2314	-0.2730	-0.2428
CE	0.1255	0.1184	0.0795	0.0602	0.1925	0.0974
PB	0.2111	0.3377	0.2773	-0.3318	-0.0411	0.2988
TH	0.4922+	0.6426*	0.6095*	-0.4341	-0.1891	0.6309*
U	-0.1440	-0.2499	-0.2376	0.3365	-0.0672	-0.2502
	SiO2	TiO2	K2O	H2O	SO3	AL

Table 18 (continued)

FE	1.0000					
MN	0.4452+	1.0000				
P	0.2346	0.5495*	1.0000			
CL	0.0396	-0.0060	0.0040	1.0000		
CR	0.4968+	0.8468*	0.4832+	-0.0186	1.0000	
NI	0.8721*	0.5264*	0.3124	-0.0841	0.5886*	1.0000
CU	0.5846*	0.6766*	0.4249+	0.1918	0.5810*	0.5320*
ZN	0.4395+	0.8210*	0.6238*	-0.0024	0.8107*	0.5244*
BR	0.1551	-0.3918	-0.4353	-0.1958	-0.2656	0.0131
SN	0.4396+	0.5542*	0.4280+	0.2481	0.5276*	0.4427+
BA	-0.3121	-0.3642	-0.2526	0.0373	-0.2366	-0.2970
CE	0.0637	0.2424	0.0149	-0.0418	0.1090	-0.0055
PB	0.2270	0.3863	0.1088	-0.1909	0.2814	0.2913
TH	0.2832	0.4362+	0.3940	0.4470+	0.6218*	0.3268
U	-0.2434 FE	-0.2718 MN	0.1015 P	-0.1576 CL	-0.2601 CR	-0.1245 NI
CU	1.0000					
ZN	0.6572*	1.0000				
BR	-0.0535	-0.2736	1.0000			
SN	0.5638*	0.2846	-0.1966	1.0000		
BA	-0.3195	-0.0288	0.4223+	-0.6648	1.0000	
CE	0.3446	0.1478	-0.3929	0.1089	-0.4152	1.0000
PB	0.2529	0.5452*	0.2379	-0.0468	0.3096	-0.0495
TH	0.3255	0.4747+	-0.2498	0.3914	-0.0835	-0.1707
U	-0.2593	-0.1653	0.0648	-0.3654	0.2474	-0.1072
	CU	ZN	BR	SN	BA	CE
PB	1.0000					
TH	0.0675	1.0000				
U	-0.1666	-0.2582	1.0000			
	PB	TH	U			

SIGNIFICANT AT 95% - SYMBOL +
SIGNIFICANT AT 99% - SYMBOL *

c) From contaminations and fractions of clay and tuff sediments within calcium borate deposits. In this manner all the major constituents of montmorillonitic and illitic clays (Si, Al, Ti, Fe, Mg, K, Mn and P) and trace elements of clays (Cr, Ni, Cu, Zn, Sn, Pb and Th) are expected to be present in small amounts in colemanite and other borates.

B₂O₃, CaO and H₂O

These three oxides constitute all of the major constituents of colemanite, the remaining elements occur in minor or trace amounts.

The B₂O₃, CaO and H₂O contents of colemanite in the northern area (Espey-Killik) are very similar to those in the southern area (Hisarcik), but the H₂O content on average is slightly lower. The arithmetic means of B₂O₃, CaO and H₂O in the southern area are 47.63%, 24.19% and 19.91% respectively (Table 16), whereas in the northern area these are 47.39%, 24.20% and 20.35% (Table 17). These results for both areas are slightly lower than the theoretical values for colemanite (50.81% B₂O₃, 27.28% CaO, 21.91% H₂O). The difference is caused by greater clay fractions and trace elements to a lesser extent. The ratio of CaO:B₂O₃ is 0.51 for both the northern and southern areas, which is close to the theoretical value of 0.54.

As expected in these relatively pure colemanite samples these three oxides are strongly positively correlated with each other (Table 18; Figs. 24, 25 and 26).

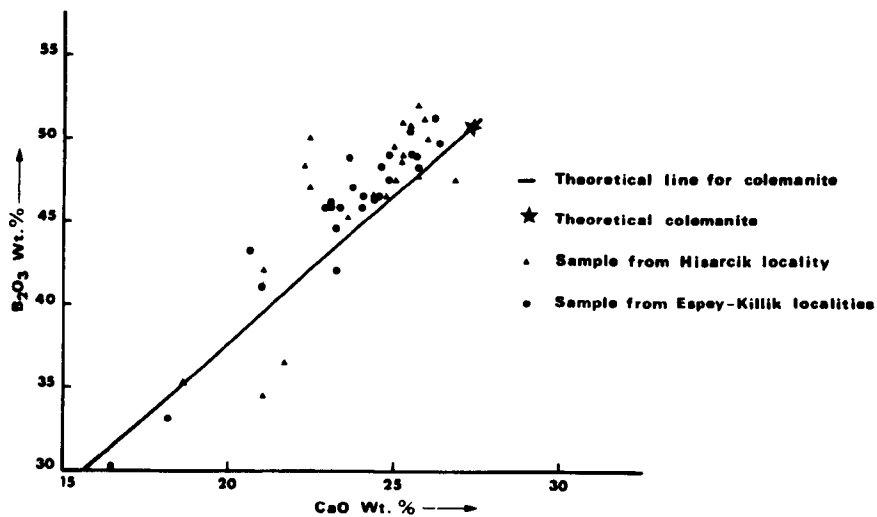


Figure 24. Plot of $B_2O_3\%$ v. $CaO\%$ for the Emet colemanites.

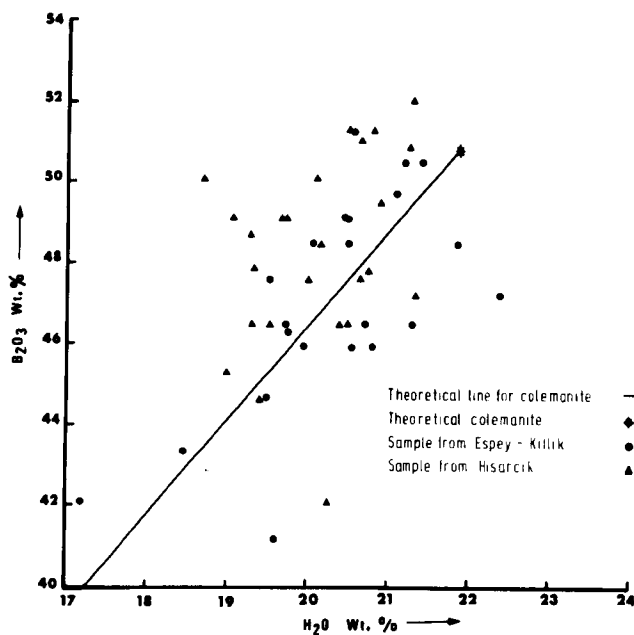


Figure 25. Scatter plot of $B_2O_3\%$ v. $H_2O\%$ for the colemanite samples.

When these three oxides are plotted against each other, some of them fall along the theoretical line for colemanite, although there are some departures from the theoretically expected proportions which need to be explained. In almost all samples the $\text{CaO} : \text{B}_2\text{O}_3$ ratio is low (see Fig. 24) either because of an excess of B_2O_3 or a deficiency of CaO . Also the ratios of $\text{B}_2\text{O}_3 : \text{H}_2\text{O}$ and $\text{CaO} : \text{H}_2\text{O}$ are high and low respectively for both the southern and northern areas. (See Figs. 25 and 26). The average compositions and oxide ratios of colemanite from the southern and northern areas in the Emet deposits are given in Table 19 with the theoretical compositions and oxide ratios of inyoite, meyerhofferite and colemanite. Among the possible reasons for the scattering in the plots are:-

- a) Analytical errors
- b) Adsorption of boron on included clays
- c) Substitution of elements such as Mg, Sr, As and Ba for Ca in the colemanite lattice.
- d) The presence of borates other than colemanite, such as hydroboracite, teruggite, cahnite, veatchite, tunellite, etc..

In the present study, B_2O_3 and CaO were analysed by atomic absorption spectrophotometry. Sources of inaccuracy in this analytical method included weighing, machine reading and volumetric measurement errors. Of these, the latter constitutes the most significant proportion of the total error. Nevertheless this value is very small ($\pm 0.474\%$) and consequently will not effect the scatter of the points in the correlation diagrams. In this method there are no specific element interferences.

	<u>Inyoite</u>	<u>Meyerhofferite</u>	<u>Colemanite</u>	<u>Colemanite (Hisarcik)</u>	<u>Colemanite (Espey-Killik)</u>
B ₂ O ₃	37.62	46.72	50.81	47.63	47.39
CaO	20.20	25.08	27.28	24.19	24.20
H ₂ O	42.18	28.20	21.91	19.19	20.35
CaO: B ₂ O ₃ ratio	0.54	0.54	0.54	0.51	0.51
B ₂ O ₃ : H ₂ O	0.89	1.66	2.32	2.39	2.33
CaO: H ₂ O	0.48	0.89	1.25	1.22	1.19

Table 19. Theoretical compositions and oxide ratios of Ca borate series compared with typical compositions and oxides ratios of Emet colemanites.

From the field and petrographic observations coupled with X-ray diffraction analyses, montmorillonite and illite are found to be associated with the borates. It is well established that illite adsorbs boron (up to 1% B_2O_3) (Ernst, 1970 and Braitsch, 1971). Boron in the illite facies is usually adsorbed on the clay minerals rather than precipitated as borates. In the Emet deposits, illite is less common than montmorillonite and therefore the adsorption of boron on clay minerals is limited. However the clay mineral content of these colemanite samples, estimated from the Al figures, has a maximum of about 2.7% clay in the Hisarcik area and 9.3% clay in the Espey-Killik area. Thus even if all the included clays were illite and this contained the maximum of 1% B_2O_3 , only up to 0.087% B_2O_3 at Hisarcik and 0.30% B_2O_3 in the northern area could conceivably be adsorbed in clay minerals. This small amount does not account for the excess of B_2O_3 over that required to form colemanite exhibited by Fig. 24. Therefore it is considered that adsorption of B by illite is an insignificant factor in explaining the scatter in the correlation diagrams.

Substitution of elements such as Sr, Mg, As and Ba for Ca in the colemanite lattice could cause the low CaO: B_2O_3 ratio in the B_2O_3 and CaO correlation diagram (see Fig. 24). Although Mg, Sr and As are present in the colemanite analyses, B_2O_3 , CaO and H_2O are negatively correlated with these and show only a weak correlation with Ba in the colemanite correlation matrices (see Table 18). Arithmetic averages of 1.45% Mg, 1.44% Sr above and 1.85% Mg, 1.28% Sr below the theoretical line for colemanite have been observed on the B_2O_3 and H_2O correlation diagram (see Fig. 25). When CaO + MgO + SrO mol. proportions are plotted against B_2O_3 mol. proportion (Fig. 27), most of the points move

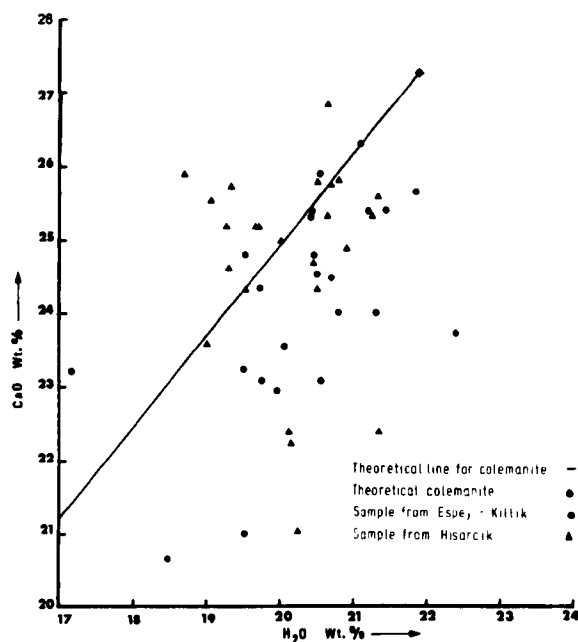


Figure 26. Scatter plot of CaO% v. H₂O% for the colemanite samples.

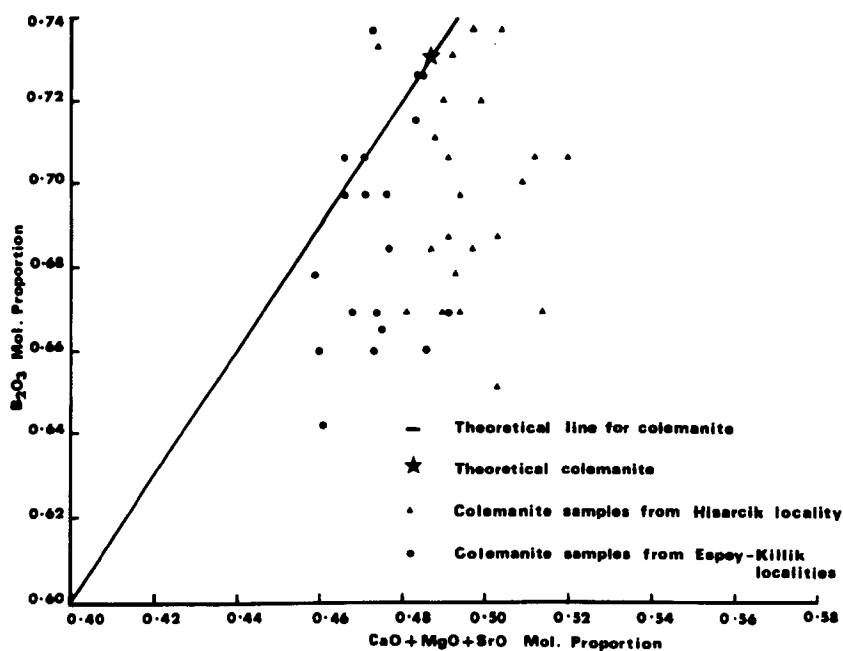


Figure 27. Plot of B₂O₃ mol. proportion against CaO + MgO + SrO mol. proportion for the colemanite samples.

to the right hand side of the theoretical line for colemanite. This implies that there is sufficient Mg and Sr in the samples to fully explain the low $\text{CaO} : \text{B}_2\text{O}_3$ ratios (see Fig. 24) by postulating replacement of Ca^{++} by Sr^{++} and Mg^{++} in the colemanite lattice. However if this were the complete explanation, the $\text{B}_2\text{O}_3 : \text{H}_2\text{O}$ ratios should be constant after allowing for the H_2O in the small amounts of clay minerals present. The wide scatter of $\text{B}_2\text{O}_3 : \text{H}_2\text{O}$ plots (Fig. 25) strongly suggests that borates other than colemanite occur in the samples analysed.

Observed borates other than colemanite were listed in Chapter VI. These borates such as meyerhofferite, hydroboracite, ulexite, teruggite, cahnite, veatchite and tunellite associated with colemanite could easily alter the $\text{CaO} : \text{B}_2\text{O}_3$, $\text{B}_2\text{O}_3 : \text{H}_2\text{O}$ and $\text{CaO} : \text{H}_2\text{O}$ ratios and would cause scattering in the correlation diagrams (see Figs. 24, 25 and 26).

The possibility that the more hydrous forms of Ca-borate (i.e. inyoite and meyerhofferite) occur has been considered. $\text{CaO} : \text{B}_2\text{O}_3$ ratios in the inyoite-meyerhofferite-colemanite series are the same (0.54), but the $\text{B}_2\text{O}_3 : \text{H}_2\text{O}$ and $\text{CaO} : \text{H}_2\text{O}$ ratios differ. Departures from the theoretical ratios for colemanite might be explained by postulating small amounts of included inyoite or meyerhofferite or both.

Fig. 25 shows that 16 of the 59 colemanite samples have excess water over that required in colemanite. Of these 5 lie so close to the theoretical $\text{B}_2\text{O}_3 : \text{H}_2\text{O}$ ratio that the discrepancy is most probably due to clay minerals. Of the remaining 11, none show decreases in both the $\text{B}_2\text{O}_3 : \text{H}_2\text{O}$ ratio and the $\text{CaO} : \text{H}_2\text{O}$ ratio consistent with inyoite and/or meyerhofferite contaminants, and a decrease in CaO as well as an addition of water is implied.

Therefore it is concluded that the scattering in the correlation diagrams is not due to the presence of more hydrous forms of Ca-borate.

Although the negligible amount of meyerhofferite was identified by the field and X-ray diffraction examinations, no inyoite was detected in the Emet borate deposits during the present study.

On Fig. 24 most of the points plotted for the B_2O_3 and CaO values of the colemanite analyses appear to fall slightly above the theoretical line for colemanite and the CaO : B_2O_3 ratio is low. This can be explained by the presence of hydroboracite, ulexite and teruggite minerals, which are commonly associated with colemanite in the deposits and have less CaO and high B_2O_3 in their compositions. Association of these minerals with colemanite can easily alter the CaO : B_2O_3 ratio in favour of B_2O_3 .

On Fig. 25, although most points plotted for the B_2O_3 and H_2O values fall above the theoretical line for colemanite, there are also some points below the line. In other words some samples have high B_2O_3 : H_2O ratios and some have low B_2O_3 : H_2O ratios. The high B_2O_3 : H_2O ratio is probably due to the presence of adsorbed boron in clay fraction, veatchite and tunellite associated with colemanite, whereas the low B_2O_3 : H_2O ratio is due to the association of hydroboracite, teruggite and cahnite minerals, which have relatively more water compared with boron in their chemical compositions.

Similarly the high CaO : H_2O ratios can be explained by the presence of cahnite, calcite and gypsum minerals, and the low CaO : H_2O ratios by the presence of other borates such as hydroboracite, ulexite, teruggite and tunellite minerals, which are characterised by high water and low calcium contents in their compositions (see Fig. 26).

In conclusion, scattering of the B_2O_3 , CaO and H_2O plots is mainly due to the presence of other borate minerals associated with the colemanite and not to the other possible causes mentioned above.

As expected B_2O_3 , CaO and H_2O are negatively correlated with the clay and tuff elements (Si, Al, Ti, Mg, K, Mn and P). The increase in the clay and tuff impurity decreases the overall amount of colemanite.

The elements Mg, Na, Sr, As and S

These elements are represented both in the evaporite phase and the clay fractions. They are strongly correlated with each other, but negatively correlated with the oxides of colemanite and weakly or insignificantly with the clay fraction elements (Si, Al, Ti, K, Mn and P). Mg and Sr are also strongly correlated with clay elements (detrital fraction) and S is weakly correlated with the oxides of colemanite (B_2O_3 , CaO and H_2O). Although these elements are not present in colemanite in the same relative proportion to each other as in the sediments, mineralogical observations and correlation matrices show that some are not detrital, but chemically (authigenic) precipitated, such as secondary borates, sulphates, sulphides and native elements. The high concentration of these elements in the colemanite analyses is due to the presence of minerals associated with colemanite which contain these elements.

The average Mg content of colemanite of the southern and northern areas is 1.92% and 1.33% respectively (Tables 16 and 17). Although Mg is negatively correlated with B_2O_3 (Fig. 28; see also Table 18) in the colemanite analyses, it is present in some of the diagenetic borates such as hydroboracite mineral. It

may also replace Ca in the colemanite composition (see Fig. 27). Its strong correlation with the oxides of clay fractions indicates its presence in montmorillonite. During the early stages of diagenesis Mg moves into the colemanite by base exchange with Mg-rich clays and tuffs, replacing some of the calcium.

The average Na content of colemanite of the southern and northern areas is 0.24% and 0.19% respectively, which is very low and close to the detection limit (Tables 16 and 17). The strong correlation between Na_2O and the SiO_2 and MgO oxides in the colemanite samples indicates its association with the tuff and clay fractions. The insignificant correlation between sodium and boron (Fig. 29, see also Table 18) rules out the presence of Na borate in the deposits. The occurrence of ulexite in the northern areas suggests that conditions were more favourable from time to time for the formation of Na-Ca borate in the thicker parts of the deposits. The insignificant correlation between sodium and Cl suggests that there is no halite present in the deposits.

The colemanite samples in the Emet deposits contain very high amounts of strontium and most of the samples analysed are comparatively enriched in strontium concentrations. The colemanite from the southern area contains an average of 1.51% strontium as compared with 1.22% strontium in the colemanite samples from the northern area (Tables 16 and 17). Although strontium is negatively correlated with B_2O_3 in the colemanite analyses (Fig. 30 and Table 18), it is present in some of the other borates in the deposits such as tunellite and veatchite minerals, which are formed after the colemanite deposition. Strontium replaces or isomorphous substitutes for Ca^{2+} in the

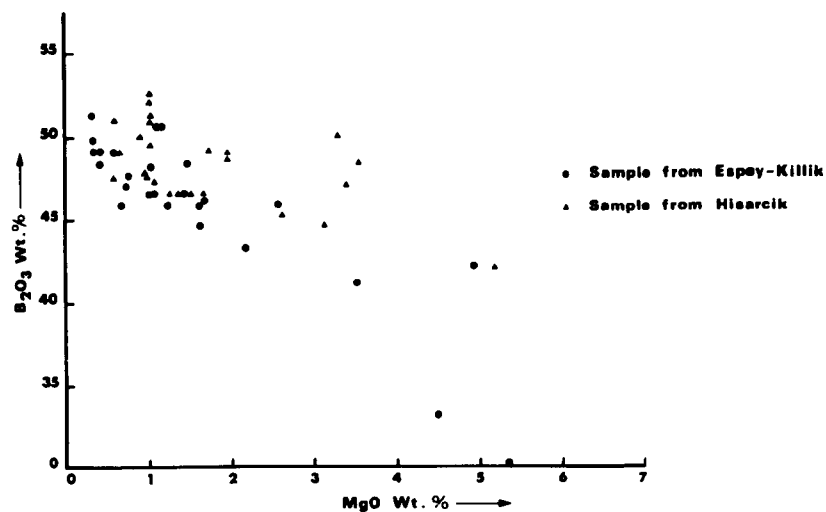


Figure 28. Correlation diagram of B₂O₃ and MgO oxides in the Emet deposits.

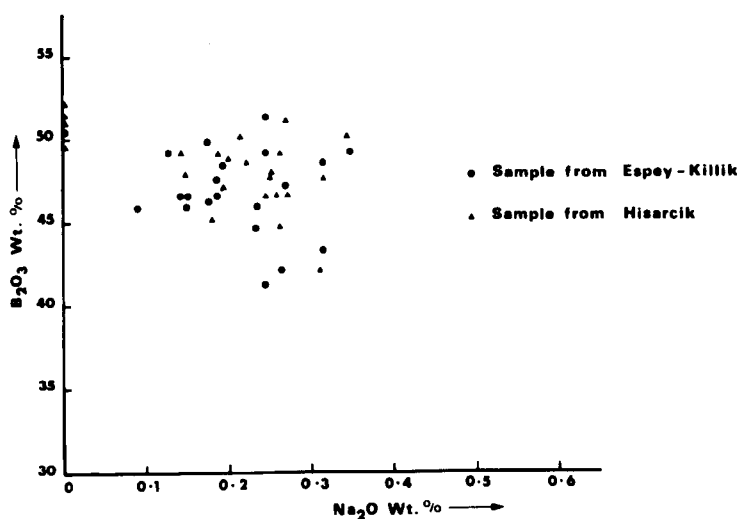


Figure 29. Correlation diagram of B₂O₃ and Na₂O oxides in the Emet deposits.

colemanite composition (see Fig. 27). Strontium also occurs adsorbed on the clay minerals (especially montmorillonite) due to its strong correlation with the oxides of SiO_2 and MgO ; mainly it occurs as an independent sulphate phase, celestite (SrSO_4) because of its correlation with SO_3 . Much of the strontium in the borate deposits is present as celestite. The concentrations of strontium in the individual colemanite samples will be discussed later on under colour variations in colemanite.

The colemanite samples contain exceptionally high arsenic concentrations, with average contents of 0.21% and 0.11% As_2O_5 , respectively for the southern and northern areas (Tables 16 and 17). Arsenic concentrations in the southern area are greater than in the northern area. The origin of the very high arsenic concentration is probably due to the widespread occurrence of hot springs connected with volcanic activity in the Emet district, as mentioned in Chapter IV. In the correlation matrices As shows a negative correlation with B_2O_3 (Fig. 31) but has a positive correlation with SO_3 and the oxides of clay fractions (Table 18). Although arsenic is present in teruggite and cahnite minerals, its main concentrations are in the sulphides and as an adsorption in the clay minerals (mainly montmorillonite). The presence of realgar and orpiment in the deposits indicates the strong relationship of As and S.

The colemanite samples analysed contain high sulphur concentration similar to arsenic. The average S content of colemanite samples of the southern and northern areas are 0.30% and 0.36% respectively, which are very close to each other (Tables 16 and 17). Very high sulphur concentrations in the deposits are most likely due to the occurrence of thermal springs and

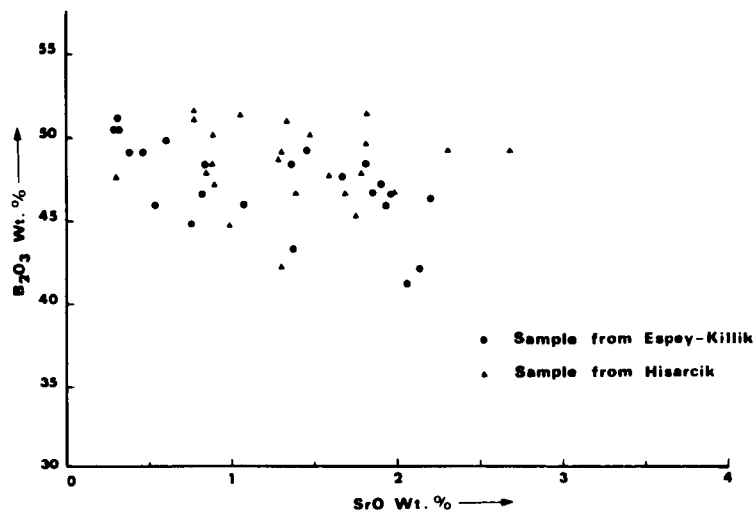


Figure 30. Correlation diagram of B_2O_3 and SrO oxides for the Emet colemanite samples.

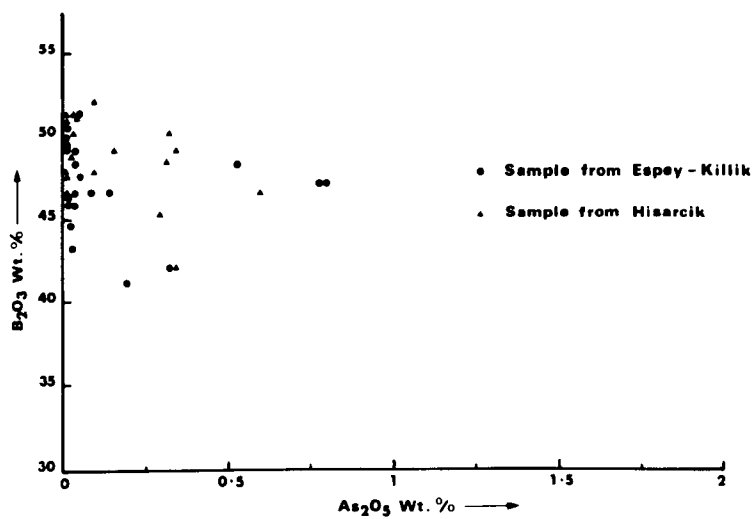


Figure 31. Correlation diagram of B_2O_3 and As_2O_5 oxides for the Emet colemanite samples.

volcanic activity in the district. In the deposits, sulphur occurs mainly in three forms: native sulphur, sulphates (as celestite and gypsum) and sulphides (as realgar and orpiment). In the colemanite analyses, sulphur is positively correlated with oxides of B_2O_3 , CaO, SrO, As_2O_5 and H_2O . A relatively weak but positive correlation between S and B_2O_3 (Fig. 32) may suggest the precipitation of minerals containing these elements under similar environments without interfering with each other. Also this may imply that these two elements came from the same source. Sulphur occurs mainly in the form of sulphates and sulphides in the deposits. The correlation of sulphur with Ca, Sr and As also proves the presence of gypsum, celestite, realgar and orpiment which are associated with colemanite.

The elements Si, Al, Ti, Fe, Mg, K, Mn and P

A considerable proportion of these minor elements represent clay and tuff impurities within the calcium borate deposits. The elements are not present in colemanite in the same relative proportion to each other as in clay and tuff (Tables 16 and 17; see also Tables 7 and 8).

Some of the Mg in clay and tuff is transferred into the borate structure by base exchange during diagenesis, which is evident from the presence of hydroboracite and teruggite minerals in the deposits. The elements Ti, Mn and P are present in relatively low concentrations (Table 16 and 17) indicating that they are mainly detrital in origin, derived from clay and tuff sediments. The concentrations of K, Mn and P are very low and the amount of Ti in colemanite samples is close to the detection limit. The Ti content of colemanite is related to the amount

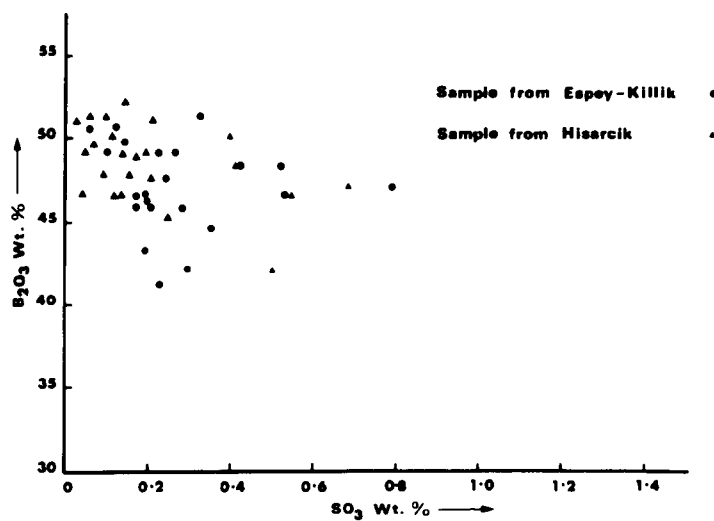


Figure 32. Correlation diagram of B_2O_3 and SO_3 oxides for the Emet colemanite samples.

of impurities (clays and tuffs) present, because usually all evaporite minerals have very little or no chemically precipitated Ti. The average content of these elements grouped together is given in Tables 16 and 17, respectively for the southern and northern areas. The concentrations of Al, Fe and K appear higher in the northern area than the southern area; probably some amounts of these elements are chemically precipitated in the thicker northern area.

A considerable amount of iron occurs in the minerals hematite and iron hydroxide. The strong correlation between iron and sulphur indicates the presence of pyrite in the deposits. The K content of evaporites represents the last stage in the evaporating sequence, depending mainly on the temperature of the evaporating body and its concentrations. The very low K and Cl content of colemanite suggests that potassium and chlorine minerals are not present. Also the high solubility of K and Mg evaporite minerals makes the amount of these minerals which are actually precipitated with colemanite extremely small.

These elements are strongly positively correlated with each other, whereas they are negatively correlated with the major oxides of colemanite (B_2O_3 , CaO and H_2O), indicating that these elements are present in the clay fractions (montmorillonite and illite) of colemanite samples (Table 18).

The elements Cl, Cr, Ni, Cu, Zn, Sn, Ce, Pb and Th.

The average contents of these elements in colemanite analyses (in ppm) are extremely low and very close to their detection limits. Their concentrations in the colemanite samples from the southern

and northern areas are given in Table 16 and 17, and these elements are evenly distributed throughout the Emet colemanite deposits.

These trace elements are strongly correlated with the oxides of clay fractions of colemanite (Si, Al, Mg and K), whereas they are negatively correlated with the major oxides of colemanite (B_2O_3 , CaO and H_2O), indicating that these elements are mainly concentrated in the clay fractions (Table 18). These elements are therefore adsorbed on mineral particles such as Fe-oxides and clay minerals (montmorillonite and illite). Their distributions will be related to their adsorption on minerals such as clays, and to their concentration in both sulphides and residual minerals.

The chalcophile elements (Cu, Zn, Pb, etc..) would only precipitate with colemanite in reducing environments, where their highly insoluble metal sulphides are readily precipitated. Reducing environments are created by the presence of SO_4 ions, which in this case are a considerable amount, and by the bacteria which would survive in the presence of sulphate ions. Nevertheless it is doubtful if these elements precipitated with colemanite and are therefore of authigenic origin.

The content of Cl and Ce elements in colemanite from both northern and southern areas is very low and very close to their detection limits. The strong correlation of Cl and Ce with the oxides of clay fractions in the colemanite analyses indicates that they are mainly adsorbed on the clay minerals.

The elements Br, Ba and U.

The average contents of these three elements for the colemanite analyses are very low and below their detection limits (Tables 16 and 18).

In the correlation matrices of colemanite analyses, these elements are positively correlated with the oxides of B_2O_3 , CaO and H_2O , whereas they show negative correlation with the oxides of clay fractions of colemanite (Table 18), suggesting that the negligible amount of these elements are associated with the evaporite minerals.

Although the bromine content is relatively high (up to 30ppm in evaporites), the non-existence of K, Na and Mg salts in the Emet deposits probably causes the low concentration of bromine.

The positive correlation between Ba and CaO in the colemanite analyses suggests that a small amount of Ba is in isomorphous substitution or probably is replacing Ca in the evaporite fraction.

Negligible amounts of uranium are redistributed in surface and ground waters and are adsorbed on mineral particles in the deposits.

3. Interpretation of chemistry

The Emet borate deposits are characterized by high Ca borate (colemanite), very low Na and relatively high Mg, Sr, As and S concentrations compared with the other borate deposits. Also the chemical analyses of the colemanite and other borate samples from the southern and northern areas indicate that there are several differences between the two areas as well as different mineral assemblages. Those samples from the southern area have on average more Mg, Sr and As, whereas the content of H_2O and K is higher in the northern area. High Mg and Sr concentrations in the southern area can be also seen on Fig. 27.

B_2O_3 , CaO, H_2O , MgO, SrO, SiO_2 and Al_2O_3 make up the bulk of the analysed samples (95% and above). B_2O_3 , CaO and H_2O are mainly restricted to the borate minerals (mainly colemanite). Si, Al, Ti, Mg, K, Mn and P are represented in the clay fractions of the samples (montmorillonite and illite). These elements are the main constituents of the clay minerals. The elements Mg, Na, Sr, As and S are represented both in the evaporite and in the clay fractions, but mainly in the latter. Although most of these elements are concentrated in the clay fraction, during diagenesis, some of these elements are transferred to the borate structure by base exchange, resulting in the formation of some diagenetic (secondary) borate and non-borate minerals such as hydroboracite, veatchite, cahnite, etc..

Most of the trace elements in the colemanite samples are in the clay and heavy minerals fractions. These trace elements which are either adsorbed on the clay minerals or within their crystal lattices in the clay fraction of the colemanite, include mainly Cl, Cr, Ni, Cu, Zn, Sn, Ce, Pb and Th. Small amounts of Br, Ba and U are included in the evaporite minerals and Ba is probably in isomorphous substitution for Ca^{++} . All the trace elements show a strong positive correlation with SiO_2 , Al_2O_3 , indicating their presence in the clay fraction rather than in the colemanite. Elements grouping in one portion of the samples, for example in detrital or evaporite minerals, show positive correlation amongst themselves.

Borate minerals, like the tuffs and clays in the borate zone, are characterised by relatively high concentrations of As, Sr and S. These elements were chemically precipitated from brines, mainly as sulphides and sulphates, which may have been partly derived

from thermal springs located adjacent to the borate deposits. Like the sediments, the borates are also characterized by a relatively high Fe_2O_3 : FeO ratio, suggesting strongly oxidising conditions of precipitation and arid to semi-arid environments of evaporation.

As can be seen from Table 18, there are strong positive correlations between the pairs of major oxides B_2O_3 - CaO , B_2O_3 - H_2O , CaO - H_2O , and negative correlations between pairs B_2O_3 - Na_2O , B_2O_3 - MgO , B_2O_3 - SrO , CaO - Na_2O , CaO - MgO , CaO - SrO . No other elements were found to show a strong positive correlation with B_2O_3 and CaO . This proves that B_2O_3 and CaO are represented in borate minerals and the unusually high concentrations of B^{+++} and Ca^{++} in the brines which gave rise to the colemanite (Ca-borate) precipitation in the deposits. It can be concluded from the correlation coefficients for B_2O_3 - CaO (positive) and B_2O_3 - Na_2O (negative) that the Emet deposits are Ca-borate (colemanite) dominant.

There is much geological and mineralogical evidence to show that secondary alterations played an important role in the modification of chemical variation within the deposits. Hydroboracite, veatchite and cahnite developed from colemanite are a good example of this process.

Boron is enriched relative to calcium due to partial replacement of colemanite by other borates during the diagenesis.

4. Colour variations in colemanite and the other borates

Although most of the borates are either white or colourless they often appear blue (Plate 106, see also Plate 95) orange and yellow (see plates 42, 63, 84 and 94) in colour. These

observed colours in borate minerals cannot always be attributed to the presence of impurities, such as clay or iron oxide, since these components are present in too small amounts to account for the observed colours. Among the possible reasons for the colouring in the borates are:-

- a) The presence of Cl in borates
- b) The presence of excess iron oxide in coloured borates
- c) The presence of clay impurities in borates
- d) The association of Sr sulphate minerals (celestite) with the borates
- e) The association of As sulphide minerals (realgar and orpiment) and native sulphur with the borates.

In the present study, it was found that the average chlorine content of colemanite from the Espey-Killik area (165ppm) is slightly higher than that of colemanite from Hisarcik area (132ppm) and both are below the detection limit of chlorine. Some individual colemanite samples have higher chlorine concentrations, e.g. sample numbers 113 and 114 contain 978ppm and 225ppm chlorine, respectively, but neither of these samples show colouring. Also blue and yellow coloured colemanite samples contain very low chlorine concentrations, in which the chlorine content is usually below the detection limit. Sample numbers 147 and 123, which are blue and yellow colemanite samples, respectively, have a chlorine content of 122ppm and 140ppm, which is also below the detection limit. Therefore it is concluded that the chlorine content of borate samples is insignificant and insufficient to colour the samples.

It has been stated previously that the sediments and borates are characterized by high Fe_2O_3 : FeO ratios indicating strongly

oxidising conditions of sedimentation and precipitation; the considerable amount of Fe^{+++} mainly in the sediments occurs in the minerals hematite and iron hydroxides, which are responsible for the colour of the sediments. The average iron content is given in Tables 7, 8, 16 and 17, respectively for clay, tuff and colemanite from the southern and northern area. In the colemanite analyses iron is fixed in the clay minerals, because of its strong correlation with the major constituents of the clay fraction. The clay and tuff fractions associated with borates are mainly green or grey in colour. This implies that the concentration of iron is not sufficient to colour the sediments and associated borates. Thus the observed colours of borates are mainly blue and orange-yellow but not brown.

Although the borate minerals are usually pure and have very few impurities, they often contain clay fraction and residual minerals. The clay minerals content of the colemanite samples have been calculated as a maximum of about 2.7% clay in the Hisarcik area and 9.3% clay in the Espey-Killik area. This suggests that the clay impurities could change the colour of borates to green or grey, although pure borates can tolerate relatively large amounts of green clay before beginning to change to a green colour.

The association of Sr-sulphates (celestite), As-sulphides and native sulphur with borates has been studied in detail in order to find out how they effect the colouring of the borates. In the present study, the average content of Sr, As and S of colemanite samples from the southern area is, 1.51%, 0.21% and 0.30%, respectively, compared with 1.22%, 0.11% and 0.36% of those colemanite samples from the northern area (see Table 16 and

17). When the individual coloured borate samples (mainly colemanite) are examined, it has been observed that those blue coloured colemanite samples such as 147 and 148 contain more than the average of SrO and SO_3 concentrations, up to 3.99% and 2.51%, respectively, and those of orange-yellow coloured samples such as 32, 34, 56 and 157 have higher As and S concentrations compared with the average values.

It has also been proved by X-ray diffraction analyses that often colemanite and other borates contain certain amounts of celestite (SrSO_4), realgar (AsS), orpiment (As_2S_3) and native sulphur (S). For instance, sample number 147, which is blue colemanite, is mixed with celestite which occurs usually blue in colour (Plate 107; see also Plate 95); its association with borates can play an important role in effecting the colour of borates.

Some samples such as 32 and 157, which are orange-yellow coloured colemanite, are associated with realgar and orpiment. Like celestite, red coloured realgar and orange coloured orpiment affect the colour of the borates (see Plates 42, 63, 84 and 94). Realgar and orpiment are also observed in the colemanite crystals as widespread spots by the microscope studies (Plate 108). Sometimes realgar and orpiment veins cut through the colemanite and other borate minerals (see Plate 56). This is often noted in field observations and microscope work.

It has been concluded that the association of iron oxide, clay, sulphate and sulphide minerals affect or change the colour of colemanite and associated borates, especially high concentrations of celestite, realgar, orpiment and native sulphur.

The blue colour of colemanite and other borates is a result of celestite; the orange-yellow colour is due to realgar, orpiment and native sulphur.



Plate 106 Colemanite sample showing blue colour from Espey underground mine.



Plate 107 Celestite associated with borates (mainly colemanite) showing distinct blue colour, Sarikaya locality.

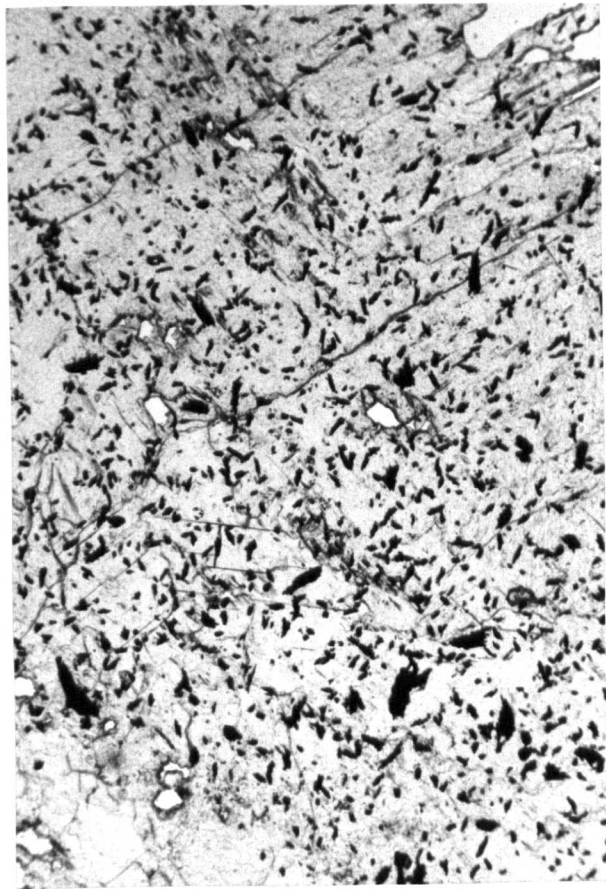


Plate 108 Widespread spots of realgar and orpiment in colemanite. Plane polarized light, x10.

Table 20. Chemical analyses of colemanite samples from Emet.

<u>Number</u>	<u>1013</u>	<u>1013a</u>	<u>4</u>	<u>6</u>	<u>8</u>
B ₂ O ₃	51.305	51.305	40.580	41.350	48.110
CaO	25.820	25.820	22.400	26.950	24.360
MgO	1.020	1.058	2.205	1.053	0.957
Na ₂ O	0.000	0.000	0.293	0.375	0.216
SrO	1.826	1.068	0.497	0.559	1.211
As ₂ O ₅	0.001	0.028	0.033	0.013	0.019
SiO ₂	0.075	0.079	12.198	5.847	3.251
TiO ₂	0.000	0.000	0.125	0.054	0.022
K ₂ O	0.000	0.000	1.987	1.039	0.517
H ₂ O	20.530	20.807	18.260	14.469	19.267
CO ₂	0.000	0.000		5.327	
SO ₃	0.102	0.066	0.390	0.190	0.462
Total	100.679	100.231	98.968	97.226	98.392
Al	128	0*	17059	8657	4010
Fe	79	69	8194	3146	1589
Mn	49	3*	80	541	102
P	44*	42*	187	112	140
Cl	216	86*	139*	141*	133*
Cr	4*	11*	97	61	25
Ni	10*	2*	120	47	29
Cu	0*	0*	20	15	24
Zn	10*	10*	20	10*	9*
Br	2*	0*	0*	2*	0*
Sn	0*	0*	31*	30	23
Ba	404	321	174*	127*	691
Ce	31*	156*	80*	55*	67*
Pb	5*	5*	11*	4*	1*
Th	0*	0*	9	4	0*
U	1*	0*	0*	2*	0*

*Indicates values below the detection limit.

Table 20. (continued)

<u>Number</u>	<u>10</u>	<u>12</u>	<u>18</u>	<u>22</u>	<u>24</u>
B ₂ O ₃	22.970	39.560	49.135	46.583	49.135
CaO	10.780	19.810	25.200	24.710	25.200
MgO	6.704	3.243	1.958	1.504	0.640
Na ₂ O	0.284	0.230	0.144	0.259	0.263
SrO	0.415	0.434	2.326	1.689	2.688
As ₂ O ₅	0.042	0.152	0.332	0.014	0.157
SiO ₂	27.767	14.216	2.771	2.050	0.653
TiO ₂	0.325	0.128	0.001	0.000	0.000
K ₂ O	3.413	1.889	0.000	0.000	0.000
H ₂ O+	13.981	16.707	19.716	20.444	19.696
CO ₂	0.596				1.554
SO ₃	0.669	0.267	0.140	0.135	0.195
Total	87.946	96.636	101.723	97.388	100.181
Al	35766	16530	639	602	338
Fe	13162	6853	656	948	608
Mn	206	127	13*	15*	3*
P	455	244	187	45*	60*
Cl	50*	127	142*	123*	151*
Cr	220	102	12	6*	6*
Ni	200	81	6*	4*	1*
Cu	38	18	31	20	36
Zn	38	19	4*	4*	5*
Br	3*	0*	0*	2*	0*
Sn	23	31	22	27	14
Ba	1406	225*	0*	78*	0*
Ce	109*	178*	262*	62*	167*
Pb	15	8*	0*	3*	4*
Th	22	13	6	0*	0*
U	2*	2*	0*	0*	0*

*Indicates values below the detection limit.

Table 20. (continued)

<u>Number</u>	<u>29</u>	<u>30</u>	<u>32</u>	<u>34</u>	<u>35</u>
B ₂ O ₃	45.307	47.859	44.668	42.116	47.604
CaO	23.590	25.760	18.200	21.070	25.060
MgO	2.617	0.976	3.115	5.206	0.989
Na ₂ O	0.181	0.252	0.263	0.311	0.251
SrO	1.751	0.856	0.996	1.307	1.594
As ₂ O ₅	0.292	0.083	1.491	0.337	0.006
SiO ₂	4.567	1.222	4.552	8.085	1.338
TiO ₂	0.025	0.000	0.000	0.025	0.000
K ₂ O	0.276	0.000	0.005	0.192	0.022
H ₂ O+	19.000	20.761	19.421	20.267	20.038
CO ₂			6.000		1.500
SO ₃	0.252	0.157	1.131	0.507	0.210
Total	97.858	97.926	99.812	99.423	98.612
Al	2534	278	610	2849	540
Fe	2318	1177	0*	1192	444
Mn	10*	13*	49	56	23
P	113	22*	801	111	39*
Cl	177 [^]	107*	108*	148*	110 *
Cr	14	8*	7*	13*	7*
Ni	9*	5*	6*	14	4*
Cu	23	23	35	45	27
Zn	9*	5*	8*	13*	5*
Br	0*	0*	0*	0*	2*
Sn	29	20	23	25	27
Ba	0 [^]	25*	0*	0*	19*
Ce	251	102*	966	267	68*
Pb	2*	2*	2 [^]	4*	2 [^]
Th	4	0*	7	5	0*
U	0*	0*	2*	1*	0*

*Indicates values below the detection limit

Table 20. (continued)

<u>Number</u>	<u>36</u>	<u>37</u>	<u>39</u>	<u>41</u>	<u>50</u>
B ₂ O ₃	46.583	46.583	47.859	46.583	47.604
CaO	24.360	24.360	25.760	24.640	26.880
MgO	1.685	1.367	1.084	1.273	0.585
Na ₂ O	0.245	0.273	0.149	0.259	0.316
SrO	3.987	1.384	1.779	1.983	0.316
As ₂ O ₅	0.030	0.590	0.015	0.008	0.026
SiO ₂	2.478	1.849	1.342	1.537	0.901
TiO ₂	0.010	0.000	0.000	0.001	0.000
K ₂ O	0.090	0.018	0.016	0.009	0.119
H ₂ O+	19.535	20.500	19.349	19.300	20.658
CO ₂					
SO ₃	0.122	0.547	0.097	0.047	0.245
Total	99.125	97.471	97.450	95.640	97.650
Al	1224	638	778	908	898
Fe	963	508	667	735	1274
Mn	15*	12*	13*	14*	5*
P	87	51*	117	14*	137
Cl	121*	114*	117*	92*	133*
Cr	10*	7*	9*	8*	11*
Ni	3*	11*	5*	3*	6*
Cu	61	26	28	32	6
Zn	10*	7*	6*	8*	5*
Br	0*	0*	3*	0*	0*
Sn	21	27	24	17	25
Ba	42*	0*	32*	0*	149*
Ce	78*	445	93*	60*	61*
Pb	2*	4*	3*	1*	0*
Th	0*	0*	0*	4	0*
U	0*	0*	0*	0*	0*

*Indicates values below the detection limit

Table 20. (continued)

<u>Number</u>	<u>54</u>	<u>56</u>	<u>58</u>	<u>61</u>	<u>63</u>
B ₂ O ₃	48.497	47.221	50.156	48.750	49.135
CaO	22.260	22.400	22.400	25.200	25.550
MgO	3.531	3.390	3.293	1.949	1.729
Na ₂ O	0.222	0.196	0.346	0.201	0.188
SrO	0.883	0.904	0.880	1.280	1.323
As ₂ O ₅	0.316	0.770	0.317	0.028	0.020
SiO ₂	5.964	5.119	1.327	2.823	2.506
TiO ₂	0.026	0.004	0.000	0.001	0.000
K ₂ O	0.369	0.047	0.000	0.028	0.015
H ₂ O+	20.160	21.346	20.128	19.294	19.080
CO ₂					
SO ₃	0.417	0.687	0.402	0.177	0.055
Total	102.645	102.084	99.249	99.731	99.601
Al	2863	1117	453	831	693
Fe	1083	628	315	927	547
Mn	31	27	44	36	45
P	248	101	29*	47*	32*
Cl	225	142*	156*	118*	124*
Cr	10*	6*	7*	4*	8*
Ni	9*	1*	5*	1*	7*
Cu	16	23	15	23	27
Zn	12*	9*	6*	7*	7*
Br	0*	0*	0*	0*	0*
Sn	24	46	20	28	24
Ba	0*	0*	0*	70*	56*
Ce	268	556	259	60*	75*
Pb	5*	2*	3*	31	6*
Th	2	0*	2	2	0*
U	1*	0*	0*	0*	0*

*Indicates values below the detection limit

Table 20. (continued)

<u>Number</u>	<u>65</u>	<u>69</u>	<u>78</u>	<u>97</u>	<u>98</u>
B ₂ O ₃	50.156	51.050	42.754	48.497	46.583
CaO	25.900	25.354	23.100	23.590	24.360
MgO	0.909	0.574	2.672	1.475	1.028
Na ₂ O	0.214	0.272	0.213	0.315	0.152
SrO	1.477	0.783	0.494	1.378	0.828
As ₂ O ₅	0.038	0.043	0.013	0.526	0.081
SiO ₂	1.059	0.477	6.929	3.662	2.902
TiO ₂	0.000	0.000	0.096	0.036	0.028
K ₂ O	0.001	0.000	1.185	0.570	0.536
H ₂ O+	18.715	20.675	19.023	20.054	19.739
CO ₂					
SO ₃	0.117	0.215	0.469	0.522	0.170
Total	98.586	99.443	96.948	100.625	96.407
Al	533	133	9301	4247	3774
Fe	57	301	4761	2681	2132
Mn	7*	7*	88	66	52
P	41*	89	267	138	110
Cl	126*	107*	181*	160*	167*
Cr	7*	6*	36	14	19
Ni	4*	3*	27	18	20
Cu	28	10	17	33	22
Zn	6*	3*	27	17	10*
Br	0*	0*	1*	0*	0*
Sn	21	22	31	31	32
Ba	28*	32*	220*	0*	45*
Ce	91*	86*	90*	387	111*
Pb	2*	0*	6*	14	7*
Th	2	1	7	0*	5
U	0*	0*	1*	0*	0*

*Indicates values below the detection limit

Table 20. (continued)

<u>Number</u>	<u>106</u>	<u>107</u>	<u>111</u>	<u>113</u>	<u>114</u>
B ₂ O ₃	45.945	43.392	33.182	47.604	28.971
CaO	22.960	20.650	18.200	24.808	25.760
MgO	1.233	2.181	4.503	0.745	5.086
Na ₂ O	0.150	0.317	0.223	0.189	0.183
SrO	1.947	1.364	1.118	1.686	1.286
As ₂ O ₅	0.015	0.029	0.037	0.056	0.022
SiO ₂	3.480	7.250	13.514	1.701	10.499
TiO ₂	0.035	0.089	0.187	0.016	0.099
K ₂ O	0.527	1.290	2.286	0.301	1.238
H ₂ O+	19.959	18.495	16.490	19.533	14.429
CO ₂			4.470	3.077	7.855
SO ₃	0.285	0.195	0.317	0.247	0.325
Total	96.536	95.252	94.527	99.963	95.753
Al	4381	9881	18623	2348	12256
Fe	2322	4914	9180	1830	6969
Mn	40	117	278	16*	492
P	102	371	201	93	177
Cl	141*	151*	153*	978	225
Cr	20	29	58	8*	37
Ni	18	42	54	7*	35
Cu	34	59	34	30	32
Zn	14*	28	37	9*	27
Br	1*	0*	0*	0*	1*
Sn	18	34	42	29	24
Ba	178*	124*	213*	176*	153*
Ce	59*	71*	111*	103*	98*
Pb	8*	15	25	4*	15
Th	4	10	9	7	2
U	0*	0*	0*	0*	1*

*Indicates values below the detection limit

Table 20. (continued)

<u>Number</u>	<u>120</u>	<u>121</u>	<u>122</u>	<u>123</u>	<u>124</u>
B ₂ O ₃	45.945	49.135	44.668	30.119	49.135
CaO	23.296	25.340	23.240	16.520	25.424
MgO	0.674	0.590	1.614	5.353	0.338
Na ₂ O	0.211	0.245	0.233	0.104	0.129
SrO	5.823	0.393	0.758	9.520	0.472
As ₂ O ₅	0.011	0.038	0.231	9.169	0.004
SiO ₂	1.021	0.946	4.991	6.088	0.227
TiO ₂	0.004	0.003	0.060	0.039	0.000
K ₂ O	0.084	0.127	0.887	0.157	0.000
H ₂ O+	18.844	20.448	19.503	17.537	20.442
CO ₂					
SO ₃	2.180	0.267	0.355	5.489	0.225
Total	98.093	97.532	96.540	100.095	96.396
Al	1175	1118	6526	3850	290
Fe	1115	457	3486	1637	1056
Mn	10*	19	65	68	9*
P	50*	48*	219	98	41*
Cl	145*	158*	157*	140*	126*
Cr	6*	9*	21	20	7*
Ni	3*	5*	25	31	1*
Cu	87	6	21	244	4
Zn	9*	6*	15*	33	3*
Br	1*	0*	0*	0*	1*
Sn	7	24	37	5	18
Ba	1393	32*	0*	0*	65*
Ce	77*	70*	227*	0*	58*
Pb	8*	3*	9*	9*	5*
Th	0*	0*	4	0*	3
U	0*	0*	0*	0*	0*

*Indicates values below the detection limit

Table 20. (continued)

<u>Number</u>	<u>129</u>	<u>131</u>	<u>133</u>	<u>139</u>	<u>140</u>
B ₂ O ₃	46.583	41.223	51.305	46.583	45.945
CaO	24.080	21.000	25.928	24.500	23.100
MgO	1.054	3.530	0.320	1.465	2.584
Na ₂ O	0.143	0.246	0.249	0.189	0.235
SrO	1.976	2.064	0.312	1.857	1.081
As ₂ O ₃	0.030	0.191	0.042	0.138	0.038
SiO ₂	1.913	8.329	0.090	2.502	4.334
TiO ₂	0.010	0.089	0.000	0.009	0.010
K ₂ O	0.211	1.169	0.000	0.265	0.244
H ₂ O+	21.314	19.613	20.544	20.710	20.550
CO ₂					
SO ₃	0.197	0.230	0.332	0.533	0.212
Total	97.511	97.684	99.122	98.751	98.333
Al	1661	8923	120	1487	1802
Fe	1176	4728	1025	1318	648
Mn	30	153	33	34	0*
P	46*	225	62*	441	114
Cl	145*	152*	104*	136*	140*
Cr	10*	28	8*	5*	8*
Ni	8*	30	27	12*	1*
Cu	36	39	6	30	16
Zn	7*	21	5*	10*	8*
Br	2*	0*	0*	0*	1*
Sn	36	36	29	29	23
Ba	239*	40*	39*	0*	176*
Ce	81*	188*	81*	162*	56*
Pb	14	13*	6*	6*	1*
Th	0*	4	0*	1	0*
U	0*	0*	0*	1*	1*

*Indicates values below the detection limit

Table 20. (continued)

<u>Number</u>	<u>143</u>	<u>147</u>	<u>148</u>	<u>149</u>	<u>150</u>
B ₂ O ₃	42.116	48.497	46.328	49.770	45.945
CaO	23.240	24.570	23.100	26.320	24.010
MgO	4.937	0.401	1.693	0.325	1.611
Na ₂ O	0.267	0.317	0.178	0.177	0.092
SrO	2.148	1.819	2.217	0.613	0.546
As ₂ O ₅	0.324	0.037	0.017	0.004	0.014
SiO ₂	3.231	0.255	3.918	0.081	3.371
TiO ₂	0.020	0.000	0.034	0.000	0.025
K ₂ O	0.323	0.003	0.676	0.000	0.557
H ₂ O+	17.195	20.510	19.760	21.110	20.805
CO ₂	3.805				
SO ₃	0.295	2.505	0.202	0.147	0.175
Total	97.901	98.914	98.123	98.547	97.151
Al	2397	338	4512	81*	2954
Fe	1417	9044	2108	333	2122
Mn	93	10*	53	2*	30
P	107	27*	169	33*	260
Cl	158*	122*	158*	126*	157*
Cr	11*	8*	15	7*	15
Ni	6*	47	18	4*	8*
Cu	46	35	36	0*	10
Zn	14*	8*	16*	5*	10*
Br	0*	2*	1*	1*	0*
Sn	23	24	25	23	32
Ba	0*	71*	95*	50*	54*
Ce	252	85*	72*	55*	60*
Pb	12*	10*	6*	6*	5*
Th	0*	0*	0*	5	2
U	0*	0*	0*	0*	0*

*Indicates values below the detection limit

Table 20. (continued)

<u>Number</u>	<u>154</u>	<u>157</u>	<u>158</u>	<u>192</u>	<u>193</u>
B ₂ O ₃	48.497	47.221	49.135	52.071	52.071
CaO	25.690	23.730	24.808	25.540	25.620
MgO	0.409	0.707	0.712	1.035	1.049
Na ₂ O	0.194	0.271	0.348	0.000	0.000
SrO	0.842	1.910	1.453	0.973	0.784
As ₂ O ₅	0.034	0.799	0.005	0.004	0.094
SiO ₂	0.488	0.762	0.419	0.043	0.141
TiO ₂	0.000	0.000	0.000	0.000	0.000
K ₂ O	0.048	0.000	0.036	0.000	0.000
H ₂ O+	21.870	22.405	20.480	20.733	21.329
CO ₂					
SO ₃	0.425	0.794	0.102	0.060	0.147
Total	98.497	98.599	97.498	100.459	101.235
Al	676	389	598	0*	0*
Fe	1826	140	1284	60	84
Mn	8*	14*	1*	2*	2*
P	82	32*	75*	57*	45*
Cl	99*	101*	124*	77*	74*
Cr	7*	10*	6*	6*	5*
Ni	19	7*	10*	3*	0*
Cu	15	35	22	0*	0*
Zn	7*	7*	8*	13*	8*
Br	0*	0*	1*	1*	0*
Sn	20	19	24	0*	1
Ba	39*	0*	108*	336	117*
Ce	87*	557	60*	69*	328
Pb	5*	1*	12*	21	7*
Th	0*	0*	0*	0*	3
U	1*	0*	0*	0*	0*

*Indicates values below the detection limit

Table 20. (continued)

<u>Number</u>	<u>194</u>	<u>198</u>	<u>202</u>	<u>206</u>
B ₂ O ₃	49.517	50.992	50.518	50.518
CaO	24.920	25.368	25.424	25.424
MgO	1.061	1.098	1.120	1.153
Na ₂ O	0.000	0.000	0.000	0.000
SrO	1.813	1.336	0.315	0.328
As ₂ O ₅	0.004	0.004	0.014	0.019
SiO ₂	0.197	0.058	0.071	0.105
TiO ₂	0.000	0.000	0.000	0.000
K ₂ O	0.000	0.000	0.000	0.000
H ₂ O+	20.901	21.285	21.213	21.435
CO ₂				
SO ₃	0.072	0.030	0.062	0.125
Total	98.485	100.101	98.737	99.107
Al	64*	0*	0*	21*
Fe	116	63	69	250
Mn	4*	4*	3*	5*
P	36*	38*	100	59*
Cl	79*	76*	69*	64*
Cr	9*	7*	4*	9*
Ni	6*	3*	0*	11*
Cu	0*	0*	0*	0*
Zn	11*	9*	9*	9*
Br	0*	1*	0*	1*
Sn	0*	0*	0*	0*
Ba	475	444	327	308
Ce	80*	0*	107*	101*
Pb	17	7*	6*	10*
Th	0*	0*	0*	0*
U	0*	0*	0*	2*

*Indicates values below the detection limit

Table 21. Chemical analyses of colemanite and clay mixtures.

<u>Number</u>	<u>2</u>	<u>47</u>	<u>49</u>	<u>77</u>	<u>128</u>
SiO ₂	10.70	14.64	14.11	10.51	10.36
Al ₂ O ₃	3.77	4.75	5.20	7.45	5.10
TiO ₂	0.07	0.12	0.13	0.13	0.11
Fe ₂ O ₃	0.37	1.79	0.83	1.08	0.84
FeO	0.32	0.19	0.18	0.24	0.18
MgO	2.03	1.42	1.80	2.09	1.66
CaO	22.33	21.00	21.70	22.40	23.10
Na ₂ O	0.20	0.20	0.30	0.24	0.20
K ₂ O	0.54	2.00	1.72	0.87	0.91
MnO	0.01	0.03	0.02	0.01	0.02
P ₂ O ₅	0.07	0.09	0.21	0.07	0.06
H ₂ O ⁺	17.90	16.94	17.17	17.14	16.26
CO ₂	0.14	0.00	0.00	0.00	0.00
B ₂ O ₃	41.48	34.54	36.53	36.69	40.20
SO ₃	0.50	0.23	0.20	0.77	0.23
Total	100.43	97.94	100.10	99.69	99.23
Cl	186	153	168	182	134
Cr	33	14	17	24	33
Ni	82	26	29	100	62
Cu	18	29	6	19	21
Zn	21	91	47	43	33
As	218	8906	368	757	153
Br	3*	0*	0*	0*	0*
Sr	3274	1355	1287	8303	6767
Ba	261	0*	187	1623	229
Ce	66	843	116	163	109
Pb	17	281	25	14	48
Th	19	7	9	11	7
U	1*	4	3*	4	0*

*Indicates values below the detection limit

Table 21. (continued)

<u>Number</u>	<u>130</u>	<u>132</u>	<u>134</u>	<u>155</u>	<u>159</u>
SiO ₂	14.74	23.22	35.01	32.61	34.96
Al ₂ O ₃	7.56	8.82	13.18	8.68	15.54
TiO ₂	0.12	0.21	0.47	0.35	0.43
Fe ₂ O ₃	0.90	1.64	3.52	3.49	3.50
FeO	0.20	0.38	0.48	1.22	0.32
MgO	4.10	6.54	4.89	4.62	7.13
CaO	20.30	15.47	11.27	12.45	10.69
Na ₂ O	0.15	0.19	0.21	0.21	0.21
K ₂ O	0.90	1.52	3.63	2.65	3.27
MnO	0.03	0.05	0.07	0.05	0.09
P ₂ O ₅	0.05	0.17	0.17	0.22	0.34
H ₂ O+	13.20	12.05	6.50	6.93	3.22
CO ₂	0.00	0.00	0.00	0.00	0.00
B ₂ O ₃	37.17	28.72	21.54	23.45	20.26
SO ₃	0.40	0.45	0.45	1.67	0.50
Total	99.82	99.43	101.39	98.60	100.46
Cl	148	101	63	66	94
Cr	37	205	296	85	77
Ni	67	82	199	200	151
Cu	55	50	30	55	34
Zn	50	73	110	107	118
As	309	1993	883	656	302
Br	0*	1*	0*	0*	1*
Sr	17342	12802	3102	3660	4594
Ba	799	72	428	455	426
Ce	91	285	228	171	166
Pb	64	35	63	113	49
Th	4*	4*	19	13	19
U	0*	0*	4	3*	7

*Indicates values below the detection limit

Table 21. (continued)

<u>Number</u>	<u>163</u>
SiO ₂	24.98
Al ₂ O ₃	9.97
TiO ₂	0.29
Fe ₂ O ₃	2.24
FeO	0.48
MgO	4.43
CaO	15.47
Na ₂ O	0.27
K ₂ O	2.70
MnO	0.06
P ₂ O ₅	0.15
H ₂ O+	10.50
CO ₂	0.00
B ₂ O ₃	28.56
SO ₃	0.25
Total	100.35
Cl	83
Cr	67
Ni	120
Cu	28
Zn	93
As	271
Br	0*
Sr	3572
Ba	337
Ce	140
Pb	66
Th	14
U	2*

*Indicates values below the detection limit

Table 22. Chemical analyses of other borate minerals from Emet.

<u>Meyerhofferite</u>				
<u>Number</u>	<u>125</u>	<u>126</u>	<u>170</u>	<u>207</u>
B ₂ O ₃	45.689	42.499	45.945	44.030
CaO	24.960	23.350	23.240	22.400
MgO	0.765	2.500	0.949	1.594
Na ₂ O	0.156	0.263	0.220	0.000
SrO	0.025	0.101	0.253	0.507
As ₂ O ₅	0.217	0.150	0.015	0.019
SiO ₂	1.057	3.886	1.626	1.881
TiO ₂	0.001	0.032	0.008	0.010
K ₂ O	0.099	0.674	0.280	0.359
H ₂ O+	26.385	24.747	25.580	26.075
CO ₂				
SO ₃	0.532	0.370	0.202	0.071
Total	99.886	98.572	98.318	96.946
Al	651	3052	1214	1447
Fe	399	2047	1101	1046
Mn	22	52	23	29
P	88	723	43*	68*
Cl	151*	178*	163*	72*
Cr	9*	21	10*	7*
Ni	2*	11*	5*	5*
Cu	0*	5	1	0*
Zn	6*	14*	8*	13*
Br	0*	0*	2*	0*
Sn	13	32	28	0*
Ba	0*	0*	90*	338
Ce	212*	168*	49*	103*
Pr	2*	7*	3*	7*
Th	3	1	1	2
U	0*	1*	0*	0*

* Indicates values below the detection limit

Table 22. (continued)

	<u>Ulexite</u>				
<u>Number</u>	<u>141</u>	<u>151</u>	<u>172</u>	<u>173</u>	<u>203</u>
B ₂ O ₃	45.689	40.580	42.611	43.647	41.605
CaO	13.328	12.250	13.664	13.524	13.524
MgO	1.034	1.241	0.851	0.904	1.383
Na ₂ O	7.881	7.459	7.943	7.667	7.112
SrO	0.103	0.593	0.325	0.263	0.096
As ₂ O ₅	0.013	0.017	0.017	0.024	0.043
SiO ₂	1.629	4.199	0.306	1.746	1.462
TiO ₂	0.008	0.052	0.000	0.018	0.007
K ₂ O	0.175	1.364	0.028	0.361	0.147
H ₂ O+	30.384	29.510	33.670	31.620	32.568
CO ₂					
SO ₃	0.445	0.552	0.317	0.477	0.168
Total	100.689	97.817	99.237	100.251	98.115
Al	977	5049	256	1894	843
Fe	856	2822	316	2307	805
Mn	17	57	7*	41	28
P	66*	273	10*	47*	68*
Cl	187	193	174*	161*	132*
Cr	8*	17	9*	10*	11*
Ni	6*	22	21	18	2*
Cu	0*	18	1	1	0*
Zn	5*	24	28	11*	11*
Br	1*	1*	0*	1*	0*
Sn	26	26	15	33	0*
Ba	101*	435	190*	139*	216*
Ce	38*	38*	30*	45*	206*
Pr	5*	34	46	9*	8*
Th	0*	3	3	3	0*
U	0*	0*	3*	0*	0*

*Indicates values below the detection limit

Table 22. (continued)

<u>Number</u>	<u>Ulexite</u>	
	<u>205</u>	<u>209</u>
B ₂ O ₃	43.392	42.116
CaO	12.990	13.664
MgO	0.871	0.851
Na ₂ O	7.348	7.566
SrO	0.276	0.112
As ₂ O ₅	0.004	0.008
SiO ₂	0.069	0.306
TiO ₂	0.000	0.000
K ₂ O	0.000	0.028
H ₂ O+	32.279	35.340
CO ₂		
SO ₃	0.168	0.139
Total	97.397	100.130
Al	26*	256
Fe	99	316
Mn	5*	7*
P	20*	10*
Cl	75*	91*
Cr	6*	11*
Ni	3*	3*
Cu	0*	0*
Zn	10*	10*
Br	2*	0*
Sn	0*	0*
Ba	374	361
Ce	40*	44*
Pr	6*	9*
Th	3	0*
U	0*	0*

*Indicates values below the detection limit

Table 22. (continued)

	<u>Veatchite mineral</u>		
<u>Number</u>	<u>142</u>	<u>145</u>	<u>210</u>
B ₂ O ₃	48.750	57.176	57.622
CaO	3.808	0.630	0.322
MgO	3.014	1.272	0.688
Na ₂ O	0.192	0.155	0.023
SrO	26.541	27.790	29.780
As ₂ O ₅	0.552	0.565	0.052
SiO ₂	4.851	1.376	0.452
TiO ₂	0.032	0.004	0.000
K ₂ O	0.233	0.008	0.000
H ₂ O+	12.030	9.948	9.745
CO ₂			
SO ₃	0.145	0.095	0.024
Total	100.148	99.019	98.708
Al	2959	734	225
Fe	1264	701	142
Mn	68	42	3*
P	131	32*	14*
Cl	108*	90*	61*
Cr	11*	10*	9*
Ni	6*	5*	9*
Cu	478	552	0*
Zn	47	21	33
Br	0*	0*	9
Sn	4	1	0*
Ba	0*	0*	305
Ce	228*	215*	159*
Pr	12*	6*	10*
Th	0*	0*	0*
U	0*	0*	0*

*Indicates values below the detection limit

Table 22. (continued)

<u>Number</u>	<u>Tunellite</u>		
	<u>211</u>	<u>211/1</u>	<u>213</u>
B ₂ O ₃	52.071	45.945	55.261
CaO	0.931	3.024	0.095
MgO	1.121	2.394	
Na ₂ O	0.058	0.000	
SrO	27.091	24.760	24.240
As ₂ O ₅	0.092	0.181	
SiO ₂	1.374	2.734	
TiO ₂	0.014	0.114	
K ₂ O	0.003	0.120	
H ₂ O+	17.544	18.892	20.240
CO ₂			
SO ₃	0.086	0.000	
Total	100.385	98.164	99.836
Al	876	2901	
Fe	369	2630	
Mn	29	220	
P	53*	228	
Cl	137*	29*	
Cr	0*	0*	
Ni	11*	0*	
Cu	0*	0*	
Zn	70	58	
Br	1*	0*	
Sn	0*	0*	
Ba	4701	5221	
Ce	164*	632	
Pb	120	30	
Th	0*	0*	
U	15	4*	

* Indicates values below the detection limit

Table 22. (continued)

	<u>Hydroboracite</u>				
<u>Number</u>	<u>59</u>	<u>72</u>	<u>138</u>	<u>144</u>	<u>153</u>
B ₂ O ₃	47.859	50.156	42.754	31.268	47.859
CaO	12.040	13.384	11.536	9.016	13.720
MgO	11.504	11.250	12.518	13.100	10.826
Na ₂ O	0.064	0.208	0.168	0.219	0.161
SrO	0.071	0.014	0.188	0.247	0.227
As ₂ O ₅	0.508	0.017	0.430	0.067	0.110
SiO ₂	1.954	0.672	4.971	16.870	1.166
TiO ₂	0.003	0.004	0.014	0.272	0.006
K ₂ O	0.020	0.032	0.097	3.155	0.106
H ₂ O+	23.955	23.885	23.089	19.118	24.650
CO ₂	1.896	0.000	2.815	2.600	0.755
SO ₃	0.604	0.292	0.936	0.609	0.415
Total	100.478	99.914	99.516	96.541	100.001
Al	610	485	1150	18491	793
Fe	871	435	3108	10176	3454
Mn	42	95	112	322	546
P	13*	22*	21*	1969	18*
Cl	135*	160*	148*	109*	150*
Cr	5*	5*	13	63	14
Ni	11*	4*	12*	52	7*
Cu	2	0*	9	21	1
Zn	6*	6*	10	71	5*
Br	0*	0*	0*	0*	0*
Sn	23	24	25	54	21
Ba	0*	126*	0*	206*	53*
Ce	429	39*	393	94*	104*
Pr	2*	4*	8*	46	4*
Th	4	4	0*	12	0*
U	0*	0*	0*	1*	0*

* Indicates values below the detection limit

Table 22. (continued)

<u>Number</u>	<u>Hydroboracite</u>			
	<u>160</u>	<u>196</u>	<u>197</u>	<u>208</u>
B ₂ O ₃	37.649	50.092	49.518	42.116
CaO	10.444	12.660	13.440	11.536
MgO	14.066	10.630	10.642	12.166
Na ₂ O	0.043	0.000	0.000	0.067
SrO	0.138	0.010	0.011	0.072
As ₂ O ₅	0.224	0.006	0.085	0.187
SiO ₂	10.779	0.032	0.062	5.448
TiO ₂	0.162	0.000	0.000	0.038
K ₂ O	0.879	0.000	0.000	0.507
H ₂ O+	23.240	25.540	25.660	23.640
CO ₂	0.000	1.417	0.254	0.787
SO ₃	0.340	0.072	0.130	0.171
Total	97.964	100.459	99.802	96.735
Al	9283	2*	14*	2689
Fe	8058	77	100	2891
Mn	250	41	31	113
P	278	30*	6*	119
Cl	136*	68*	68*	78*
Cr	51	6*	7*	11*
Ni	53	2*	7*	6*
Cu	11	0*	0*	0*
Zn	24	11*	9*	20
Br	0*	0*	0*	0*
Sn	34	0*	0*	0*
Ba	10*	306	58*	0*
Ce	217*	32*	351	832
Pb	11*	13*	6*	9*
Th	5	4	0*	2
U	2*	0*	1*	0*

* Indicates values below the detection limit

Table 22. (continued)

<u>Number</u>	<u>Teruggite</u>		
	<u>70</u>	<u>71</u>	<u>195</u>
B ₂ O ₃	34.139	34.139	33.182
CaO	17.360	17.430	16.800
MgO	3.200	3.604	4.171
Na ₂ O	0.225	0.256	0.000
SrO	0.117	0.177	0.024
As ₂ O ₅	18.689	18.689	18.165
SiO ₂	0.499	1.246	0.054
TiO ₂	0.000	0.000	0.000
K ₂ O	0.000	0.000	0.000
H ₂ O+	25.437	24.300	27.294
CO ₂			
SO ₃	0.102	0.267	0.017
Total	99.768	100.108	99.707
Al	146*	362	3*
Fe	845	518	63
Mn	40	67	25
P	34*	38*	27*
Cl	155*	235	157*
Cr	11*	8*	7*
Ni	4*	11*	3*
Cu	152	153	141
Zn	22	27	24
Br	0*	0*	0*
Sn	14	9	0*
Ba	0*	0*	0*
Ce	0*	0*	0*
Pb	0*	6*	9*
Th	0*	1	4
U	0*	0*	1*

*Indicates values below the detection limit

Table 22. (continued)

<u>Number</u>	<u>Cahnite</u>	
	<u>212</u>	<u>214</u>
B ₂ O ₃	23.355	16.591
CaO	32.480	29.120
MgO	1.800	
Na ₂ O	0.000	
SrO	0.654	
As ₂ O ₅	31.376	34.673
SiO ₂	2.024	
TiO ₂	0.048	
K ₂ O	0.750	
H ₂ O+	9.144	9.361
CO ₂	0.000	
SO ₃	0.000	
Total	101.631	89.745
Al	3313	
Fe	3368	
Mn	118	
P	200	
Cl	131*	
Cr	0*	
Ni	0*	
Cu	66	
Zn	36	
Br	0*	
Sn	0*	
Ba	0*	
Ce	0*	
Pb	0*	
Th	0*	
U	2*	

*Indicates values below the detection limit

Table 23. Chemical analyses of non-borate minerals from Emet.

Realgar

<u>Number</u>	<u>73</u>
B ₂ O ₃	0.153
CaO	0.077
MgO	1.998
Na ₂ O	0.000
SrO	0.001
As	69.160
SiO ₂	0.000
TiO ₂	0.000
K ₂ O	0.000
H ₂ O+	0.061
CO ₂	
S	28.180
Total	99.630

Al	312
Fe	0*
Mn	116
P	9*
Cl	654
Cr	0*
Ni	0*
Cu	173
Zn	33
Br	0*
Sn	0*
Ba	0*
Ce	0*
Pb	7*
Th	0*
U	0*

*Indicates values below the detection limit

Table 23. (continued)

<u>Number</u>	<u>Celestite</u>		
	<u>9</u>	<u>11</u>	<u>199</u>
B ₂ O ₃	3.829	4.467	0.080
CaO	0.560	0.371	0.140
MgO	1.976	0.436	0.476
Na ₂ O	0.130	0.163	0.032
SrO	45.398	52.918	55.475
As ₂ O ₅	0.035	0.005	0.013
SiO ₂	7.355	0.058	0.004
TiO ₂	0.056	0.000	0.000
K ₂ O	0.473	0.000	0.000
H ₂ O+	1.462	0.242	0.431
CO ₂	0.000	0.000	
SO ₃	35.058	40.865	42.840
Total	96.332	99.527	99.491
Al	10951	180	74*
Fe	1667	454	49
Mn	19	12*	2*
P	147	23*	10*
Cl	91*	69*	42*
Cr	2*	5*	4*
Ni	22	2*	8*
Cu	496	499	0*
Zn	31	14*	47
Br	7	18	11
Sn	0*	2	1
Ba	9286	870	1039
Ce	143*	133*	161*
Pr	0*	0*	122
Th	0*	0*	0*
U	0*	0*	0*

*Indicates values below the detection limit

Table 23. (continued)

<u>Number</u>	<u>Gypsum</u>				
	<u>80</u>	<u>81</u>	<u>83</u>	<u>84</u>	<u>200</u>
B ₂ O ₃	1.276	0.160	1.276	0.000	0.160
CaO	31.500	31.530	31.500	31.010	31.530
MgO	0.430	0.405	0.398	0.450	0.757
Na ₂ O	0.254	0.239	0.261	0.160	0.082
SrO	0.106	0.033	0.034	0.076	0.033
As ₂ O ₅	0.004	0.004	0.004	0.004	0.004
SiO ₂	0.666	0.514	0.526	0.768	0.242
TiO ₂	0.000	0.000	0.000	0.000	0.000
K ₂ O	0.014	0.008	0.005	0.020	0.000
H ₂ O+	19.683	17.968	18.170	19.030	19.686
CO ₂					
SO ₃	44.957	46.782	46.621	45.295	45.628
Total	98.890	97.643	98.795	96.813	98.122
Al	878	664	705	986	269
Fe	704	249	1119	668	216
Mn	19	17	0*	11*	9*
P	201	5*	15*	162	20*
Cl	46*	58*	47*	53*	45*
Cr	10*	9*	11*	10*	12
Ni	3*	3*	6*	8*	8*
Cu	16	15	16	18	10
Zn	3*	4*	5*	4*	7*
Br	1*	1*	2*	1*	1*
Sn	36	22	29	23	0*
Ba	68*	75*	108*	88*	442
Ce	30*	44*	32*	29*	38*
Pb	3*	1*	4*	4*	7*
Th	4	2	3	1	0*
U	1*	0*	0*	1*	0*

* Indicates values below the detection limit

Table 23. (continued)

Gypsum

<u>Number</u>	<u>201</u>
B ₂ O ₃	0.000
CaO	31.080
MgO	0.764
Na ₂ O	0.109
SrO	0.072
As ₂ O ₅	0.006
SiO ₂	0.231
TiO ₂	0.000
K ₂ O	0.000
H ₂ O+	19.276
CO ₂	
SO ₃	46.026
Total	97.564
Al	286
Fe	191
Mn	5*
P	223
Cl	67*
Cr	7*
Ni	34
Cu	13
Zn	10*
Br	3*
Sn	0*
Ba	404
Ce	31*
Pb	6*
Th	0*
U	1*

* Indicates values below the detection limit

Table 23. (continued)

<u>Calcite</u>					
<u>Number</u>	<u>136</u>	<u>137</u>	<u>169</u>	<u>175</u>	<u>204</u>
B ₂ O ₃	0.080	1.276	0.160	0.000	0.000
CaO	52.920	50.540	49.700	51.800	52.920
MgO	0.628	1.772	1.842	0.914	2.581
Na ₂ O	0.191	0.200	0.124	0.332	0.000
SrO	1.100	1.438	0.701	0.018	1.961
As ₂ O ₅	0.153	0.265	0.076	0.001	0.011
SiO ₂	0.387	2.149	1.932	1.464	0.041
TiO ₂	0.000	0.005	0.007	0.003	0.000
K ₂ O	0.015	0.206	0.321	0.045	0.000
H ₂ O+	0.419	0.681	0.847	0.561	0.389
CO ₂	41.580	39.710	39.577	40.700	41.950
SO ₃	0.170	0.202	0.612	0.125	0.155
Total	97.643	98.444	95.899	95.963	100.008
Al	514	2197	2821	2090	0*
Fe	419	888	1088	820	116
Mn	12*	62	41	138	13*
P	139	142	162	333	129
Cl	130*	112*	203	285	77*
Cr	7*	8*	13	7*	6*
Ni	1*	9*	7*	5*	0*
Cu	27	30	31	21	0*
Zn	6*	10*	12*	7*	9*
Br	0*	0*	8	2*	2*
Sn	19	22	26	20	0*
Ba	89*	0*	103*	36*	335
Ce	191*	244*	150*	123*	93*
Pb	0*	4*	10*	3*	5*
Th	4	23	8	12	0*
U	0*	1*	25	0*	0*

*Indicates values below the detection limit

CHAPTER VIII

ORIGIN AND DIAGENESIS OF THE EMET BORATE DEPOSITS

1. The geological setting:

Stratigraphical evidence presented in detail in Chapters III and V suggests that the Emet borate deposits were formed in two separate basins, possibly part of a chain of inter-connected lacustrine lakes. The clastic sediments in both basins are similar but are very much thicker in the Northern basin (Espey-Killik area). Petrographically and geochemically they can not be distinguished (Chapter IV); both share the same characteristics which indicate a dominantly volcanic source and deposition under strongly oxidising conditions. Like the volcanic rocks of the surrounding hinterland (Chapter III) the clays and tuffs interbedded with the borates are rich in K^+ relative to Na^+ (Chapter IV).

Although the interbedded sediments are indistinguishable the borates show mineralogical (Chapter VI) and geochemical (Chapter VII) features in the two basins which are sufficiently different to suggest that the chemical compositions of ground and surface waters in the two basins differed at least from time to time.

The Emet borate deposits and associated sediments are dislocated by the NW-SE and NE-SW trending gravity faults, which both occurred after the deposition of borates, but NW-SE trending gravity faults are still active (Chapters III and V). Thermal springs, which at present deposit travertine and sulphur, are believed to play a very important role during the deposition of borates (Chapter III). They were related to the extensive volcanic activity during the existence of the borate lakes at Emet.

2. Source of the Boron, Arsenic, Sulphur, Calcium, Sodium, Magnesium and Strontium:

The geochemical association of boron, arsenic and sulphur suggests a common origin for all three elements at Emet. Arsenic sulphides and native sulphur, although present in minor quantities, are as widely distributed as colemanite and hence it may be assumed that the initial brines at all times were fed by an abundance of calcium and boron with minor amounts of arsenic and sulphur. Several possible sources for these elements have been considered. A marine origin may be dismissed, because all the evidence indicates that the Emet borates were deposited in non-marine lacustrine environments (see Chapters III and V).

Among the possible sources for these elements are:-

- a) Leaching of buried borate deposits by spring system
- b) Volcanic exhalation and associated thermal springs.

It is quite possible that B, As and S were transported to the deposits from the older buried borate deposits which could be located in the adjacent area. Because many of the borate deposits have no extensive drainage areas, the buried deposits must be fairly close to the more recent deposits. The geology of the Emet district clearly shows that the basement and surrounding rocks are metamorphic and consist of marble, micaschist and calcschist (Chapter III). Although local thermal springs now carry certain amounts of boron, arsenic and sulphur (Chapter III), there is no evidence that these springs leach older buried deposits. However, there is evidence that thermal and surface waters, which leach volcanic rocks, (Chapter III) in the Emet region, might produce substantial amounts of soluble boron for accumulation in the borate lakes of Middle Oligocene age in the Emet area.

During the present study, thermal springs, which are widespread in the district, were analysed for boron and arsenic. They contain considerable amounts of these elements (see Table 6) and sulphur concentration in these springs is much higher (see Plate 11).

Because of the temporal and spatial distribution of volcanic activity during the existence of the lakes at Emet and thermal springs activity in the region around the lakes, it is very likely that the concentration of boron, arsenic and sulphur were then much higher. The association of volcanics with boron bearing thermal springs is quite common elsewhere in the world such as Steamboat Springs, Nevada, Yellowstone National Park, Amedee Hot Springs, California, etc..

In view of the lack of boron and arsenic and the rarity of sulphur in rocks likely to be exposed in the catchment area, a thermal spring source connected to the volcanic activity for boron, arsenic and sulphur seems most probable. In the Emet area, the extensive volcanic tuffs were interbedded with the borates, indicating that much of the sediments were derived from volcanic terrain and source. Therefore, geochemical investigations suggest that the most likely sources of B, As and S were from:-

- a. The weathering products of Tertiary volcanic rocks transported into the borate basins by streams.
- b. Volcanic ash deposited directly into the borate basins.
- c. Thermal springs.

Surface streams may have carried some Na^+ , Ca^{++} , Sr^{++} , Mg^{++} and other elements in solution into the basins as the result of weathering of rocks exposed in the catchment area but the major source of Ca^{++} , Mg^{++} and Sr^{++} , by analogy with present day hydrology, is considered to be due to leaching of underlying Tertiary limestone by thermal springs (see Table 6).

The sources of Ca^{++} could be summarised as follows:-

- a. Weathering of the basement rocks and transport by surface or groundwaters.
- b. Weathering of exposed Lower Limestone and transport by surface of groundwaters.
- c. Leaching of the basement rocks and Lower Limestone by thermal and other groundwaters.
- d. Volcanic exhalations.

It seems very likely that most of the calcium was introduced to the basins by thermal springs and weathering of the basement rocks and the Lower Limestone.

Probable sources for Na^+ are connate water; volcanic tuffs associated with borates and thermal springs.

There are several alternatives for the source of Mg^{++} . Among the most probable origins are thermal springs, volcanic tuffs and clay associated with the borates, basement rocks and leaching from the Lower Limestone. The magnesium concentrations of the present thermal springs were given in Table 6. Clays and volcanic tuffs are extremely rich in magnesium (see Tables 7 & 8), indicating that a very high amount of magnesium was concentrated in the clays and tuffs.

Strontium concentration of the sediments and borates in Emet is high, as mentioned previously. Strontium may have been introduced to the brines in several ways. Among the possible sources for strontium are:- Upper Limestone, volcanic tuff and clay, leaching from Lower Limestone and thermal springs and volcanic rocks, which occurred in the adjacent area.

It is possible that strontium leached from the Upper Limestone during the diagenesis. As it is well known, aragonite can hold more Sr^{++} in its lattice than calcite. If aragonite were deposited originally and converted to calcite during diagenesis, a large amount of strontium would have come out, but no aragonite was detected by X-ray diffraction analysis. Also strontium would have been preferentially concentrated in the upper part of the borate zone, because of the impermeable nature of interbedded clays, whereas strontium is quite high all through the borate zone. Therefore, it may be concluded that the source of Sr^{++} is not the Upper Limestone. Strontium content of the thermal springs was already given on Table 6 and volcanic rocks in the district and volcanic tuffs in the deposits contain very high strontium

concentrations (see Tables 5 and 13). Geochemical investigations suggest that the most likely sources of Sr were from: volcanic rocks, interbedded volcanic tuffs and clays, thermal springs and probably leaching from the lower limestone.

3. Mineral phases formed penecontemporaneously with the clastic sediments:

The composition of non-marine evaporites is much more variable than that of marine evaporites, for it depends to a varying degree upon climate, the nature of the rocks exposed in the catchment area and the composition of thermal spring waters. The crystallization of the borate minerals in the lake deposits is closely dependant on surface conditions, temperature range and pH of the lake brines, duration of time and chemical composition of the lake waters. This last point includes concentration of B, Ca, Na, etc. ions in the lake brines.

Origin of the early formed colemanite:

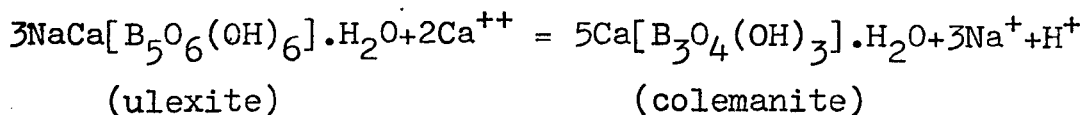
As it was mentioned in Chapter VI, colemanite occurs in many different forms such as nodular, massive, disseminated crystals, fibrous layers, thin layers and vugh fillings. Nodular forms (see Plates 30, 31 and 32), massive granular (see Plates 33, 34 and 35) and disseminated crystals in clay matrix (see Plates 36, 37 and 38) have been considered as early formed colemanite (Chapter VI). Vugh fillings (see Plate 42), fibrous (see Plates 39 and 40) and thin layers (see Plate 41) of colemanite are believed to be late diagenesis products. Different forms of colemanite are often found to appear together in the same colemanite nodule (Plate 109).

It has been argued (p154) that this early formed colemanite was deposited penecontemporaneously with the unconsolidated sediments. It is probable that it was formed within the clays and tuffs below the sediment/water interface and probably continued to grow as the sediments were compacted (see Plates 36, 37, 38 and 55).

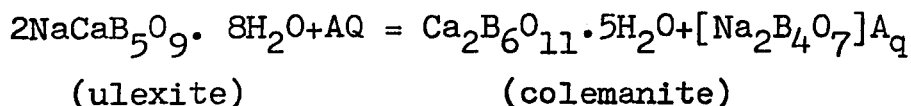
Whether early formed colemanite was formed by the breakdown of ulexite as suggested by Foshag (1921), Noble (1926) and Özpeker (1969); or by the dehydration of inyoite or meyerhofferite proposed by Rogers (1919), Hanshaw (1963), Christ et al (1967) Christ (1972) and Inan (1973); or by direct precipitation from solution as concluded by Kurnakova and Nikolaev (1948), Bowser and Dickson (1963) and Bowser (1965), is problematical.

The genesis of colemanite by the breakdown of ulexite was first suggested by Foshag (1921) for deposits in California but does not appear to be applicable to the Emet Valley colemanite for the following reasons:-

- a. Ulexite is rare even in the northern area (Espey-Killik).
- b. Nowhere is colemanite found intergrown with or apparently replacing ulexite.
- c. Nowhere have cores of colemanite been found in indurated masses of "cotton ball" ulexite as at Kramer, California (Bowser, 1965; Bowser and Dickson, 1966).
- d. Colemanite and ulexite always occur as separate nodules.
- e. Interbedded clays at Emet are notably deficient in Na^+ (see Table 7) and not enriched as they theoretically should have been if the following chemical reaction, suggested by Özpeker (1969), took place by base exchange between ulexite and the clays:-



f. Interbedded sediments (clays and tuffs, mainly) and borates at Emet are notably deficient in both Na and Cl, and not enriched as they theoretically should have been if the following chemical reaction, suggested firstly by Foshag (1921) and postulated to occur at temperature above 70°C, by Kemp (1956), in the presence of percolating sodium chloride solutions.



g. Suggestions that alteration of ulexite leads to the formation of the mineral pair colemanite and borax is inapplicable to the Emet area, where neither borax or any other Na-bearing mineral other than negligible ulexite occurs.

Alternative suggestions concerning the genesis of colemanite are equally difficult to substantiate. Metasomatic replacement of limestone (Gale, 1913) is improbable since the colemanite beds do not pass laterally into limestone nodules and no partially altered limestones have been found (see Chapters III and V).

Petrographic evidence from elsewhere, e.g. Death Valley, California (Rogers, 1919), Bigadiç area, Turkey (Meixner, 1952; 1953 and 1956) suggest that the higher hydrate inyoite ($\text{Ca}[\text{B}_3\text{O}_3(\text{OH})_5] \cdot 4\text{H}_2\text{O}$) was the first formed Ca borate mineral, which on burial and diagenesis was dehydrated to the denser meyerhofferite or more commonly to colemanite. The presence of drusy cavities (see Plate 44), often containing water, and of rare septarian cracks, filled with a clear colemanite (see Plate 109; see also Plates 32 and 45), suggest that reduction in volume

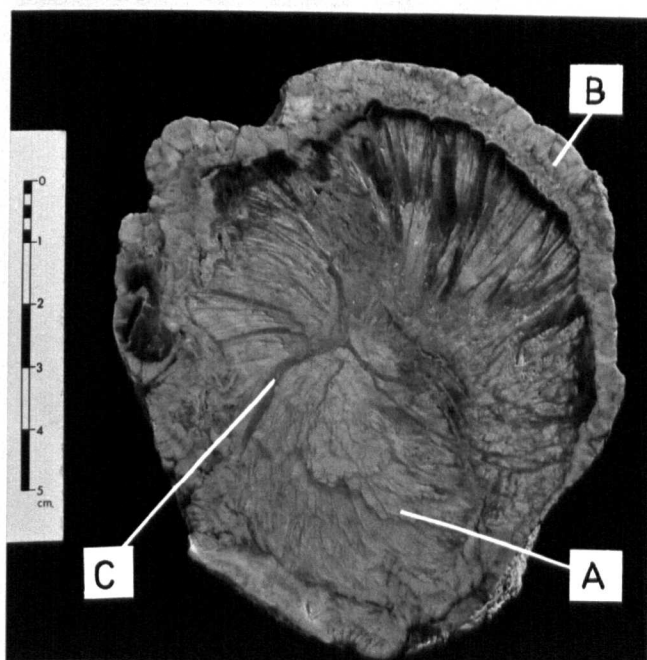


Plate 109. Section of colemanite nodule showing three generations of colemanite;

- A. massive colemanite crystals,
- B. fibrous colemanite crystals, and
- C. coarsely crystalline colemanite in cracks (possibly of septarian origin).

has occurred in some colemanite nodules. However, no inyoite has been found in the Emet district and no pseudomorphs of colemanite after inyoite have been recorded (Gawlik, 1956; Özpeker, 1969; Helvaci, 1974); shrinkage cracks and drusy cavities need not be due to dehydration of inyoite. Also Bowser and Dickson (1966) concluded that the colemanite in those nodules from the Kramer deposit, which are similar to those from Emet, apparently grew from solution in unconsolidated sediments and need not have formed by alteration of pre-existing ulexite or dehydration of inyoite. Whether inyoite was ever formed at Emet remains an open question.

Inyoite is the only Ca borate mineral found in modern deposits (Muessig, 1966) and experimental work by Inan, Dunham and Esson (1973) showed that pressure is required to form colemanite. At 1 atmosphere and below 38°C in their experiments, inyoite was the stable Ca borate mineral in contact with calcium borate solutions and above 38°C it transformed to meyerhofferite and not to colemanite. At 500 atmospheres and 38°C inyoite was replaced by colemanite + H_2O . Although they did not establish the threshold conditions for this reaction, their work implies that colemanite will not form at the pressures found in shallow lakes or unconsolidated lacustrine muds. Thus many strands of evidence from field-work, petrology and experiments indicate that colemanite forms by diagenetic replacement of inyoite on burial, or directly from calcium borate solutions above 38°C under comparatively high pressures during post depositional mineralisation. If inyoite has been replaced by colemanite at Emet, the replacement has been remarkably complete, since in spite of the most diligent search no relics or pseudomorphs of inyoite have been

found. Could it be that notwithstanding the experimental evidence colemanite did form as a primary mineral in physico-chemical conditions not yet defined or experimentally investigated? As Christ (1972) stated, the hydrated calcium borates form a more complex series than do the sodium borates, and experimental physical-chemical data should prove correspondingly more revealing for an understanding of the behaviour of hydrated minerals in general. Such an experimental study would be difficult. Unlike the sodium borates, the calcium borates are relatively insoluble in water, and for this and possibly other reasons, the crystalline solids and aqueous solution are not readily brought into equilibrium.

The Emet borate zones are characterised by relatively high arsenic and strontium contents and the effect of these elements on the crystallisation of the Ca borates is unknown. Similarly the effects of low partial pressures of H_2O have yet to be investigated.

In the present study preliminary experiments have shown that colemanite and calcite form when the evaporation products of 1:1 and 1:2 mixtures of colemanite and calcite dissolved in HCl are exposed to the atmosphere for several months (at least 5 or 6 months). This reaction takes place at atmospheric pressures, laboratory temperatures and pH about 7 or 8, suggesting that the deep burial and high pressures may not be necessary for the solution and reprecipitation of colemanite in natural conditions. Similar experiments with ulexite and calcite results in calcite reprecipitation, probably due to deficiency of Ca^{++} in the solutions.

In the borate zone, rhythmic deposition of colemanite, clay, tuff and limestone beds (see Plates 20, 21, 22, 25 and 26;

Figs. 15 and 16) indicates that when the brines were oversaturated with B and Ca, colemanite was deposited and during the period when B concentration decreased calcite was precipitated. Clays and tuffs were continuously deposited. In the thin section, clay and tuff inclusions in the early formed colemanite have been commonly observed (see Plates 32, 37, 45, 48, 49, 50, 55, and 59) and it is difficult to believe that these textures would have been preserved had the colemanite replaced inyoite or ulexite.

During the deposition, like colemanite, meyerhofferite, ulexite and teruggite nodules appear to have developed penecontemporaneously within and not on the sediments. Their sporadic occurrence indicates that the precipitation of these minerals was limited to certain parts of the deposits, possibly due to localised thermal springs. Realgar and small amounts of celestite were also precipitated with the sediments. The fine-grained realgar crystals enclosed in early formed massive colemanite and sediments demonstrate that some of the realgar was formed at an early stage (see Plates, 56, 63, 94 and 108). Small amounts of celestite were also formed penecontemporaneously within the sediments and borates (see Plate 106).

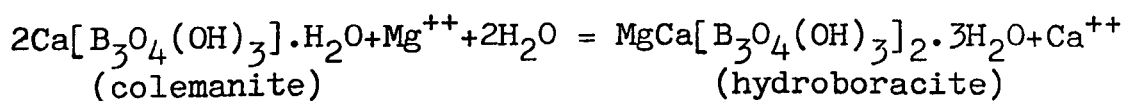
4. Diagenetic mineralization:

After the burial of the deposits by younger sediments, B and Ca bearing solutions circulating through the early borates and sediments were responsible for precipitation of later generations of colemanite such as vugh fillings (see Plate 42), fibrous (see Plates 39 and 40) and thin layers (see Plate 49) of colemanite. Plate 109 clearly indicates this secondary fibrous colemanite

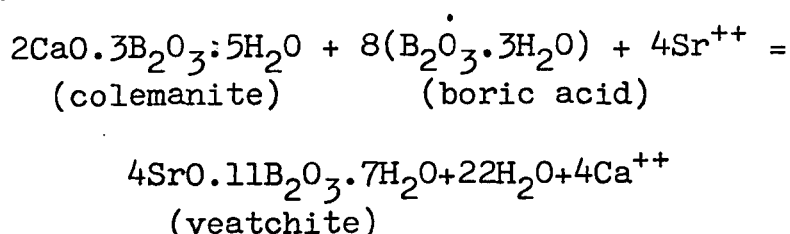
surrounding nodules and coarsely crystalline colemanite in cracks and vughs. Vugh fillings and coarsely crystalline euhedral colemanite crystals are very common and occur usually in the vughs of colemanite nodules as previously described in Chapter VI. Very thin layers of colemanite occur sporadically throughout the deposits.

The Emet deposits in general do not show much post-depositional deformation and most of the original stratification is preserved. During the diagenesis of the deposits common alteration products of colemanite are hydroboracite and calcite, and rarely a form of veatchite and cahnite. These have been clarified by the field observations, X-ray examinations, staining technique, microscope studies and chemical analyses (see Chapters VI and VII).

All colemanite samples analysed have a certain amount of hydroboracite which is commonly intimately intergrown with colemanite (see Plate 62) and is sometimes cut by later colemanite veins (see Plate 63). The transformation of colemanite to hydroboracite involves only the substitution of Mg^{++} for Ca^{++} and the addition of H_2O viz:-

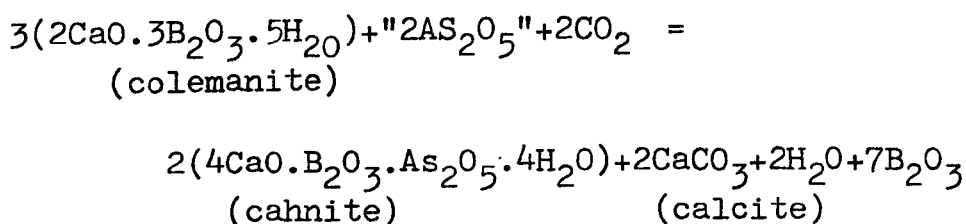


involves no substantial reduction in volume but does result in an enrichment in boron. It is tentatively postulated that interstratal boron rich brines, depleted in Ca^{++} and enriched in Sr^{++} reacted with the colemanite in a manner similar to that shown by the following hypothetical reaction:-



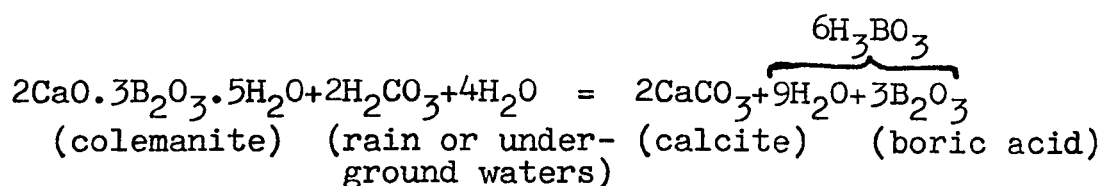
Such a dehydration reaction seems likely to occur with burial and compaction.

Cahnite occurs as a coating on euhedral colemanite crystals in vughs in colemanite nodules in the Espey-Killik area (see Plate 61). Colemanite, cahnite and calcite are usually associated together. The transformation of colemanite to cahnite and calcite could be formulated as follows:

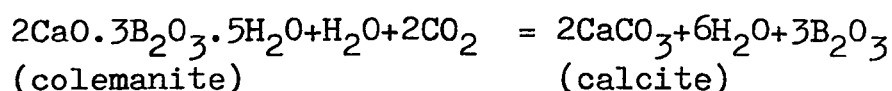


Alteration of colemanite to calcite is clearly seen by field observations (see Plates 64 and 103), staining techniques (see Plates 65 and 66) and microscope studies (see Plate 104). Colemanite alters to calcite mainly near the surface and near the fault zones. Alteration takes place along the radiating structure of colemanite nodules due to the action of rain or underground waters. If CO_2 saturated rain water, which furnishes H^+ , reacts

with exposed colemanite directly, or as ground water with near surface material, Ca^{2+} will be removed from the system and fixed as calcite, and the $\text{CaO}:\text{H}_2\text{O}$ ratio will decrease. For instance in the Hisarcik area, the colemanite horizons, which are on the slopes of mesas and plateaux, have completely disintegrated or been replaced by calcite on the surface. The transformation of colemanite to calcite can be explained as follows:-



or



Boron is very likely to be washed away by surface waters, e.g. the Emet River and surface waters carry up to 15 and 50ppm B_2O_3 , respectively.

Calcite also occurs in surface outcrops and adjacent to faults as a result of modern weathering. Much of the calcite may therefore be of very recent origin.

All the evidence indicates that hydroboracite, veatchite and cahnite often replaced colemanite and it is tentatively suggested that these minerals formed during diagenesis as a result of the addition of Mg^{++} , Sr^{++} and As^{5+} , respectively and the loss of Ca^{++} . Colemanite, in restricted parts of the deposits, was replaced by either hydroboracite; hydroboracite and calcite; cahnite and calcite; or cahnite. Cahnite may have formed as a result of dehydration of teruggite as observed in the Hisarcik area (see Plates 87 and 89). In addition to these diagenetic changes there is field and mineralogical evidence of at least three generations

of colemanite (see Plate 109) and separate post-depositional crystallization of tunellite, cahnite, celestite, native sulphur, gypsum, realgar and probably orpiment. On weathering colemanite is readily replaced by calcite and realgar by orpiment.

Tunellite commonly occurs as thin tabular shaped crystals (see Plate 77) and as small white nodules (see Plate 79) which have apparently grown in the interbedded clays. Often thin tabular shaped tunellite crystals have nucleated on ulexite (see Plate 78). Tunellite appears to have formed during diagenesis with enrichment of Sr^{++} in some places (in the northern area only) which led to formation of tunellite either from hydrous borates or small tunellite nodules which have grown in the interbedded clays. Tunellite does not appear to be replacing any other borate minerals in the deposits.

Alteration products of the colemanite (maximum 4% of the deposits) are insignificant as compared to the overall amount of colemanite (95% and above of the deposits). This suggests that colemanite has not undergone an extensive diagenetic alteration.

Interbedded tuffs are often altered to montmorillonite bearing clays. This is however incomplete and the transition between tuffs and montmorillonitic clay has been observed in progress (Chapter IV). The montmorillonite shows very little diagenetic alteration, as understood by the absence of chlorite, though illite occurs frequently in the deposits. The illite is believed to be detrital in origin and not an alteration product from montmorillonite.

5. Depositional and post-depositional history:

From the foregoing discussion it is concluded that the Emet borates were formed in playa lakes, in seismically active areas, fed partly by thermal springs and partly by streams draining the catchment areas. The bulk of the interbedded clastic sediments appear to be derived from volcanic terrain but Tertiary limestone might also have been exposed and erosion of these may have contributed Ca^{++} and Sr^{++} to the lake waters. Alternatively Ca^{++} and Sr^{++} may have leached from the underlying limestones and basement rocks by the thermal spring waters.

Since Ca borate makes up over 95% of the deposits, it is reasonable to assume that the original brines were enriched in Ca^{++} and boron. Arsenic sulphides, strontium sulphate and small amounts of native sulphur, although present in minor quantities, are as widely distributed as the Ca borate and hence it may be assumed that the initial brines at all times contained an abundance of calcium and boron with minor amounts of arsenic and sulphur. Strontium and sodium may also have been present in the initial brines or alternatively may have been added to the mineralising solutions periodically.

All early precipitated minerals seem to have formed within the clastic sediments. Probably the brines were never sufficiently concentrated to allow borate precipitation until the lakes partially or wholly dried up. Brines were evidently rich in Ca^{++} and in both northern and southern basins and Ca borates are present at every horizon throughout the sequence. Co-precipitation of the Ca-Na borate, ulexite, and later diagenetic formation of the Sr borate, tunellite, occurs only rarely in the northern basin and not at all in the southern area. Experimental evidence from

the system $\text{CaO-Na}_2\text{O-SrO-B}_2\text{O}_3\text{-H}_2\text{O}$ is not available but field and textural evidence clearly indicates the sequence Ca borate \rightarrow Ca-Na borate \rightarrow Sr borate. Arsenic bearing borates and Sr borates do not occur together in the Emet deposits although arsenic sulphides do occur at the same horizon as Sr borates and sulphate.

Field and petrological evidence already discussed (Chapters III, V and VI) demonstrates that Ca borates, ulexite, and teruggite crystallized within the sediments and did not precipitate from open water.

The composition of the brines would be changed with each influx of water-borne sediment; with the addition of material from thermal springs and due to crystallisation. Because of these variables no unambiguous sequence of crystallisation emerges either as "gross phase zoning" or "oscillatory zoning" as described by Inan, Dunham and Essen (1973) from the Kirka deposit. Some general tendencies have been established but owing to the rarity of borate minerals other than colemanite it is not known if these trends are universally valid.

Both lateral and vertical changes from calcite-marls to colemanite bearing clays have been observed and a gross zoning both laterally and vertically from calcite to colemanite and back to calcite seems to be general in both areas. In the southern area the sporadic occurrence of gypsum suggests that where sulphates are present the sequence is calcite-gypsum-colemanite.

In the northern basin the early colemanite phase and ulexite crystallise before tunellite, implying that Sr borates will not crystallise from solution until Ca borates and Na-Ca borates have

been precipitated. The retention of Sr^{++} in the interstratal brines may account for both the diagenetic replacement of colemanite by a veatchite mineral in the northern basin and the late post-depositional crystallisation of celestite (SrSO_4) in both the northern and southern basins. Sr borates and arsenic bearing borates have not been found together in the same bed. It is not known whether this is a genuine incompatibility or merely a reflection of the scarcity of teruggite and cahnite.

The history of the Emet deposits may therefore be tentatively summarised as follows:

a) Establishment of playa lakes in seismically active areas fed by thermal springs and surface streams at the end of Eocene or early Oligocene.

b) In these lakes clay and volcanic ash were deposited and Ca borate nodules developed within the unconsolidated sediments during periods of evaporation. In the northern basin ulexite was also periodically formed and the arsenic bearing borate (teruggite) was precipitated occasionally in the southern basin. Small amounts of sulphur, celestite and realgar were also formed within the sediments penecontemporaneously with the borates.

c) After burial the Ca borate nodules, most probably colemanite, continued to grow. Inyoite, if formed, dehydrated to colemanite and colemanite was precipitated in vughs together with realgar and more rarely celestine and cahnite.

d) Chemical reaction between Mg-rich clays and colemanite leading to the formation of hydroboracite.

e) Reaction between Sr-rich interstratal brines and colemanite leading to its partial replacement by a veatchite mineral.

f) Solution and reprecipitation of colemanite in veins and around colemanite nodules, as fibrous and thin layers.

g) Uplift and erosion leading to the weathering of colemanite and its replacement by calcite in surface outcrops and adjacent to faults. Alteration of realgar to orpiment on exposure to air.

In many parts of the deposits the colemanite appears to be unaltered apart from recrystallisation, so that the post-depositional changes d and e above apply only to restricted parts of the deposits. Realgar, celestite and sulphur appear to have been deposited both during and after the formation of the Ca borates.

CHAPTER IX

COMPARISON OF THE FORMATION OF CALCIUM BORATES OF EMET WITH THE KIRKA DEPOSIT AND OTHERS IN TURKEY

1. Introduction:

In this thesis, an attempt has been made to explain some problems concerning the geology (Chapter V), mineralogy (Chapter VI), geochemistry (Chapter VII), origin, diagenesis and depositional history (Chapter VIII) of the Emet borate deposits. The Emet borate deposits are here compared and contrasted with other Turkish borates with particular reference to the Kirka deposit. For a general discussion of known Turkish borates see pages 23-26 and location map (see Fig. 1).

The unique character of the borate deposits in Turkey indicates that the conditions of formation of these deposits are different from those that lead to the formation of the more

typical non-marine evaporite deposits. Colemanite, a very common calcium borate, is the dominant mineral in all the deposits apart from Kirka. The detailed mineralogy of the Turkish borate deposits varies considerably and they are classified as Ca and Na borates (see page 25). Mineralogical studies have shown that the Emet borate deposits are far more complex than was first thought (see Tables 3, 4 and 14; Helvacı and Firman, 1976). Tables 3 and 4 show that each deposit has its characteristic assemblage of minerals. Several non-borate minerals associated with the borates at Emet are also recorded (see Table 15). These are totally absent in the other Turkish borate deposits.

The most important difference between the Emet deposits and the others is the large contribution of thermal springs to the Emet borate-rich lakes, which at this time are supposed to have formed an interconnecting chain. In addition the Emet area is characterised today by many thermal springs and by analogy with modern South American borate deposits (Muessig, 1966) it seems probable that hot springs were a characteristic feature when borate deposits were forming. Active thermal springs are still widespread in the Emet Valley and these still carry small amounts of boron, arsenic and sulphur (see Chapter III). The chemical analyses of the spring waters from the Emet district were given in Table 6.

Major chemical variation between the Emet, Bigadiç and Kirka deposits is shown on a $\text{CaO-B}_2\text{O}_3\text{-Na}_2\text{O}$ ternary diagram (Fig. 33) in which these components represent the bulk of the borate minerals found in the deposits. The Emet and Bigadiç deposits are Ca-rich whereas the Kirka deposit is Na-rich. Na borates do not occur in the Emet and other Turkish deposits and even Ca-Na borates occur

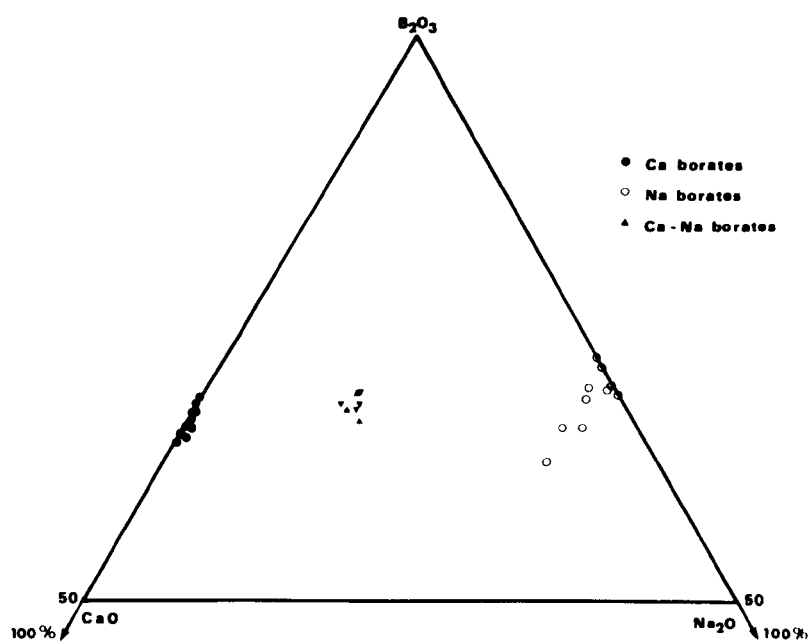


Fig. 33. The chemical composition, in terms of wt. % B₂O₃, CaO and Na₂O of samples from the Emet, Kirka and Bigadiç borate deposits.

only in very small amounts when compared with the Kirka deposit.

The trace element contents of the Emet deposits (see Tables 5, 13, 20, 21, 22 and 23) differ from the Kirka deposit (Inan, Ph.D. thesis, 1973) mainly in S, As and Sr. This is also reflected by the sulphide, sulphate, Ca-As and Sr borate content of the Emet deposits. Realgar, orpiment and gypsum do not occur in the Kirka deposit whereas these minerals are abundant throughout the Emet deposits (see Chapter VI). New occurrences of veatchite, teruggite and cahnite are also restricted to the Emet deposits (see Helvaci and Firman, 1976; also Tables 4 and 14; Chapter VI).

In conclusion, the mineralogy (Chapter VI) and geochemistry (Chapter VII) of the Emet borate deposits are unique amongst Turkish borate deposits, because of unusual occurrences of Ca-As and Sr borates and the high content of S, As and Sr as trace elements.

The Emet borate deposits differ in detail from other Turkish Ca borate and Kirka deposits but have the following features in common:-

a) They are restricted to Tertiary lacustrine sediments deposited in a non-marine environment under arid or semi-arid climatic conditions.

b) They were apparently deposited in sedimentary intermontane basins of limited extent in regions where fresh-water limestone deposition was widespread both before and after borate formation.

c) In addition to borates these basins were the repositories for fine grained clastic sediments, i.e. conglomerate, sandstone, clay, marl and tuff, much of which are of volcanic origin.

d) Although the lithology of the borate deposits shows some differences from one to another, sediments in the borate lakes often show clear evidence of cyclicity.

e) All Turkish borate deposits appear to be associated with volcanic activity and they are classified in deposits related to volcanic activity (Aristarain and Hurlbut, 1972).

f) Borate occurrences are associated with volcanic rocks. Both intrusive and extrusive volcanic rocks are common in the neighbourhood of the borate basins.

g) Borates in the Turkish deposits are not associated with more typical evaporite minerals, such as halite and trona.

h) At Emet, as elsewhere in Turkey, the palaeogeographic scenario seems to have consisted of shallow lakes fed partly by hot springs and partly by streams which carried sediments from the surrounding volcanic, limestone and basement terrain. The rocks which may have been exposed in the catchment areas appear to be in restricted and closed basins.

2. Kernite and other borate minerals from the Kirka deposit:

After the outstanding discovery of the Kirka borate deposit (Dunn, 1966; Arda, 1968; Inan 1972) many scientists have been attracted to Kirka, because of the uniqueness of the deposit and the large number of borate minerals occurring there, several of them new occurrences.

Although a number of papers appeared shortly after the sodium borate deposit was discovered, the first major paper to be published was by Inan, et. al., (1973) on the mineralogy and chemistry of the borates. The mineralogy and geochemistry of the Kirka borate deposit was also studied by Inan, 1973 (unpublished Ph.D. thesis).

During the present study, this deposit was visited several times and borate samples were collected and analysed (Table 24) for comparison with those borates occurring in the Emet deposits. Kernite has been found during the present investigation, in addition to the minerals previously recorded (Inan, 1973). Table 4 (see page 26) also lists the borate minerals so far recorded in this deposit.

Kernite ($\text{Na}_2[\text{B}_4\text{O}_6(\text{OH})_2] \cdot 3\text{H}_2\text{O}$)

Kernite has a restricted distribution and is found only at one locality in the underground workings of the Sarikaya (Kirka) mine. New kernite crystals may be found when the underground workings advance. It is developed in the deeper part of the sodium borate body at Kirka.

It occurs as colourless, transparent but sometimes white elongated needle-shaped, or group of needle-shaped, crystals which are surrounded by a zone of borax. Individual crystals vary in their length, which is up to 10cm. Kernite alters by dehydration to white tincalconite which occurs as fine-grained coatings on kernite crystals that have been exposed to the atmosphere (Plate 110). Partial chemical analyses of the Kirka kernite have been performed and are enclosed (Table 25).

Although kernite crystals have not been observed intergrowing with borax crystals, there is no evidence which clarifies the origin of kernite in the deposit. Hence it is unknown whether kernite was formed directly from solution under high temperature and pressure during the diagenesis, or was derived from borax by dehydration. In any case the restricted occurrence of kernite within the deposit indicates that the conditions (of either deposition or diagenesis) varied on a very localised basis.

Table 24. Chemical analyses of some borate minerals from the Kirka deposit.

<u>Number</u>	<u>176</u>	<u>177</u>	<u>178</u>	<u>179</u>	<u>180</u>
B ₂ O ₃	45.945	43.392	40.573	41.223	54.878
CaO	0.112	13.524	3.598	13.356	0.157
MgO	0.409	0.793	2.902	0.837	0.528
Na ₂ O	21.304	7.980	18.071	8.274	0.136
SrO	0.004	1.688	0.238	0.214	27.455
As ₂ O ₅	0.001	0.001	0.009	0.001	0.017
SiO ₂	0.064	0.556	2.093	2.414	0.128
TiO ₂	0.000	0.000	0.000	0.018	0.000
K ₂ O	0.000	0.000	0.049	0.649	0.000
H ₂ O+	31.322	32.169	30.487	31.970	18.464
CO ₂					
SO ₃	0.544	0.345	0.497	0.577	0.060
Total	99.705	100.448	98.517	99.533	101.823
Al	49*	381	232	2357	138
Fe	438	730	624	1641	389
Mn	0*	7*	19	64	1*
P	2*	5*	11*	5*	8*
Cl	282	151*	270	253	134*
Cr	7*	7*	58	4*	5*
Ni	2*	4*	0*	7*	2*
Cu	0*	18	0*	0*	477
Zn	4*	4*	1*	5*	18
Br	0*	1*	0*	4*	3*
Sn	10	24	14	46	2
Ba	130*	86*	129*	87*	1070
Ce	0*	47*	2*	73*	108*
Pb	2*	0*	1*	3*	0*
Th	0*	1	0*	0*	0*
U	0*	3*	0*	0*	0*

* Indicates values below the detection limit

176 - Tincalconite

179 - Ulexite

177 - Ulexite

180 - Tunellite

178 - Borax and tincalconite mixture

Table 25. Partial chemical analyses of kernite samples from Kirka.

NUMBER	I	II
B_2O_3	50.092	50.092
CaO	0.000	0.000
MgO	0.009	0.002
Na_2O	20.100	20.680
SrO	0.000	0.000
H_2O	25.720	24.780
TOTAL	95.921	95.554

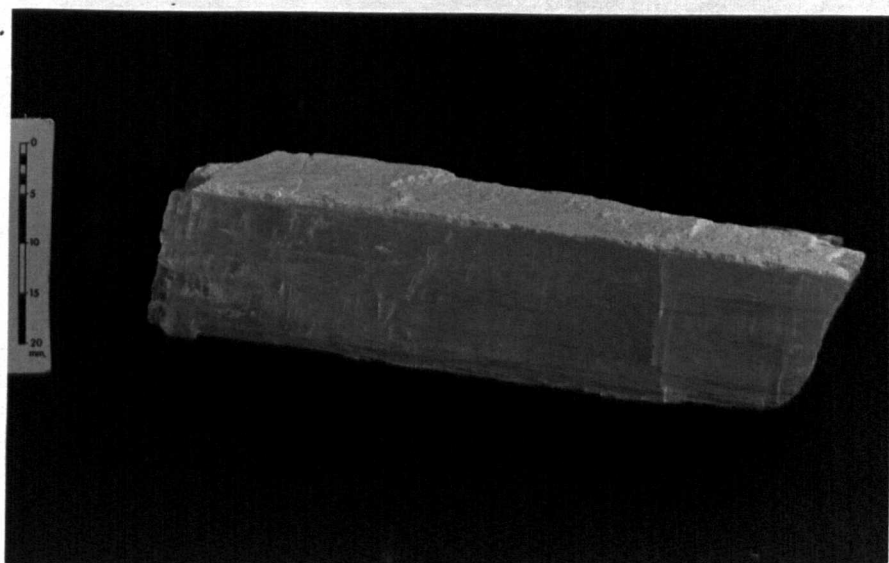


Plate 110. Kernite crystals with tincalconite occurring as a thin fine-grained coat on upper surface.

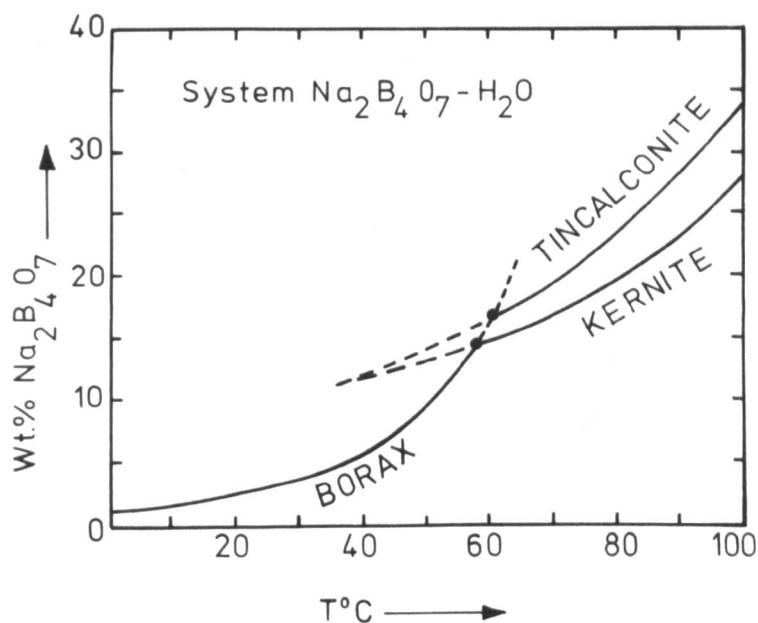


Fig. 34. Solubility-temperature relations in the system $\text{Na}_2\text{B}_4\text{O}_7 - \text{H}_2\text{O}$ (simplified after Bowser, 1964).

Previously the kernite was thought to be absent from Kirka and hence the temperature of formation of this deposit was thought to be below 60°C (see Inan, 1973; and Fig. 34). However since kernite has now been found, then at some time during the history of the deposit the temperature must have exceeded 60°C (either during deposition or in diagenesis).

3. Inyoite mineral from Bigadiç deposits:

Inyoite ($\text{Ca}[\text{B}_3\text{O}_3(\text{OH})_5] \cdot 4\text{H}_2\text{O}$) samples were collected from the Bigadiç deposits and one sample was analysed for comparison with the chemical analyses of colemanite and meyerhofferite from the Emet deposits.

Inyoite occurs locally at some of the mines (B. Günevi, K. Günevi, Acep and Salmanli localities) in the Bigadiç deposits (see also Özpeker, 1969). It coexists with meyerhofferite, colemanite, ulexite and hydroboracite in the borate zone which consists mainly of clay, marl, limestone, tuff and sandstone.

Inyoite occurs as intergrown crystal masses and discrete tabular crystals and crystal groups, colourless to white (Plate 111). A few of the crystals are 2.5cm or larger, but most are microscopic in scale and altered. Some of the inyoite in the main mass had altered to meyerhofferite and/or colemanite. Sometimes it occurs as clear, coarse-grained, euhedral aggregates. A partial analysis of inyoite is given on Table 26.



Plate 111. Large inyoite aggregate showing tabular crystals.

Table 26. Partial chemical analysis of inyoite from Bigadiç.

NUMBER	I
B_2O_3	37.100
CaO	20.870
MgO	0.050
Na_2O	0.009
SrO	0.011
H_2O	40.250
TOTAL	98.290

CHAPTER X

ECONOMIC ASPECTS AND FUTURE PROSPECTS

1. Economic aspects:

Turkey is currently the second largest producer of boron minerals and has the world's largest reserves. The level of output is rapidly rising towards that of the USA and has been continuously expanded to meet increasing demands of world consumers. Production was more than doubled in 1974, to more than one million tonnes (1 075 533 tonnes); and further increases, particularly of borax from Kirka, are likely to lead to Turkey dominating the world markets. Already Turkey is the major world producer of colemanite, much of which comes from the Emet valley (see Table 1). Proved and probable reserves of all boron minerals are vast in relation to output and are measured in hundreds of years supply, even by the most conservative estimates.

Although quantitatively known reserves in the Emet district are more than adequate, their quality is less assured. Arsenic sulphides (realgar and orpiment) are ubiquitous in the Emet borate deposits and the arsenic-bearing borates, teruggite and cahnite, occur sporadically (see Chapter VI; Tables 14 and 15; Figs 15 and 16). Washing and gravity separation removes most of the clays which contain the bulk of the sulphides and sulphur. The bright colours of realgar and orpiment contrast with colemanite to make it comparatively easy to upgrade the colemanite by hand-picking. Teruggite and cahnite are, however, similar in colour to colemanite (see Chapter VI) and cannot be easily identified on a moving belt. Their distribution in the unworked parts of the borate basin is unknown but should they occur in substantial amounts, separation problems would be severe, if high grade colemanite with low arsenic and sulphur should be required. Thus the discovery of teruggite and cahnite has commercial significance because arsenic separation techniques may need to be modified to take account of this additional source of arsenic contamination.

No adequate mineralogical and geochemical studies were made on cores from the exploratory boreholes, so no regional pattern of the distribution of arsenic and sulphur can be discerned and thus it is impossible to define high and low arsenic areas (if they exist) with any degree of confidence. Should further boreholes be sunk, it would seem desirable that as much mineralogical and geochemical information as possible should be gleaned from them to plan future workings, so that the high-grade and the purest deposits may either be reserved to meet special demands, or blended with arsenic-rich material to produce acceptable grades.

The percentage of B_2O_3 , as shown in Table 1 on page 7, is adequately high in all areas, but it varies with the mineralogy (see Chapter VI), and, in particular, is lowest adjacent to faults and near surface outcrops, where colemanite is partially or wholly altered to calcite (see Chapters V, VI and VIII; Plates 64, 65, 66, 103 and 104). Detailed mapping of the Emet deposits (see Figs. 11, 13 and 14) has shown that the area is far more faulted than was previously thought; hence, lower grades of B_2O_3 in narrow fault zones may be encountered more frequently.

Notwithstanding the mineralogical complexities enumerated in this study, however, the Emet borates are high-grade colemanite deposits, and should supply a substantial quantity of the world's needs for many years.

2. Future prospects:

The mineralogical and geochemical studies of the Emet borate deposits have commercial implications connected with the planning of the present workings; ore processing; future developments and exploration.

As shown on Figs. 20 and 21, sufficient boreholes were sunk to prove the viability of the deposits; but not to adequately define the size and shape of the borate basins (see also Figs. 18 and 19). Colemanite and calcite were recorded from the boreholes but no detailed mineralogical study was considered necessary. Since the cores are not available for further study, the present knowledge of the distribution of minerals is based solely on natural and artificial exposures. The present understanding of the geology and mineralogy suggests that in several respects the borehole data may be misleading.

Early tests on some of the borehole cores from the Hisarcik and Espey localities underestimated the thickness of the borate zone. More recent tests on the surviving cores; numbered 15, 20 and 30 in the Espey locality (see Figs. 15 and 21); by the present author, show this thickness to be much greater than previously estimated; thus the actual borate reserves may be considerably greater than indicated in Table 1 (see page 7).

From detailed mapping of the area coupled with information from the surrounding geology, as is mentioned previously (see Chapters III and V), it is suggested that the area is more faulted than has hitherto been thought. Because of the throw of these faults, the boreholes sunk on both sides of the faults have not cut through the borate zone. These faults occur in the Espey and Hisarcik areas, particularly in the Kapikaya locality (Hisarcik) (see Figs. 11, 13 and 14). Therefore, estimated reserves were considerably less than actual reserves.

Some small faults with brecciated colemanite-clay gouge, together with land-slides in the quarries of the Hisarcik opencast mine, cause problems during mining. Unfolded beds above and below the borate zone are very gently dipping, varying between horizontal and 20° towards the northeast (see Fig. 14). Small faults, the effects of underground and surface waters, thick interbedded clays, the weight of waste dumps and the recent Gediz earthquake (see Fig. 2 and Plate 28) caused these land-slides in the opencast mine workings (Plate 112; see also Plate 27). Because of these, the stripping and mining operations have not been as successful as had been hoped.

Also it is necessary to take records from the quarries during the whole mining operation, because there are quite noticeable



Plate 112. Land-slides caused by the weight of the waste dumps near the Hisarcik opencast mine.

differences between the actual position of the strata and that shown by the data provided from the borehole logs. These records may eventually lead to a correct interpretation of the geological structure of the quarries and of the deposition of the beds.

In some parts of the Hisarcik opencast mine (between the Sarıkaya and Kapıkaya localities) waste materials have also been stored; on top of the extension of the colemanite beds (see Plate 27; Figs. 11 and 14). These waste dumps will in the future increase the cost of production since they will have to be removed before the overburden as the mining progresses to the northeast.

The detailed mapping and geology also suggest that other colemanite beds, which are supposed to correlate with the lower beds of the Killik mine, may be present below the height of 850 metres in the Espey mine. Therefore, it seems desirable that further boreholes ought to be sunk 30 or 50 metres downwards from the 850 metres level (see Figs. 13, 17, 19 and 21).

The colemanite of the Emet Valley is so abundant that there is very little incentive to prospect for further reserves. That other borate deposits could be found is suggested by the discovery by the present author of typical colemanite nodules, now weathered to calcite in surface outcrops at Çerte (see Fig. 12), 20 kilometres east of Emet; an area where no borate deposits have previously been found.

CHAPTER XI

SUMMARY AND CONCLUSIONS

The Emet deposits are located in the middle of the known borate deposits of Western Anatolia, between the Eskişehir and Bigadiç districts (see Fig. 1). They were deposited in Tertiary lacustrine sediments during volcanic activity, which commenced in the early Tertiary and continued at least until the beginning of the Quaternary. Borate minerals were formed as chemical sediments in separate or possibly inter-connected lake basins under arid or semi-arid climatic conditions.

Emet borates were considered by previous authors to be of Neogene age. Palaeontological evidence from the Emet area acquired during the present investigation suggests that the deposits are in fact older than was previously thought. Some ostracods from the Upper Limestone that overlies the borates indicate brackish-fresh water deposits of Middle Oligocene age.

The sediments consist of the following predominantly lacustrine sequence; from top to bottom: upper limestone with clay, marl and chert layers; clay, tuff and marl with borate deposits; red formation - conglomerate, sandstone, clay, marl and limestone with coal and gypsum bands; and thin bedded lower limestone with lenses of marl and tuff. This sequence rests directly on a Palaeozoic(?) metamorphic complex containing marble, mica schist, calc-schist and chlorite schist, with angular unconformity. Sediments in the borate lakes show clear evidence of sedimentary cycles. Much of the sediment in the borate basins seems to have been derived from a volcanic terrain.

Volcanic rocks, which are closely related to the Middle Oligocene lacustrine sediments, are mainly spherulitic rhyolite, dacite, pyroxene andesite and olivine-augite basalt. Volcanic tuffs interbedded with the lacustrine sediments occur in the borate basins also.

The Middle Oligocene sedimentary formations strike roughly parallel to the Emet River, their dip ranging from nearly horizontal to over 20° , and they are dislocated by NW-SE trending gravity faults, many of which are still active. NE-SW trending gravity faults occurred after the deposition of the borates, but these are not active at present. The predominant faults are normal with dips ranging from 30° to the vertical.

The Emet lake beds are preserved in an elongate structural basin which trends roughly north-south. The thickness of the Tertiary sediments varies from one place to another, probably because of deposition in a chain of inter-connected lakes. The maximum thickness exceeds 750m. The borate zone varies in thicknesses between 0-100 metres and reaches its maximum thickness at

the Espey and Killik localities. Beyond the commercial areas, the borate zone is very thin or absent and it shows lateral and vertical facies changes throughout.

Detailed mapping (see Figs. 13 and 14) has shown that the Middle Oligocene sedimentary formations, including the borate zone, are far more faulted than was previously thought.

The depositional basin is aligned north-south, and outcrops on the east side of the Koca Çay (Emet River) from Dereköy north almost to Killik.

Thermal springs, which at present deposit travertine and sulphur, are active west of the Emet River. New springs were generated by movement of northwest-southeast-trending faults during the Gediz earthquake in 1970. Although these springs do not contain appreciable amounts of boron and arsenic, it seems likely that similar springs were important sources of B, As, S and probably Ca and Sr when the borates formed.

Mineralogical studies have shown that the borate deposits in the Emet district are far more complex than was first thought. Meyerhofferite, hydroboracite, a form of veatchite, tunellite and cahnite have been found during the present investigation, in addition to the minerals previously recorded (see Table 2). Also ulexite was found in the Espey and Killik areas, but it has not been observed in the Göktepe and Hisarcik localities where it was previously recorded by Özpeker. Table 14 lists the borate minerals so far recorded in these deposits.

A number of non-borate minerals associated with the borates occur throughout the deposits (see Table 15). Realgar, orpiment and celestite are the common ones, but native sulphur, fibrous gypsum, selenite, calcite and quartz also occur. Calcite also

occurs frequently in surface outcrops and adjacent to faults as a result of recent weathering. Montmorillonite and illite are the only clay mineral groups identified, and the former is the dominant mineral in all the samples. The occurrence of the clay minerals, sulphide and sulphate minerals in the deposits is ubiquitous.

Colemanite occurs in many different forms ranging from minute stellate clusters of crystals in clay to ovoid nodules up to 0.5 metre in diameter. The individual crystals which make up the nodules are colourless, grey, pink and dark blue. Other borate minerals occur sporadically and are restricted to certain parts of the deposits. Cahnite has not previously been identified from borate deposits.

The principal borate mineral assemblages observed are:- colemanite-meyerhofferite; colemanite-ullexite-hydroboracite; colemanite-hydroboracite; colemanite-veatchite; colemanite-ullexite-tunellite; colemanite-teruggite-cahnite; colemanite-cahnite; ullexite-hydroboracite; ullexite-tunellite and teruggite-cahnite (see Figs. 22 and 23). Colemanite-hydroboracite; colemanite-veatchite; colemanite-cahnite and teruggite-cahnite assemblages are believed to be developed during the secondary processes. As shown in Figs. 22 and 23, assemblages of minerals in the borate zone differ at different levels in the sequence. There is also an overall difference between the northern area (Espey-Killik) and the southern area (Hisarcik) sufficient to suggest that they were deposited in separate (but possibly interconnected) basins.

Brines in the Emet borate deposits (palaeolakes) were evidently rich in Ca^{++} and B^{+++} in both northern and southern basins and the Ca borate mineral (colemanite) is present at

at every horizon throughout the sequence. Hydroboracite and cahnite occur sporadically throughout the deposits. Present observations suggest that meyerhofferite, ulexite, tunellite and the veatchite mineral are restricted to the north and teruggite to the southern basin. Chemically this implies that conditions were more favourable from time to time for the formation of Na-Ca borates and Sr borates in the thicker northern deposits than in the south (see Figs. 22 and 23).

Petrography of the basement metamorphic complex, volcanic rocks, Middle Oligocene sediments and borates are described in detail and they were given in relevant chapters. (see Chapters III, IV and VI).

The chemical analyses of the volcanic rocks from the Emet district fall into high-Al basalt, high-K andesite, dacite and rhyolite volcanic rock groups. The Harker variation and KCN diagrams (see Figs. 9 and 10) of the volcanic rocks associated with the Emet borate deposits indicate that these volcanic rocks are very rich in potash and soda in comparison to Cascade volcanic province.

Most of the clay minerals in the Emet deposits seem to be formed by the breakdown or alteration of volcanic tuff. A complete gradation (transition) exists between tuff and clay in the Emet borate zone sediments and is reflected in their geochemistry. These two different rock types vary due to the different stages of alteration. Clays on average have less SiO_2 and K_2O and significantly more Fe_2O_3 , MgO , NO_2O and H_2O than the average tuff at Emet. Both tuffs and clays are characterised by high $\text{Fe}_2\text{O}_3:\text{FeO}$ ratios indicating strongly oxidizing conditions of sedimentation. Unusually high concentrations of B, As, Sr and S

suggest the formation of suites of evaporite and hydrothermal minerals within the sediments similar to those found in the interbedded borate layers. Low Cl and negligible Br tend to confirm the non-marine character of the sediments. Like the volcanic rocks of the surrounding hinterland the clays and tuffs interbedded with the borates are rich in K^+ relative to Na^+ .

CaO and CO_2 make up the bulk of the analysed limestone samples (90% and above). The analysed elements are restricted either to the carbonate fraction or the detrital fraction. Si occurs in two different forms in the limestone such as in the detrital fraction (clay) and in the chemically precipitated chert. The detrital clay fraction of limestone includes the major elements Si, Al, Fe, Mg and K. Most of the trace elements in the limestone are in the clay and heavy minerals fraction. Dolomite does not occur in the limestone, although it has a fairly high concentration of magnesium (1.01%). Like the tuffs and clays the upper limestone is also characterized by a relatively high concentration of B, As, Sr and high $Fe_2O_3:FeO$ ratio which indicates strongly oxidising conditions of sedimentation and arid to semi-arid environments with a very low rate of leaching.

The Emet borate deposits are characterized by high Ca borate (colemanite), very low Na and relatively high Mg, Sr, As and S concentrations compared with the other borate deposits. Also the chemical analyses of the colemanite and other borate samples from the southern and northern areas indicate that there are several differences between the two areas as well as different mineral assemblages. Those samples from the southern area have on average more Mg, Sr and As, whereas those from the northern area contain more H_2O and K.

B_2O_3 , CaO, H_2O , MgO, SrO, SiO_2 and Al_2O_3 make up the bulk of the analysed samples (95% and above). B_2O_3 , CaO and H_2O are mainly restricted to the borate minerals whereas Si, Al, Ti, Mg, K, Mn and P are represented in the clay fractions of the samples. The elements Mg, Na, Sr, As and S are represented both in the evaporite and in the clay fractions. Some of these elements are transferred to the borate structure by base exchange during the diagenesis of the deposits. Most of the trace elements in the borate samples are in the clay and heavy minerals fractions, including mainly, Cl, Cr, Ni, Cu, Zn, Sn, Ce, Pb and Th. Like the sediments, the borates are also characterized by a relatively high $Fe_2O_3:FeO$ ratio, suggesting strongly oxidising conditions of precipitation and arid to semi-arid environments of evaporation.

The association of iron oxide, clay, sulphate and sulphide minerals changes the colour of colemanite and associated borates, especially high concentrations of celestite, realgar, orpiment and native sulphur. The blue colour of colemanite and other borates is a result of celestite; the orange-yellow colour is due to realgar, orpiment and native sulphur.

The geochemical association of boron, arsenic and sulphur suggests a common origin for all three elements at Emet. The geochemical investigations suggest that the most likely sources of B, As and S were from the Tertiary volcanic rocks. Weathering products may have been transported into the borate basins by streams, or volcanic ash may have been deposited directly into the borate basins. Thermal springs may also have leached B, As and S from the volcanic rocks.

Surface streams may have carried some Na^+ , Ca^{++} , Sr^{++} , Mg^{++} and other elements in solution into the basins as the result

of weathering of rocks exposed in the catchment area but the major source of Ca^{++} , Mg^{++} and Sr^{++} , by analogy with present day hydrology, is considered to be due to leaching of underlying basement rocks and Tertiary limestone by thermal springs.

The early formed colemanite was deposited penecontemporaneously with the unconsolidated sediments. It is probable that it was formed within the clays and tuffs below the sediment/water interface and probably continued to grow as the sediments were compacted. During the deposition, meyerhofferite, ulexite and teruggite nodules like colemanite, appear to have developed penecontemporaneously within and not on the sediments. Their sporadic occurrence indicates that the precipitation of these minerals was limited to certain parts of the deposits, possibly due to localised thermal springs. Realgar and small amounts of celestite were also precipitated with the sediments.

After the burial of the deposits by younger sediments, boron and calcium-bearing solutions circulating through the early borates and sediments were responsible for precipitation of later generations of colemanite such as vugh fillings (see Plate 42), fibrous (see Plates 39 and 40) and thin layers (see Plate 49) of colemanite. During the diagenesis of the deposits common alteration products of colemanite are hydroboracite and calcite, and rarely a form of veatchite and cahnite. All the evidence indicates that hydroboracite, veatchite and cahnite often replaced colemanite and it is tentatively suggested that these minerals formed during diagenesis as a result of the addition of Mg^{++} , Sr^{++} and As^{5+} and the loss of Ca^{++} . In addition to these diagenetic changes there is field and mineralogical evidence of at least three generations of colemanite (see Plate 109) and separate

post-depositional crystallization of tunellite, cahnite, celestite, native sulphur, gypsum, realgar and probably orpiment. On weathering, colemanite is readily replaced by calcite and realgar by orpiment. Interbedded tuffs are often altered to montmorillonite-bearing clays. This is, however, incomplete and the transition between tuffs and montmorillonitic clay has been observed in progress (see Chapter IV).

Both lateral and vertical changes from calcite-marls to colemanite-bearing clays have been observed and a gross zoning, both laterally and vertically from calcite to colemanite and back to calcite, seems to be general in both areas. In the southern area the sporadic occurrence of gypsum suggests that where sulphates are present the sequence is calcite-gypsum-colemanite. In the northern basin the early colemanite phase and ulexite crystallize before tunellite, implying that Sr borates will not crystallize from solution until Ca borates and Na-Ca borates have been precipitated. Experimental evidence from the $\text{CaO-Na}_2\text{O-SrO-B}_2\text{O}_3\text{-H}_2\text{O}$ system is not available but field and textural evidence clearly indicates the sequence Ca borate- Ca-Na borate - Sr borate. Sr borates and arsenic-bearing borates do not occur together in the same bed. Realgar, celestite and sulphur appear to have been deposited both during and after the formation of the Ca borates.

Major chemical variation between the Emet, Bigadiç and Kirka deposits is shown on a $\text{CaO-B}_2\text{O}_3\text{-Na}_2\text{O}$ ternary diagram (see Fig. 33) in which these components represent the bulk of the borate minerals found in the deposits. The Kirka deposit is Na-rich whereas the others, including Emet, are Ca-rich. Na borates do not occur and Ca-Na borates occur only in very small amounts in

the Emet deposits. In conclusion, the mineralogy and geochemistry of the Emet borate deposits are unique amongst the Turkish borate deposits, because of unusual occurrences of Ca-As and Sr borates and the high content of S, As and Sr in trace element form.

Kernite, a sodium borate, has been found during the present investigation, in addition to the minerals previously recorded from the Kirka deposit (Inan, 1973). Previously the kernite mineral was thought to be absent from Kirka and hence the temperature of formation of this deposit was thought to be below 60°C (Inan, 1973). However since kernite has now been found, then at some time during the history of the deposit the temperature must have exceeded 60°C (either during deposition or in diagenesis), at least, on a very localised basis.

Turkey is the major world producer of colemanite, much of which comes from the Emet Valley (see Table 1). Although quantitatively known reserves in the Emet district are more than adequate, their quality is less assured. Notwithstanding the mineralogical complexities enumerated in this study, however, the Emet borates are high-grade colemanite deposits, and should supply a substantial quantity of the world's needs for many years.

Detailed mineralogical and geochemical studies should be made on cores from the further boreholes in certain parts of the deposits. These would help to establish the regional pattern of the distribution of arsenic and sulphur. Thus it would be possible to define high and low arsenic areas (if they exist) with a degree of confidence.

The colemanite of the Emet Valley is so abundant that there is very little incentive to prospect for further reserves; but it is suggested that further prospecting and drilling should take

place between Emet and Çerte to establish the eastward extent of these deposits (see Fig. 12).

The Emet borate zones are characterized by relatively high arsenic and strontium contents and the effect of these elements on the crystallisation of the Ca borates is unknown. Similarly the effects of low partial pressures of H_2O have yet to be investigated. Experimental studies would be necessary on the system $CaO-Na_2O-SrO-B_2O_3-H_2O$.

It seems desirable that S^{32}/S^{34} and O^{16}/O^{18} isotope analyses of borate and non-borate minerals from Emet should be undertaken. These analyses may provide data on temperature of formation of borate minerals, origin of water involved in mineral crystallisation and the origin of colemanite with relation to other borate minerals.

APPENDIX A

SAMPLE COLLECTION AND PREPARATION

1. Collection:

11 volcanic rocks; 84 clay, tuff, marl and limestone; 59 colemanite; 11 colemanite with clay fractions; 31 other borate minerals and 15 non-borate mineral samples were collected from the top of the red formation, mainly from the borate zone, and from the upper limestone from several vertical sections along the borate zone in the Emet borate deposits (see Figs. 12, 13 and 14).

Most of the samples were obtained from the open pit in the Hisarcik locality (see Fig. 16), the underground workings and borehole cores of Espey and Killik mines (see Figs 15 and 17) and from natural exposures throughout the deposits, including the Göktepe and Dereköy localities (see Figs. 6 and 12). Additional samples were also collected from the Kirka and Bigadiç deposits (see Fig. 1).

Hand specimens of varying sizes and one relatively large specimen of pure massive colemanite, for 'spiking' and calibration, were collected and photographed to illustrate the mode of occurrence and relevant structures of borates (see Plate 33 and Chapter VI).

Details of the sample localities of all the rocks and minerals analysed during this study are given in Table 27.

2. Preparation:

All hand-picked rock specimens, commercial borate samples and the standard colemanite (1013) were broken up by hand or by rock splitter and hammer into smaller pieces, some of which were allocated for thin sectioning, mineralogical and textural studies. The rest were further broken up to small chips. Excessive detrital material and clay fraction have been avoided from borate samples. Sample chips were carefully scraped off to remove iron oxide impurities picked up from the hammer.

The chips were then crushed by a cast iron jaw-crusher to a size of about 1mm and stored in polythene bags immediately. About 100-200 grams of each were further crushed by an agate tema mill to a fine powder passing through 250 mesh nylon. Finally this fine crush was thoroughly mixed to prevent mineral segregation before storing in plastic containers.

Table 27: Sample numbers and localities.

<u>Sample No.</u>	<u>Locality</u>
1 - 13	Dereköy
14 - 28	Akdere
29 - 46	Kapıkaya
47 - 68	Sarıkaya
69 - 73	Hisarcık*
74 - 84	Göktepe
85 - 100	Borehole 15, Espey
101 - 109	Borehole 20, Espey
110 - 116	Borehole 30, Espey
117 - 137	Espey*
138 - 152	Kıllık*
153 - 174	Whole area*
175	Çerte
176 - 180	Kırka*
181 - 191	Emet (volcanic rocks)*
192 - 214	Emet*

* Random sampling: This means the samples were collected over the whole deposits and not systematically.

APPENDIX B

MAJOR ELEMENT ANALYSIS BY WET CHEMICAL METHODS

Atomic absorption spectrophotometry and wet chemical analyses were carried out on the elements B, Ca, Mg, Na, Sr, FeO, H₂O and CO₂. The Mg, Na and Sr analyses were undertaken for only a small number of samples. FeO and CO₂ analyses were carried out on rock and selected mineral samples.

B₂O₃ was determined by atomic absorption spectrophotometry on 0.5 grams samples dissolved in 25 ml warm HCl. Excessive heating was avoided to prevent any boron loss by volatilization and the containers were covered with watch glasses during heating. After filtering and dilution these were stored in polythene bottles. The boric acid standard solution was used for calibration. Readings ppm on these solutions were obtained using an EEL 240 Atomic Absorption Spectrophotometer. Results were corrected to account for dilution and converted from %B to %B₂O₃ (multiply by 3.1906). The detection limit of this method is 50 ppm B.

Operating conditions used:-

Wavelength	249.7	Fuel Acetylene	3.5
Lamp	B	Oxidiser	N ₂ O 5.4
Lamp current	15 ma	Slid width	4
Coarse setting	4	Flame height	6.0
Damping	High	Direct.	

CaO, MgO, Na₂O and SrO were also determined using the EEL 240 Atomic Absorption Spectrophotometer. Lanthanum is used in the solution to overcome interfering elements on CaO and MgO determination. With SrO determination NaCl is used to prevent the Sr ionisation. Suitably diluted "solution B's" were used for these determinations. Standards of CaO, MgO, Na₂O and SrO were prepared for calibrations from analytical grade CaCl₂, MgCl₂, NaCl and SrCl₂ standard solutions. With this method the detection limits for Ca, Mg, Na and Sr are 0.2, 0.01, 0.05 and 0.3ppm respectively. An EEL technical publication has been used for A.A.S. work.

FeO (ferrous iron) was determined by the conventional titrimetric method using standard dichromate solution with diphenylamine sulphonic acid as indicator (Sarver, 1927).

0.25 grams of sample was decomposed in sulphuric and hydrofluoric acids. The solution was washed with boric acid into a saturated boric acid solution, and was titrated against the standard dichromate solution to a purple end point. At least one U.S.G.S. standard rock and a departmental standard were analysed with each batch of samples and the results obtained were in good agreement with the published recommended values.

Water (H_2O) was determined by using the modified Penfield method (Shapiro and Brannock, 1956). This method involves heating a sample and then collecting the water evolved on a filter paper. Errors are caused by oxidation, pyrolysis of unstable compounds, emission of other volatiles and variations in atmospheric water. In view of these factors results were remarkably consistent. For samples containing appreciable amounts of sulphur, anhydrous sodium tungstate (3 grams) was mixed with the sample powders.

Carbon dioxide (CO_2) produced from the reaction of orthophosphoric acid on the sample, was determined by measuring the amount of the carbon dioxide which reacts with a solution of barium hydroxide by back titration against hydrochloric acid with thymolphthalin as an indicator. This method is described by Bush (1970). It is an accurate, rapid and inexpensive method.

APPENDIX C

MAJOR AND TRACE ELEMENTS ANALYSES BY X-RAY FLUORESCENCE SPECTROMETRY

1. Introduction:

All major and trace elements analyses (excluding those using 'rapid' wet chemical methods) were carried out using a P.W.1212 Phillips, automatic X-ray fluorescence spectrometer. Two methods were used: The fusion technique for major elements (in rocks, excluding Na) and the resin pellet method for major (in minerals only) and trace elements (rocks and minerals).

The operating conditions, calibrations and analyses results for Colemanite (1013) standard are given in Tables 28, 29, 30 and 31. The analysis results for individual samples are given in the text in relevant chapters (see Tables, 5, 13, 20, 21, 22, 23 and 24).

Element	Mg	Na	Sr	As	Si	Ti	K	S
Date Run	11/74	11/74	6/74	6/74	7/74	7/74	1/75	10/74
Tube	Cr	Cr	Mo	Mo	Cr	Cr	Cr	Cr
Line	K α	K α	K α	K α	K α	K α	K α	K α
2 θ Peak	43.55	53.04	35.87	48.82	108.84	86.02	50.50	110.73
2 θ Bk.1	45.30	51.54	34.97	46.97	106.64	89.00	54.62	113.73
2 θ Bk.2			36.95	49.97				
B.factor			0.54	0.38				
Kv	50	50	80	80	60	60	60	60
mA	40	40	24	24	24	24	24	24
Collimator	Coarse	Coarse	Fine	Fine	Coarse	Coarse	Coarse	Coarse
Crystal	KAP	KAP	LiF220	LiF220	P.E.	LiF200	P.E.	Ge
Counter	F	F	S	F+S	F	F	F	F
Time (secs)	40	40	20	20	20	20	20	20
Ratio Std	1005/50/A	1005/50/A	1005/50/A	1005/50/A	1005/50/A	1005/50/A	1005/50/A	1005/50/A

Slope	3.87	4.39	1214	74.99	180558	0.74	2.20	1158
Intercept	0.39	0.36	-17247	-12.08	-308	-0.01	-0.07	-61.09
Std. Err.	1.44	0.10	100	8.86	85.47	0.03	0.09	244.4
Spike	*	*	SrCO ₃	As ₂ O ₃	SiO ₂	*	*	Gypsum

Calibration Results

*Calibrated by international standards

Table 28: Major elements analyses (Colemanite Standard, 1013): Operating conditions using P.W. 1212 XRFs. Analyses on resin pellets.

Table 29: Major elements analyses of colemanite standard, 1013.

<u>Oxide</u>	<u>Analysis</u>		
	<u>1</u>	<u>2</u>	<u>3</u>
B ₂ O ₃	51.304	51.305	52.071
CaO	25.820	25.820	25.540
MgO	1.020	1.058	1.035
Na ₂ O	0.000	0.000	0.000
SrO	1.826	1.068	0.973
As ₂ O ₅	0.001	0.028	0.004
SiO ₂	0.075	0.079	0.043
TiO ₂	0.000	0.000	0.000
K ₂ O	0.000	0.000	0.000
H ₂ O	20.530	20.807	20.733
CO ₂	0.000	0.000	0.000
SO ₃	0.102	0.066	0.060

<u>Analysis</u>	<u>Method</u>
B ₂ O ₃	Atomic Absorption
CaO	Atomic Absorption
H ₂ O	Penfield
CO ₂	Volumetric (Bush, 1970)
(MgO-SO ₃)	Resin Pellets (XRFS)

<u>El.</u>	<u>Tube</u>	<u>Line</u>	<u>20 p</u>	<u>20 Bk.1.</u>	<u>20 Bk.2.</u>	<u>f</u>	<u>Kv</u>	<u>mA</u>	<u>Colli.</u>	<u>Crystal</u>	<u>Counter</u>
Al	Cr	K α	144.80	137.85			60	24	Coarse	P.E.	F
Fe	Cr	K α	57.42	55.19			60	24	Coarse	LiF200	F
Mn	W	K α	95.18	93.18			60	32	Fine	LiF220	F+S
P	Cr	K α	140.92	138.92			50	40	Coarse	Ge	F
Cl	Cr	K α	92.70	95.70			60	24	Fine	P.E.	F
Cr	W	K α	69.36	67.25			60	32	Fine	LiF200	F
Ni	W	K α	71.25	72.13			60	32	Fine	LiF220	F+S
Cu	Mo	K α	65.53	66.53			80	24	Fine	LiF220	F+S
Zn	Mo	K α	60.54	59.25			80	24	Fine	LiF220	F+S
Br	Mo	K α	29.96	29.06	30.16	0.18	80	24	Fine	LiF200	S
Sn	W	K α	14.00	13.30			50	40	Coarse	LiF200	S
Ba	W	L β	128.84	131.84			50	40	Coarse	LiF220	F+S
Ce	W	L β	111.65	109.65			60	32	Coarse	LiF220	F+S
Pb	Mo	L β	40.33	39.79	40.80	0.48	80	24	Fine	LiF220	S
Th	Mo	I α	39.17	38.76	39.79	0.57	80	24	Fine	LiF220	S
U	Mo	I α	37.25	36.83	38.76	0.78	80	24	Fine	LiF220	S

f : Background factor

F : Gas flow proportional counter

S : Scintillation counter and long secondary collimator

Analysis time, 20 secs., throughout (except P, 40 secs.).

Table 30: Minor and trace elements analyses (Colemanite Standard, 1013): Operating conditions using P.W. 1212 XRFs.

Table 31: Minor and trace element calibrations;
Colemanite Standard, 1013.

<u>El.</u>	<u>Date Run</u>	<u>Slope</u>	<u>Inter.</u>	<u>S.E.</u>	<u>D.L.</u>	<u>M/C Std.</u>	<u>Spike</u>
Al	7/74	67153	-22.52	73.30	82	1005/50/A	Al ₂ O ₃
Fe	10/74	35644	-108.3	24.02	29	"	Fe ₂ O ₃
Mn	6/74	862.0	-37.0	18.32	16	"	Mn ₃ O ₄
P	7/74	1010	-22.30	6.85	75	"	NaH ₂ PO ₄
Cl	7/74	334	-26.32	4.72	186	"	KCl
Cr	12/74	189.8	-1.74	3.68	11	"	Cr ₂ O ₃
Ni	4/74	137.1	-4.63	1.06	12	"	NiO
Cu	6/74	251.5	-34.88	6.46	53	"	CuO
Zn	6/74	136.1	-5.04	0.66	16	"	ZnO
Br	2/75	87.93	-3.74	2.96	9	"	CsBr
Sn	10/74	873.5	3.94	3.40	41	"	SnO ₂
Ba	4/74	2387	-127.8	9.14	296	"	Ba(NO ₃) ₂
Ce	4/74	675.3	-60.38	5.86	247	"	CeO ₂
Pb	6/74	141.0	-1.98	2.16	13.5	"	PbO
Th	11/74	261.7	-3.38	5.27	6	"	ThO ₂
U	6/74	113.3	2.16	1.68	5	"	U ₃ O ₈

Inter. : Intercept
S.E. : Standard Error
D.L. : Detection Limit (ppm)
M/C Std. : Ratio Standard

2. Preparation of fusion beads:

This method of analysis for major elements is based on that described by Norrish and Hutton (1969) and improved by D.M. Taylor (1972, unpublished Ph.D. thesis). It is thoroughly discussed and evaluated in Harvey et al (1973).

A fusion disc, about 2mm thick and 29.5mm in diameter, is prepared from 2g of flux (Lithium tetraborate, Lithium carbonate, Lanthanum oxide and Sodium nitrate) and 0.37 g of rock powder. The mixture is melted in a muffle furnace at 1000°C, in a platinum crucible. Ignition loss is calculated by weighing the cooled melt. The mixture is then remelted, poured on to an aluminium disc and a plunger brought down rapidly to produce a flat bead.

Inter-element absorption and enhancement effects are not completely eliminated and for accurate analysis, these effects were corrected by a computer program, written by Harvey et al (1973).

The data reduction and final calculation of corrected analyses were made by computer programmes, (X09 , X08 and X02) which are available in the department.

Six elements at a time (Si, Al, Ti, Fe, Ca and K) were analysed on the Cr tube. Mg and P were also analysed on the same tube. Mn was analysed on W tube. Calibration is very quick to perform, and makes use of a small number of particularly well analysed standards. Calibration for major elements were made by using the international standards (USGS): DTS-1, BCR-1, PCC-1, GSP-1, G-2 and AGV-1, and the Nottingham University Geology Department standards: 1000 (olivine gabbro), 1001 (muscovite granite), 1002 (gypsum), 1003 (red marl), 1005 (hornblende andesite), 1006 (charnockite), 1007 (slate), and

3. Preparation of powder pellets:

Powder pellets were used to analyse for major elements in minerals and trace elements in both minerals and rocks. Trace element determinations are based on a method modified after Leake, et al (1969).

A resin pellet is prepared by thoroughly mixing 6g of rock powder with 1g of phenol-formaldehyde resin in a plastic phial containing plastic balls to assist the mixing. The powders are thoroughly mixed by placing the phial in an electric shaker and shaking for about 15 minutes. The balls were then removed and the mixture placed in a die between two tungsten carbide or stainless steel platens and pressed, under vacuum, at 30 tons pressure for 5 minutes using a hydraulic press. The resulting pellet was baked for 30 minutes at 85°C, labelled and stored between tissues in a cardboard box.

4. Calibration procedure:

Element calibrations were carried out by the spiking method. An accurately weighed spectrographically pure compound of a particular element was added to about 30 grams of dried rock standard powder (1013 Colemanite), to give an added concentration of about 10,000ppm. of that element. This initial mix (A) was thoroughly mixed by an electric shaker and successively diluted with the standard rock powder to give the concentration of 5000, 2500, 1000, 750, 500, 250, 100, 75, 50, 25, 10 and 5ppm. of the particular element added. The compounds used for spiking are given in Table 31. To reduce preparation time some elements were added together in the preparation of mix A

(multiple spikes) while others, because of the problems of interference and absorption, were spiked individually. The following multiple spikes were made:- As + Fe + U; Mn + Pb; Si + Al + P + Br; Cl + Zn; Cu + Ni + Ba and Sr + Ce.

The departmental standards 1003 and 1005 were used for the rock samples and calibration for each element was carried out with spikes on these standards (Aljubouri, 1972; Taylor, 1972; both unpublished Ph.D. theses). Additional spikes of As, S and Br were made using these standards.

After preparation of the spiked mixes at the values required, a resin pellet for each mix was prepared. A calibration slope for an element was obtained by running spiked pellets, with the machine standard, in the range of 10,000 to 5ppm and with a pellet of the standard rock to serve as a blank.

The slope was obtained by regression analysis of x (count ratio to the machine standard) and y (element concentrations). The negative intercept was taken to be equal to the amount of element present in the rock.

The standard error of calibration was also calculated (see Table 31) to give an estimate of precision of calibration which is affected by weighing and mixing the spike powders during preparations.

Detection limits for 1013 at the 95% confidence level are also given in Table 31 and are based on the formula given by Leake et al. (1969). Variations in the detection limit of an element in different matrices are caused by variations in the absorption characteristics of these matrices (Jenkins and de Vries, 1972).

5. Determination of unknowns:

The count ratio data for samples of unknown composition were converted to parts per million (ppm) in two stages. The first stage was the multiplication of the count ratios by the relevant slope factors, obtained from the calibration, to give uncorrected ppm. values.

The slope factors used were strictly only valid for rocks of identical composition to the standard rock used in the calibration process as a result of mass absorption effects. The second stage in the processing was the minimisation of these effects. This was achieved by ratioing the theoretical mass absorption values for the unknowns to those of the standard, for the wavelengths at which each of the elements were determined, and multiplying the uncorrected ppm. values by the factors obtained. Corrections for mass absorption were carried out for all trace elements using tungsten and molybdenum tube lines.

6. Corrections for contamination and interference:

Chlorine contamination from the handling can be very serious, if pellets are not properly handled. For this reason, all pellets were picked up, with a piece of tissue to avoid contact with the skin. Necessary care was taken in handling and storing pellets and chlorine results appear constant.

The overall Cu contamination from the target tube was corrected by using international standards, during systematic analysis of samples by the X-ray fluorescence spectrometer. A correction factor of -45ppm. was obtained and applied to all results.

The BaL β 1,4 peak was overlapped by CeL α . The interference was corrected, by running the Ce spikes on the Ba 2 θ peak. The Ba concentration was calculated by the following formula:-

$$\text{Ba ppm} = \text{Uncorrected Ba ppm} - \text{Ba slope} \times \left(\frac{\text{Ce ppm}}{\text{Ce slope at Ba } 2\theta} \right).$$

REFERENCES

- ALJUBOURI, Z. (1972) Geochemistry, Origin and Diagenesis of some Triassic Gypsum Deposits and associated sediments in the East Midlands. Unpublished Ph.D. Thesis, University of Nottingham.
- ANGINO, E.E., and BILLINGS, G.K. (1972) Atomic absorption spectrometry in geology (2nd edition), Elsevier, Amsterdam, London, New York.
- ARDA, T. (1968) Borate deposits of Eskişehir-Kirka province. M.T.A. report (unpublished Turkish text) Ankara.
- ARISTARAIN, L.F. and HURLBUT, C.S. Jr. (1968) Terruggite $4\text{CaO} \cdot \text{MgO} \cdot 6\text{B}_2\text{O}_3 \cdot \text{As}_2\text{O}_5 \cdot 18\text{H}_2\text{O}$, a new mineral from Jujuy, Argentina. *Amer. Min.*, 53, p.1815-1827.
- ARISTARAIN, L.F. and HURLBUT, C.S. Jr. (1972) Boron minerals and deposits (Part I. Uses, distribution and economic minerals of boron.) *Min. Record*, 3, p.165-172.
- ARISTARAIN, L.F. and HURLBUT, C.S. Jr. (1972) Boron minerals and deposits (Part II. Geological environments and classification of boron deposits.) *Min. Record*, 3, p.213-220.
- BAYSAL, O. (1972) Tunellite, a new hydrous strontium borate from the Sarikaya borate deposits in Turkey. *Bulletin of the Mineral Research and Exploration Institute of Turkey*, No.79. p.22-29, Ankara.
- BAYSAL, O. (1973) The genesis of the Kirka (Sarikaya) borate deposit. *Türkiye madencilik bilimsel ve teknik kongresi* p.255-277 (Turkish text with English abstract).
- BEEVERS, C.A. and STEWART, F.H. (1960) p-veatchite from Yorkshire. *Mineralogical Magazine and Journal of the Mineralogical Society*, 32, p.500-501.
- BOWSER, C.J. (1965) Geochemistry and petrology of the sodium borates in the non-marine evaporite environment. Ph.D. dissertation, University of California, Los Angeles.
- BOWSER, C.J. and DICKSON, F.W. (1963) Mechanism of borax deposition and the chemical composition of Pliocene lake waters at Kramer, California: (abs.), *Geol. Soc. America, Ann. meetings*, New York.
- BOWSER, C.J. and DICKSON, F.W. (1966) Chemical zonation of the borates of Kramer, California. *Second Symp. on Salt*, 1, p.122-132, *Northern Ohio Geol. Soc.*, Cleveland Ohio.

- BRAITSCH, O. (1959) Über p-veatchit, eine neue veatchit - varietat aus den Zechsteinsalz. Beiträge zue Mineralogie und Petrographie, 6, p.352-356.
- BRAITSCH, O. (1960a) Mineralparagenesis und Petrologie der Stassfurtsalze in Reyereshausen, Kali und Steinsalz, No.1, 1-4.
- BRAITSCH, O. (1960b) Die Borate und Phosphate im Zechsteinsalz Südhannovers, Fortschr. Mineralogie, 38, 190-191
- BRAITSCH, O. (1971) Salt deposits; their origin and composition. Springer-Verlag, Berlin, Heidelberg, New York.
- BROWN, W.W. and JONES, K.D. (1971) Borate deposits of Turkey in CAMPBELL, A.S. (ed) Geology and History of Turkey. The Petroleum Exploration Society of Libya, Tripoli.
- BÜGGE, Jens A.W. (1951) Minerals from the skarn iron ore deposits at Arendal, Norway. Cahnite from Klodeborg mine. K.Norske Vidensk, Selskab. Förh, Vol.24, p.79-81.
- BUSH, P.R. (1970) A rapid method for the determination of carbonate carbon and organic carbon. Chem.Geol. 6, p.59-62.
- CARROLL, D. (1958) Role of clay minerals in the transportation of iron. Geochim. Cosmichm. Acta, 14, p.1-27.
- CARROLL, D. (1970) Clay minerals: a guide to their x-ray identification. Boulder, Geol.Soc.America, Special Paper 126.
- CHRIST, C.L. (1960) Crystal chemistry and systematic classification of hydrated borate minerals. Am.Min. vol.45, p.334-340.
- CHRIST, C.L. (1972) Some contributions of crystal chemistry to geochemistry. Journal of Geological Education, Special issue, Volume XX, No.5.
- CHRIST, C.L. and CLARK, J.R. (1956) The structure of meyerhofferite, $2\text{CaO} \cdot 3\text{B}_2\text{O}_3 \cdot 7\text{H}_2\text{O}$, a $\text{P}\bar{1}$ crystal, determined by the direct method of Hauptman and Karle: Acta Cryst. 9, 830.
- CHRIST, C.L. and CLARK, J.R. (1960) The crystal structure of meyerhofferite, $\text{CaB}_3\text{O}_3(\text{OH})_5 \cdot \text{H}_2\text{O}$: Z.Krist. Vol.114, p.321-342.
- CHRIST, C.L., CLARKE, J.R. and EVANS, H.T. Jr. (1958) Studies of borate minerals (III): the crystal structure of colemanite, $\text{CaB}_3\text{O}_4(\text{OH})_3 \cdot \text{H}_2\text{O}$, Acta. cryst. vol.II, p.761-770.
- CHRIST, C.L. and GARRELS, R.M. (1959) Relations among sodium borate hydrates at the Kramar deposit, Boron, California. Amer.Jour.Sci., Vol.257, p.516-528.

- CHRIST, C.I., TUESDELL, A.H. and ERD, C.R. (1967) Borate mineral assemblages in the system $\text{Na}_2\text{O}-\text{CaO}-\text{MgO}-\text{B}_2\text{O}_3-\text{H}_2\text{O}$. *Geochim. Cosmochim. Acta*, 31, p.313-337.
- CLARK, J.R. (1959) Studies of borate minerals, IV: the crystal structure of inyoite, $\text{CaB}_3\text{O}_3(\text{OH})_5 \cdot 4\text{H}_2\text{O}$. *Acta Cryst.*, Vol.12, p.162-170.
- CLARK, J.R. and APPLEMAN, D.E. (1964) Pentaborate polyanion in the crystal structure of ulexite, $\text{NaCaB}_5\text{O}_6(\text{OH})_6 \cdot 5\text{H}_2\text{O}$. *Science* 145, 1295-1296.
- CLARK, J.R. and CHRIST, C.L. (1971) Studies of borate minerals XVI. Veatchite: Crystal structure and correlations with p-veatchite. *Am.Mineralogist*, V.56, p.1934-1954.
- D'ACHIARDI (1934) Ginorite. *Per. Min.*, 5, 22.
- DICKSON, J.A.D. (1965) A modified staining technique for carbonates in thin section. *Nature*, 205, p.587.
- DICKSON, J.A.D. (1966) Carbonate identification and genesis as revealed by staining. *J.Sed.Petrol.*, 36, p.491-505.
- DONNAY, G. and BUERGER, M.J. (1950) The determination of the crystal structure of tourmaline. *Acta Cryst.*, Vol.3. p.379.
- DUNN, P.S. (1966) Boron. *Eng.Min.Jour.*, 168, p.126-128.
- EEL, Technical Publication. Atomic Absorption Analytical Methods. Volume 2. Ref.No. 001 97 028. Evans Electroselenium Limited, England.
- EMBREY, P.G. (1960) Cahnite from Capo di Bove, Rome. *Min.Mag.*, Vol.32, p.666-668.
- ERD, R.C., MORGAN, V. and CLARKE, J.R. (1961) Tunnelite, a new hydrous strontium borate from the Kramer borate district, California. *U.S. Geol.Survey Prof. Paper* 424-C, C294-C297.
- ERING, S. (1971) The Gediz earthquake of 1970 in CAMPBELL, A.S. (ed) *Geology and History of Turkey*. The Petroleum Exploration Society of Libya, Tripoli.
- ERNST, W. (1970) *Geochemical facies analysis*. Elsevier Publishing Company, Amsterdam.
- FOSHAG, W.F. (1921) The origin of the colemanite deposits of California. *Econ. Geol.*, 16, p.199-214.
- GALE, H.S. (1913) The origin of colemanite deposits. *U.S. Geol. Survey. Prof. Paper* 85-A.
- GATES, G.R. (1959) Clay mineral composition of borate deposits and associated strata at Boron California. *Science*, Vol.130, No.3367, July 10, p.102.
- GAWLIK, J. (1956) Borate deposits of the Emet Neogene basin. *M.T.A. Report No. 2479*, Ankara. (Turkish and German text).

- GILES, H. (1903) Bakerite (a new borosilicate of calcium) and howlite from California. *Min.Mag.*, 13, p.353-355.
- GOLDSCHMIDT, V.M. (1954) *Geochemistry*. Oxford University Press, Oxford.
- HANSHAW, B.B. (1963) Preliminary relations in the system $\text{Na}_2\text{B}_4\text{O}_7\text{-Ca}_2\text{B}_6\text{O}_{11}\text{-H}_2\text{O}$. Prof. Paper U.S.Geol.Surv., 475-B, p. 24-27.
- HARDER, H. (1961) Incorporation of boron in detrital clay mineral. *Geochim et Cosmochim acta*, Vol.21, p.284-294.
- HARVEY, P.K. et al, (1973) An accurate fusion method for the analysis of rocks and chemically related materials by x-ray fluorescence spectrometry. *X-ray Spectroscopy*, Vol.2.
- HELVACI, C. (1974) Contribution to discussion of a paper by Inan, K., Dunham, A.C. and Esson, J. *Trans.Inst. Min.Metall. (Section B. Appl.earth sci.)* 83, B.36.
- HELVACI, C. and FIRMAN, R.J. (1976) Geological setting and mineralogy of Emet borate deposits, Turkey. *Trans. Inst. Mining Metall. (Section B. Appl.earth sci.)*, 85, B.142-152.
- INAN, K. (1972) New borate district, Eskişehir-Kirka province, Turkey. *Inst.Mining and Met.*, Vol.81. p.B163-165.
- INAN, K. (1973) The mineralogy and geochemistry of the Kirka borate deposit, Turkey. Unpublished Ph.D. Thesis, University of Manchester.
- INAN, K., DUNHAM, A.C. and ESSON, J. (1973) The mineralogy, geochemistry and origin of the Kirka borate deposit, Eskişehir province, Turkey. *Trans.Inst.Min.Metall. (Sect.B. Appl.earth sci.)*, 82, B.114-123.
- JENKINS, R. and DE VRIES, J.L. (1972) *Practical x-ray spectrometry* (2nd edition). Macmillan, London and Basingstoke.
- KEMP, P.H. (1956) *The chemistry of the borates; Part I: Borax Consolidated Limited*, London SW1, 90p.
- KITANO, Y. (1963) Geochemistry of calcareous deposits found in hot springs. *J.Earth Sci., Nagoya Univ.* 11, p.68-100.
- KRAUSKOPF, K.B. (1956) Factors controlling the concentrations of thirteen rare metals in sea water. *Geochim et Cosmochim. Acta* 9, 1-32.
- KURMAN, I.M. and USACHEVA, Z.M. (1937) Geology and origin of the datolite deposits of the laccoliths of the Mineral Spring region (North Caucasus). *Trans. Sci. Inst. Fertilizers and I. Fung.*, No.142, p.124, and *Min Abst.* v.7, p.442.

- KURNAKOVA, A.G. and NIKOLAEV, A.V. (1948) The solubility isotherm of the system $\text{Na}_2\text{O}-\text{CaO}-\text{B}_2\text{O}_3-\text{H}_2\text{O}$ at 25°C . Akad. Nauk. U.S.S.R., Izv. Otd. Khim. Nauk 1, p.377-382 (Russian text).
- LADREGREN, S. (1945) Contribution to the geochemistry of boron II. The distribution of boron in some Swedish sediments and iron ores. The boron cycle in the upper lithosphere. Arkiv. Kim. Mineral. Geo., 19a, No.26,1.
- LEAKE, B.E. et.al. (1969) The chemical analysis of rock powders by automatic x-ray fluorescence. Chem. Geol. 5, p.7-86.
- MALINKO, S.V. (1966) First find of caninite in the U.S.S.R. Dokl.Acad.Sci. U.S.S.R., Earth Sci.Sect., 166, p.116-120. Transl. from Dokl.Acad. Nauk U.S.S.R., 166, p695-697.
- MEIXNER, H. (1952) Einige Boratminerale (colemanit und Tertschit, ein neues Mineral) aus der Türkei. Fortschr. Mineralogie, Vol.31, p.39-42.
- MEIXNER, H. (1953) Neue Türkische boratlagrstatlen; Berg. u. huttenmann Monatsh, vol.98, p.86-92.
- MEIXNER, H. (1953) Mineralogische Beobachtungen an Colemanit, Inyoit, Meyerhofferit, Tertchit und Ulexit aus neum Türkischen Boratlagerstätten. Heidelb. Beitr. Miner. Petrogr., 3, p.445-455.
- MEIXNER, H. (1956) Due neue Türkische boratprovinz un Iskelekoy bei Bigadic im Vilayet Balikesir. Sonderabdruck aus Kali und Steinsalz, part 2, p.43-47, Essen, Verlag Glockauf.
- MORIMOTO, N. (1956) The crystal structure of borax. Min.J. Japan 2, 1-18.
- MUESSIG, S. (1958) First known occurrence of inyoite in a playa at Laguna Salinas, Peru. Am.Mineral., Vol.43, p.1144-1147.
- MUESSIG, S. (1959) Primary borates in playa deposits; mineral of high hydration. Econ.Geol., Vol.54, No.3, p.495-501.
- MUESSIG, S. (1966) Recent South American borate deposits. Second symp. on Salt, 1, p.151-159, Northern Ohio Geol. Soc., Cleveland, Ohio.
- MURDOCH, J. (1957) Crystallography and x-ray measurements of howlite from California. Am.Min., 42, 521.
- NEGRO, A.D., KUMBASAR, I. and UNGARETTI, L. (1973) The crystal structure of teruggite. American Mineralogist, 58, p.1034-1043.
- NOBLE, L.F. (1926) Note on a colemanite deposit near Shoshone, California, with a sketch of the geology of a part of Amargosa valley. U.S.Geol.Survey, Bull. 785, p.63-73.

- NORRISH, K. and HUTTON, J.J. (1969) An accurate X-ray spectrographic method for the analysis of a wide range of geological samples. *Geochim. Cosmochim. Acta*, 33, p.431-455.
- ÖZPEKER, I. (1969) Western Anatolian borate deposits and their genetic studies. Ph.D dissertation (Turkish text). Technical University of Istanbul.
- PALACHE, C. and BAUER, L.H. (1927) Cahnite, a new borate-arsenate of calcium from Franklin, New Jersey. *Amer. Min.*, Vol.12, p.149-153.
- PALACHE, C., BERMAN, H. and FRONDEL, C. (1951) Dana's system of mineralogy. Vol.2, John Wiley, New York.
- PREWITT, C.T. and BUERGER, M.J. (1961) The crystal structure of cahnite $\text{Ca}_2\text{B}_4\text{O}_{10}(\text{OH})_4$. *Amer. Min.*, 46, p.1077-1085.
- RANKAMA, K. and SAHAMA, Th.G. (1950) *Geochemistry*. Univ. Chicago Press, Chicago.
- ROGERS, A.F. (1919) Colemanite pseudomorphous after inyoite from Death Valley, California. *American Mineralogist*, Vol.4. p.135-139.
- RUMANOVA, I.M. and ASHIROV, A. (1964b) Determination of the crystal structure of hydroboracite. $\text{CaMg B}_3\text{O}_4(\text{OH})_{32} \cdot 3\text{H}_2\text{O}$. *Soc.Phys.Cryst.* 8, p.665-680.
- RUMANOVA, I.M., KURBANOV, Kh.M. and BELOW, N.B. (1966) Crystal structure of probertite, $\text{CaNa}[\text{B}_5\text{O}_7(\text{OH})_4] \cdot 3\text{H}_2\text{O}$. *Soc.Phys.Cryst.* 10, p.513-522.
- SARVER, L.A. (1927) The determination of ferrous iron in silicates. *Am.Chem.Soc.Jour.*, v.49, p.1472-1477.
- SCHALLER, W.T. (1927) Kernite, a new sodium borate. *Am. Mineral.*, Vol.2. p.24-25.
- SCHALLER, W.T. and MROSE, M.E. (1960) The naming of the hydrous magnesium borate minerals from Boron, California. A preliminary note. *Am.Mineral.*, Vol.45. p.732-734.
- SCHLUTER, A. (1928) Das Pandemit vorkommen von Sultancayiri, Abh.2. prakt. Geol. u Bergwirtschaftslehre, v.17.
- SHABYNIN, L.I. (1955) On the diagnosis of borates in magnesium skarns. *Mem.Soc.Russe Min.*, Ser.2, Vol.84. p. 308-320.
- SHABYNIN, L.I. (1957) Distribution and formation conditions for boron concentration in endogenetic borates of skarn deposits. *Izvestiya Akad Nauk S.S.S.R. Ser.Geol.* p.63-70.
- SHAPIRO, L. and BRANNOCK, W. (1956) Rapid analysis of silicate rocks. *U.S. Geol.Surv. Bull.* 1036C.
- STEWART, F.H., CHALMERS, R.A. and PHILLIPS, R. (1954) Veatchite from the Permian evaporites of Yorkshire. *Miner. Mag.*, Vol.30. p.389.

- STRECKEISEN, A.L. (1967) Classification and nomenclature of igneous rocks. N.Jb.Mineral.Abh., 107, p.144-240.
- SVERDRUP, H.U., JOHNSON, M.W. and FLEMING, R.H. (1942) The oceans. Prentice Hall, Inc., New York.
- TAYLOR, D.M. (1972) The petrology and geochemistry of the andesites and associated rocks from an area of the Ochil Hills, Dunning, Perthshire. Unpublished Ph.D. Thesis, University of Nottingham.
- TAYLOR, S.R. (1969) Trace element chemistry of andesites and associated cal-alkaline rocks. Oregon Dept. Geol. Min.Ind.Bull., 65, p.43-64.
- TILLEY, C.E. (1951) The zoned contact-skarns of the Broadford area, Skye: a study of boron-fluorine metasomatism in dolomites. Min.Mag. Vol.29, p.631-666.
- VOGEL, A.I. (1961) A textbook of quantitative inorganic analysis. 3rd edition. Longmans, London.
- WATANABE, T. (1939) Kotiot ein neues gesteinsbildendes Magnesium borat, Tschermak Miner. Petr. Mitt., 50, 441-463.
- WATANABE, T. (1964) Geochemical cycle and concentration of boron in the earth's crust. V.I.Verdenskii Inst. Geochim. and anal.chem. U.S.S.R. Vol.2, p.167-177.
- WEAST, R.C. (1971) Handbook of Chemistry and Physics, 52nd edition. Cleveland, Ohio: The Chemical Rubber Co.Ltd.
- WEDEPOHL, K.H. (1969) Handbook of geochemistry. Vol.II. Springer-Verlag, Berlin, Heidelberg, New York.
- YARAR, R., DEMIR, H., KUMBASAR, N. and TRUPIA, A. (1970) Gediz depremi incelemelerine ait on rapor: Deprem muhendisligi yayinlari, No.1, Technical University, Istanbul, Insaat Fakultesi.
- ZACHARIASEN, W.H. (1954) The precise structure of orthoboric acid. Acta Cryst. 7, 305-310.